JOURNAL OF THE AERONAUTICAL SCIENCES

VOLUME 11 APRIL, 1944 NUMBER 2

Research for Aeronautics—Its Planning and Application

The Seventh Wright Brothers Lecture*

W. S. FARREN†

Royal Aircraft Establishment

FOREWORD

The invitation of your Council to deliver the Wright Brothers Lecture in commemoration, on this occasion, of forty years' development in aviation is an honor of which I am deeply sensible. The responsibility of doing justice to it would be heavy at any time. The turn of the tide of our joint fortunes in this war makes it greater rather than less. For the burden of success, whether in war or in peace, is far greater than that of failure. But so also is the stimulus to our courage.

INTRODUCTION

THE EXCEPTIONAL CIRCUMSTANCES of the times make it impossible for me to observe the letter of what I know is the Institute's wish in the choice of a subject, though I believe I can conform to it in spirit. The Institute desires that the lecturer shall deal with some scientific or technical subject on which he is, or has been, personally engaged, and shall not indulge in broad surveys. There will come a time when the lecturer's chief difficulty will be to choose from the embarrassingly rich store of knowledge which has accumulated during this war. But for the time being the door of that store cannot be opened in public. Moreover, I doubt whether the part that I have played in a large number of fascinating and exciting investigations during the last 4 or 5 years is such that I could fairly deprive those who have done the work of the privilege of speaking about it. This is a difficulty that has always faced those who hold such positions as mine, and one of which your Council were no doubt well aware when they invited me.

I have long been concerned with the problems that arise in applying the advances in knowledge which research for aeronautics has brought us and with the problems of planning the course of current research and of providing appropriate and timely resources for future research. I believe that these are matters that might with advantage be surveyed as a whole, in a scientific spirit. Moreover, I believe that the subject can usefully be treated in a purely personal way, and I have throughout drawn on my own experience.

From this it follows that any conclusions I draw apply only to the circumstances in my own country, or rather to my own interpretation of what they have been and may be. It will be for you, not for me, to say whether you find them in any way relevant to circumstances in the United States. But the intimate re-

W. S. Farren.

* Presented before the Institute of the Aeronautical Sciences in the U.S. Chamber of Commerce Auditorium, Washington, D.C., December 17, 1943.

† Director.

lations that have existed between workers in America and in England, in the field in which my interests and responsibilities lie, give me the courage to believe that a summary of my experience may be of interest to you, and worthy of this occasion.

The Aim of Research

Research is one of the things we all understand but find difficult to define. In the foreword to a recent pamphlet on *Industrial Research*, Sir Harold Hartley defined it as "a habit of mind which makes us attack every problem, big or small, in an orderly, systematic way, using if possible the advantages that modern science can give us." I remember Lord Rutherford, in a characteristically expansive and emphatic mood, using almost the same words. I invite you to note the two words "if possible." There are limits to what "modern science" can do for us. In research, as in other human activities, we depend a good deal on our wits. There is limitless opportunity for intuition and initiative.

The aim of research is to produce a theory firmly supported by experimental evidence. Though necessarily incomplete, it must be a close enough approximation to serve the man who has to make things work. I trust you will not infer from this statement that I am interested in research only for what I can get out of it. I have known the thrill of working solely for the fun of it. But I am interested, for the time being, in research with a clear and unmistakable objective—the discovery of how to make better aircraft. It is my experience that, for such research to be not only fruitful but timely, it is essential that the practical problems involved in its eventual application shall always be clear to those who are doing it. This need not in any way restrict their freedom. Indeed, they can gain immensely from contact with those upon whom the burden of applying their work is placed.

The theme I have taken is indeed that it is only by intimate and wholehearted collaboration between the research worker, the designer, the constructor, and the user that research can be intelligently planned, pursued, and applied.

The Independent Worker in Research

As a preliminary I propose to give you an example from my earlier experience which I feel puts the point as it appears to the independent research worker.

I have been personally concerned with research in flight for nearly 30 years. The two chief aerodynamic problems have been, and still are, the reduction of drag and the improvement of stability and control. Throughout, these problems have been attacked in the light of the practical questions thrown up by continuous contact, on the one hand, with those who design and build aircraft and, on the other, with those who use them. In my experience it has been this intimate relation between the three parties which has made this work so continuously exciting and, I believe, profitable. On looking back I cannot find any example that convinces me that we should have moved more quickly or more certainly had work on the fundamentals been divorced from that on problems of the moment.

It is true that at times, while we were developing our theory, we had the advantage—and this adds to my point—of individual work going on in flight, under conditions which I now believe to have been ideal. When I was one of the team who worked on these subjects at Cambridge, we often felt that we could do more, or do it more quickly, if only we had more of something—men, airplanes, workshops—but chiefly more hours in the day. In truth, I think we did as much as was physically possible without enlarging our organization, and, if we had done that, our work would have changed in character and would, I believe, have been less effective. That it had effect, and quickly, was due to our close relation with the establishments that had the necessary resources to exploit it for practical purposes with which they were intimately acquainted. They seized it and rapidly developed it. Its practical effect can now be seen not only in many aircraft but in the research equipment and programs of work.

You will remember Sir Melvill Jones's first Wright Brothers Lecture, in which he described some of the work I have just referred to on the boundary layer. From my own share in that work I can say that we were profoundly excited by the problems themselves and by the fascination of trying to solve them by experiments in flight. But we were stimulated, and all our discussions were illuminated, by the realization of the potential application of their results. This we obtained from our constant personal contacts with the Experimental Establishments and with aircraft designers.

Thus my experience leads me to the conclusion that, while there should be no explicit attempt to divorce work on basic problems from that on immediate ones of narrower range, the fullest encouragement and practical support should be given to independent workers. What form this should take I hesitate to define. My own preference is not for large endowments to institutions in the hope that they may attract good men. I would rather make generous finance available through some semi-independent advisory organization when the need is made clear by the development of the work. This may be either in cash or in kind. We at Cambridge had very little money, but the country supplied us with airplanes and maintained and renewed them. My only concern is that the ponderous workings of the machinery of government, when finance is involved, may result in the essential help coming too late. One day we shall learn to trust our scientific advisers with a reasonable fraction of our money on a block-grant basis and ask no account except at longish intervals.

Research on a Large Scale

I come now to that class of research for aeronautics whose scale is such that success depends on planning of large experimental resources and on planning so that application to practice may meet the foreseen needs of design and its capacity to exploit new discoveries.

We must, in my view, plan research for aeronautics in three phases. First, we must relate all our main effort to advances in basic theory. Odd pieces of information without a clear, strong framework are worth little. Second, we must provide the experimental information by which theory may be built up and its limitations recognized and reduced. Third, we must ensure that experimental application is made in such conditions that the practical value of the theory is confirmed.

There are three chief parties to this undertaking: first, those who are by trade workers in the field of theory and those who have the flair for the associated exploration by experiment; second, those who make use of the results in the design and construction of aircraft; and third, those who use the aircraft and on whom we rely to exploit the product of the efforts of the first and second. The extent to which these should enter into planning of research can be illustrated by an example—the problem of reducing the cooling drag of power plants.

That it is possible to reduce the power wasted in cooling an airplane power plant to 2 per cent or less of the brake horsepower was established many years ago. Indeed, it was shown that, at flight speeds that were then within sight and have now been passed, the cooling could be made to help to propel the airplane. But the cooling of a power plant is a matter that goes far beyond broad conceptions of this kind. It involves complex flows of air and liquids, demanding regulation to meet the varying conditions of flight and high standards of reliability in functioning and of ease of maintenance, which are of the greatest concern to the user.

It was not until other developments had reduced the rest of the drag so much that the power-plant drag was a dominating factor that the designer became convinced that the problem demanded his serious attention. He has finally succeeded in producing cooling systems that are no less reliable and have a much lower drag. The user accepts the slight additional embarrassment to maintenance in return for the higher speed and greater range.

But the practical problems of achieving the full result are still only partially solved. Few power plants will stand up to critical examination on such points as low-loss ducting or airtight cowlings. It is a difficult engineering problem to design and make such features at the same time light and easily removable and replaceable without damage.

Throughout the whole history of this development there has been intimate association between the three parties chiefly concerned. But in my view we can now see that a better planning of the enterprise as a whole would have saved much time and waste of work. In particular, an earlier realization by the designer of the outstanding advance that was within his grasp would have brought him to a closer cooperation, on strictly practical lines, with his only source of specific information—the research establishments. They in turn were backward in that they did not provide themselves with the right material by which alone convincing information, directly applicable to practical problems, could be obtained. This is a case in which I believe the enlightened user, if correctly advised, could have forced the pace.

A Survey of 25 Years' Achievement

The final criterion of our success in using the knowledge with which we have been supplied is the extent to which the product of our efforts has improved as time has passed. The curve of advance is not a smooth one. Over longish periods we often see little beyond a slow rise in achievement, and we tend to believe that there is little more to be expected. Then there comes something in the nature of a transformation. It is often ascribed to a single cause and, generally, one can say that there is an outstanding stimulus. But if we compare the final product—in this case, the airplane itself—before and after the event, allowing a long enough time for the situation to reach a fairly stable state, we can make a fair assessment of the relative weight of all the influences which have contributed to the change. I believe such an examination of the advance of the airplane, between say 1917 and 1942, is useful in providing us not only with a means of examining how far we have been successful in using the results of research but also a guide to the part played by sheer engineering skill and initiative. Finally, it may serve as a base from which we may survey some of the potential advances that are now opening out to us and judge what resources we shall need in order to achieve them.

I shall take two typical aircraft that were in general and successful use in 1917 and compare them with two modern aircraft of similar duties. Naturally there are striking differences, and we shall find no difficulty in tracing them to their sources. But perhaps equally striking are the characteristics that have apparently undergone little change. I think, however, that we shall see that the effort to preserve them unchanged has made as high a demand on research and engineering skill as that required to produce the more obvious improvements.

During the last war the Royal Aircraft Factory (which became the Royal Aircraft Establishment in April, 1918) produced many designs for aircraft which were constructed in large numbers. One of the most

successful was the S.E.5, a single-seat fighter with a 180-hp. Hispano Suiza engine. It had a creditable history as a fighter. I propose to compare it with a Spitfire. Then I shall take the Handley Page 0/400 twin-engined heavy bomber and compare it with a Lancaster.

I shall not be giving away any information to our enemies. They are well acquainted, in more ways than one, with both Spitfires and Lancasters. Some of them may even remember the S.E.5 and the 0/400. For my purpose it is quite sufficient to take examples of marks of the modern types whose performance has long been surpassed.

Let us first look at them in general outline. Fig. 1 shows the 1917 fighter. In Fig. 2 its specifically military features have disappeared and around it is the outline of the Schneider Trophy streamlined monoplane, the essential product of the period between the two world wars. Fig. 3 shows the 1942 fighter. In Figs. 4, 5, and 6 is shown the transition from the 1917 bomber, through the streamlined airliner, to the 1942 bomber. The most obvious differences are the change from biplane to monoplane and the general cleaning-up due to enclosing the crew, abolishing external wing bracing, and retracting the undercarriage. Comparing them type by type, the overall dimensions are not very different. The Spitfire has the same wing surface as the S.E.5, about half the drag, nearly twice the strength, three times the speed, four times the total weight, four times the military load, and seven times the power. The Lancaster has about half the drag of the Handley Page 0/400 on the same span of wings and about three-quarters the wing surface. Its total weight is nearly five times as great; the wing loading, over six times; the power, seven times; and the military load, with a 25 per cent greater range, over eight times. Let us inquire how some of these improvements have been made.

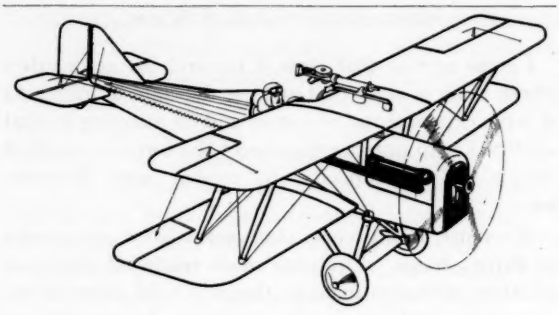

FIG. 1.

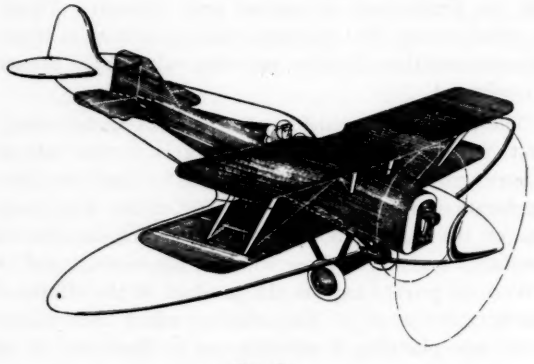

FIG. 2.

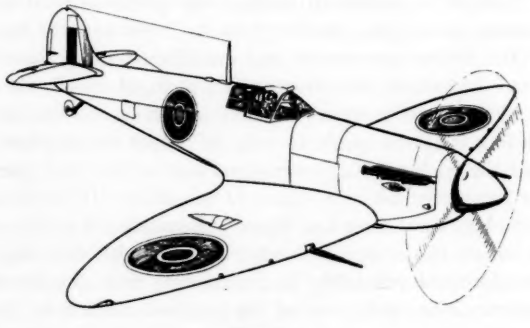

FIG. 3.

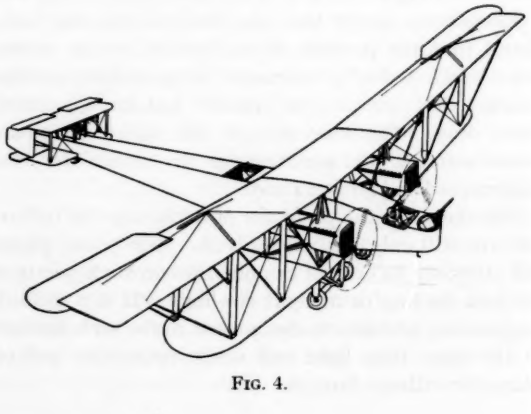

FIG. 4.

DRAG REDUCTION

The change in drag coefficient C_{D_0} is of first interest. I have not found it possible to get accurate figures for the older aircraft, but they are approximately 0.039 for the fighter and 0.046 for the bomber. The corresponding modern figures are 0.022 for the Spitfire and 0.030 for the Lancaster. Thus, per square foot of wing surface, the total drag has been reduced to about 55 and 65 per cent of the 1917 standard.

Comparing the two fighters in more detail, we find first that the wing surface is the same for both. Disregarding induced drag (or assuming it to be the same fraction of the whole in each), the top speed at the same height will be proportional to the cube root of the thrust power divided by the drag coefficient. Since the propeller efficiency is near enough the same for both, we may use brake power. Taking ground level powers in both cases—180 hp. for the Hispano and

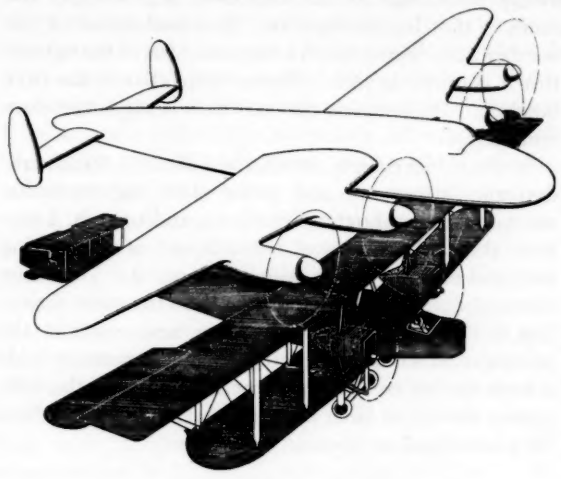

FIG. 5.

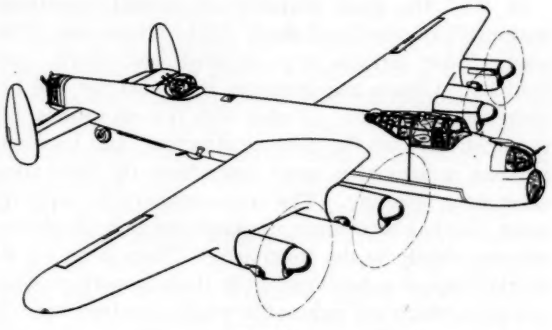

FIG. 6.

1250 for the Merlin—the ratio is about 7. Thus the contributions to increase of speed are:

$$\text{by reduction of drag } \left(\frac{0.039}{0.022}\right)^{1/3} = 1.21$$

$$\text{by increase of power } (7)^{1/3} = 1.92$$

The product of these figures is 2.33.

If we assume that by supercharging it is possible to keep the Merlin power constant up to say 25,000 ft., where the density is approximately halved, we shall get a further rise:

$$\text{by supercharging } (2)^{1/3} = 1.26$$

The total ratio of increase is therefore nearly 3.

At this point I feel that the engine people are feeling very pleased—and we have good reason to acknowledge the success of their effort. But these figures as they stand do less than justice to the aerodynamic contribution. All the cooling required by the seven-times increased power has been provided and yet the aircraft has no more than half the drag per square foot of wetted surface.

How have these improvements been made? Let us look first at the drag account (Table 1). To the saving of 47 lbs., the most obvious contributions are from the elimination of wing bracing and undercarriage—31 lbs. in all. But the body and cooling drag is actually reduced by over 10 per cent in spite of the seven-fold increase of power.

TABLE 1

	S.E.5 Drag at 100 Ft. per Sec.	Spitfire Drag at 100 Ft. per Sec.
Wings	28	20
Wing bracing	15	...
Body and cooling	44	38.6
Tail surfaces	7	4.4
Undercarriage	16	...
Total	110 lbs.	63 lbs.
C_{D_0}	0.039	0.022

TABLE 2

	S.E.5	Spitfire	FW 190
Structure	29.7%	28.9%	30.9%
Power plant	37.1	38.0	35.7
Fuel	15.4	16.6	14.3
Load	17.8	16.5	19.1
Total	100.0%	100.0%	100.0%
Primary load factor	6	10	...

For the bomber, the reduction in C_{D_0} is rather less than for the fighter on account of the drag of defensive armament, but otherwise the influences operating have been much the same.

Toward the end of my paper I shall say something about what further improvements in drag are in sight and what problems we have to solve in order to achieve them.

WEIGHT ANALYSIS

Let us look next at the weight picture. The Spitfire weighs four times as much as the S.E.5; the Lancaster, nearly five times as much as the 0/400. What has made it possible to carry so much additional weight per square foot of wing surface—for the fighter four times, for the bomber six times as much? In the airplane itself, first, the development of flaps giving higher maximum lift coefficient and higher drag; second, power plants of much greater power per unit weight; and, third, constant-speed propellers to make the power fully available over a wide speed range. But larger and better airfields, permitting higher take-off and landing speeds and better flying technique, have contributed even more. The effective maximum lift coefficient has risen by about 65 per cent. Even so, the

TABLE 3

	Handley Page 0/400	Lancaster
Structure	40.4%	31.4%
Power plant	22.0	16.4
Fuel	19.3	19.8
Load	18.3	32.4
Total	100.0%	100.0%

touch-down and take-off speeds, with the higher wing loadings, are 50 to 80 per cent higher.

A comparison of the weight analyses and load factors of the fighters is given in Table 2. As a matter of interest, I have given also the weight analysis for the FW 190.

How has this remarkable similarity of weight distribution been maintained? From the structural point of view, it is essentially by increasing wing loading four times that it has been possible to go from braced biplane to monoplane with nearly double the primary strength, from fabric covering to a metal skin, and from a fixed to a retractable undercarriage with no significant changes in percentage structure weight.

From the point of view of the power plant, we have to record a rise in the net output per pound of complete plant in the ratio of about 7 to 4. The complete plant of 1942 includes both constant-speed propeller and supercharging arrangements by which the power is maintained up to heights at which the air density is half, or even less than half, of that at ground level.

For the same percentage fuel weight the range is some 40 per cent better at a much higher cruising speed. Specific fuel consumption is much the same in spite of the great improvement in specific performance achieved in the face of the burden of supercharging. We must acknowledge here the tremendous contribution of high-octane fuel.

We are left in both cases with about one-sixth of the total weight for the man, his equipment, and armament. The weight of the man is the same as it was. In 1918 it exceeded that of his whole fighting equipment. Today it is but a fraction of it. The weight of the bullets alone in the modern fighter exceeds that of the whole armament of the S.E.5.

For the bombers, weight analyses are strikingly different from those of the fighters (Table 3). In 1917 we thought it natural for the structure weight of a large bomber to be greater than that of a small fighter—40.4 per cent compared with 29.7 per cent. In fact there was a view, widely held and expressed somewhat forcibly by Dr. Lanchester, that aircraft of larger span than say 100 ft. would be uneconomical because of the operation of the square-cube law characteristic of geometrically similar structures. Designers, aided by research, have managed to avoid the consequences of this law. They have been so successful that the structure weight percentage for the Lancaster is practically the same as that for the Spitfire. The load factor of the bomber is, of course, much lower than that of the fighter. But it is probably little different from that of the 1917 bomber. The progress that has been made is therefore remarkable.

In the achievements summarized above I think aerodynamic, structural, and power-plant improvements can fairly claim about equal shares, and to each, I suggest, the contributions of research and of engineering skill and ingenuity have been about equal. To pursue the analysis would lead me away from my main theme. But I think we may, with advantage, examine the history of effort in the structural and aerodynamic fields a little further in order to show the nature of the difficulties that have been met and the methods by which they have been overcome.

STRUCTURAL DEVELOPMENTS

In 1917 the great majority of aircraft structures were made of wood and steel. Light alloys were little used. Wing surfaces were covered with fabric, and torsional stiffness requirements were met by the biplane wing structure. Today with few exceptions, we use light alloy for the primary structure, and torsional stiffness is derived in most cases from the light-alloy sheet wing covering. The very considerable improvement that has been made in aluminum-rich alloys contributes chiefly to the wing spars. There is as yet no marked sign of a development in their properties or application which will reduce the weight involved in meeting torsional stiffness requirements. This is, of course, because these involve stability rather than strength characteristics.

I do not suggest that the enormous effort that has been put into improving aircraft materials has not contributed to the maintenance of structure weight at a remarkably low figure in spite of increases of speed, strength requirements, and size. But it is significant that the Mosquito airplane, which is made almost entirely of wood, has a structure weight as low as that of the equivalent metal airplane.

One feature of the modern aircraft which has undoubtedly contributed to a more economical wing structure, in particular, is the great increase of wing loading and therefore of wing weight per unit area, which has made it possible to employ the material to much greater advantage—i.e., to have a smaller percentage of relatively lowly stressed material. This brings me to one of the outstanding contributions of research to aeronautics—namely, that derived from the investigation of the strength of actual structures in close association with theoretic analysis. It is by such work that it has been possible to increase greatly the useful load of practically all aircraft now in use. The most thorough mechanical testing of aircraft structures undoubtedly pays a high dividend. These tests have

not only shown us that our methods of design have led to general forms of structure well adapted to meet the demands on them, and fundamentally economical in character, but have enabled us to discover where our knowledge of the detailed distribution of stresses is inadequate and at the same time to improve that knowledge and to strengthen the structure against unforeseen local weaknesses.

The determination of the loads that the structure is called upon to bear is fundamentally a more difficult problem. We are greatly indebted to such methods as the V.G. recorder, but these give us only overall figures that, useful as they are, throw little light on the load distribution in flight. We have now available a method of great potency in the electrical resistance strain gauge. This is being used with great effect on a large scale in laboratory tests, and its application to measurements in flight is being rapidly developed. It will undoubtedly prove to be one of the greatest contributions of the research worker to improvement in the structures of aircraft.

Possibly the greatest achievement of the research worker in the field of aircraft structures is in discovering how to avoid the dangers of what we comprise in the term "flutter." In my view, there is in the whole of aircraft engineering no better example of the power of mathematical analysis, of ingenuity in experiment, and of skill in interpretation. The successful attainment of very high speeds, with a remarkably small number of serious failures, can only be ascribed to the most skilled use of all these resources, guided by systematic review of the results of their application. Direct experiment in flight—the only satisfactory check—is almost impracticable. Laboratory determination of reliable numerical values of the essential quantities involved is extremely difficult. Much more information on these is essential for progress, and here the designer can justifiably demand all that research can provide.

Stability and Control

Up to this point I have said nothing of the contribution of research to the production of stable and controllable aircraft. I am glad to say that the time is now long past when lack of stability is regarded by anyone as a virtue in an aircraft. In fact it is unquestionably a most serious defect, whatever the duty of the aircraft. But it has always been difficult to define the necessary or desirable margins of stability and the associated general stability and control characteristics. The designer must, however, have the requirements expressed in terms that can be reflected in his layout, both as a whole and in detail. He must be able to judge fairly accurately how the changes inevitable as a design develops will react on the stability and control, and he must have at his disposal means of dealing economically with the consequences both of the variation of load distribution resulting from operational conditions and of the changes involved in the development of the aircraft.

There is a good deal about the stability and control of aircraft in which there has been little apparent change over the period covered by the examples I have taken. I believe, however, that this is simply because the desirable general characteristics were attained by about 1918. Since then our main problems have been, first, to preserve them substantially unchanged in spite of the profound changes in the form of aircraft and, second, to enable the same man to control much larger and much faster aircraft.

The foundations of stability and control theory were laid, and well laid, long ago. Much labor has been spent on expanding it to embrace new developments, such as structural distortion, and on the analysis of the controlled and uncontrolled motion of aircraft. A vast amount of experimental evidence has been accumulated. Much of this, however, is related rather to specific problems than to the systematic development of an understanding of the matter. There is room here for a wholesale improvement, particularly by an attack on a wider front in flight. I am not among those who criticize our record here on the grounds that we did not undertake enough basic work at the time when the airplane, as we now know it, first crystallized. I regret that circumstances made it impossible to give this work high priority. Had we been able to do so, we might have avoided many troubles and saved much labor. But I do not believe that, on the balance, we would have reached our objective—usable aircraft—more quickly. We relied on our past experience, on our ability to improvise, and—most significant of all—on our conviction that the theory available was soundly founded on experimental evidence. We discovered, by the attacks we were forced to make on troubles as they arose, much more about stability and control than most of us believed there was to learn. Thus, and I believe only thus, could we have advanced at the rate we did. It is an excellent example of the interworking of research and application.

In the field of control balance we have made tremendous advances in the face of difficulties that are sometimes hardly appreciated. The 1917 bomber operated at speeds—80 to 100 m.p.h.—at which the pilot could provide the forces necessary for control with little or no aerodynamic balance. Take the 0/400 ailerons. The maximum hinge moment required was probably equivalent to a force on the pilot's hand of the order of 50 lbs., with ailerons on which the aerodynamic balance was probably no better than one-half. In the Lancaster the same movement of surfaces of about the same size is required at 300 m.p.h., requiring nine times the forces. The pilot is no stronger, so the aerodynamic balance must reduce the hinge moment to say one-

eighteenth of that of unbalanced ailerons. This is a difficult requirement but it has been met.

Suppose we put up the weight at the same wing loading to 100,000 lbs., one and one-half times that of the Lancaster. The linear dimensions will rise in the ratio $1.5^{1/2}$ and the hinge moment at the same speed in the ratio $1.5^{3/2}$. The aerodynamic balance must therefore reduce the hinge moment in the ratio

$$1/(2)(1.5)^{3/2}(3)^2 = 1/30$$

A similar argument leads to a figure of 1/400 if the weight is increased to 500,000 lbs. We can certainly achieve 1/30 and possibly 1/400 in ideal conditions. But it is doubtful whether this is a wise policy, since we can hardly expect to define or to maintain the shapes of surfaces sufficiently closely. Power-operated controls have been avoided so far, but it is unwise to assume that we can neglect them indefinitely. There seems to be no good reason to be doubtful of our ability to make them reliable.

Power Plant Developments

I do not propose to extend this survey to the two other main factors that have contributed to the changes we have seen in aircraft—the power plant and the propeller. I have already quoted some figures that show how remarkably the reciprocating engine has advanced. I have also said that there have since been further advances, which, however, serve rather to emphasize the comparisons I have made than to invalidate them. This is because there have been accompanying changes in weight and other characteristics that leave the main conclusions substantially unaffected. Our debt to the engineers who, aided by research, have achieved these results is immense.

To the constant-speed propeller the performance of aircraft must also acknowledge a great debt. But the flying man is even more grateful for what it has provided—almost complete freedom from his chief anxiety, namely, the liability to misuse his engine. We now look forward confidently to new methods of propulsion for aircraft. But I believe the propeller has a long and useful future before it and one in which research will play an outstanding part.

Summary—the Task of Research

I trust that this short survey has gone some way to show why I am convinced that the research worker and the engineer must work together if we are to make significant progress. In his James Forrest Lecture to the Institution of Civil Engineers in England, Dr. Southwell said that "Aeronautical Engineering is ordinary engineering made more difficult." If that was true in 1930, as I believe it was, it is more than ever true now. We can see clear prospects of great advances in aircraft in size, in performance, and in safety. The curve of improvement against time shows no real signs of flattening out. But we shall need all our ingenuity to avoid or to overcome the barriers which we can see ahead.

I think the engineer has made good use of the outstanding contributions of research for aeronautics. If at times he has appeared slow to appreciate the significance of new developments, he has a good excuse in his preoccupation with producing something on which we can rely. This is a sufficiently serious responsibility and one that he has borne with credit. But it is this very preoccupation that emphasizes the need for employing as part of an engineering organization men competent to detect those advances in knowledge which are potentially valuable and to work out the technique of applying them.

The research worker himself is not blameless in this respect. We can call to mind the case of Mendel, the significance of whose work in genetics was not recognized until he had been dead many years. His case is an example of discovery not appreciated because it is too far in advance of the general state of development of the science. Dr. Lanchester's books *Aerodonetics* and *Aerodynamics* contained much which may perhaps be regarded in the same way.

The instances I have mentioned may, of course, be garded as classic examples of the difficulty of disseminating knowledge. As the volume of knowledge increases, this difficulty grows. In the hall of Trinity College, Cambridge, there hangs the portrait of William Whewell, sometime Master. It is said that he was the last man to know all knowledge. He died in 1866.*

But the research worker has, in my view, a part to play in "putting across" the results of research. It is reasonable to ask that he should put his results in such a form that they can be used. To those who feel that this is hardly worthy of so much of their time and attention, as it certainly demands if it is to be well done, I would commend the example of one of the greatest workers in aeronautics, Hermann Glauert. Every one of his outstanding contributions to aerodynamics was finished in such a form that the method of its application was made clear. I am not aware that this in any way detracted from the value of his work on whatever basis it may be judged. And I know, from my long and intimate friendship with him, that he regarded it as the natural method, and indeed the only one that would satisfy his sense of craftmanship.

---

* Oxford may feel that their claim has been overlooked. It is preserved in the rhyme:

> My name is Benjamin Jowett
> Everything that's known, I know it.
> What I don't know isn't knowledge
> And I am Master of Balliol College.

Jowett died in 1893.

Problems of the Immediate Future

If this review leaves us confident of our powers to use effectively the results that an alliance between research and engineering ingenuity can provide, as I think it should, how should we shape our plans for the future? Let us look for a moment into what the future may hold for us in one field alone: still further improvement in performance—in speed and in range.

Within the limits of our present knowledge the most economical way to fly faster is to fly higher. Let us suppose that we can extend the range of operation of power plants so that propulsive power is independent of height. Taking an airplane with the characteristics of the Spitfire (Table 1), and assuming that $C_{D_0} = 0.022$ under all conditions, the curve of speed against height is shown in Fig. 7 labeled A. The line of sonic speed, Mach number = 1, is crossed at 65,000 ft. In practice the effect of the compressibility of air begins to be felt at about $M = 0.65$ at 33,000 ft. at a speed of about 430 m.p.h., and the rapid rise of C_{D_0} with M brings the curve for greater heights down to about the level of curve A_1. The loss of speed is very large.

If, by devising forms that will ensure some measure of laminar flow, we can halve C_{D_0} and at the same time avoid compressibility effects, we get curve B. But if compressibility has the same kind of effect as on the original airplane, the result will be to depress the speed to curve B_1. Similarly, reducing C_{D_0} to one-quarter of the original value, we get curves C and C_1.

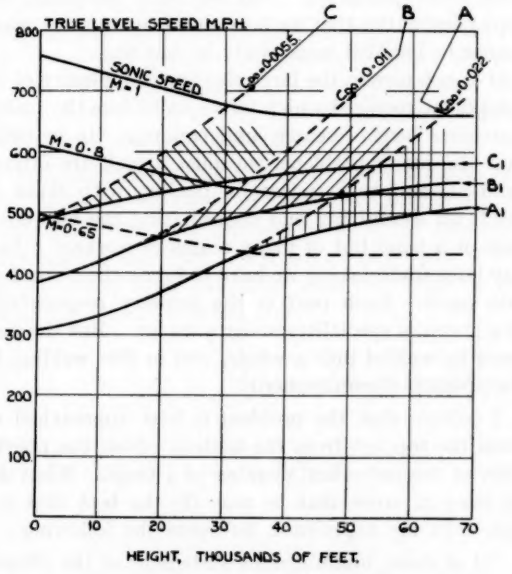

TRUE LEVEL SPEED VS HEIGHT.
SHOWING INFLUENCE OF REDUCTION OF C_{D_0} & OF COMPRESSIBILITY.
PROPULSIVE POWER 4·5 I.H.P./SQ.FT. WING SURFACE.
WING LOADING 28 LBS/SQ.FT.
ASPECT RATIO 5·6

FIG. 7.

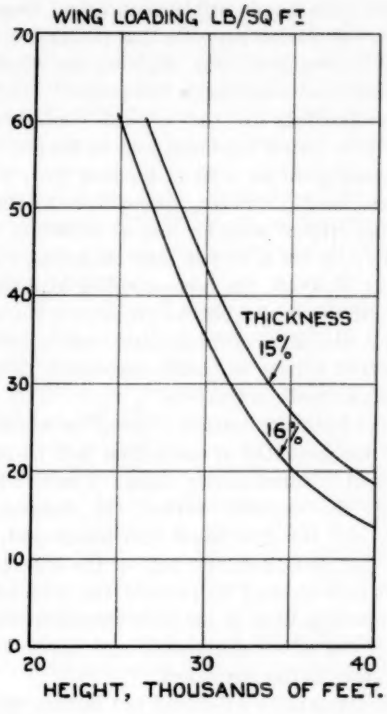

CRITICAL WING LOADING VS. HEIGHT.
TRUE LEVEL SPEED 450 M.P.H.
FLOW LAMINAR UP TO 60% OF CHORD.
AIRFOIL THICKNESS 15% & 16%

FIG. 8.

If we are to reach really high speeds economically, it is clear that we must devote at least as much effort to avoiding or reducing the effect of compressibility as to reducing the "low speed" value of C_{D_0}. On the other hand, at speeds at which it is likely to be economical to cruise for long distances, compressibility will for some time be relatively unimportant and laminar flow forms offer outstanding prospects. In round figures range and economical cruising speed are inversely proportional to the square root of C_{D_0}. If we can halve C_{D_0}, both range and cruising speed will rise by 40 per cent.

We must not dismiss too lightly the possibility of cruising economically, at great height, at very high speeds—speeds at which compressibility may well have a dominating influence on design. With a laminar flow extending over the majority of the surface of the airplane we may reasonably expect to be able to cruise at 450 m.p.h.—a Mach number of about 0.7. Considering the airfoil alone, because of necessary thickness and camber, sonic speed will occur at a point near the surface when the lift coefficient reaches a certain value. Hence, the wing loading must not exceed a figure dependent on the height. At the heights at which

it is likely that such speeds will be economical, from the power aspect, calculation suggests that rather low wing loadings will be required. Fig. 8 shows the results of some preliminary calculations on this point. The wing loading corresponding to the critical conditions is sensitive both to airfoil thickness and to height. For example, assuming 60 per cent of laminar flow, 15 per cent thickness, and a camber appropriate to the lift coefficient, the critical wing loading at 35,000 ft. is 28 lbs. per sq.ft.; or for a 16 per cent thickness, 20 lbs. per sq.ft. At 30,000 ft. the corresponding loadings are 44 and 35. If these calculations are sound, the effect on the general economics of the situation will be marked. Here is another reason to justify extensive theoretic and experimental work in this field.

Thus we see both the barriers to progress which now face us and the potential rewards that will be ours if we can succeed in surmounting them. I return to my main theme—the research worker, the designer, the constructor, and the user must join forces and, each fortified by the confidence and help of the others, plan the work that is needed to provide the information, pursue the investigations in the conviction that the aim is worthy of the effort demanded, and apply the results to produce better airplanes.

From aerodynamics we demand not merely the bare solution of the problem of forms providing laminar flow, relatively immune from effects of compressibility. We require specific information covering the whole airplane, including its propulsion, stability, and control. It may be that the whole layout of the aircraft will be different from that to which we have been accustomed. It is for the aerodynamic people to say, but they must base their opinions on a sound foundation of experiment.

From structural research we require to know what schemes of structural design are most likely to provide the necessary precision of form and superficial smoothness and how to cope with new strength and stiffness requirements. Aerodynamics must supply information on the loads that will be met in flight, and much thought must be given to the meteorologic conditions that will be encountered.

In the future it will be impossible to consider the airplane engine and the airplane as separate enterprises with conflicting requirements. The thermodynamic problems will be aerodynamic also. Their joint solution will throw up more than enough of the design problems at which the power-plant engineer excels.

Will the transformation of the energy of the fuel into thrust demand a propeller or a jet or a combination? There is no single answer. It will depend on the duty of the airplane. But the propeller designer will find that his task will tax all his ingenuity.

Upon the airplane designer will fall the burden of combining into a working proposition the contributions of all his collaborators. He will need to provide for pressurized cabins, ice-free surfaces, and the many indispensable aids to control, navigation, take-off, and landing.

To the user the prospects are such that he should spare no pains in encouraging the research worker and the engineer in their difficult tasks. He must support them to the full in obtaining the resources, in men and material, which will be essential for solving their problems. And he must contribute, as a member of the team, the operational information that will guide their efforts at all stages.

The experimental resources that such work demands are large. They must be generously planned to provide the greatest possible scope and flexibility. It will take time to devise and to create them, and during this time we shall inevitably meet further difficulties whose exact nature we cannot yet foresee. We may be confident in our ability to adapt and to improvise, but we must ensure that the basic equipment is on an adequate scale.

The Management of Research for Aeronautics

I have left until last such remarks as I have to make on an aspect of planning research for aeronautics to which you may feel I should have paid more attention—namely, the organization and management of the work on the scale that the scope and complexity of the problems demand. In what I said earlier I have emphasized my belief in the value of the independent small team of workers, who necessarily work on a small scale with relatively small equipment, and on one or at most a few problems. But we must recognize, perhaps reluctantly, that we have problems to solve which cannot be handled successfully in that way.

It is not merely the large size and complexity of the equipment required which forces us to face the task of managing large research undertakings. It is rather that the many problems we must attack are interdependent, and that success in dealing with them depends on assembling and coordinating the efforts not only of a team but of many teams of workers. As in any large undertaking we have to break the work down into parts. Each part is the primary responsibility of a group of specialists under a leader. But the parts must be welded into a whole, and in this welding lies the problem of management.

I believe that the problem is best approached not from the top but from the bottom—from the point of view of the individual member of a team. What does he need in order that he may do the best that is in him? In my experience, he needs the following:

(1) A clear, unambiguous statement of the ultimate objective. This must be more than a statement of the specific problem. It must relate it to the general picture of which it is a part. Thus he will know *why* the work is being done.

(2) An opportunity to give his own views on the value of the underlying ideas. The basic plan must

be, in part, his own. Thus he will start with a sound conviction that the plan is a good one.

(3) An immediate leader in whom he has confidence, who will inspire him, help him, and keep him up to date in all the relevant parallel work on related problems. Thus he will retain the good spirits in which he starts.

(4) Sufficient resources to enable his work to progress at what is, in his judgment, a speed commensurate with the importance of the objective. Thus he will feel that the value of his work is recognized in the only way that means anything to him.

This formula can, in my experience, be applied to groups of workers under a central management or to separate establishments under a central direction. And the difficulties that one meets in applying it arise not from its shortcomings but from conscious or unconscious neglect of its essentials.

Looked at in this way, such questions as the ideal size of research establishments cease to be of any great significance. Just as a team must have a leader who knows all about the work being done by its members, so a group of teams must have a leader who is recognized by them to know enough about their work for him to be able to guide it to its common objective. The limit of economical size of a complete unit is set not by some arbitrary formula but by the simple fact that no one man can know enough about work in more than a few fields to be able to inspire real confidence in his team leaders or their teams. The control of large equipment, the management of numbers of skilled industrials, and the commonplace daily problems of facilities are matters of consequence, but they are not the real determining factors. In any event they are well understood and can be broken down and shared among a properly balanced staff.

I would summarize my views on this question as follows. There is no single or simple formula by which to determine the best method of handling research. But I believe there are a few simple principles in the light of which each particular situation may be reviewed and a good solution found.

Conclusion

You will see that my experience has led me to the view that the record of science and engineering in aeronautics is a creditable one. It justifies us in demanding the means of extending our efforts into those new fields that we can now clearly see. The task of organizing and managing the work, of devising and constructing the equipment, and, above all, of leading those upon whose efforts success will in the end depend is one of absorbing interest.

What the world will make of our efforts is a matter on which I regard it as unprofitable to speculate, at any rate here and at this time. I am an engineer in a world where good engineering, skillfully used, means survival and bad engineering means the end of what I believe to be a good way of living. So I am content for the time being to confine my efforts to the work in hand and to leave philosophic speculations on its value, on some absolute scale which I confess eludes me, to those who can find time or inclination for it. For this reason I have confined my attention primarily to research for aeronautics as used in war. There is another reason—I have spent the best part of my life on work with this as its first aim in the conviction that it had to be done.

But I am an incurable optimist. I believe that we shall succeed in our present effort—in which the share of research is to provide information by which aircraft and their equipment can be steadily improved and used to greater effect. When we have achieved our immediate aim, I do not doubt that much of our work will be put to uses that are more to my taste and to yours.

In the end, however, it is with the scientific and technical advances in the means of flight that we are here concerned. So far we have had a mere 40 years in which to show what we can do. It has been my purpose to point, in the light of my experience, to what we must do now to discharge the responsibility that is laid on us so that those who will follow us may find a fair field in which to explore the endless vista of opportunity which will lie before them.

(*Discussion of the Lecture follows on pages 106–109*)

Discussion of the Lecture

Dr. Hugh L. Dryden, Chief of the Mechanics and Sound Division, National Bureau of Standards, acted as Chairman of the Lecture. At the conclusion of the Lecture Dr. Dryden read his prepared discussion and called for the other prepared comments on the subject.

Dr. Hugh L. Dryden, Chief of Mechanics and Sound Division, National Bureau of Standards: "It is widely recognized that aeronautical progress now is dependent mainly, as it was 40 years ago, on aeronautical research and that the gains realized will be proportionate to the time, effort, and skill expended in the orderly study of the numerous problems confronting the aeronautical designer. Anyone who studies the early history of the Wright Brothers will find that their ultimate success was the outcome of research on the aerodynamic, structural, and thermodynamic problems of powered flight. They devised new instruments of research, conducted extensive experimental programs, and successfully applied the results.

"Mr. Farren has ably presented a thumbnail sketch of the accomplishments of aeronautical research during the past 25 years and has outlined the problems of the immediate future and the change in character of the needed research equipment and organization that have arisen from the maturing of aeronautical development. The large size and complexity of the research equipment requires the planning of tests months in advance, the careful engineering design of the experimental setup itself, its construction by skilled workmen, extensive instrumentation, a comparatively short period of actual testing, and a longer period for analysis of the data. Months elapse between the conception of a new idea and its experimental test. Many of us look back with some longing to the days of the small wind tunnel and small group of workers when new ideas could be examined experimentally within a few days or even hours before the thrill and enthusiasm which accompanied the new idea faded. I agree with Mr. Farren that even today a place should be provided for the independent worker and small research group.

"Mr. Farren has stated the aim of research as twofold, (1) 'the discovery of how to make better aircraft' and (2) 'to produce a theory firmly supported by experimental evidence.' It is important to recognize the substantial identity of these aims. The discovery of how to make better aircraft depends upon obtaining a clear understanding of the fundamental characteristics of the flow of fluids under various circumstances, the elastic and plastic behavior of structure, and the transformation of energy in its various manifestations. In other words, the discovery of how to make better aircraft results from the discovery of rational 'theories firmly supported by experimental evidence.' Under present circumstances we are living principally on the accumulated fat of basic research and spending much of our effort in developmental research; that is, research to answer the specific foreseen needs of design. This emphasis is proper under present conditions, but with the return of peace it is hoped that the present large-scale facilities can be used to an increasing extent for the specific aim of producing theories firmly supported by experimental evidence as the surest method of producing better aircraft."

Dr. J. C. Hunsaker, Head of the Department of Mechanical Engineering and Aeronautical Engineering, M.I.T.; Chairman, N.A.C.A.: "The Institute of the Aeronautical Sciences has been most fortunate in its selection of the seventh Wright Brothers lecturer. I doubt if anyone else could have shown us, from experience as an actual participant, the course of British aeronautical research over the past 30 years. His advice as to the planning and management of research is firmly based on experience, and I am sure his hopeful forecast regarding possible rewards for future research will be accepted with satisfaction by workers in this country.

"I was especially interested in Mr. Farren's stipulation that fruitful research must have as an aim the creation of better airplanes and that this requires the collaboration of three interested parties: the researcher, the designer, and the user. It is not enough that the user wants improvement. He always does. His advice can stimulate research, however, only when he can express his need in terms that limit the problem. In turn, the designer and his industrial partner, the constructor, must further formulate the problem in terms that indicate possible points of attack for the research team.

"Many problems also work in reverse to involve the three parties. The research man may evolve a new wing section of improved drag characteristics. Unless he can show the builder how to apply the new section without too many uncertainties it will not be tried. Furthermore, unless the user wants the improvement enough to accept some interference with current production, adoption may be indefinitely postponed. The research has missed its aim unless supported by convincing experimental evidence, reported in a form to make its application clear, and evaluated so that the user can judge it.

"Mr. Farren brings out another matter of extreme importance to us all by distinguishing between the independent research team with rudimentary experimental facilities and organized research on a large scale. Mr. Farren has been on both sides of the fence which unfortunately separates the two kinds of workers. At

Cambridge University the three-man research team of Farren, Taylor, and Jones was extremely productive in adding to our fundamental knowledge of boundary layer mechanics, turbulence, profile drag, and other aerodynamic factors. Their basic work led to organized research on specific applications at the R.A.E. and elsewhere and eventually affected current designs such as the Spitfire, whose combat performance is so well appreciated by the Luftwaffe.

"The lesson for us is to encourage such independent research teams by modest financial support and by putting them in contact with the builder and the user.

"Organized aeronautical research by government is necessary but involves some risk. There is first the risk of neglecting the potentially fruitful efforts of independent persons and, second, the risk that an official research program may become sterile or take a wrong direction. A great industry should not be dependent for its fundamental technology on a single source of design information.

"Mr. Farren has shown that the first risk can be avoided by encouragement and support of the independent research teams. The second risk can be minimized if we follow Mr. Farren's advice and see to it that research programs are planned by the joint judgment of the researcher, the designer, and the user.

"I am happy to observe that the N.A.C.A. policy seems to comply with Mr. Farren's advice. The Committee now has outstanding 78 contracts for research reports by independent groups and is looking for further opportunities.

"The official Research Program of the Committee is based on recommendations of subcommittees composed of representatives of the three interested parties: researcher, designer, and user. Just now some 280 people are giving their time without compensation to 23 committees of experts in as many special areas of the general field of aeronautical research.

"I am greatly encouraged to learn from Mr. Farren that we are in agreement on the basic policies of managing research, and I hope that we shall be successful in achieving the progress in the art that research now indicates to be possible. The postwar future of aviation we cannot see clearly now, but I am sure it contains rich rewards for research. When so many likely spots to dig are already marked down in the research laboratories, surely some of them will yield treasure.

"Mr. Farren has shown us in his survey the remarkable advance made by the Wright Brothers' airplane in the past 25 years. He was somewhat cautious in not claiming more than half of this advance as due to research. The rest he attributes to ingenuity and design. But the research man also applies ingenuity and design to his investigations and experiments. In the final summation, perhaps all technical progress comes from ingenuity and design.

"But truly creative invention occurs only at rare intervals. Let me close with a note of humility by observing that the airplane was created by the Wright Brothers 40 years ago this morning, and, despite 40 years of the application of ingenuity and design, it is still fundamentally the Wright Brothers' airplane that we are planning to go on improving for the next 40 years."

Dr. Th. von Kármán, Director, Daniel Guggenheim Graduate School of Aeronautics, California Institute of Technology: "I am glad to discuss Mr. Farren's Wright Brothers Lecture, not only in view of the excellent content and form of the paper, but also because of the personality of the author. Mr. Farren mentioned the 'Cambridge Team' in connection with a flight test program that made practical use of basic research initiated at Cambridge University. As a matter of fact, the Cambridge group, of which he was one of the most useful members, had a great influence on the development of engineering science and research in England in a very broad sense. After the so-called World War No. 1, scientifically minded engineers of almost all countries felt that between the abstract aims of the mathematical sciences and the mere empiricism of engineering research there must be a place for a new kind of Applied Mechanics which would push forward the mathematical calculations until they actually approached the facts of experience and clear up the conditions and methods of experimental engineering research until the experiments allowed a clear theoretical interpretation. The first International Congress for Applied Mechanics gave the opportunity for a reunion of sympathetically minded research men of the mentioned type. English science and engineering was there prominently represented by a group of young engineering scientists from Cambridge. I always considered my close scientific and personal relations with their group over more than two decades a great honor and pleasure.

"On the other hand, I am somewhat embarrased to discuss Mr. Farren's article. It is a real pleasure to discuss a paper if you disagree with the author. After receiving the preprint of Mr. Farren's paper I tried very hard to find some points of which I did not approve; however, I had no success. Thus, I shall restrict myself to underlining a few of his statements from the point of view of a man who is, according to Mr. Farren's definition, by trade a worker in the field of theory but who at least likes to have associates with a flair for the associated exploration by experiment.

"First, I wish to endorse the statement of the author concerning the importance of independent workers in research. I recognize that our governmental planners and managers of research, civilian and military, are fully aware of the importance of basic research, and I gratefully acknowledge that both encouragement and practical support are given to basic research. However, I also feel, as does Mr. Farren, that research planned on a

large scale and using elaborate equipment does not make superfluous a kind of more individualistic research work. In fact, in many cases one starts out to solve a specific problem, and then half way to the goal one may encounter some intrinsic difficulty that puts out of reach the expected result just as the Fata Morgana disappears as one comes nearer. However, one finds new aspects of the problem, new aims that are even more attractive and important than those which were originally striven for. The handling of such changes in aim and direction is a rather difficult matter when one is working under research contracts with well-defined limited objectives. If Christopher Columbus contracted for the discovery of a western sea lane to India, in the eyes of the contract section of his government he was a complete failure. Nevertheless, he discovered America.

"I agree with Mr. Farren that governments should trust their scientific advisers with a reasonable, or I would rather say, a reasonably small fraction of their funds on a block-grant basis and ask no account except at longish intervals.

"Concerning the review of 25 years' progress in basic aircraft design, I believe Mr. Farren presented a fair distribution of the credit due to aerodynamicists, structural men, and engine people. However, it seems to me that in one point we have not been sufficiently progressive. We permitted the development of these three branches to proceed too far without close correlation. It is true that the engine people learned to appreciate aerodynamics, and, especially in the last few years, the engine companies are extremely anxious to secure the services of aerodynamicists. Nevertheless, the airframe builder is often faced with the problem of building-in ready-made power-plant units with more or less inflexible requirements in regard to space and arrangement. It seems to me that in the era of submerged engines, gas turbines, and jets this procedure will no longer be possible and that the airplane and its power plant will have to be considered more than ever before a single unit. We hope it will not always be the aerodynamicist who is forced to make compromises to the advantage of the other two branches.

"I found what Mr. Farren said about flutter research very interesting. I also have the feeling that flutter is one field in which, through lack of appropriate experimental methods, aircraft designers have surrendered unconditionally to the mathematician; and frankly, though a mathematical theorist by trade myself, I often wonder why the designer has such a boundless faith in flutter calculations, in view of the many crude approximations incorporated in the flutter theories. It seems to me that here a great field is still open to able and ingenious experimenters.

"Whereas in the field of flutter we are guided by the theorists, it appears to me that in the field of control and stability the opposite situation prevails. There is no doubt that the foundation of the theory of dynamic stability is sound, but somehow I have the feeling that the theory still does not analyze sufficiently the influence of the essential factors that cause the pilot to like one airplane and dislike another. Mr. Farren remarks that, after all, we can allow ourselves to be led by previous experience in determining what makes a usable aircraft. This is all right as long as the general layout of the airplane remains similar to previous satisfactory designs. However, if one starts to experiment with unorthodox types, the lack of correlation between theory and flight characteristics makes the job extremely difficult.

"I am sure that it was a great pleasure for all of us to listen to Mr. Farren's clear and inspiring lecture. In the rush caused by the duties of the day it is refreshing and valuable to consider certain problems in the light of history even if the history extends only as far back as the years in which the older men in this audience together with myself were young and I dare say naïve in their approach to the new art and science of aeronautics."

Dr. Edward P. Warner, Vice-Chairman, Civil Aeronautics Board: "This is another notable occasion in the history of the Institute of the Aeronautical Sciences. It has been the usual custom of those who have given the Wright Brothers Lecture to fix upon the existing state of the art or upon the discussion of recent progress in some particular compartment of aeronautical science. The lecturer today has taken a broader canvas. Not only has he ranged the whole area of aeronautical development; he has also provided a frame of reference for judging the future by reviewing the nature and the sources of the progress already made. The accomplishments of aeronautical research are most easily dramatized in terms of the intermittent spectacular discovery. Mr. Farren has appraised them by the more comprehensive and enduring standard of summary of their total achievement over a protracted period.

"He sets the Spitfire side by side with the S.E.5 for our inspection, and they appear to have come from different worlds; yet there is no single change, except the introduction of forced induction by a rotary impeller, to which more than 10 per cent of the difference in performance could be directly ascribed. No single step has been decisive, but the final product has been much more than the result of a series of disconnected efforts to operate separately upon each part and characteristic of the aircraft. Mr. Farren has dwelt with special emphasis upon the interdependence of the various facets of progress and upon the growing need, both in design and in planning aeronautical research, of dealing with the aircraft as an integrated whole. As the individual parts become progressively more refined and more complex, it becomes progressively more impracticable to treat them separately.

"To give properly specialized attention to each problem, and at the same time to make certain that all problems are viewed and studied in a proper relation-

ship to one another, calls for a large and skillfully devised organization. It is a defect of large organization that its very complexity can lull us into the illusion that its operation is automatic. Mr. Farren has warned us of that illusion, and he has dwelt to our advantage upon the vital importance both of the inventive and imaginative spark in the individual researchers and the qualities of their leaders. Aeronautical research is not conducted by wind tunnels but by men.

"Mr. Farren's own distinguished contributions in these fields are written large in the record of the progress of the last 25 years. In his present position, as personal embodiment of the personal leadership upon which so much of the success of a research organization depends, he has a large part in shaping the image of the future. The post that he now occupies, as the head of an establishment with more than 30 years of steadily accumulating achievement to its credit, is one of the world's best watchtowers from which to appraise the progress of aeronautical research and one of the world's best points from which to guide and control and accelerate that progress. It is a great privilege to have a share in expressing our appreciation of Mr. Farren's lecture and our appreciation also of the opportunity of welcoming the head of so famous an institution and so distinguished a representative of the great tradition of British aeronautical science."

Dr. George W. Lewis, Director of Aeronautical Research, National Advisory Committee for Aeronautics: "I should like to express the pleasure of aircraft people in general and research workers in particular that Mr. Farren has been able to come to this country to give us the benefit of his views on a subject with which he has been associated so intimately, for so long, and with such obvious success. His lecture has dealt with a difficult subject, and he has provided us with a thought-provoking discussion. Before remarking on some details of the Lecture, I should like to indicate the appreciation of research workers in this country for his clear presentation of the problems of planning and applying research for aeronautics.

"The appraisal of the relative importance of attaining laminar flow and avoiding compressibility difficulties is interesting and timely. Mr. Farren's statement that 'at speeds at which it is likely to be economical to cruise for long distances, compressibility will for some time be relatively unimportant, and laminar flow forms offer outstanding prospects,' together with Fig. 7, which indicates the dependence of performance on drag coefficient, emphasizes the need for continuous and vigorous research on the problem of drag reduction.

"Mr. Farren's statement that 'with a laminar flow extending over a majority of the surface of the airplane, we may reasonably expect to be able to cruise at 450 m.p.h.—a Mach number of about 0.7' is a most important observation and points again to the tremendous advances that are in sight through the application of laminar flow principles and carries an important implication of economic operating speeds of such a magnitude as to permit utilization of the jet propulsion principle.

"Mr. Farren, in touching upon the problems that lie before us in aerodynamic research, structures research, and power-plant research, has hinted at the interdependence of the work in aerodynamics and power plants. I feel that this observation is very well taken and that, as a matter of fact, the progress has been so rapid in what may be called the pure applications of either aerodynamics or power plants that those problems requiring the *joint* efforts of workers in these two fields have suffered comparative neglect. It may well be that our greatest progress in the immediate future will come through the effective combination of our knowledge, abilities, and techniques of individual fields in the solution of the important problems that lie between the two fields. Mr. Farren has mentioned aerodynamics and power plants; I should like to suggest that aerodynamics and structures have similar intimate relation in that each is an increasingly important controlling factor of the other: The type of airflow and aerodynamic characteristics depends upon the shapes defined in detail by the aircraft structure, and the structure required depends in turn both upon the aerodynamics of the body in general and details of the flow in particular.

"I consider that Mr. Farren's statement regarding the necessity of close cooperation between the research worker, the designer, and the constructor is most important. It is clear that unless the research worker has a knowledge and a sympathy with the practical problems to be met by the designer and constructor in applying new principles, the research worker cannot properly choose the variables and their range so as to provide the aircraft industry, for instance, with the information required. It is also clear that the rate at which new concepts are introduced into practice, and therefore our rate of technical progress, depends fundamentally on the confidence of the designer and constructor in the research results and their willingness to attempt to make the gains that are indicated through research."

Methods of Analysis for Torsion with Variable Twist

TH. VON KÁRMÁN* AND N. B. CHRISTENSEN†

Northrop Aircraft, Inc.

Abstract

The object of this paper is to give a simple method for the analysis of thin-walled sections (open, closed, or combination of open and closed sections) that have variable twist when loaded in torsion. The method is applied to the problem of torsion with axial constraint. The application to torsion of sections with variable torsional rigidity (for example, tapered structures or structures with large communication cutouts in the skin) will be treated in a later paper.

Notations

A = area swept by the radius vector drawn from the center of rotation O of the beam to an arbitrary point on the centerline of the wall
C = equivalent polar moment of inertia
C' = warping strength of a section
E = Young's modulus of elasticity
F = concentrated force acting on an imaginary beam
G = shear modulus
K = curvature of a longitudinal strip in the plane of the strip
M = concentrated moment acting on an imaginary beam
O = center of rotation or shear center of a section
S = total length of periphery
T = twisting moment or torque carried by primary shear
T' = twisting moment or torque carried by secondary shear
$\bar{T}$ = $T + T'$, total twisting moment applied to a beam
a = cross-sectional area of the wall of a section
p = fictitious load acting on an imaginary beam
q = $t\tau$, primary shear flow, i.e., shear flow with no axial restraint
q' = $t\tau'$, secondary shear flow, i.e., shear flow produced by axial restraint
r = the normal distance from a wall element centerline to the center of rotation, or shear center
s = length of arc measured along the wall centerline
t = wall thickness
l = running twisting moment or running torque
w = axial displacement of an arbitrary point of the wall centerline
x = coordinate parallel to the longitudinal axis of the structure
γ = τ/G shear strain
ϵ_x = axial strain produced by restraint
σ_x = axial stress produced by restraint
τ = primary shear stress produced with no axial restraint
τ' = secondary shear stress produced by axial restraint
ϕ = angle of twist
θ = $d\phi/dx$ rate of twist

Received September 23, 1943.

* Consultant on Aerodynamics and Structural Engineering. Also Director, Daniel Guggenheim School of Aeronautics, California Institute of Technology.

† Stress Engineer.

Introduction

The theory of torsion of cylindric beams with arbitrary cross sections, first developed by St. Venant, assumes the absence of longitudinal stresses; in other words, the warping of the cross section is not restrained and the distortion of every cross section is the same. The exact solution of the torsion problem for given end conditions is extremely complex and laborious. However, for thin-walled sections an approximate theory can be obtained by a procedure first used by Timoshenko[1] for structures with straight walls and generalized by Wagner[4] in the treatment of the problem of buckling of torsionally weak sections. This theory was further applied to several cases of the general buckling problem by Kappus[5] and, more recently, by Goodier.[6, 7] Timoshenko's theory of straight-walled sections was extended by several authors. A list of papers is given by Timoshenko[2] and A. Ostenfeld.[3] The nature of the approximation used by these authors, and also adapted in this paper, is discussed in the section on "The Shear Flow Produced by Variable Twist."

The shear flow resulting from an applied torque consists of two parts: the primary shear flow produced by pure twist without axial restraint and the secondary shear flow produced by axial stresses due to "bending" in the plane of the thin-walled elements.

The method of calculating the first component is generally known and is discussed in this paper merely for the sake of completeness. For the calculation of the second component a simple graphic method is developed. This method makes use of an analogy found between the secondary shear stresses in a thin-walled section and the bending moments existing in a fictitiously loaded beam.

The Shear Flow Produced by Pure Twist

Open Section

In the case of pure twist the average shear flow in the direction of the thin-walled elements of an open section is zero. The torsional rigidity of the section is practically the same as that of a flat plate with the same distribution of thickness t over the length S.

Consider a longitudinal strip of unit width. In the twisted state the axis of such a strip is a helicoidal line, the angle of inclination between the axis of the strip and the x axis being equal to $r\theta$ (Fig. 1). Since the resultant shear stress in the cross section $t\,ds$ is zero, this

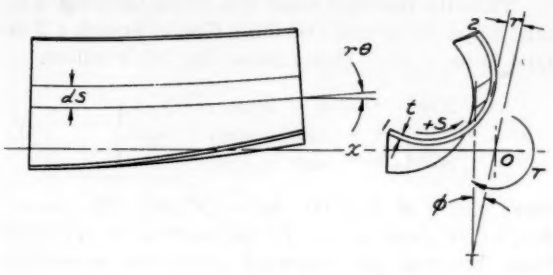

FIG. 1.

helicoidal line remains normal to the element $t\,ds$, i.e., the cross section is rotated by the same angle $r\theta$. Therefore the inclination of a cross-sectional element $t\,ds$ relative to a plane normal to the axis of the twisted beam is equal to

$$dw/ds = -r\theta \tag{1}$$

The difference between w_1 and w_2 (1 and 2 being the two end points of the open section) is, therefore,

$$w_2 - w_1 = -\theta \int_2^1 r\,ds \tag{2}$$

$$w_2 - w_1 = -2\theta A \tag{3}$$

where A is the area swept by the radius vector drawn from the center of rotation to an arbitrary point of the cross section (shaded area in Fig. 2; the diagram on the right side illustrates the distribution of w).

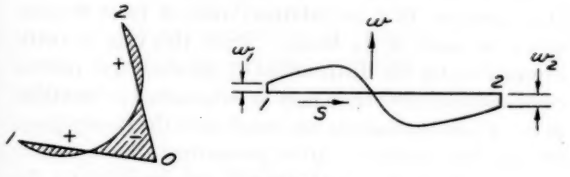

FIG. 2.

Closed Section

In the case of a closed section there is a constant shear flow, because of twist only, through every element of the wall. This constant shear flow is equal to

$$q = t\tau = T/2A \tag{4}$$

Since the points 1 and 2 coincide (see Figs. 3 and 4), A, in this case, is the area enclosed by the centerline of the wall and T is the applied torque. The shear strain corresponding to the shear stress τ is equal to $\gamma = T/G$. Hence, again considering a longitudinal strip of unit width, it is seen that the angle between the helicoidal line with the inclination $r\theta$ and the plane of the section is equal to $[90° - (\tau/G)]$. Therefore, from Fig. 5

$$dw/ds = -[r\theta - (\tau/G)] \tag{5}$$

Since $w_2 - w_1 = 0$,

$$-2\theta A + \oint (\tau/G)\,ds = -2\theta A + \oint (q/Gt)\,ds \tag{6}$$

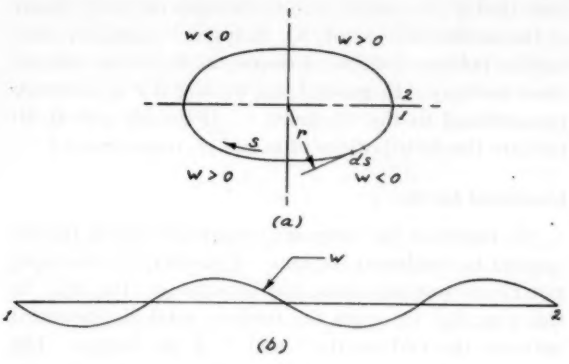

FIG. 3.

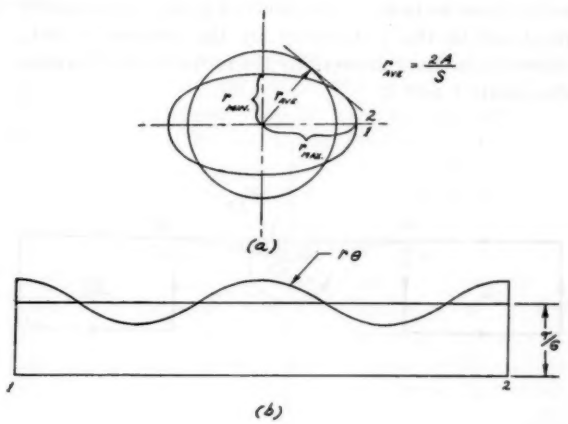

FIG. 4.

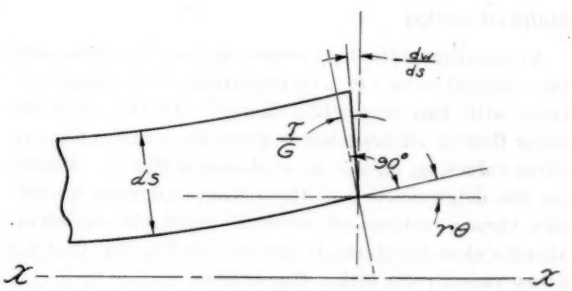

FIG. 5.

or because $q = t\tau = \text{const.}$, $\oint \tau\,ds = t\tau \oint ds/t = 2G\theta A$ and

$$\tau/G = 2A\theta/(t \oint ds/t) \tag{7}$$

Substituting this value in Eq. (5)

$$dw/ds = -\theta[r - (2A/t \oint ds/t)] \tag{8}$$

It is seen that if $t = \text{const.}$

$$dw/ds = -\theta[r - (2A/S)] \tag{9}$$

where S is the circumference and $2A/S$ is the mean value of r. In fact, $(1/S)\oint r\,ds = 2A/S$ (Fig. 4). It is also

seen that if t = const., dw/ds vanishes for every point of the section if $r = 2A/S$. A typical example is any regular polygon (which, of course, includes the circular cross section). In general, $dw/ds = \theta$ if r is inversely proportional to the thickness t. (Figs. 3b and 4b illustrate the distributions of w and $r\theta$, respectively.)

Combined Section

The results of the foregoing paragraphs can be readily applied to combined sections. Consider, for example, two closed sections connected by a flange (Fig. 6). In this case Eq. (3) gives the relative axial displacement between the end points 1 and 2 of the flange. The warping of the closed sections can be computed as before. (r is measured from the shear center O of the entire cross section.) The points 1 and 2 are relatively displaced in the x direction by the amount $-2\theta A_{12}$ where A_{12} is the area swept by the radius vector between the points 1 and 2.

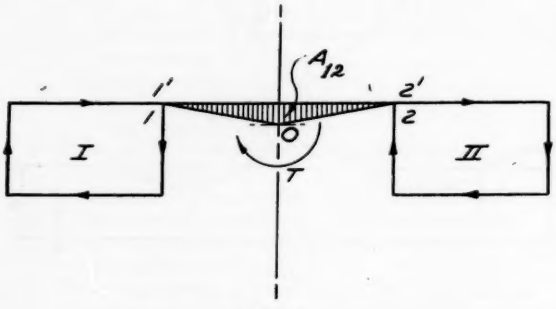

FIG. 6.

Multicell Section

As another example, consider a closed section with two internal webs, i.e., a combination of two closed sections with two connecting flanges. In this case the shear flow in all branches is given by combinations of three values, q_1, q_2, and q_3, as shown in Fig. 7. Hence, for the determination of these three unknown quantities, three equations are needed. From the consideration for closed sections, it follows (cf. Eq. (6)) that for every closed path within the section:

$$-2G\theta A + \oint (q/t)\, ds = 0 \qquad (10)$$

Eq. (10), applied to the three closed paths (I), (II), (III), yields three equations which determine the three shear flows.

The shear flow is built up by superposition of the three closed circuits of the intensity q_1, q_2, and q_3 (Fig. 7). Then the resultant shear flow in the branch DA is equal to $(q_2 - q_1)$ and the shear flow in branch CB is equal to $(q_3 - q_2)$. Hence, from Eq. (10) it follows

$$\left.\begin{aligned} 2G\theta A_1 &= \alpha_{11}q_1 - \alpha_{12}q_2 \\ 2G\theta A_2 &= -\alpha_{12}q_1 + \alpha_{22}q_2 - \alpha_{23}q_3 \\ 2G\theta A_3 &= -\alpha_{23}q_2 + \alpha_{33}q_3 \end{aligned}\right\} \qquad (11)$$

where $\alpha_{11} = \oint ds/t$ (I), $\alpha_{22} = \oint ds/t$ (II), $\alpha_{33} = \oint ds/t$ (III), and $\alpha_{12} = \int_A^D ds/t$ and $\alpha_{23} = \int_B^C ds/t$. These integrals are extended along the respective boundaries of the three closed sections and along the two respective intermediate webs. The solution of the three simultaneous linear equations gives the values of q_1, q_2, and q_3 for a given value of θ. If this calculation is carried out, q_1, q_2, and q_3 can be written in the form

$$\left.\begin{aligned} q_1 &= 2G\theta(\bar{A}_1/\alpha_{11}) \\ q_2 &= 2G\theta(\bar{A}_2/\alpha_{22}) \\ q_3 &= 2G\theta(\bar{A}_3/\alpha_{33}) \end{aligned}\right\} \qquad (12)$$

where $\bar{A}_1$, $\bar{A}_2$, and $\bar{A}_3$ appear as linear combinations of A_1, A_2, and A_3 multiplied by certain numerical factors. For example,

$$\bar{A}_1 = (\alpha_{11}/\Delta)\,[(\alpha_{22}\alpha_{33} - \alpha_{23}^2)A_1 + \alpha_{12}\alpha_{33}A_2 + \alpha_{12}\alpha_{23}A_3]$$

where $\Delta = \alpha_{11}\alpha_{22}\alpha_{33} - \alpha_{23}^2\alpha_{11} - \alpha_{12}^2\alpha_{33}$.

THE SHEAR FLOW PRODUCED BY VARIABLE TWIST (SECONDARY SHEAR FLOW)

The fundamental idea of this theory is as follows: It is assumed that an arbitrary rate of twist θ exists along the span of the beam. From this rate of twist, expressions for the distribution of the shear and normal components of the strain may be determined as functions of θ. These expressions are based upon the theory given in the first section. After computing the resulting strains, values of normal stresses are obtained by the use of the fundamental relationship between stress and strain. If the normal stresses are known, the condition of equilibrium in the axial direction gives the magnitude of the additional or secondary shear stresses. It is evident that such shear stresses involve a change in the shear strain distribution obtained before. This change is neglected in this theory; however, it is possible to take it into account and obtain a second approximation if desired.

Now, if the rate of twist is constant, the curvature (measured in a plane tangential to the median surface) of an initially straight line parallel to the beam axis remains zero; in other words, no bending occurs in this plane. In order to compute the axial strain caused by a variable rate of twist, the deformation of a longitudinal strip must be considered. If the twist is variable, such a strip is bent in its own plane and it is readily seen that its curvature is equal to $K = -r(d\theta/dx)$.

In the case of an open section where the primary shear strain $\gamma = (\tau/G)$ vanishes, the axial strain is

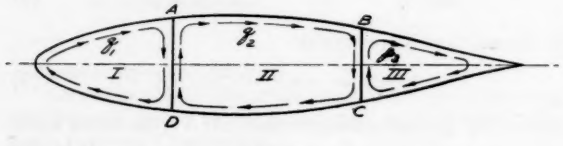

FIG. 7.

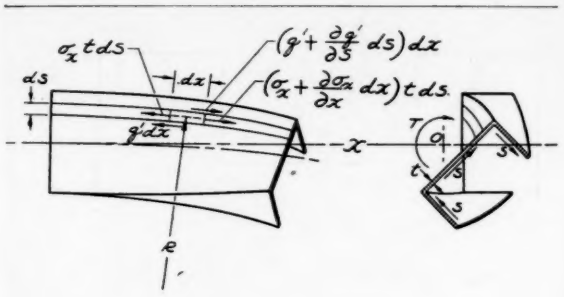

FIG. 8.

determined by curvature alone. If a strip of the width ds (Fig. 8) is considered bent in its own plane, an element of this strip, whose length is originally equal to unity, is deformed upon loading so that the length of one longitudinal edge is equal to $[1 + \epsilon_z + (\partial\epsilon_z/\partial s) \times (ds/2)]$ and the length of the other longitudinal edge is equal to $[1 + \epsilon_z - (\partial\epsilon_z/\partial s)(ds/2)]$. The difference of these lengths divided by ds is equal to $1/R$ or K where R is the radius of curvature of the strip considered. Hence, $\partial\epsilon_z/\partial s = -r(d\theta/dx)$.

In the case of a closed section, the axial strain also depends on the shear strain produced by the twist. The axial strain is defined by the derivative of the axial displacement w with respect to x, i.e., $\epsilon_z = \partial w/\partial x$ by differentiating the expression

$$\partial\epsilon_z/\partial s = \partial^2 w/\partial s\partial x = (\partial/\partial x)(\partial w/\partial s) \qquad (13)$$

It is noted that $\partial w/\partial s$ is the inclination between an arbitrary warped cross-sectional element and a plane normal to the beam axis and, according to Eq. (5), is equal to:

$$-\partial w/\partial s = [r\theta - (\tau/G)] = \theta\{r - [2A/(t\oint ds/t)]\} \qquad (14)$$

The first term in the bracket expresses the contribution of the pure bending; the second term expresses that of the primary shear. Substituting Eq. (14) in Eq. (13), the following formula is derived and found valid for open and closed sections:

$$\partial\epsilon_z/\partial s = -(d\theta/dx)\{r - [2A/(t\oint ds/t)]\} \qquad (15)$$

In order to apply this formula for multicell sections, the actual enclosed areas $A_1, A_2 \ldots$ are to be replaced by $\bar{A}_1, \bar{A}_2 \ldots$ (cf. Eq. (12)); also for the intermediate webs, the contributions to τ computed from the two adjoining closed circuits are to be added.

Introducing the axial stress σ_z by the relation $\epsilon_z = \sigma_z/E$ into Eq. (15), the following is obtained:

$$\partial\sigma_z/\partial s = -E(d\theta/dx)\{r - [2A/(t\oint ds/t)]\} \qquad (16)$$

Consider now the equilibrium of an element of the wall as illustrated by Fig. 8.

The equilibrium condition in the longitudinal direction requires that

$$(\partial\sigma_z/\partial x) + (\partial q'/t\partial s) = 0 \qquad (17)$$

where q' is the secondary shear flow. A differential equation for q' is obtained by taking the partial derivative of Eq. (16) with respect to x and the partial derivative of Eq. (17) with respect to s and then combining the results so that

$$\frac{\partial}{\partial s}\left(\frac{\partial q'}{t\partial s}\right) = E\,\frac{d^2\theta}{dx^2}\left(r - \frac{2A}{t\oint ds/t}\right) \qquad (18)$$

It is convenient to use the increment $da = t\,ds$ instead of ds, where the variable a denotes the integrated area of the wall cross section measured between two arbitrary points along the wall centerline. Then Eq. (18), with $d^2\theta/dx^2 = \ddot{\theta}$, becomes

$$\frac{\partial^2 q'}{\partial a^2}\frac{1}{E\ddot{\theta}} = \left(\frac{r}{t} - \frac{2A}{t^2\oint ds/t}\right) \qquad (19)$$

Eq. (19) suggests a simple graphic or numerical method for the determination of the secondary shear flow q'. It is known that the load per unit length p acting on a straight beam is equal to the second derivative of the bending moment M. Hence, an imaginary beam may be introduced by developing the wall centerline in a straight line and expanding the elements ds proportional to the thickness. In other words, the longitudinal coordinate of this beam is given by a. Then, if a fictitious load distribution given by the right side of Eq. (19) is applied to the beam, the moment distribution will represent the quantity $q'/E\ddot{\theta}$, i.e., a quantity directly proportional to the secondary shear flow q'.

The application of this idea is demonstrated for various cases in the following paragraphs:

EXAMPLE SOLUTIONS OF q' AS A FUNCTION OF θ

Open Symmetric Channel Section

Since for an open section the enclosed area A does not exist, Eq. (19) reduces to

$$(\partial^2 q'/\partial a^2)(1/E\ddot{\theta}) = r/t$$

It is noted that, if q' is considered positive in the direction of integration from 1 to 2, positive q' in the flanges produces clockwise torque about O and positive q' in the web tends to rotate the section in a counterclockwise direction. Therefore r is negative for the elements in the web. This conclusion leads to the convention that if positive shear in the element tends to rotate clockwise about the center of rotation, r is positive, and, if it tends to rotate it counterclockwise, r is negative.

Fig. 9b is the load diagram of the imaginary beam; the length of the beam is proportional to the cross-sectional area of the wall. Since the channel is symmetric, r/t for the flanges equals $h/2t$ and for the web r/t equals $-(e/t)$. The sign is determined in accordance with the preceding paragraph.

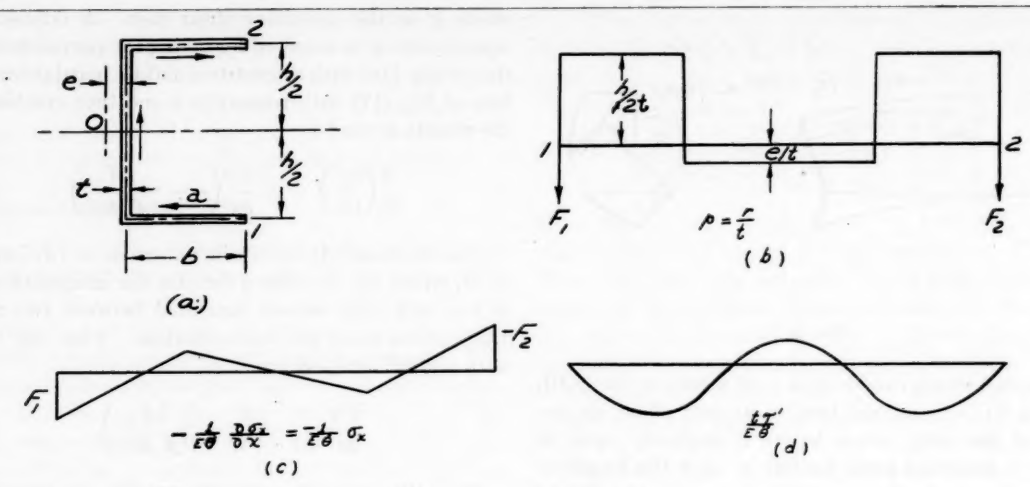

FIGS. 9a, 9b, 9c, and 9d.

From the fictitious load distribution, the fictitious shear and moment diagrams are readily determined. It is to be noticed that the shear diagram gives the distribution of $-(1/E\ddot{\theta})(\partial\sigma_z/\partial x)$. This follows from Eq. (17), which can be written in the form

$$-(\partial\sigma_z/\partial x) = \partial q'/\partial a$$

Substituting $q'/E\ddot{\theta} = M_a$ (where M_a is the ordinate of the moment diagram) it is seen that $-(\partial\sigma_z/\partial_z)(1/E\ddot{\theta}) = \partial M_a/\partial a$. Since the derivative $\partial M_a/\partial a$ of the fictitious moment is the fictitious shear force on the imaginary beam, $-(\partial\sigma_z/\partial x)(1/E\ddot{\theta})$ is given by the fictitious shear force. For example, the value of $-(\partial\sigma_z/\partial x)(1/E\ddot{\theta})$ at the end point is numerically equal to the reaction force F_1 acting at this end point of the imaginary beam.

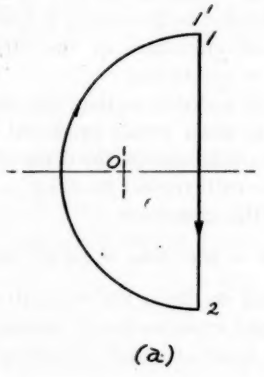

FIG. 10a.

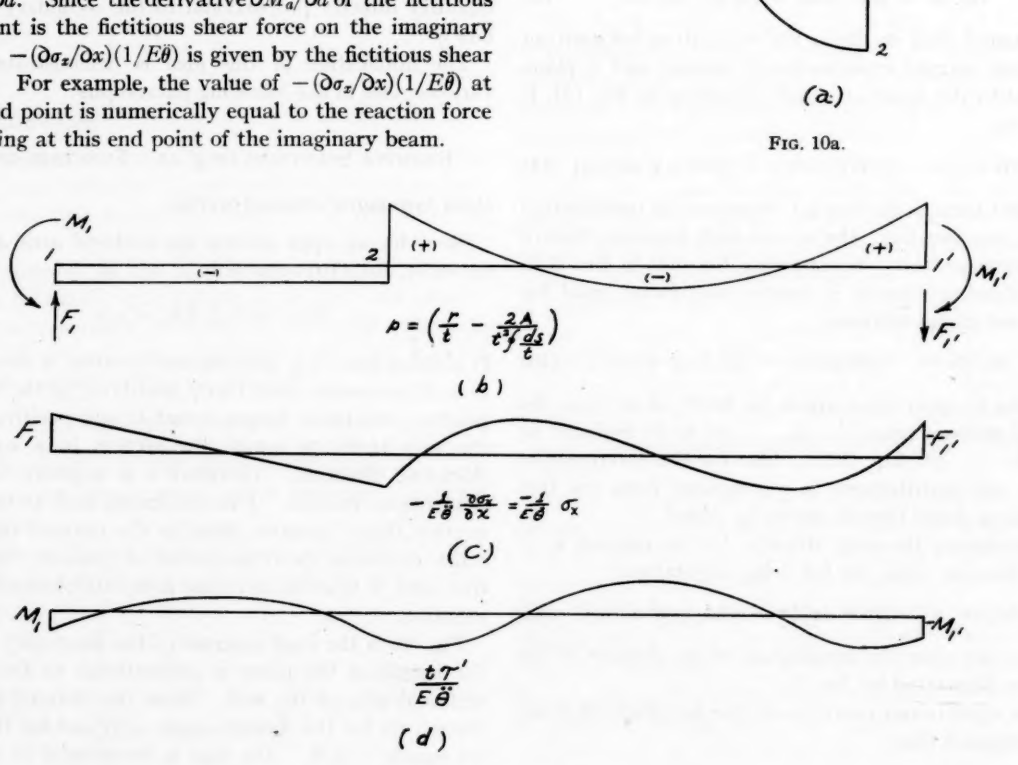

FIGS. 10b, 10c, and 10d.

Since $\partial\sigma_z/\partial x$ has the form $E\ddot{\theta}f(a)$,* σ_z is equal to $E(d\theta/dx) = E\dot{\theta}$ multiplied by the same function of a. Consequently, $(d\sigma_z/dx)(1/E\ddot{\theta}) = \sigma_z/E\dot{\theta}$. In other words, the *shear diagram* of the *imaginary beam* can be used for direct determination of σ_z. The diagrams for $-(\partial\sigma_z/\partial x)(1/E\ddot{\theta})$ and $-(\sigma_z/E\dot{\theta})$ differ in the scale of their ordinates only. The stress σ_z at any point of the wall becomes

$$\sigma_z = -E\dot{\theta}[F_1 + \int_0^a (r/t)\, da] \tag{20}$$

By integrating again, the desired expression of q' is obtained. The ordinate for this curve (Fig. 9d) is now

$$q'/E\ddot{\theta} = 1/E\dot{\theta} \int \sigma_z\, da = \int [F_1 + \int_0^a (r/t)\, da]\, da$$

Since q' is zero at the points 1 and 2, q' may now be expressed as follows:

$$q' = E\ddot{\theta} \int_0^a [F_1 + \int_0^a (r/t)\, da]\, da \tag{21}$$

Closed Section

Fig. 10 is a line diagram of a D section. The method of solution is much the same as that used for the open sections. The wall is assumed to be cut at $1 - 1'$ and then developed into a straight line or an imaginary beam (Fig. 10b).

The load on the beam is in accordance with the right-hand side of Eq. (19). The end moments M_1 and M_1' are readily seen to represent q' and $-q'$ at the points 1 and 1'. Since points 1 and 1' coincide, q' must be the same for both points; consequently, $M_1 + M_1' = 0$. By the same reasoning, the shear forces, which are proportional to σ_z, at 1 and 1' must also be equal. If F_1 and F_1' are the reaction forces at the two ends of the beam $F_1 + F_1' = 0$. The magnitude of F_1 and F_1' is determined in the same manner as that for the open section.

The integral of the load curve is illustrated by Fig. 10c and its significance is the same as that discussed for the open channel. By integrating the shear curve a moment curve is obtained that results in a zero value at 1 and 1', and its ordinates may be expressed as

$$\int_1^a \{F_1 + \int_1^a [(r/t) - (2A/t^2 \oint ds/t)]\, da\}\, da$$

This curve must be corrected by addition of an amount M_1 so as to satisfy the condition

$$\int_1^{1'} q'\, ds/t = \int_1^{1'} q'\, da/t^2 = 0$$

It is readily seen that the condition is satisfied if

$$\int_1^{1'} \frac{da}{t^2} \int^a \left[F_1 + \int_1^a \left(\frac{r}{t} - \frac{2A}{t^2 \oint ds/t}\right) da\right] da + M_1 \int_1^{1'} \frac{da}{t^2} = 0$$

from which

$$M_1 = -\int_1^a \frac{da}{t^2} \left\{ \frac{\int_1^a \left[F_1 + \int_1^a \left(\frac{r}{t} - \frac{2A}{t^2 \oint ds/t}\right) da\right] da}{\oint da/t^2} \right\}$$

The expression for q' may now be written as

$$q' = E\ddot{\theta}\left\{\int_1^a \left[F_1 + \int_1^a \left(\frac{r}{t} - \frac{2A}{t^2 \oint ds/t}\right) da\right] da + M_1\right\} \tag{22}$$

Combined Section

The procedure for a combined section is in accordance with the fundamentals illustrated for the open and closed sections treated individually.

The combined section may be developed in either of two ways—i.e., the closed section may be divorced from the overhanging portion of the beam and the two parts solved independently (remembering that r is measured from a common point) or the section may be treated as a unit. If the two sections are treated independently, additional reactions are required at the point 2. It is evident that the reaction force for the closed section at point 2 is equal, but opposite in direction, to the reaction force for the overhanging portion. Therefore, by connecting the two sections these forces are eliminated. Figs. 11b, 11c, and 11d illustrate the case of a combined section.

Multicell Section

Fig. 12a represents a symmetric multicell section that has a constant wall thickness t. The solution, which is regarded by the authors to lead to less difficulty, is one that treats each cell separately.

The values of $\bar{A}_1$, $\bar{A}_2$, and $\bar{A}_3$, introduced in the section on "The Shear Flow Produced by Pure Twist," are found to be as follows:

$$\bar{A}_1 = \alpha_{11}/\Delta[(\alpha_{22}\alpha_{33} - \alpha_{23}^2)A_1 + \alpha_{12}\alpha_{33}A_2 + \alpha_{12}\alpha_{23}A_3]$$

where $\Delta = \alpha_{11}\alpha_{22}\alpha_{33} - \alpha_{23}^2\alpha_{11} - \alpha_{12}^2\alpha_{33}$. $\bar{A}_2$ and $\bar{A}_3$ are found to be

$$\bar{A}_2 = (\alpha_{22}/\Delta)(\alpha_{12}\alpha_{33}A_1 + \alpha_{11}\alpha_{33}A_2 + \alpha_{11}\alpha_{23}A_3)$$
$$\bar{A}_3 = (\alpha_{33}/\Delta)[\alpha_{12}\alpha_{32}A_1 + \alpha_{11}\alpha_{32}A_2 + (\alpha_{11}\alpha_{22} - \alpha_{12}^2)A_3]$$

By treating each cell separately, three imaginary beams are used. The imaginary beam for cell I is represented by the line A,B,1,2,A (Fig. 12b-I); for cell II, the line A,C,D,B,A (Fig. 12b-II); for cell III, the line C,3,4,D,C (Fig. 12b-III).

The load p, as represented by the right side of Eq. (19), must be adjusted so as to be consistent with the

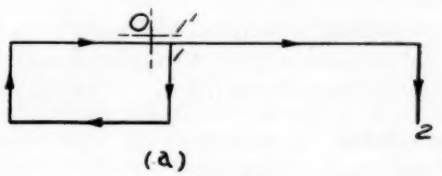

FIG. 11a.

* It is seen that the function f(a) depends on the shape and dimensions of the section only. It is identical to the "unit warping" used by the authors quoted in the introduction.

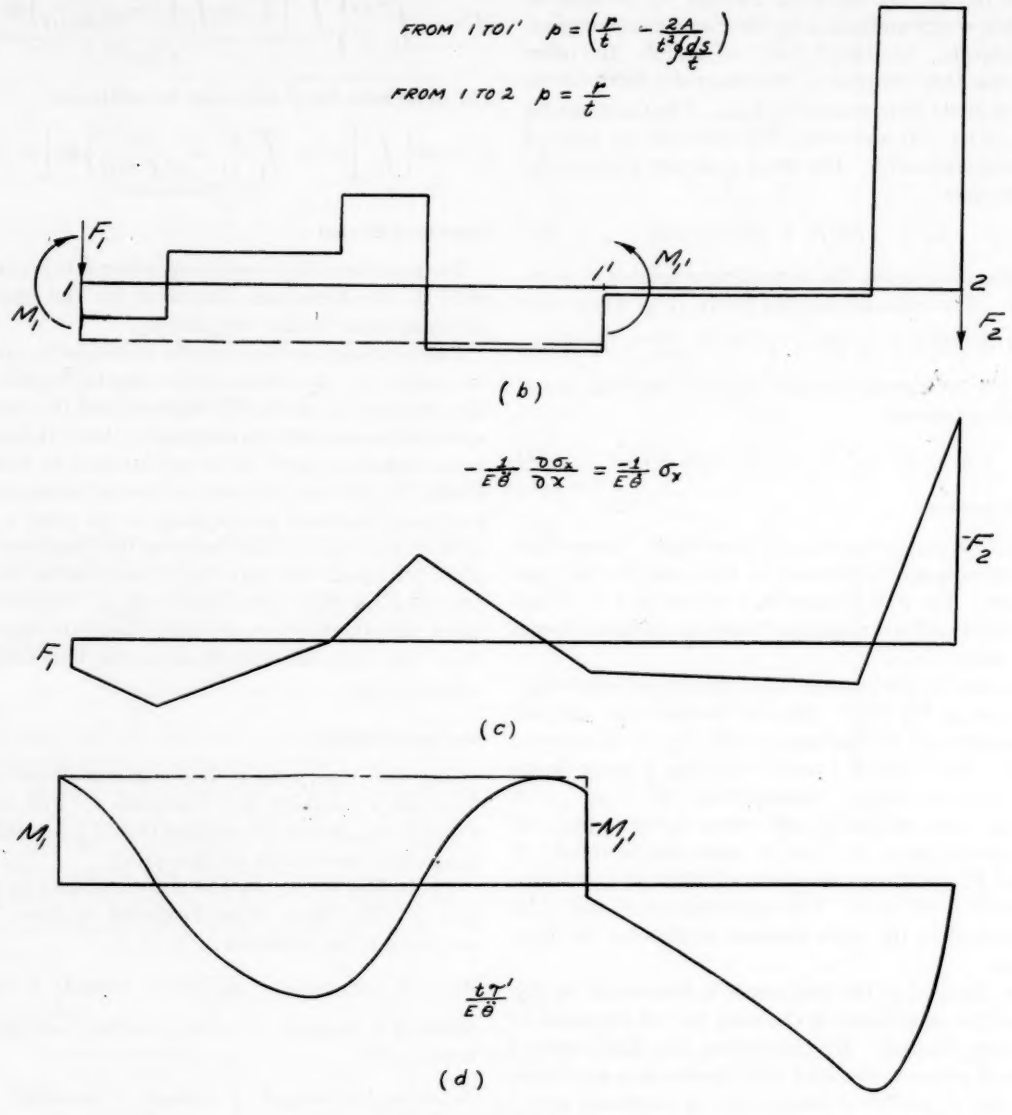

FIGS. 11b, 11c, and 11d.

theory developed for the multicell section. It is expressed as follows:

For cell I,

$$p]_A^B = (r/t) - (2/t^2)[(\bar{A}_1/\alpha_{11}) - (\bar{A}_2/\alpha_{22})]$$
$$p]_B^A = (r/t) - (2A_1/t^2\alpha_{11})$$

For cell II,

$$p]_A^C \text{ and } p]_D^B = (r/t) - (2\bar{A}_2/t^2\alpha_{22})$$
$$p]_C^D = (r/t) - (2/t^2)[(\bar{A}_2/\alpha_{22}) - (\bar{A}_3/\alpha_{33})]$$
$$p]_B^A = (r/t) - (2/t^2)[(\bar{A}_2/\alpha_{22}) - (\bar{A}_1/\alpha_{33})]$$

and for cell III,

$$p]_C^D = (r/t) - (2\bar{A}_3/t^2\alpha_{33})$$
$$p]_D^C = (r/t) - (2/t^2)[(\bar{A}_3/\alpha_{22}) - (\bar{A}_2/\alpha_{32})]$$

The ordinates in Figs. 12b-II, and 12b-III represent the values of p for the respective cells. The force reactions are determined in the same manner as for the previous examples.

Again, by integrating the load curves, the shear

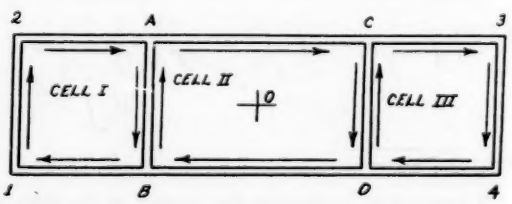

(a)

FIG. 12a.

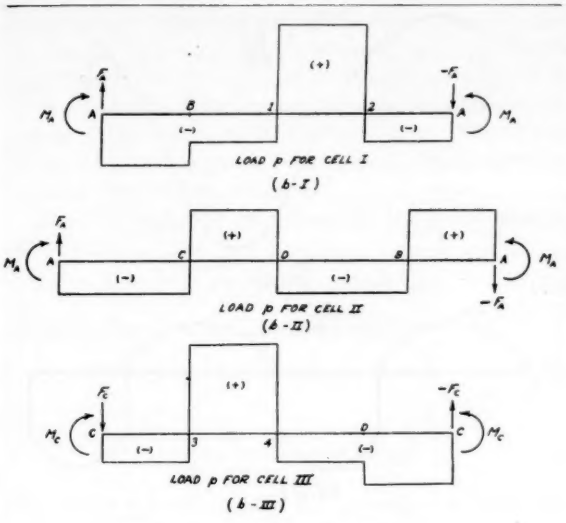

FIGS. 12b-I, 12b-II, and 12b-III.

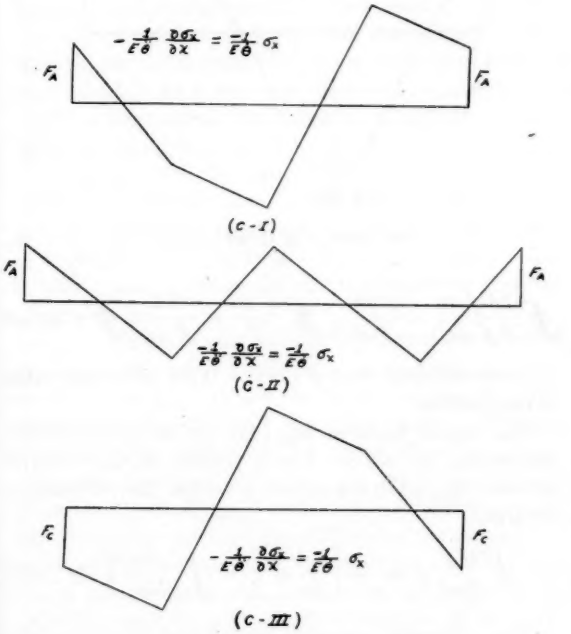

FIGS. 12c-I, 12c-II, and 12c-III.

curves are obtained (Figs. 12c-I, 12C-II, and 12c-III), from which values of the normal stress σ_x may be obtained by multiplying the ordinates by $(-E\theta)$.

Integration of the shear curves furnishes bending moment curves that do not take concentrated moments into account. The concentrated moments appear as constants of integrations (which satisfy the end conditions, which express the fact that there is no relative displacement between the edges of the cuts). This is the same condition that was satisfied for the single-cell example. However, in the case of a multicell section, a constant additive correction cannot be used for a complete single cell, since the correction for cell I along the member AB affects the correction for cell II and vice versa. Hence, a similar method must be used to that used in computing the values of A_1, A_2, and A_3.

The net shear in each element may be thought of as consisting of two parts. The first part is the one indicated by the continuous curve divided by $E\theta$. The second part is then the amount that must be added so as to satisfy the end conditions.

In order to simplify the following expressions, the first variable parts are denoted by q_1', q_2', and q_3' and the additive corrections are set equal to q_1' for cell I, q_{II}' for cell II, and q_{III}' for cell III. The values of q_1', q_{II}', q_{III}' are determined by the following relations:

For cell I

$$\oint_{I} \frac{q'\,da}{t^2} = \oint_{I} \frac{q_1'\,da}{t^2} + \int_A^B (q_1' - q_{II}')\frac{da}{t^2} + \int_B^A q_1'\frac{da}{t_2} = 0 \quad \text{(clockwise)}$$

For cell II

$$\oint_{II} \frac{q'\,da}{t^2} = \oint_{II} \frac{q_2'\,da}{t^2} + \int_A^C q_{II}'\frac{da}{t^2} + \int_C^D (q_{II}' - q_{III}')\frac{da}{t^2} + \int_D^B q_{II}'\frac{da}{t^2} + \int_B^A (q_{II}' - q_1')\frac{da}{t^2} = 0$$

For cell III

$$\oint_{III} \frac{q'\,da}{t^2} = \oint_{III} \frac{q_3'\,da}{t^2} + \int_C^D q_{III}'\frac{da}{t^2} + \int_D^C (q_{III}' - q_{II}')\frac{da}{t^2} = 0 \quad \text{(clockwise)}$$

These equations are of a type identical to those used for the determination of $\bar{A}_1$, $\bar{A}_2$, and $\bar{A}_3$; therefore the same method of solution may be used.

Relation Between Twist and Torsional Moment

It was shown in the introduction that the total twisting moment is composed of the moment T of the primary shear stresses produced by the twist θ without axial restraint, and the additional moment T' produced by secondary shear stresses resulting from the restraint.

The moment produced by the twist alone is equal to $CG\theta$, where CG is the torsional rigidity of the section. The quantity C has the dimension of a moment of inertia; it is called the "equivalent polar moment of inertia." The magnitude of C is small for an open section (of the order of St^3); also, in a combined section, the contribution of the open portion is negligible in comparison with the contribution of the closed parts. For a closed section, C is comparatively large and may be computed in the following manner:

According to Eq. (7) the shear flow is equal to

$$t\tau = q = [2AG\theta/(\oint ds/t)]$$

On the other hand, the moment produced by the shear stresses about the center of rotation is equal to

$$T = \oint qr\,ds = q\oint r\,ds = 2qA \tag{23}$$

By substituting the value of q

$$T = 4A^2G\theta/(\oint ds/t) \tag{24}$$

Hence, the equivalent polar moment of inertia of the closed section is

$$C = 4A^2/(\oint ds/t) \tag{25}$$

In the case of a section consisting of n cells, the values of $q_1, q_2, \ldots q_n$ have to be calculated by the method given under the heading "Multicell Section," and Eq. (23) is to be replaced by the expression

$$T = 2(A_1q_1 + A_2q_2 + \ldots + A_nq_n) \tag{26}$$

In order to calculate the moment T' resulting from the secondary shear stress τ', the following integral must be computed:

$$T' = \oint q'r\,ds = \oint q'(r/t)\,da \tag{27}$$

Since q' and r/t were determined before, T' is easily obtained by multiplying the ordinates of the diagrams for q' and r/t and integrating the product. Noting that q' is proportional to $E\ddot{\theta}$ and that the average value of the product $q'(r/t)$ is negative, it follows that the expression for T' has the form

$$T' = -C'E\ddot{\theta} \tag{28}$$

The quantity C' has the dimension of the sixth power of a length and may be expressed as

$$C' = -\oint (q'/E\theta)(r/t)\,da \tag{29}$$

In many cases it is simpler to compute C' from the diagram of $-(\sigma_x/E\theta)$. It is remembered that according to Eq. (19)

$$\frac{\partial^2 q'}{\partial a^2} = E\ddot{\theta}\left(\frac{r}{t} - \frac{2A}{t^2\oint ds/t}\right)$$

Hence

$$r/t = (2A/t^2\oint ds/t) + (1/E\ddot{\theta})(\partial^2 q'/\partial a^2) \tag{30}$$

Substituting this expression in Eq. (29)

$$C' = -\frac{1}{E\ddot{\theta}}\oint \frac{2Aq'\,da}{t^2\oint ds/t} - \frac{1}{E^2\ddot{\theta}^2}\oint \frac{\partial^2 q'}{\partial a^2}\,q'\,da \tag{31}$$

It is noted that the first term on the right side of the equation is to be extended over the circumference of closed sections or closed portions of combined sections only, since for all other cases A does not exist. Now any portion of the integral in this first term taken over the circumference of a closed section vanishes, since

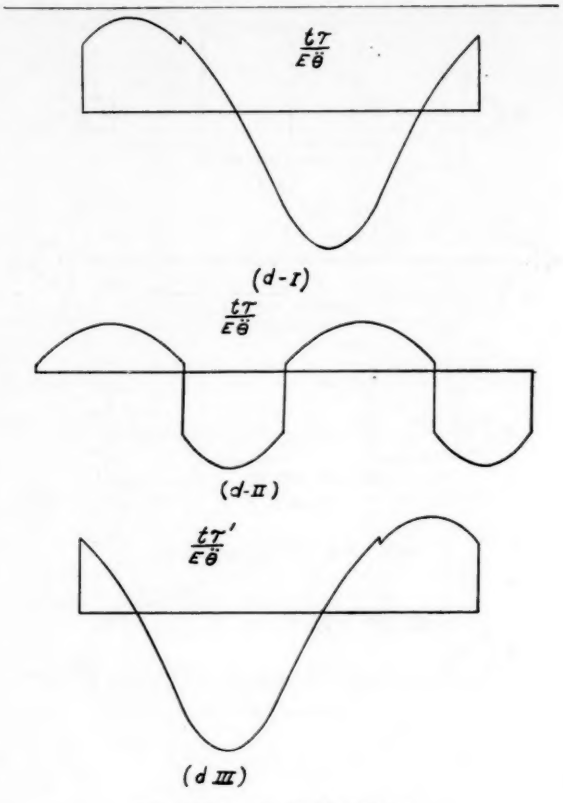

FIGS. 12d-I, 12d-II, and 12d-III.

$$\oint \frac{2Aq'\,da}{t^2\oint ds/t} = \frac{2A}{\oint ds/t}\oint \frac{q'\,da}{t^2} = \frac{2A}{\oint ds/t}\oint \tau'\,ds = 0$$

It is remembered that $\oint \tau'\,ds = 0$ for all closed paths of integration.

The second term in Eq. (31) can be computed by integrating by parts. For a portion of the integral between the arbitrary points m and n, the following is obtained:

$$\int_m^n \frac{\partial^2 q'}{\partial a^2}\,q'\,da = \left[\frac{\partial q'}{\partial a}\,q'\right]_m^n - \int_m^n \left(\frac{\partial q'}{\partial a}\right)^2 da \tag{32}$$

The following consideration shows that the sum $\sum_m\sum_n[(\partial q'/\partial a)q']_m^n$ vanishes. First, assume that a point m or n represents a free edge; then at such point $q' = 0$, since at a free edge the shear flow must be equal to zero. The rest of the expression consists of values taken at intermediate points, at which at least three webs of the section converge. Consider the contributions from such a point—for example, from point A of Fig. 12a. The terms in which the point A occurs are $[(\partial q'/\partial a)q']_2^A + [(\partial q'/\partial a)q']_A^B + [(\partial q'/\partial a)q']_A^C$; the contribution of the point A is, therefore, $[(\partial q'/\partial a)q']^A + [(\partial q'/\partial a)q']_A + [(\partial q'/\partial a)q']_A$. Now the value at $\partial q'/\partial a$ must be identical in all three terms, since $\partial q'/\partial a = -(1/t)(\partial\sigma_x/\partial_x)$ and $(\partial\sigma_x/\partial x)$ has a unique

value at A. Since the sum of the three terms is equal to $(\partial q'/\partial a)[q_{zA}' - q_{AB}' - q_{AC}']$, where $q_{zA}', q_{AB}', q_{AC}'$ denote the shear flows converging to or diverging from point A, it is evident that the sum in the bracket vanishes because of the continuity of the shear flow. This is true of all intermediate points; therefore the whole sum considered must be equal to zero.

Eq. (31) may now be reduced to the simple expression:

$$C' = (1/E^2\dot{\theta}^2) \oint (\partial q'/\partial a)^2 \, da \tag{33}$$

since $\partial \sigma_z/\partial x = -(\partial q'/\partial a)$ and therefore

$$C' = [1/(E\dot{\theta})^2] \oint (d\sigma_z/ds)^2 \, da \tag{34}$$

or

$$C' = (1/E^2\dot{\theta}^2) \oint \sigma_z^2 \, da \tag{35}$$

Since $\sigma_z/E\dot{\theta}$ involves only the geometric data of the cross section (as developed in the section on "Example Solutions of q' as a Function of θ"), C' is a geometric constant of the cross section. Also, since σ_z and E have the same dimension and $\dot{\theta}$ has the dimension radians/-unit length^2, C' has the dimension of the sixth power of unit length. As it was mentioned above, the quantity $\sigma_z/E\dot{\theta}$ is identical to the "unit warping" used by the authors cited in the introduction.

It appears to the writers of this paper that the method presented here operates with notions and graphic methods familiar to practical engineers, and it is hoped, therefore, that it will appeal to them. The following sections illustrate the application of the foregoing material.

In certain cases the quantity C' can be interpreted in a simple manner. Consider as an example the twisting of an I section. From the method explained in this paper the relation $C' = 2e^2\,(th^3/12)$ is obtained, where $2e$ is the height of the section, h is the width of the flanges, and t is the thickness of the flanges. Since the moment of inertia of each flange is equal to $I = th^3/12$, the quantity C' may be obtained by multiplying the moment of inertia of the two flanges by the square of their distance to the shear center and adding the products. It is easily seen that the same result is obtained by calculating the torsion in an I beam from the bending of the two flanges. In fact, if z denotes the deflection of the flanges considered as beams, the rate of twist of the I beam is equal to $\theta = (1/e)(dz/dx)$. On the other hand, the twisting moment is equal to $2Ve$ where V is the shear force in one flange. Hence,

$$T' = 2Ve = 2EI(d^3z/dx^3)e = 2e^2EI(d^2\theta/dx^2)$$

Comparing this expression with Eq. (28), it is seen that $C' = 2Ie^2$ as it was obtained above.[3]

The simple example of the I beam suggests that the quantity C' be expressed as the product of one of the "flexural moments of inertia," I, and the square of a length e, which can be considered as the "eccentricity parameter" of the section. With this notation Eq. (28) for the secondary twisting moment can be written in the form

$$T' = -IEe^2(d^2\theta/dx^2)$$

whereas the primary twisting moment is given by $T' = CG\theta$.

The product IE is called the flexural rigidity; the product CG, the torsional rigidity of the section; finally, the product $C'E$ or Ie^2E, its warping rigidity.

Sample Calculations of C'

A Channel Section

For this particular case $h = 4$ in., $b = 2$ in., $t = 0.20$ in., and e is calculated to be 0.81 in. The ordinates of the load diagram (Fig. 9b) are, therefore: $h/2t = 10$, $e/t = -4.05$, and $F_1 = F_2 = -2.38$. Since the section is symmetric and it is the square of the ordinate of the shear curve that is required to solve for C', expressions for $\sigma_z/E\theta$ are needed only over half of the developed beam.

The ordinate of the shear diagram is expressed in two parts: from one free edge to the web, and from one flange to the center of the web. The expression for the first part is

$$-(1/E\theta)\sigma_z]_{0.4}^{0.4} = -2.38 + \int_0^a 10 \, da = -2.38 + 10a$$

and for the second part is

$$-(1/E\theta)\sigma_z]_{0.4}^{0.8} = -2.38 + \int_0^{0.4} 10 \, da - \int_{0.4}^{a} 4.05 \, da = 3.24 - 4.05a$$

Substituting these values into Eq. (35)

$$C' = 2[\int_0^{0.4} (2.38 - 10)^2 \, da + \int_{0.4}^{0.8} (3.24 - 4.05)^2 \, da] = 1.88 \text{ in.}^6$$

The value of C for such a section is $St^3/3$ (see the section on "Relation Between Twist and Torsional Moment") or $8 \times 0.20^3/3 = 0.02133$ in.^{4}

AZ Section

In this example the dimensions of the web and flange are the same as that of the channel section illustrated in the preceding example. For this case the shear center is located at the c.g. of the section; therefore $e = 0$. The value of C' is determined in the same manner as that shown for the channel section and is found to be $C' = 2.667$ in.^{6} This value compared with 1.88 in.^{6} for the channel section illustrates that the Z has greater torsional rigidity than the channel, since the value of C for the Z section is identical to that of the channel.

A Single-Cell Closed Section

In the simple example of Fig. 13a it is assumed that the effective bending material is distributed into an equivalent thickness of 0.20 in., which will not buckle under load. The length $AB = 40$ in. and $BC = 10$ in.

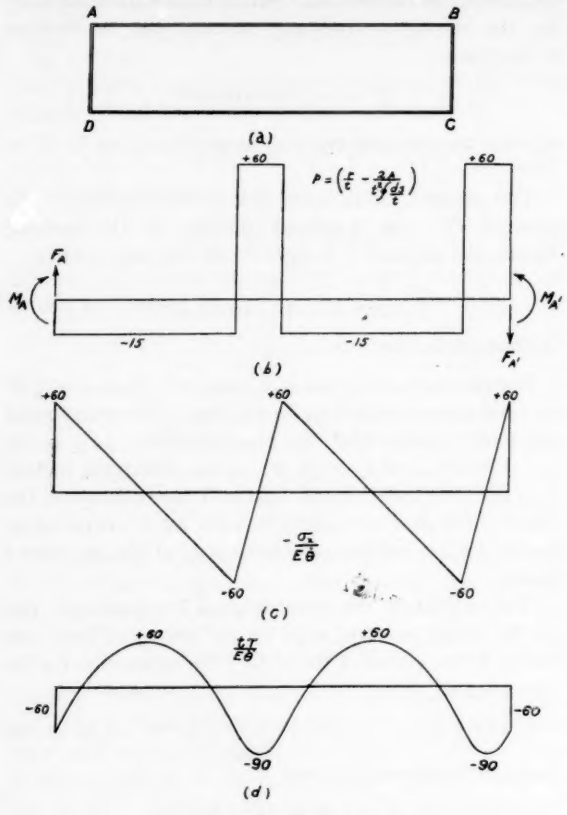

FIGS. 13a, 13b, 13c, and 13d.

Again, since the section is symmetric, only half of the developed area need be used. From Fig. 13c it is seen that

$$\frac{-1}{E\theta}\sigma_x\Big]_A^B = 60 - 15a \text{ and } \frac{-1}{E\theta}\sigma_x\Big]_B^C = -540 + 60a$$

Hence, Eq. (35) yields

$$C' = 2[\int_0^8(60 - 15a)^2\,da + \int_8^{10}(-540 + 60a)^2\,da] = 24{,}000 \text{ in.}^6$$

From Eq. (25) $C = 1280$ in.^{4}

The Solution of Differential Equation of $\theta = f(x)$

In the previous section the torsional moment was shown to be related to the twist by the differential equation

$$\bar{T} = T + T' = GC\theta - C'E\ddot{\theta} \tag{36}$$

The general solution for this type of differential equation may be expressed as

$$\theta = A \sinh \lambda x + B \cosh \lambda x + (\bar{T}/CG) \tag{37}$$

where

$$\lambda^2 = CG/EC' \tag{38a}$$

where A and B are constants determined from the end conditions as defined for a given problem. It is seen that $1/\lambda$ is a characteristic length of the problem. Using the notations of the foregoing section

$$1/\lambda = e\sqrt{ET/CG} \tag{38b}$$

In other words, $1/\lambda$ is equal to the eccentricity parameter multiplied by the square root of the ratio of the flexural to the torsional rigidity of the section. Hence $1/\lambda$ is especially large if e is not small, and the torsional rigidity is small compared with the flexural rigidity, as in open sections; it is extremely small for closed sections with small eccentricity and has moderate values for closed sections with eccentric material distribution.

Comparison of Results of Elementary Method of Torque Analysis to the Presented Method

A Cantilever Beam with a Torque Applied at the Free End

For this particular example there is no warping at the built-in end ($x = 0$) and at the free end ($x = L$) the beam is free to warp.

Since dw/ds is proportional to θ and σ_x is proportional to $\dot{\theta}$, the end conditions are: at $x = 0$, $\theta = 0$; at $x = L$, $\dot{\theta} = 0$. From these known end conditions the values of A and B in Eq. (37) are found to be

$$A = (\bar{T}/CG) \tanh \lambda x \qquad \text{and} \qquad B = -\bar{T}/CG$$

Substituting values of A and B, Eq. (37) becomes

$$\theta = (\bar{T}/CG)\{1 - [\cosh \lambda(L - x)/\cosh \lambda L]\} \tag{39}$$

The corresponding value according to the elementary solution is known to be

$$\theta = \bar{T}/CG \tag{40}$$

A comparison of Eqs. (39) and (40) shows that, when $x = 0$, Eq. (39) becomes equal to zero and Eq. (40) remains the same as that for any value of x.

The total angle of twist may be compared by integrating the two expressions. From Eq. (39)

$$\phi_L = (\bar{T}/CG)[L - (\tanh \lambda L)/\lambda] \tag{41}$$

and from Eq. (40)

$$\phi_L = \bar{T}L/CG \tag{42}$$

It is to be noticed that if $\lambda L > 5$ for practical purposes Eq. (41) may be reduced to

$$\phi_L = (\bar{T}/CG)[L - (1/\lambda)] \tag{43}$$

Furthermore, if λ is large, Eq. (39) approaches the value of Eq. (40).

With the value of θ known for the presented theory, Eq. 36 may be developed so that T and T' can be expressed as a function of x.

$$T = CG\theta = \bar{T}\left[1 - \frac{\cosh \lambda(L - x)}{\cosh \lambda L}\right] \tag{44}$$

$$T' = C'E\ddot{\theta} = \bar{T}\left[\frac{\cosh \lambda(L - x)}{\cosh \lambda L}\right] \qquad (45)$$

These expressions show that at the built-in end ($x = 0$), the total torque $\bar{T}$ is carried in the form of secondary shear stress. They also show that the ratio of T and T' at the free end ($x = L$) is dependent upon the length of the beam as well as the cross-sectional shape.

From Eqs. (44) and (45) general expressions for τ, τ', and σ_z may be developed. The primary shear stress is equal to

$$\tau = \frac{3\bar{T}}{ST^2}\left[1 - \frac{\cosh \lambda(L - x)}{\cosh \lambda L}\right] \qquad (46)$$

or introducing the numerical values for S and t,

$$\tau = 9.37\bar{T}\left[1 - \frac{\cosh \lambda(L - x)}{\cosh \lambda L}\right]$$

As to the magnitude of the secondary shearing stress it was found previously that the quantity $q'/E\ddot{\theta}$ depends on the shape and the dimensions of the cross section only. This quantity has the dimensions of the moment of inertia, and it is variable along the centerline of the thin-walled section. This quantity will be denoted by β_s, where the subscript s indicates that it varies with s. Then

$$\tau' = \beta_s(E\ddot{\theta}/t)$$

or substituting $E\ddot{\theta}$ from Eq. (39)

$$\tau' = \left(\frac{\beta_s\lambda^2}{t}\right)\left(\frac{E}{G}\right)\left(\frac{\bar{T}}{C}\right)\left[\frac{\cosh \lambda(L - x)}{\cosh \lambda L}\right]$$

This equation can also be written in the form

$$\tau' = \left(\frac{\beta_s}{t}\right)\left(\frac{\bar{T}}{C'}\right)\left[\frac{\cosh \lambda(L - x)}{\cosh \lambda L}\right] \qquad (47)$$

The value of β_s and C' can be taken from the curves derived in the section on "Example Solutions of q' as a Function of θ."

The magnitude of the normal stress σ_z can be determined in a similar way. It was found that the quantity $\sigma_z/E\ddot{\theta}$ depends again on the shape and dimensions of the cross section. This quantity has the dimensions of an area and is denoted by α_s. Then

$$\sigma_z = \alpha_s E\dot{\theta}$$

or substituting the value of $\dot{\theta}$ from Eq. (39)

$$\sigma_z = \alpha_s\left(\frac{E}{G}\right)\left(\frac{\bar{T}}{C}\right)\lambda\left[\frac{\cosh \lambda(L - x)}{\cosh \lambda L}\right] \qquad (48)$$

From Fig. 9c, it is seen that the maximum tension stress is the same as the maximum compression stress as to be expected for a symmetric section. Since the ordinates are shown as negative values of $\sigma_z/E\ddot{\theta}$, the maximum tension is at point 1 and the maximum compression stress is at point 2. From "Sample Calculations of C'" F_1 or $\alpha_{s_{max.}} = -(\sigma_z/E\ddot{\theta})$ at point 1 is found to be -2.38.

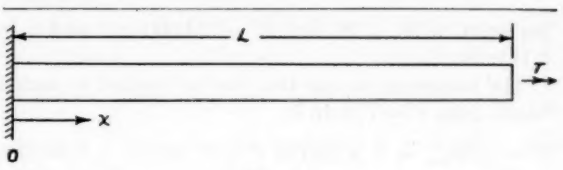

FIG. 14.

Substituting the given numerical values into Eq. (48) the maximum tension stress is found to be

$$\sigma_{max.} = 19.5\bar{T} \tanh \lambda L$$

Since $\tanh \lambda L$ is limited to unity, the maximum torque that can be applied to the beam as far as normal stresses are concerned is

$$\bar{T} = 56{,}000/19.5 = 2{,}870 \text{ in.lbs.}$$

The maximum value of the shearing stress τ' can be calculated from Eq. (47). From Fig. 9d the maximum value of β_s is found to be equal to -0.283. Substituting this value and numerical values for t and C', Eq. (47) becomes

$$\tau' = \left(\frac{0.283\bar{T}}{0.20 \times 1.88}\right)\left[\frac{\cosh \lambda(L - x)}{\cosh \lambda L}\right] = 0.745\bar{T}\left[\frac{\cosh \lambda(L - x)}{\cosh \lambda L}\right]$$

The maximum value of τ' is at the built-in end and is found to be

$$\tau_{max.}' = 0.745\bar{T}$$

The maximum value of τ, however, is at the free end ($x = L$). Therefore

$$\tau_{max.} = 9.37\bar{T}[1 - (1/\cosh \lambda L)]$$

Adding the primary and secondary shearing stresses, the total shearing stress is found to be

$$\tau + \tau' = \bar{T}\left[9.37 - 8.625\,\frac{\cosh \lambda(L - x)}{\cosh \lambda L}\right]$$

It is seen that $\tau_{max.}$ is limited to $9.37\bar{T}$ when $L = \infty$. Therefore the maximum allowable torque that can be applied to such a beam without exceeding the ultimate shearing stress is

$$\bar{T} = 34{,}000/9.37 = 3{,}630 \text{ in. lbs.}$$

These results show that for this particular beam the shearing stresses are never critical, regardless of the length of the beam.

Closed Section

This box beam is assumed to be constructed of 24ST duraluminum sheet and has an arbitrary length L. Also $E = 10.5 \times 10^6$ lbs. per sq.in., $G = 3.9 \times 10^6$ lbs.

per sq.in., $C = 1{,}280$ in.^{4}, $C' = 24{,}000$ in.^{4}, and $\lambda = 0.1410$ in.$^{-1}$.

The maximum torque that can be applied to such a beam, from $\tau = \bar{T}/2At$, is

$$\bar{T} = 2At\tau_{ult.} = 2 \times 400 \times 0.2 \times 34{,}000 = 5{,}440{,}000 \text{ in.lbs.}$$

From the presented theory this value is reduced as follows: At the built-in end $x = 0$, Eq. (47) becomes

$$\tau' = -(t\tau'/E\ddot{\theta})/(\bar{T}/tC')$$

or

$$\bar{T} = t\tau'_{ult.}C'/\ (-\ t\tau'/E\ddot{\theta})$$

Substituting given numerical values and $t\tau'/E\ddot{\theta} = -90$ cu.in. (refer to Fig. 13d)

$$T = \frac{0.20 \times 34{,}000 \times 24{,}000}{90} = 1{,}810{,}000 \text{ in.lbs.}$$

It is of interest to note that for the closed section the secondary shearing stresses are considerably greater than the primary shearing stresses, whereas, in the case of the open section, the opposite was found to be true.

The maximum normal stress occurs when $L = \infty$ and is found as follows:

$$-(\sigma_x/E\dot{\theta}_{max.}) = \pm 60 \text{ (refer to Fig. 13c)}$$

Substituting $x = 0$ and $L = \infty$ into Eq. (48)

$$\sigma_x = (\sigma_x/E\dot{\theta})(\bar{T}/\lambda C')$$

Now,

$$\sigma_x = \frac{60\bar{T}}{0.141 \times 24{,}000} = 0.0177\bar{T}$$

Substituting $\bar{T} = 1{,}810{,}000$ in.lbs.

$$\sigma_{max.} = 32{,}000 \text{ lbs. per sq.in.}$$

From these results it appears that the type of closed section investigated here is only to be designed on shear allowables, whereas in the open sections either normal stresses or shearing stress may be critical. This conclusion, however, is based upon the physical properties of present-day materials that would be used for such a structure.

A Cantilever Beam Loaded with a Concentrated Torque at an Intermediate Point Between Its Two Ends

Since the span is divided into two parts, separate equations are required. Therefore, from Eq. (37) the following may be expressed:

$$\theta\Big]_{x=0}^{x=a} = A_a \sinh \lambda x + B_a \cosh \lambda x + (T_a/CG) \quad (49)$$

$$\theta\Big]_{x=a}^{x=L} = A_b \sinh \lambda(x-a) + B_b \cosh \lambda(x-a) + (T_b/CG) \quad (50)$$

In the above equations the subscripts designate the portion of the span over which the constant applies.

Since there is no restraint at $x = L$ and since the beam is free to rotate at this point, $T_b = 0$ and $T_a = \bar{T}$. Eqs. (49) and (50) therefore reduce to

$$\theta\Big]_{x=0}^{x=a} = A_a \sinh \lambda x + B_a \cosh \lambda x + (\bar{T}/CG) \quad (51)$$

$$\theta\Big]_{x=a}^{x=L} = A_b \sinh \lambda(x-a) + B_b \cosh \lambda(x-a) \quad (52)$$

It is seen that the above equations have a total of four constants which are to be determined from end conditions. By reasons given in "The Solution of Differential Equation of $\theta = f(x)$," the following may be said: at $x = 0$, $\theta = 0$; at $x = L$, $\dot{\theta} = 0$. From these end conditions Eqs. (51) and (52) reduce to

$$\theta\Big]_{x=0}^{x=a} = A_a \sinh \lambda x + (\bar{T}/CG)(1 - \cosh \lambda x) \quad (53)$$

$$\theta\Big]_{x=a}^{x=b} = -D \cosh \lambda(L-x) \quad (54)$$

Since the beam is continuous across B, the warpage and the normal stress across B must be consistent. Therefore,

$$\theta_{-B} - \theta_{+B} = 0 \quad \text{and} \quad \dot{\theta}_{-B} - \dot{\theta}_{+B} = 0$$

The values of A_a and D are found to be:

$$A_a = \frac{\bar{T}}{CG}\left[\tanh \lambda L - \frac{\sin \lambda b}{\cosh \lambda L}\right]$$

and

$$D = (\bar{T}/CG)[(1 - \cosh \lambda a)/\cosh \lambda L]$$

If a and b are greater than $5/\lambda$ the above values may be reduced to the approximate values as follows:

$$A = (\bar{T}/CG)[1 - (e^{\lambda b}/e^{\lambda L})]$$

$$D = (\bar{T}/CG)[(2 - e^{\lambda a})/e^{\lambda L}]$$

These results show that, although there is no resulting torque in the overhanging section, normal stresses and shear stresses exist and their magnitude may be readily calculated.

A Cantilever Beam Loaded with a Concentrated Torque at an Intermediate Point Between the Two Ends; the Free End is Free to Warp but Not Free to Rotate

This case is the same as the preceding case except there is no rotation at point C (Fig. 15). Consequently, Eqs. (49) and (50) are valid for this case. It is now seen that two more unknown constants (T_a and T_b) are introduced. The requirements needed for these two added unknowns are met by the following relationships:

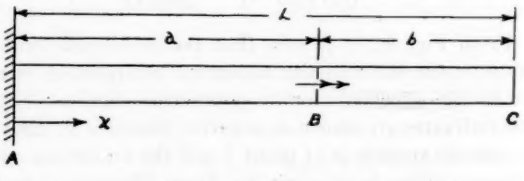

FIG. 15.

$$T_a - T_b = \bar{T} \tag{55}$$

and

$$\phi_C = \int_0^L \theta\, dx = \frac{A_a}{\lambda}(\cosh \lambda a - 1) + \frac{B_a}{\lambda} + \frac{aT_a}{CG} + \frac{A_a}{\lambda}(\cosh \lambda b - 1) + \frac{B_b}{\lambda}\sinh \lambda b + \frac{bT_b}{CG} = 0 \tag{56}$$

The remaining conditions to be met are

$$\theta_A = B_a + (T_a/CG) = 0 \tag{57}$$

$$\theta_C = \lambda A_b \cosh \lambda b + \lambda B_b \sinh \lambda b = 0 \tag{58}$$

$$\theta_{-B} - \theta_{+B} = A_a \sinh \lambda a + B_a \cosh \lambda a + (T_a/CG) + B_b - (T_b/CG) = 0 \tag{59}$$

$$\dot{\theta}_{-B} - \dot{\theta}_{+B} = \lambda A_a \cosh a + \lambda B_a \sinh \lambda a - \lambda A_b = 0 \tag{60}$$

Eqs. (55), (56), (57), (58), (59), and (60) give six relationships from which the six unknowns can be determined.

$$A_a = \left(\frac{\bar{T}}{CG}\right)\left(\frac{\lambda b \sinh \lambda L - \lambda L \sinh \lambda b}{\lambda L \cosh \lambda L - \sinh \lambda L}\right)$$

$$A_b = \left(\frac{\bar{T}}{CG}\right)\sinh \lambda b \left(\frac{\sinh \lambda a - \lambda L \cosh \lambda a + \lambda b}{\lambda L \cosh \lambda L - \sinh \lambda L}\right)$$

$$B_a = \left(\frac{\bar{T}}{CG}\right)\left(\frac{\sinh \lambda b - \lambda b \cosh \lambda L}{\lambda L \cosh \lambda L - \sinh \lambda L}\right)$$

$$B_b = \left(\frac{\bar{T}}{CG}\right)\cosh \lambda b \left(\frac{\lambda L \cosh \lambda a - \lambda b - \sinh \lambda a}{\lambda L \cosh \lambda L - \sinh \lambda a}\right)$$

$$T_a = \bar{T}\left(\frac{\lambda b \cosh \lambda L - \sinh \lambda b}{\lambda L \cosh \lambda L - \sinh \lambda L}\right)$$

$$T_b = \bar{T}\left(\frac{\sinh \lambda L - \lambda a \cosh \lambda L - \sinh \lambda b}{\lambda L \cosh \lambda L - \sinh \lambda L}\right)$$

It is of interest to note that in this case there are not only differences of shear and normal stresses between this solution and the elementary solution (as illustrated in the first example) but also the ratio of T_a to T_b differs from that determined by the elementary solution. This may be illustrated by applying the above results to the channel section previously discussed.

Let $L = 20$ in. and $a = b = 10$ in. From the elementary solution the applied torque $\bar{T}$ is equally divided so that $T_a = T_b = \bar{T}/2$, or $T_a/T_b = 1$. From the expressions given for T_a and T_b

$$\frac{T_a}{T_b} = \frac{\lambda b \cosh \lambda L - \sinh \lambda b}{\sinh \lambda L - \lambda a \cosh \lambda L - \sinh \lambda b} = 1.96$$

A Cantilever Beam with the Free End Free to Rotate Loaded with a Uniform Running Torque $\bar{t}$

For this case Eq. (36) is valid, but, instead of $\bar{T}$ being a constant, it is a function of x—namely,

$$\bar{T} = \bar{t}(L - x) \tag{61}$$

Eq. (36) then becomes

$$CG\theta - C'E\ddot{\theta} = \bar{t}(L - x) \tag{62}$$

from which

$$\theta = A \sinh \lambda x + B \cosh \lambda x + (\bar{t}/CG)(L - x) \tag{63}$$

when $x = 0$, $\theta = 0$, and, therefore, $B = \bar{t}L/CG$; when $x = L$, $\theta = 0$, and, hence

$$A = (\bar{t}L/CG)[\tanh \lambda L + (\operatorname{sech} \lambda L)/\lambda L]$$

Substituting into Eq. (63),

$$\theta = \frac{\bar{t}L}{CG}\left[\left(\tanh \lambda L + \frac{\operatorname{sech} \lambda L}{\lambda L}\right)\sinh \lambda x - \cosh \lambda x + \left(\frac{L - x}{L}\right)\right] \tag{64}$$

The value for the total angle of twist, as determined from the elementary solution, is

$$\phi = \bar{t}L^2/2CG$$

and from the presented solution

$$\phi = \frac{\bar{t}}{CG}\left[\frac{L^2}{2} - \frac{1}{\lambda^2}\left(\frac{1 + \lambda L \sinh \lambda L}{\cosh \lambda L} - 1\right)\right]$$

which, when λ becomes large, reduces to

$$\phi = (\bar{t}L^2/2CG)\,[1 - (2/\lambda L)]$$

A Cantilever Beam Loaded with a Uniform Torque $\bar{t}$ Along the Span; One End Being Fixed and the Other End Free to Warp but Not Free to Rotate

Eq. (36) is also valid for this case, but again $\bar{T}$ is a function of x. This function is expressed as follows:

$$\bar{T} = T_0 - \bar{t}x \tag{65}$$

T_0 represents the torsional moment at the fixed end; $x = 0$. T_L hereafter designates the reaction at $x = L$.

This introduces two additional unknowns over the previous case; therefore two additional conditions are required. These conditions may be stated as:

$$-T_0 + T_L + \bar{t}L = 0 \tag{66}$$

and, when $x = L$, $\phi = 0$. Now

$$\theta = A \sinh \lambda x + B \cosh \lambda x - (\bar{t}/CG)x + (T_0/CG) \tag{67}$$

when $x = 0$

$$B + (T_0/CG) = 0 \tag{68}$$

when $x = L$

$$\int^L \theta\, dx = \phi_L = \frac{A}{\lambda}(\cosh \lambda L - 1) + \frac{B}{\lambda}\sinh \lambda L - \frac{\bar{t}L^2}{2CG} + \frac{T_0 L}{CG} = 0 \tag{69}$$

$$\dot{\theta} = \lambda A \cosh \lambda L + \lambda B \sinh \lambda L - \frac{\bar{t}}{CG} = 0 \tag{70}$$

From Eqs. (66), (68), (69), (70) the values of the four constants are found to be

$$T_0 = iL\left[\frac{1}{2} + \frac{\lambda L \sinh \lambda L - 2\cosh \lambda L + 2}{2\lambda L(\lambda L \cosh \lambda L - \sinh \lambda L)}\right]$$

$$T_L = iL\left[-\frac{1}{2} + \frac{\lambda L \sinh \lambda L - 2\cosh \lambda L + 2}{2\lambda L(\lambda L \cosh \lambda L - \sinh \lambda L)}\right]$$

$$A = \frac{iL}{CG}\left[\frac{2\lambda L + (\lambda^2 L^2 - 2)\sinh \lambda L}{2\lambda L(\lambda L \cosh \lambda L - \sinh \lambda L)}\right]$$

$$B = -\frac{iL}{CG}\left[\frac{1}{2} + \frac{\lambda L \sinh \lambda L - 2\cosh \lambda L + 2}{2\lambda L(\lambda L \cosh \lambda L - \sinh \lambda L)}\right]$$

It is seen that because of the restrained warping at the fixed end the reaction moment at the fixed end is larger than that at the end free to warp; whereas, according to the elementary theory, the two reaction moments are equal.

Conclusions

The method presented in this paper permits the computation of the stress distribution in thin-walled structures of constant cross section which are subjected to variable twist. The computation requires simple mathematical operations, and a method is proposed which reduces this calculation to a sequence of graphic integrations analogous to that used in dealing with transversely loaded beams.

The numerical examples carried out show that the results of the theory deviate considerably from the usual theory of torsion in cases where the axial warping is considered restrained. For example: in one case of a closed section, the maximum secondary shearing stress equals three times the maximum primary stress. Since the theory is based upon the idea of successive approximations, it will be necessary to compare the results with those of the exact theory of elasticity applied to shells of simple geometric shapes before its application in such extreme cases can be recommended.

References

[1] Timoshenko, S., Einige Stabilitätsprobleme der Elastizitätstheorie, *Zeitschrift für mathematik und physik*, Vol. 58, p. 361, 1910.

[2] Timoshenko, S., *Strength of Materials*, Part II, 2nd Edition; D. Van Nostrand Company, Inc., New York, 1941.

[3] Ostenfeld, A., Copenhagen, Polytekniske laereanstalt, Laboratorium for bygningsstatik Meddelelse, No. 6; 1931.

[4] Wagner, H., *Torsion and Buckling of Open Sections*, N.A.C.A. T.M. No. 807, 1936.

[5] Wagner, H., and Pretschner, W., *Torsion and Buckling of Open Sections*, N.A.C.A. T.M. No. 784, 1936.

[6] Goodier, J. N., *Buckling of Compressed Bars by Torsion and Flexure*, Bulletin 27, Engineering Experiment Station, Cornell University, December, 1941.

[7] Goodier, J. N., *Torsional and Flexural Buckling of Bars of Thin-Walled Open Section Under Compressive and Buckling Loads*, Journal of Applied Mechanics, Vol. 9, No. 3, September, 1942.

[8] Kappus, Robert, *Twisting Failure of Centrally Loaded Open-Section Columns in the Elastic Range*, N.A.C.A. T.M. No. 851, 1938.

[9] Hoff, N. J., *Stresses in Spaced-Curved Rings Reinforcing the Edges of Cut-Outs in Monocoque Fuselages*, The Journal of The Royal Aeronautical Society, Vol. XLVII, No. 386, p. 35, February, 1943. (This article was not known to the authors at the time of preparation of this paper. It contains, in many points, a similar approach to the problem.)

The Effect of Combined Stresses on the Ductility and Rupture Strength of Magnesium-Alloy Extrusions

E. G. THOMSEN* AND J. E. DORN†
University of California

ABSTRACT

The effect of combined stresses on the rupture strength and ductility of three tubular magnesium extrusions was investigated. The data reveal that the materials investigated obey the critical shear stress law for rupture. The rupture stress, however, depends upon the conditions of anisotropy, ductility under combined stresses and work hardening.

The ductility of magnesium-alloy extrusions under combined stresses agrees fairly well with predictions based on the Ros and Eichinger equations. Anisotropy, however, modifies the results.

INTRODUCTION

SOME PROGRESS HAS BEEN MADE in the past few years in determining the effect of complex stresses on the properties of metals. Of these properties, elastic failure, total deformation before rupture, rupture strength, and endurance strength are important. Numerous reports are available in the literature on the effect of combined stresses on plastic yielding and the endurance strength. There have been relatively few investigations, however, on the effect of combined stresses on the rupture strength and permanent deformations at rupture. Up to the present no satisfactory theory for the rupture of polycrystalline metals has been presented.

The most recent extensive investigation on the rupture of metals under combined stresses is that of Siebel and Maier[1] and Maier[2] who obtained combined stresses by applying internal pressure and longitudinal tension to hollow, cylindric test bars. From the loads and the corresponding cross sections of the specimens at rupture they obtained the true stresses at rupture in the axial and tangential or circumferential direction. Unfortunately, their experimental points are so few and the range of combined stresses so limited that no decisive conclusions as to the criterion for rupture under combined stresses may be obtained from these data.

Another investigation of importance is that of Bridgman.[3, 4, 5] Bridgman loaded solid cylindric specimens biaxially with a high external hydrostatic pressure and with a zero load in the axial direction. He observed that the rupture obtained under these conditions resembled the rupture that results from a simple tensile stress in the axial direction. This he called the "pinching-off effect." Siebel and Maier[1] and Maier[2] carried out experiments similar to those of Bridgman and their results were in qualitative agreement with those obtained by Bridgman.

The subject of rupture strength and plastic deformation at rupture under combined stresses has been reviewed recently by Gensamer.[6] This review illustrates that the critical maximum principal tensile stress has been generally accepted as the guiding criterion for rupture of ductile metals under combined stresses. Gensamer carefully illustrates, however, that the data in support of this criterion are limited and that this criterion is in disagreement with Bridgman's pinching-off effect. Brittle materials, such as cast iron, which fracture under simple compression stresses are generally believed to provide shear types of rupture. The only evidence that has been presented in these cases in support of a shear type of rupture resides in the known fact that the plane of failure coincides approximately with that plane on which the shear stress is a maximum. Careful microscopic examination of fracture planes, however, reveal that the planes are irregular and frequently consist of numerous steps. The microscopic fracture plane, therefore, does not coincide with the macroscopic fracture plane and, consequently, any proof of a criterion for rupture based on the direction of the fracture as revealed by macroscopic studies is open to serious criticism.

The effect of combined stresses on the rupture strength and ductility plays an important role in the plastic forming of metals. In all but a few of the simple forming operations the metal is subjected to combined stresses in order to produce the desired shape. Consequently, the limitations of forming processes are dependent upon the detailed knowledge of the response of materials to combined stresses. The effect of combined stresses on rupture are also important in certain types of design problems.

The purpose of the current investigation is to secure additional data on the rupture strength and ductility of metals under combined stresses in order to provide a broader background for establishing a sound theory for the rupture of metals.

Received July 30, 1943.

* Instructor, Department of Mechanical Engineering.
† Assistant Professor, Department of Mechanical Engineering.

TABLE 1
Composition of Tubular Magnesium-Alloy Extrusions*

Alloy	Percentage									
	Al	Cd	Cu	Fe	Mn	Ni	Pb	Si	Sn	Zn
J–1	5.8	0.01	0.01	0.001	0.22	0.001	0.032	0.01	0.004	0.74
O–1	7.8	0.01	0.01	0.001	0.27	0.001	0.018	0.01	0.004	0.43
FS–1	2.4	0.01	0.01	0.009	0.27	0.001	0.006	0.01	0.004	0.90

* Spectrochemical analyses by courtesy of The Dow Chemical Company.

MATERIALS

The materials used in this investigation are given in Table 1. The tubular extrusions were fabricated under laboratory conditions and do not necessarily conform with standard specifications for these materials. The microstructures characterizing these materials are shown in Fig. 1. It may be observed that the microstructure is different for each of these alloys. FS–1 did not contain undissolved B constituent but the microstructure revealed the presence of Mn in the form of small sphereoids scattered uniformly over the bar section. The microstructure for J–1 alloy revealed a small amount of undissolved B-constituent in addition to the Mn sphereoids noted in FS–1. Although the patches of the B-constituent were aligned in the direction of extrusion, the bands were discontinuous. As noted in the microstructure for O–1 alloy, pronounced banding of the B-constituent in the direction of extrusion was prevalent. The bands formed more or less continuous stringers of the lamellar precipitate of the B-constituent. The alloys that were investigated, therefore, exhibited three different degrees of microscopic homogeneity.

Pole figures for the alloys in the as-received condition are given in Fig. 2. Each alloy has a different degree of preferred orientation. FS–1 with a central pole has the highest degree of preferred orientation, whereas O–1 with four poles has the lowest degree of preferred orientation. Thus the alloys investigated cover a range of orientations.

EXPERIMENTAL TECHNIQUE

The method selected to secure combined stresses in the current investigation consisted of applying internal pressure and axial tension or compression to tubular specimens. The internal oil pressure was obtained by the use of a two-cylinder, Bosch Diesel, fuel-injection pump modified to provide uniform pressures. The pressure of the oil in the specimens was measured with a 10,000 lbs. per sq.in. Crosby Bourdon type gauge. The gauge was calibrated at frequent intervals with an American Dead Weight Gauge tester and was found to yield a reproducible accuracy of 10 lbs. per sq.in. The maximum pressure pulsations from the pump were determined to be less than 20 lbs. per sq.in.

The axial tensile loading was accomplished with a 60,000-lb. Olson testing machine with least scale reading equal to 10 lbs. The axial compression load was obtained with a 30,000-lb. Riehle Testing Machine having a 3000-lb dial and least scale divisions of 5 lbs.

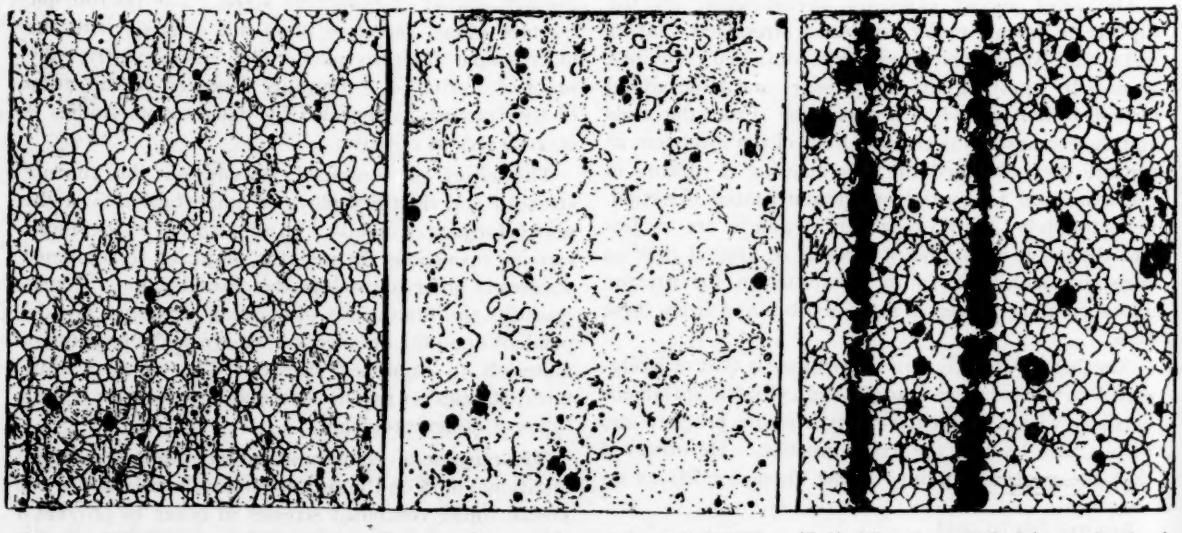

FIG. 1. Microstructure of magnesium-alloy extrusions near inner tube wall (×100). (*Left*) Alloy J–1. Etched in acetic glycol for 15 sec. (*Middle*) Alloy FS–1. Etched in 2 per cent nitric acid and 5 per cent malic acid for 5 sec. (*Right*) Alloy O–1. Etched in acetic glycol for 6 sec.

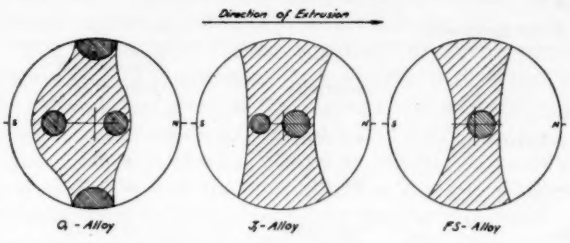

FIG. 2. Pole figures of the basal planes of magnesium-alloy tubular extrusions in the as-received condition.

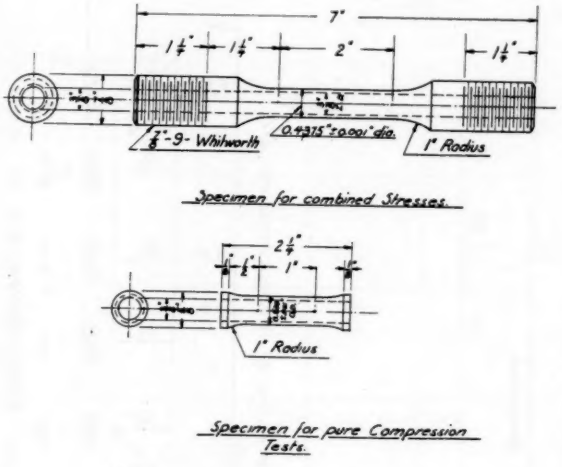

FIG. 3. Specimen design.

The specimens were screwed into special spherically seated, self-aligning grips to which the pressure-generating unit was connected by means of a high-pressure oil line.

Two methods of loading the specimens were used.

(1) The specimen was loaded in such a way that the ratio of axial stress to tangential stress (based on the original section) remained constant throughout the test.

(2) The specimen was loaded by first applying a predetermined axial (or tangential) load and holding it constant until the tangential (or axial) load had been increased to its value at rupture.

It was found that within the limits of accuracy of this investigation neither rupture strength nor ductility was influenced by the method of loading.

SPECIMENS

The specimen design selected for this investigation is given in Fig. 3. This design is in close agreement with the A.S.T.M. standard tensile test specimen, except that the gauge section has a constant diameter. The internal diameter was left in the as-extruded condition. The outside diameter was machined by placing the specimen blank on a carefully ground, snugly fitting mandrel. The specimen for pure compression tests is also shown in Fig. 3. This design was developed to prevent crimping and buckling and does not conform to standard specifications.

The following symbols are used to designate the specimen dimensions:

d_{ii} = initial inside diameter
d_{io} = initial outside diameter
l_i = initial gauge length (2 in.)
t_i = initial wall thickness
d_{fi} = final inside diameter
d_{fo} = final outside diameter
l_f = final length of gauge section
t_f = final wall thickness

These quantities are interrelated by

$$t_i = (d_{io} - d_{ii})/2 \tag{1}$$

$$t_f = (d_{fo} - d_{fi})/2 \tag{2}$$

$$\ln \frac{l_f}{l_i} + \ln \frac{t_f}{t_i} + \ln \frac{d_{fo} + d_{fi}}{d_{io} + d_{ii}} = 0 \tag{3}$$

The third equation assumes that the volume is the same before and after permanent deformation and that no local necking has occurred. These assumptions are valid within the limit of accuracy required for this investigation. Numerous checks on the specimen dimensions revealed that local necking was less than the experimental accuracy. The measurements of the initial dimensions of the specimens are given in Table 2. The values used in calculations are the average values of several carefully executed readings.

TABLE 2

Initial Dimensions of Specimen

Dimension	Technique	Sensitivity, In.	Approximate Percentage Error
d_{ii}	Tapered plug gauge	±0.0001	0.02
d_{io}	Zeiss optimeter	±0.00005	0.01
l_i	Scale and calipers	±0.01	0.5
t_i	By Eq. (1)	.....	0.5

In order to determine the true stress at rupture, the final dimensions of the specimen at the point of fracture were determined. Each type of fracture given in Fig. 4 required a different technique for measurements. The procedure finally selected for the evaluation of the final dimensions is given in Table 3.

RESULTS

The stresses in a thick-walled cylinder that is subjected to an internal pressure and a longitudinal load are well known. Turner[14] has demonstrated that within the proportional limit

$$\sigma_l = (L + \pi a^2 P)/\pi(b^2 - a^2) \tag{4}$$

TABLE 3
Final Dimensions of the Specimens

Type of Fracture	Dimension	Technique	Sensitivity, In.	Approximate Percentage Error
A	d_{fi}	Toolmakers' microscope	±0.0001	0.02
	t_f	Zeiss optimeter	±0.00005	0.01
	l_f	Scale and calipers	±0.01	0.5
	d_{fo}	By Eq. (2)	.....	0.03
B and C	t_f	Zeiss optimeter	±0.00005	0.015–0.02
	l_f	Scale and calipers	±0.01	0.5
	d_{fo}	By Eqs. (2) and (3)	.....	0.5
	d_{fi}	By Eqs. (2) and (3)	.....	0.5

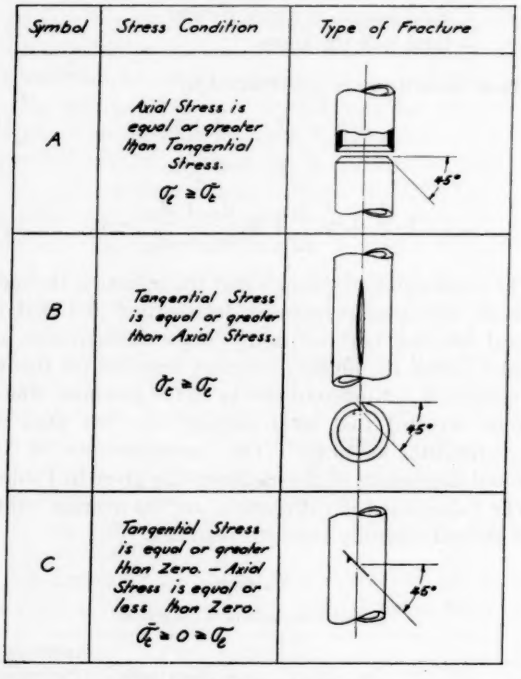

FIG. 4. Diagrams of fracture.

$$\sigma_t = Pa^2[1 + (b^2/r^2)]/(b^2 - a^2) \qquad (5)$$

$$\sigma_r = -Pa^2[1 - (b^2/r^2)]/(b^2 - a^2) \qquad (6)$$

where

σ_l = stress in the longitudinal direction
σ_t = stress in the tangential direction
σ_r = stress in the radial direction
L = load in the longitudinal direction
P = internal pressure
b = outer radius
a = inner radius
r = any radial point between a and b

Accordingly, the system of stresses employed in this investigation is a limited triaxial system in which the ratio of the radial to tangential stress is a constant at each radial position—namely,

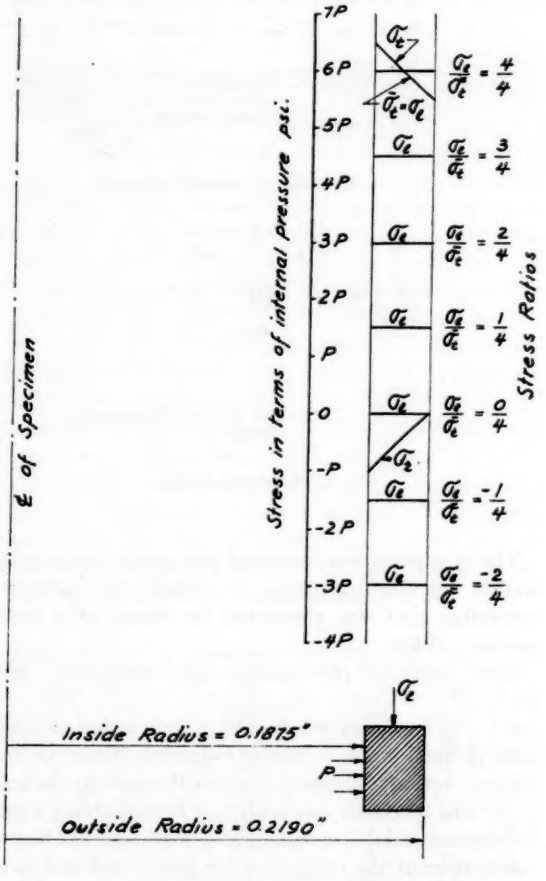
Stress in terms of internal pressure psi.
7P
6P
5P
4P
3P
2P
P
0
-P
-2P
-3P
-4P
Stress Ratios
$\frac{\sigma_l}{\sigma_t} = \frac{4}{4}$
$\frac{\sigma_l}{\sigma_t} = \frac{3}{4}$
$\frac{\sigma_l}{\sigma_t} = \frac{2}{4}$
$\frac{\sigma_l}{\sigma_t} = \frac{1}{4}$
$\frac{\sigma_l}{\sigma_t} = \frac{0}{4}$
$\frac{\sigma_l}{\sigma_t} = \frac{-1}{4}$
$\frac{\sigma_l}{\sigma_t} = \frac{-2}{4}$
$\sigma_t = \sigma_l$
σ_l
σ_t
σ_l
σ_l
σ_t
σ_l
σ_t
σ_l
$\sigma_t

outer wall. For each ratio σ_l/σ_t employed in the test the corresponding values of σ_l are given in Fig. 5.

The application of these equations to the plastic region may be questioned. It is obvious that σ_l may be calculated as given in Eq. (4) for the plastic region since it merely represents the total load divided by the area. It is also obvious that $\sigma_r = -P$ at the inside wall and $\sigma_r = 0$ at the outside wall as a result of the boundary conditions irrespective of whether the strains are elastic or plastic as well as elastic. The trend of σ_r with the radial position may be altered as a consequence of plastic deformation, but, as will be demonstrated later, the variation of σ_r with the radial position does not enter into the final discussion and does not alter any of the proposed analyses on rupture. The only question regarding the application of the above-mentioned formulas to the case where severe plastic deformation may be encountered therefore centers about σ_t. As pressures above the proportional limit are applied it is anticipated that plastic motion first occurs at the inner wall. This will cause σ_t at the inner wall to exhibit a smaller variation with the radial position than exists at lower pressures. In view of the limited existing knowledge on this subject it was believed advisable to approximate the true conditions by assuming that the value of the tangential stress is the average value—namely, $\bar{\sigma}_t = 5.95P$. Eq. (5) then reduced to the thin wall equation

$$\bar{\sigma}_t = Pa/(b - a) \tag{8}$$

As will be shown later the experimental data yield results that agree with this approximation and therefore substantiate this procedure.

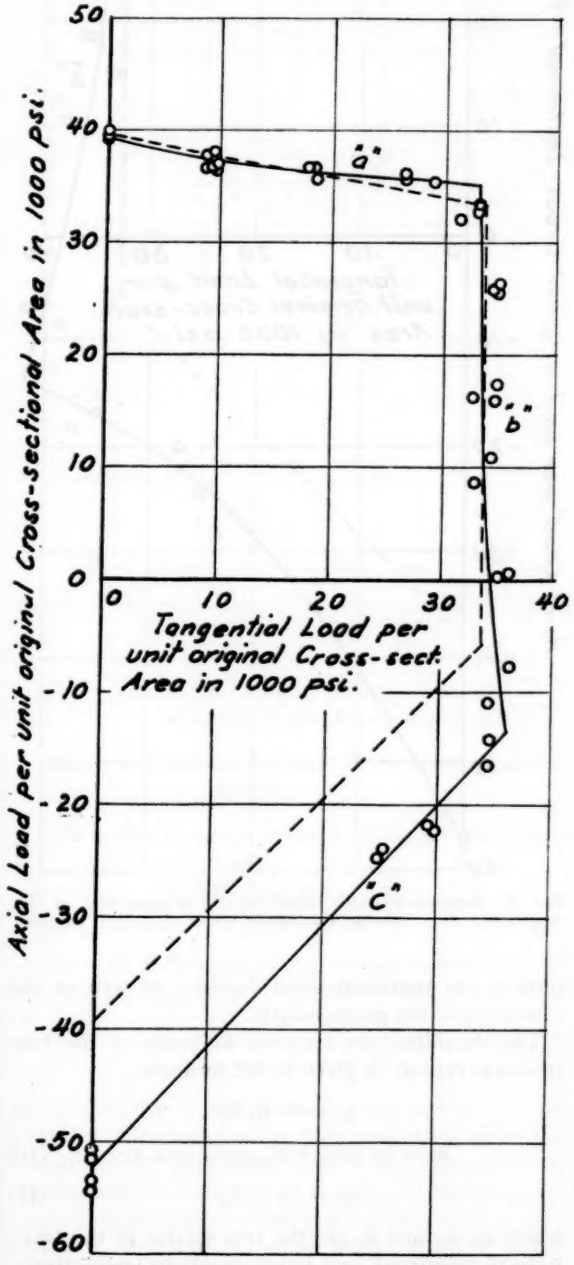

FIG. 6. Rupture strength based on the original area of J-1 magnesium-alloy tubular extrusions under combined stresses.

Although the stress system is triaxial, the conditions of rupture may be plotted on a biaxial stress diagram, since the radial stress is constant for each tangential stress. In Figs. 6, 7, and 8, the stresses at rupture based on the original area in the longitudinal and tangential directions are presented. The upper half of each graph represents a field of combined tension whereas the lower half represents the field of longitudinal compression and tangential tension. The solid curve through the experimental points gives the average values of the stress (load per unit original area) at rupture. All of the magnesium-alloy extrusions investigated gave similar trends of the load per unit original area with combined loading even though they exhibited differences in composition, preferred orientation and microstructure.

Although knowledge of the load per unit original area at rupture is important in certain types of design problems, the true stress at rupture permits a more accurate scientific analysis of the rupture of metals. Therefore, the true stresses at rupture are given in Figs. 9, 10, and 11. Again the general similarity between the alloys may be noted.

The true stresses for rupture follow three different curves, "a," "b," and "c." In the combined tension field where $\sigma_l > \bar{\sigma}_t$, the rupture conditions are given by curve "a," but where $\bar{\sigma}_t > \sigma_l$, the rupture conditions follow curve "b." In the field of combined tension and compression the rupture conditions are given by curve "c," which is at approximately 45° to the coordinate system. Curves "b" and "c" intersect below the $\sigma_l = 0$ axis, the reason wherefore will be analyzed in the discussion.

Corresponding to curve "a," "b," and "c" three types of fractures were noted as given in Fig. 4. Type

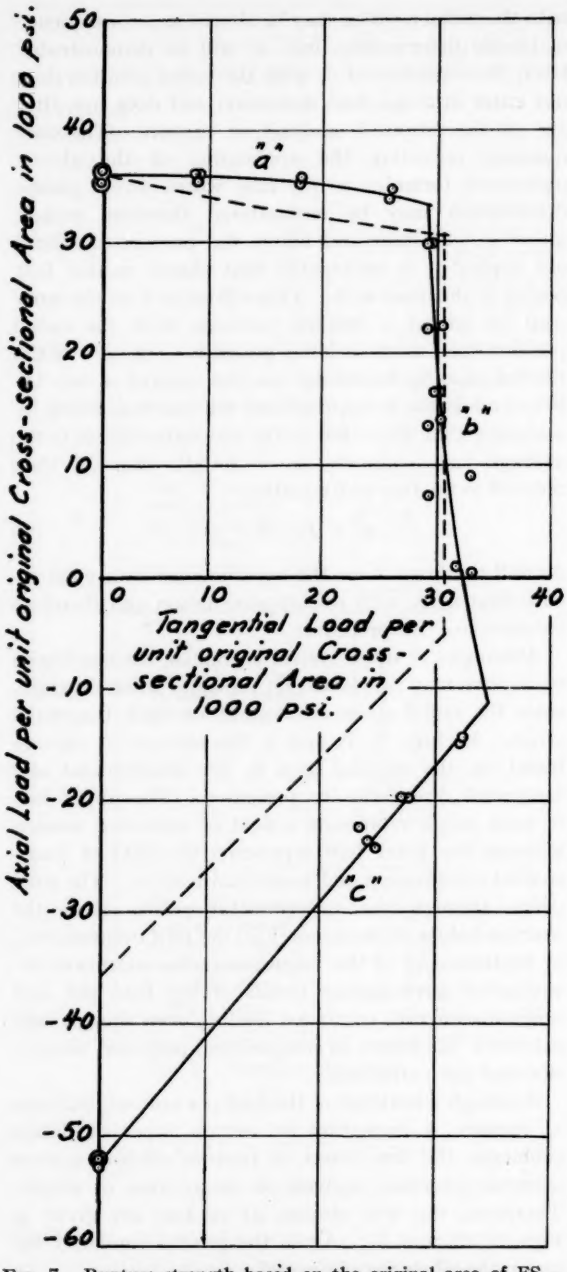

FIG. 7. Rupture strength based on the original area of FS_{-1} magnesium-alloy tubular extrusions under combined stresses.

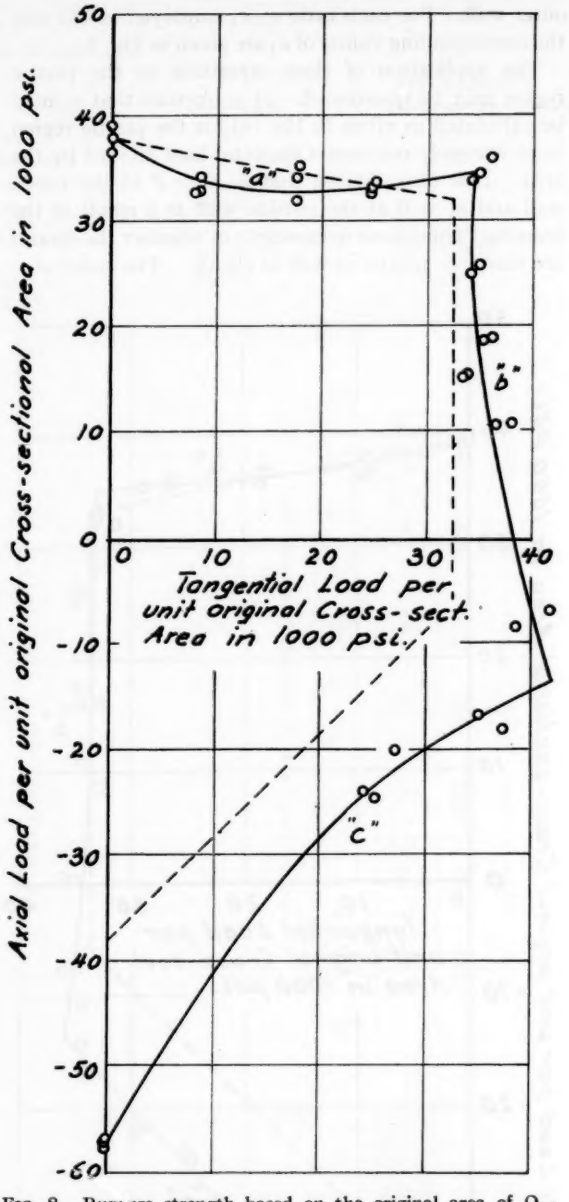

FIG. 8. Rupture strength based on the original area of O_{-1} magnesium-alloy tubular extrusions under combined stresses.

A rupture was obtained along curve "a"; type B, along curve "b"; and type C, along curve "c." The macroscopic angles as nofed in the figure were approximately at 45° to the maximum and minimum principal stress directions.

The ductility of the three alloys was also evaluated in terms of combined stresses because of the importance of this subject in the forming of metals. Inasmuch as these materials did not exhibit local necking, the ductility is the maximum local ductility as well as the average over the gauge length.

The ductilities are recorded in terms of the true strains at rupture as given by the formulas

$$\phi_l = \ln (l_f/l_i) \tag{9}$$

$$\phi_t = \ln [(d_{fo} + d_{fi})/(d_{io} + d_{ii})] \tag{10}$$

$$\phi_r = \ln (t_f/t_i) \tag{11}$$

where ϕ_l, ϕ_t, and ϕ_r are the true strains in the longitudinal, tangential, and radial directions, respectively, and

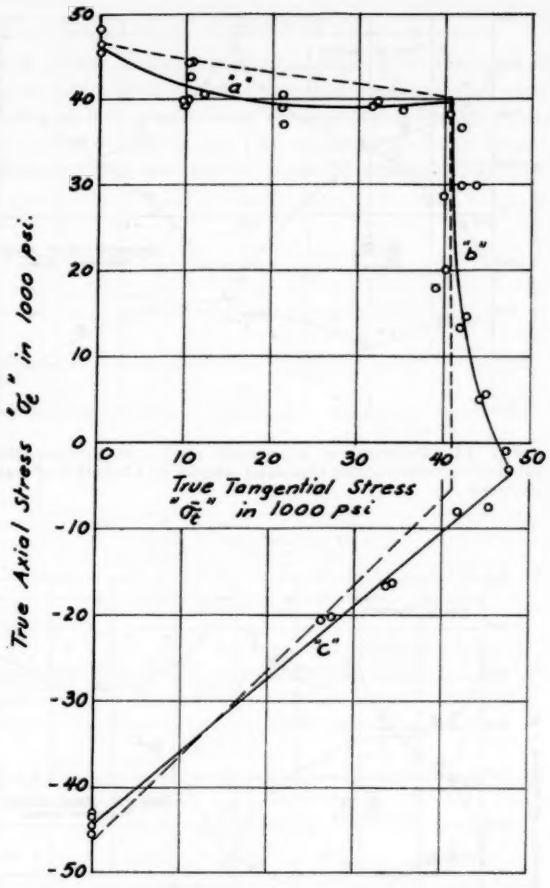

FIG. 9. True rupture strength of J_{-1} magnesium-alloy tubular extrusions under combined stresses.

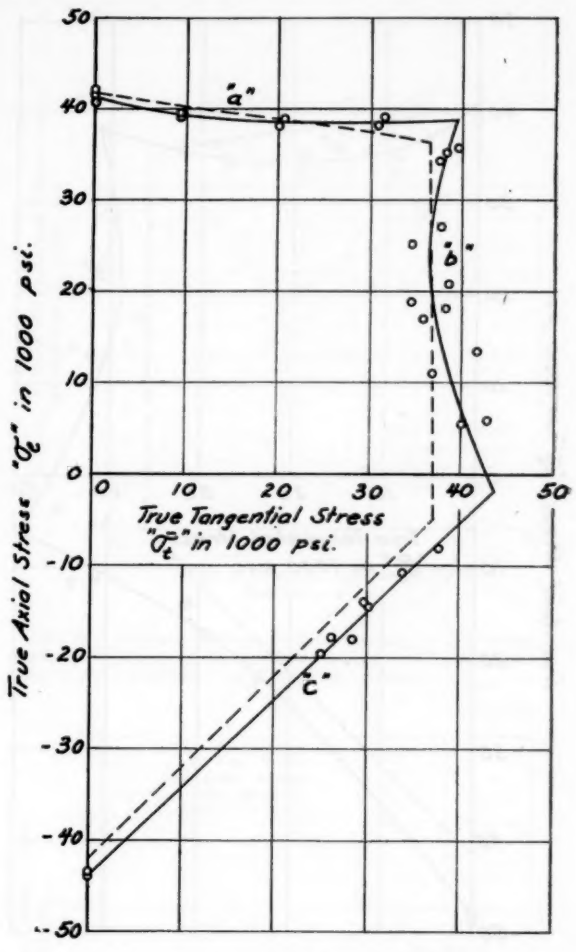

FIG. 10. True rupture strength of FS_{-1} magnesium-alloy tubular extrusions under combined stresses.

l_f = final longitudinal gauge length
l_i = initial longitudinal gauge length
$\frac{\pi}{2}(d_{fo} + d_{fi})$ = final average circumferential gauge length
$\frac{\pi}{2}(d_{io} + d_{ii})$ = initial average circumferential gauge length
t_f = final thickness
t_i = initial thickness

On the basis of the constancy of volume before and after deformation the above equations are interrelated by

$$\phi_l + \phi_t + \phi_r = 0 \qquad (12)$$

The ductility of the alloys is given in Figs. 12, 13, and 14. The ordinates are the various values of the true strain and the abscissae are those of the arbitrary dimensionless function $(\bar{\sigma}_t - \sigma_l)/|\sigma_{max.}|$, where $\sigma_{max.}$ is $\bar{\sigma}_t$ or σ_l, depending on which is a maximum. For pure tension $\bar{\sigma}_t = 0$ and $(\bar{\sigma}_t - \sigma_l)/|\sigma_{max.}|, = -1$. Under conditions of equal biaxial tension, $\sigma_l/\bar{\sigma}_t = 4/4$ and $(\bar{\sigma}_t - \sigma_l)/|\sigma_{max.}|, = 0$. For pure tangential tension, $\sigma_l = 0$ and $(\bar{\sigma}_t - \sigma_l)/|\sigma_{max.}|, = +1$. For equal longitudinal compression and tangential tension $\sigma_l/\bar{\sigma}_t = -4/4$ and $(\bar{\sigma}_t - \sigma_l)/|\sigma_{max.}|, = +2$; for pure longitudinal compression $\bar{\sigma}_t = 0$ and $(\bar{\sigma}_t - \sigma_l)/|\sigma_{max.}|, = +1$. All three of the alloys exhibited approximately the same relationships of the true strains with combined stresses. One difference was shown by the O_{-1} alloy, which yielded a different type of curve over the range of $(\bar{\sigma}_t - \sigma_l)/|\sigma_{max.}|$, from 1 to 2 from the other alloys. The discontinuities in the strains with changes in combined stress, however, are more significant than this singularity. The discontinuities in the true strains agree with the discontinuities in the true stress curves at rupture as a function of combined stresses. Uniform changes in the true strains with changes in stress are noted over curve "a" corresponding to the A type of fracture. When the stress curve changes abruptly to type "b," the fracture becomes type B and the true strains exhibit a similar discontinuity. Discontinuities are also observed in the true strains as the true rupture stresses

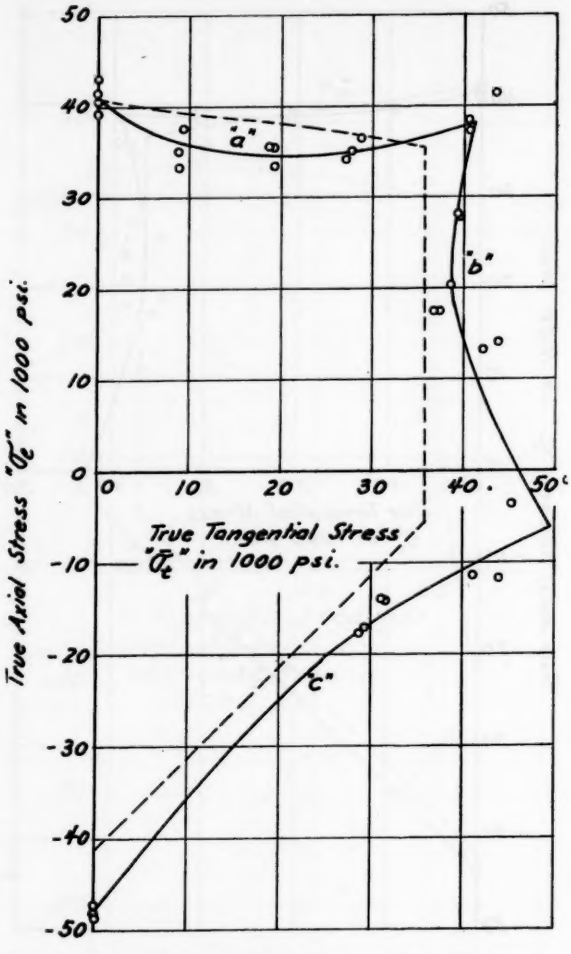

FIG. 11. True rupture strength of O_{-1} magnesium-alloy tubular extrusions under combined stresses.

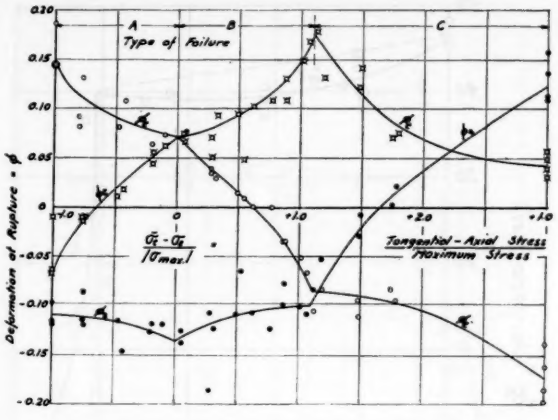

FIG. 12. Deformation at rupture of J_{-1} magnesium-alloy tubular extrusions under combined stresses as a function of state of stress.

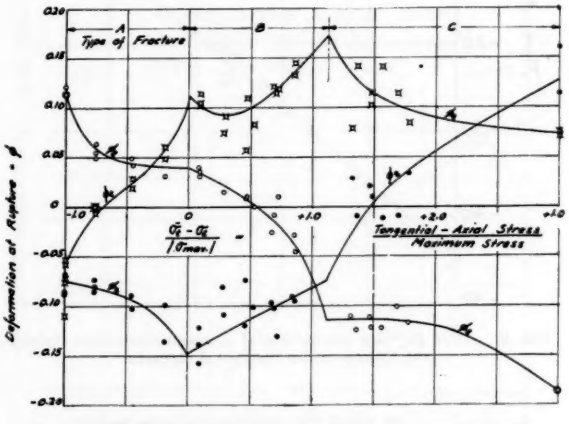

FIG. 13. Deformation at rupture of FS_{-1} magnesium-alloy tubular extrusions under combined stresses as a function of state of stress.

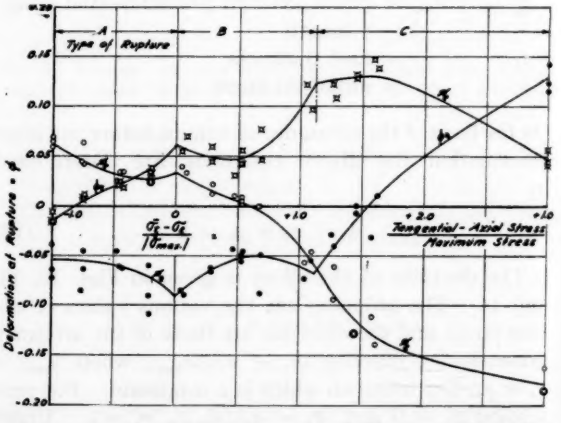

FIG. 14. Deformation at rupture of O_{-1} magnesium-alloy tubular extrusions under combined stresses as a function of state of stress.

change from curve "b" to curve "c" and the fracture changes from type B to type C.

In order to evaluate the effect of work hardening on the data it is necessary to obtain a measure of the strain. In simple longitudinal tension or compression this is easily accomplished by using the absolute value of the true strain in the longitudinal direction. For combined stresses a somewhat similar measure can be used. As can be seen from Eq. 12 the absolute value of the maximum principal strain is equal to one-half of the sum of the absolute values of the true strains or

$$2|\phi_{max.}| = |\phi_t| + |\phi_t| + |\phi_r| \qquad (13)$$

The sum of the absolute values of the true strains as a function of combined stresses is shown in Figs. 15, 16, and 17, and twice the principal shear stress at rupture is plotted as a function of the sum of the absolute values of the true strains at rupture, which is shown in Figs. 18, 19, and 20. For the latter, three curves are obtained for each graph corresponding to the three types of fractures.

Discussion

A review of the important literature[6] on the rupture of metals reveals that it is generally believed that ductile metals fracture when the maximum tensile stress exceeds a critical value. An idealized curve for tensile rupture under pure biaxial stresses is shown in Fig. 21a. Comparison of this figure with Figs. 9, 10, and 11 reveals that this mode of failure was not obtained in the current investigation. The stress combinations at rupture based on the critical shear stress law are shown in Fig. 21b. This curve is in qualitative agreement with the observations, indicating that the ruptures that were obtained were shear-type ruptures.

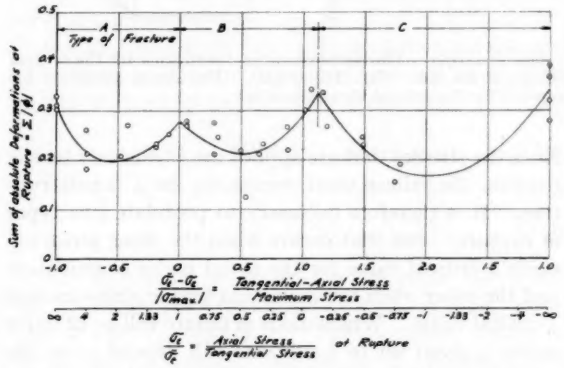
A
Type of Fracture
B
C
Sum of absolute Deformations at Rupture = Σ/ϕ/
Tangential - Axial Stress / Maximum Stress
Axial Stress / Tangential Stress at Rupture

FIG. 15. Sum of absolute principal deformations of J_{-1} magnesium-alloy tubular extrusions under combined stresses as a function of a state of stress.

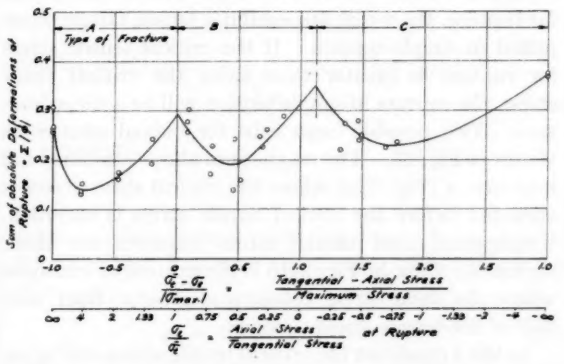
A
Type of Fracture
B
C
Sum of absolute Deformations at Rupture = Σ/ϕ/
Tangential - Axial Stress / Maximum Stress
Axial Stress / Tangential Stress at Rupture

FIG. 16. Sum of absolute principal deformations of FS_{-} magnesium-alloy tubular extrusions under combined stresses as a function of state of stress.

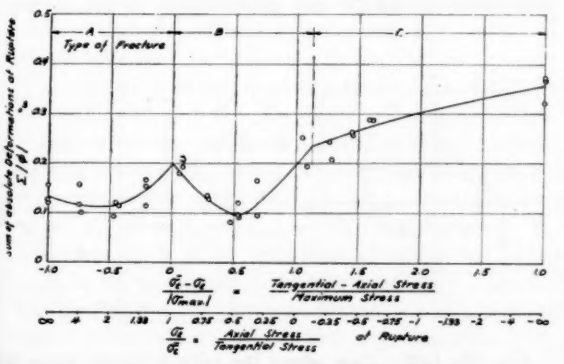

FIG. 17. Sum of absolute principal deformations of O_{-1} magnesium-alloy tubular extrusions under combined stresses as a function of state of stress.

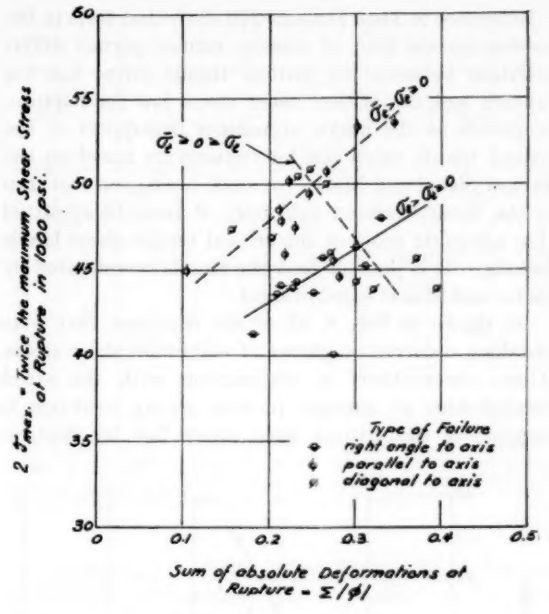
2 τmax. = Twice the maximum Shear Stress at Rupture in 1000 psi.
Sum of absolute Deformations at Rupture = Σ/ϕ/
Type of Failure
right angle to axis
parallel to axis
diagonal to axis

FIG. 18. Maximum shear stress at rupture as a function of the sum of absolute principal deformations for J_{-1} magnesium-alloy tubular extrusions under combined stresses.

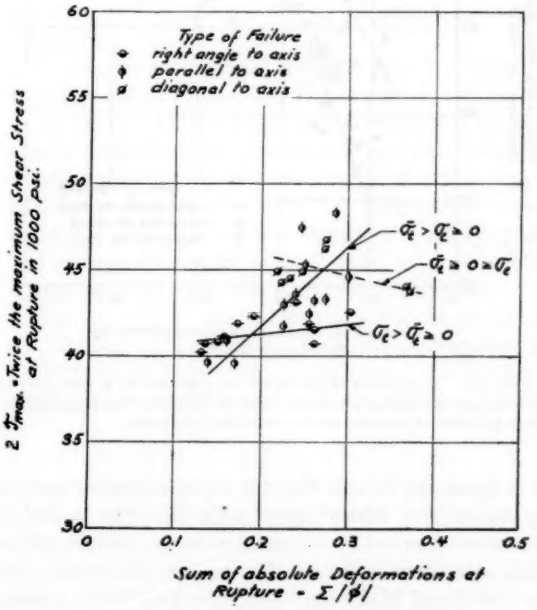
Type of Failure
right angle to axis
parallel to axis
diagonal to axis
2 τmax. = Twice the maximum Shear Stress at Rupture in 1000 psi.
Sum of absolute Deformations at Rupture = Σ/ϕ/

FIG. 19. Maximum shear stress at rupture as a function of the sum of absolute principal deformation for FS_{-1} magnesium-alloy tubular extrusions under combined stresses.

Reference to Figs. 21a and 21b show that tests in the tension-tension field of stresses cannot permit differentiation between the critical tensile stress law for rupture and the critical shear stress law for rupture. Inasmuch as the major arguments in support of the critical tensile stress law for rupture are based on the data of Siebel and Maier[1] for steel, brass, and cast iron in the tension-tension field only, it must be admitted that adequate proof of the critical tensile stress law is lacking. It is possible that the metals investigated by Siebel and Maier[1] failed in shear.

As shown in Fig. 4, all of the fractures that were obtained occurred on planes of maximum shear stress. These observations in conjunction with the stress relationships at rupture provide strong evidence in support of the critical shear stress law for rupture.

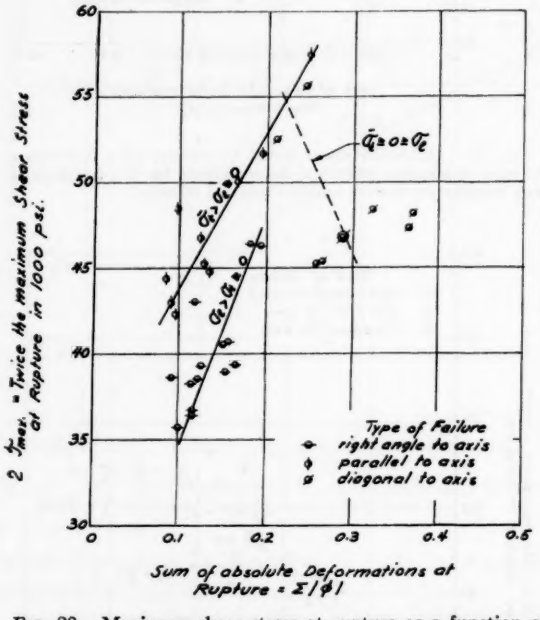

FIG. 20. Maximum shear stress at rupture as a function of the sum of absolute principal deformations for O_{-1} magnesium-alloy tubular extrusions under combined stresses.

It is significant to note that the rupture planes observed by Siebel and Maier[1] agree with the type A and B fractures observed by the authors on magnesium alloys. This agreement indicates that the metals investigated by Siebel and Maier may also have failed with a shear rupture.

Not all fractures can be shear fractures. Ductile metals in pure compression are subjected to high shear stresses. When their limit of ductility is exceeded they generally burst open on a plane parallel to the compression stress. This may result from the fact that the specimen acquires a barrel shape that induces circumferential tensile stresses. Metals under equal triaxial tension are not subjected to a shear stress. Nevertheless, a metal subjected to these stresses will fracture.

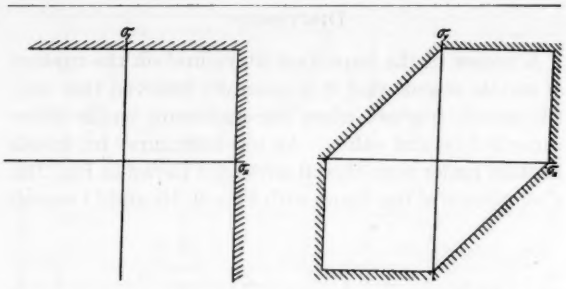

FIG. 21a (*left*). The stress condition for rupture for the critical tensile stress law. FIG. 21b (*right*). The stress condition for rupture for the critical shear stress law.

Since the stresses that are applied are exclusively tensile stresses, the failure must necessarily be a tensile rupture. It is therefore necessary to postulate two types of rupture: one that occurs when the shear stress exceeds a critical value for the metal under examination and the other when the maximum tensile stress exceeds a critical value. Which mode of failure will be effective under a given set of conditions will depend upon the relative magnitudes of the critical tensile stress and the critical shear stress for the metal, as well as the combination of stresses applied. If the critical tensile stress for rupture is less than two times the critical shear stress for rupture, the metal will exhibit a tensile failure when pulled in simple tension. If the critical tensile stress for rupture is greater than twice the critical shear stress, the rupture in simple tension will be a shear fracture. Two possible cases exist for biaxial stresses as shown in Fig. 22. The magnesium alloys examined fall into case a (Fig. 22a) where the critical shear stress is exceeded before the critical tensile stress is exceeded. Consequently, all biaxial stress fractures are shear ruptures. Case b(Fig. 22b) is illustrative of examples where the shear stress cohesion is greater than one-half of the tensile stress cohesion.

In the I quadrant the critical tensile stress will be exceeded before the critical shear stress and a tensile rupture will result. Since there are no tensile stresses in the III quadrant, shear ruptures will occur here. Quadrants II and IV may exhibit shear or tensile rup-

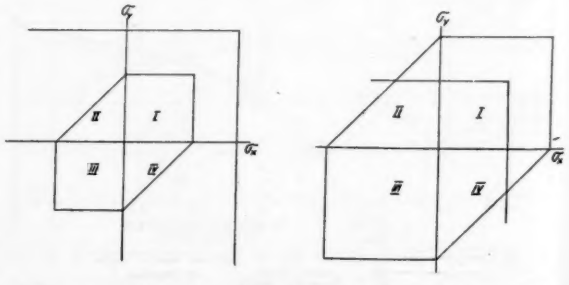

FIG. 22a (*left*). Case where the critical tensile stress for rupture is greater than twice the critical shear stress for rupture. Fig. 22b (*right*). Case where the critical tensile stress for rupture is less than twice the critical shear stress for rupture.

tures dependent upon the stress ratios and the relative orders of magnitude of the critical shear stress and the critical tensile stress. If, in case b, the critical shear stress for rupture of a given metal is infinitely great, only tensile ruptures will be obtained. The determination of the critical conditions of rupture of metals should prove a fertile field of investigation not only because of the theoretic significance attached to such studies but equally because of the practical importance of this topic.

Ros and Eichinger[9] have suggested that the relationship between stresses and plastic strains for isotropic metals is given by the following equations:

$$\phi_l = (1/D)[\sigma_l - {}^1/_2(\sigma_t + \sigma_r)] \tag{14}$$

$$\phi_t = (1/D)[\sigma_t - {}^1/_2(\sigma_r + \sigma_l)] \tag{15}$$

$$\phi_r = (1/D)[\sigma_r - {}^1/_2(\sigma_l + \sigma_t)] \tag{16}$$

These equations are analogous to those for elastic strains where Young's modulus E replaces D and where Poison's ratio μ replaces $^1/_2$. The coefficient $^1/_2$ appears in the above equations because of the assumption of constancy of volume under plastic deformation.

In the present investigation the average stress in the tangential direction is

$$\bar{\sigma}_t = 5.95P \tag{17}$$

and the average stress in the radial direction is

$$\bar{\sigma}_r = -0.5P \tag{18}$$

Therefore

$$\bar{\sigma}_r = -0.083\bar{\sigma}_t \tag{19}$$

Assuming that these average values may be introduced into Ros and Eichinger's equations, the following is obtained:

$$\phi_l = (1/D)(\sigma_l - 0.459\bar{\sigma}_t) \tag{20}$$

$$\phi_t = (1/D)(1.041\bar{\sigma}_t - 0.5\sigma_l) \tag{21}$$

$$\phi_r = (1/D)(0.583\bar{\sigma}_t - 0.5\sigma_l) \tag{22}$$

The value of $1/D$ may be determined from the deformation and the critical shear stress for rupture in simple tension. For example, in the case of J_{-1} alloy, ϕ_l at rupture in simple tension is 0.145, $\sigma_l = 46{,}500$ lbs. per sq.in., and $\bar{\sigma}_t = 0$. Therefore $1/D = 0.145/46{,}500 = 3.12 \times 10^{-6}$. Assuming that the critical shear stress law applies and neglecting differences in work hardening, rupture will occur when $\sigma_l - \sigma_{r\ max.} = 46{,}500$ along curve "a," when $\bar{\sigma}_t - \sigma_{r\ max.} = 46{,}500$ along curve "b," and when $\bar{\sigma}_t - \sigma_l = 46{,}500$ along curve "c," where $\sigma_{r\ max.}$ is the minimum radial tensile stress. Introducing these values into Ros and Eichinger's equations for plastic deformations yields a first approximation of the deformations at fracture. The calculated values given in Fig. 23 may be compared with the experimental data of Fig. 12. The good agreement between the calculated

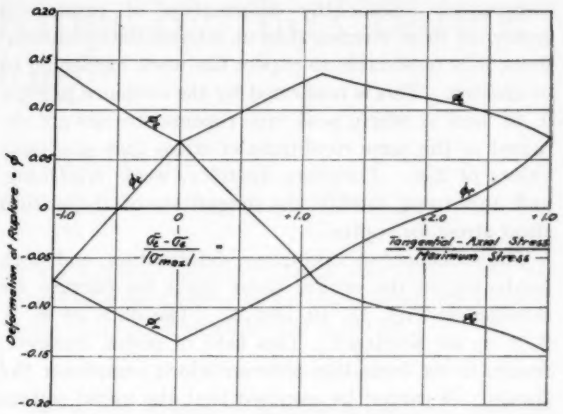

FIG. 23. Predicted deformation at rupture of J_{-1} magnesium-alloy tubular extrusions under combined stresses as a function of state of stress as calculated from Eqs. (20), (21), and (22) and the maximum critical shear stress law for rupture.

and experimental results proves the utility of Ros and Eichinger's relationships. It is possible to calculate the deformations of isotropic materials under combined stresses from the simple tensile stress strain data and a knowledge of the type of rupture. In the cases of FS_{-1} alloy and O_{-1} alloy, the agreement is not so good as for J_{-1} alloy. This is attributed to the greater isotropy of J_{-1} alloy.

It has been suggested by previous investigators[10] that the values in Ros and Eichinger's equations may be a function of the stress combinations. This point can be determined by plotting the calculated $\Sigma|\phi|$ as a function of the combined stresses as shown in Fig. 24 and by comparing this with Fig. 15 obtained experimentally. The fair agreement between the calculated and experimental data indicates that, for the combined stresses investigated, D is practically a constant.

Figs. 15, 16, 17, and the theoretic Fig. 24 reveal that the absolute value of the maximum deformation has peak values in pure axial tension, equal axial and tangential tension, pure tangential tension, and pure axial

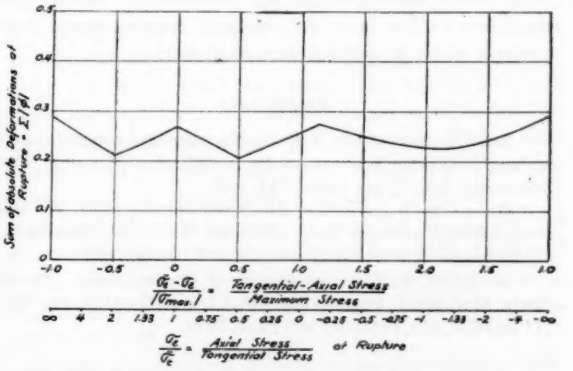

FIG. 24. Predicted sum of absolute principal deformations of J_{-1} magnesium-alloy tubular extrusions under combined stresses as calculated from Eqs. (20), (21), and (22) and the maximum critical shear stress law for rupture.

compression. Since the deformation at rupture is greater at these stresses than at intermediate combinations, it is reasonable to expect the work hardening to be greater. This is confirmed by the evidence in Figs. 9, 10, and 11 where peak true rupture stresses are obtained at the same conditions of stress that give peak values of $\Sigma|\phi|$. Therefore ductility, work hardening, and anisotropy modify the magnitude of the critical shear stress for rupture.

The influences of anisotropy, deformation, and work hardening on the critical shear stress for rupture are recorded in Figs. 18, 19, and 20. The data for $\sigma_t \geq 0 \geq \sigma_l$ are scattered. This field of stress, however, results in the formation of twins which complicate the trends. It cannot be assumed that the metal softens in this field with increasing deformations. It is more probable that those stresses that provide greater deformations are most effective in producing twins. This question was not completely analyzed in the present investigation.

The broken curves of Figs. 6 to 11 were calculated on the basis of knowledge of the deformations and rupture strength in simple tension. The deformations under combined stresses were assumed to be given by the Ros and Eichinger equations, and the critical shear stress law for rupture was assumed to be valid. In this calculation work hardening and anisotropy were neglected. The good agreement between the calculated and experimental curves are conclusive proof of the validity of the critical shear stress law for rupture.

Conclusions

(1) Under biaxial stresses magnesium-alloy extrusions rupture in accordance with the critical shear stress law for rupture.

(2) The deformations obtained for magnesium-alloy extrusions under biaxial stresses agree with predictions based on Ros and Eichinger's equations.

(3) The critical shear stress at rupture is a function of anisotropy, ductility under combined stresses, and work hardening.

(4) Two laws of rupture are postulated: the critical shear stress law and the critical tensile stress law. General cases of rupture were discussed.

References

[1] Siebel, E., and Maier, A. F., *Einfluss des Spannungszustandes auf das Formanderungsvernogen der Metallischen Werkstoff*, VDI Zeitschrift, Vol. 77, pp. 1345–1349, 1933.

[2] Maier, A. F., *Einfluss des Spannungezustandes auf das Formanderungsvermogen der Metallischen Werkstoffe*, dissertation for the degree of Doktor-Ingenieur, V.D.I., Berlin, 1934.

[3] Bridgman, P. W., *Consideration of Rupture under Triaxial Stress*, Mechanical Engineering, Vol. 61, Nos. 2 and 6, pp. 107–111 and 477, 478, February and June, 1939.

[4] Bridgman, P. W., *Reflections on Rupture*, Journal of Applied Physics, Vol. 9, pp. 517–528, 1938.

[5] Bridgman, P. W., *Recent Work in the Field of High Pressures*, American Scientist, Sigma Xi Quarterly, Vol. 31, No. 1, pp. 1–35, January, 1943.

[6] Gensamer, M., *Strength of Metals under Combined Stresses*, 106 pp.; American Society for Metals, Cleveland, 1941.

[7] Morell, L. G., and Hanawalt, J. D., *X-ray Study of the Plastic Working of Magnesium Alloys*, Physics, a Journal of General and Applied Physics, Vol. 3, No. 4, pp. 161–168, October, 1932.

[8] Barrett, C. S., *The Stereographic Projection*, Transactions of the Institute of Metals Division, Institute of Metals, New York, 1937.

[9] Ros, M., and Eichinger, A., *Versuche zu Klarung der Frage der Bruchgefahr*, Diskussions, Bericht Nummer 34, Materialprufungsanstalt an der E. T. H., Zürich, 1929.

[10] Nadai, A., *Plasticity;* McGraw-Hill Book Company, Inc., New York, 1931.

[11] Lessels, J. M., and Macgregor, C. W., *Certain Phases of the Combined Stress Problem*, Proceedings of the Fifth International Congress of Applied Mechanics, Cambridge, Mass., pp. 201–206, September, 1938.

[12] Lessels, J. M., and Macgregor, C. W., *Combined Stress Experiments on a Nickel-Chrome Molybdenum Steel*, Journal of the Franklin Institute, pp. 163–181, August, 1940.

[13] von Kármán, Th., *Mitteilungen über Forschungsarbeit*, VDI Vol. 118, 1913.

[14] Turner, L. B., *Stresses in a Thick Hollow Cylinder Subjected to Internal Pressure*, Cambridge Philosophical Transactions, Vol. 21, p. 50, 1908–1912.

[15] Taylor, G. I., and Quinney, H., *The Plastic Distortion of Metals*, Philosophical Transactions of the Royal Society, Vol. 230, pp. 323–362, November, 1931.

[16] Gough, H. J., and Pollard, H. V., *The Strength of Metals under Combined Alternating Stresses*, Proceedings of the Institution of Mechanical Engineers, Vol. 131, pp. 3–103, 1935.

[17] Timoshenko, S., *Theory of Elasticity;* McGraw-Hill Book Company, Inc., New York, 1934.

[18] Lode, W., *Versuche über den Einfluss der mittleren Hauptspannung auf die Fliessgrenze*, Zeitschrift für angewandte Mathematik und Mechanik, Vol. 5, pp. 142–144, 1925.

[19] Marin, J., *A Method of Defining Failure in Members Subjected to Combined Stresses*, Transactions, American Society for Metals, pp. 1013–1021, December, 1941.

[20] Marin, J., *Failure Theories of Materials, Subjected to Combined Stresses*, American Society of Civil Engineers Proceedings, Vol. 61, No. 6, August, 1935.

[21] Beck, A., *The Technology of Magnesium and Its Alloys;* F. A. Hughes and Co., Limited, London, 1940.

[22] *Dowmetal Laboratory Methods*, Bulletin No. D.M. 41, The Dow Chemical Company, Midland, Mich., 1941.

[23] Bakarian, P. W., *Preferred Orientation in Rolled Magnesium and Magnesium Alloys*, Technical Publication No. 1355, American Institute of Mining and Metallurgical Engineers, Inc., August, 1941.

[24] Davey, W. P., *Study of Crystal Structure and Its Applications;* McGraw-Hill Book Company, Inc., New York, 1934.

[25] Clark, G. L., *Applied X-rays;* McGraw-Hill Book Company, Inc., New York, 1932.

[26] Glocker, R., *Materialprufung mit Rontgenstrahlem;* Julius Springer, Berlin, 1937.

[27] Schmid, E., and Boas, W., *Kristallplastizitzt;* Julius Springer, Berlin, 1935.

Analysis of Fuselage Rings by the Column Analogy

DONALD A. DUPLANTIER*

Consolidated Vultee Aircraft Corporation

INTRODUCTION

THE PURPOSE OF THIS PAPER is to review the column analogy method of analyzing beams, arches, and rigid frames and illustrate its applicability to the analysis of airplane fuselage rings. It is acknowledged that the subject of ring analysis has already received considerable attention, but it is believed that the column analogy method has specific advantages that merit its presentation. In general, an analogy is useful for the purpose of making computations semiautomatic, free from confusion of signs, and comparatively rapid. The column analogy method accomplishes these objectives, and its usefulness increases with the complexity of loading.

The method was developed by Cross,[1] of Yale University, and subsequently received a lucid discussion by Grinter,[2] of the Illinois Institute of Technology, to whom the author is indebted for the development of the basic concept presented herein. The analogy is most useful when applied to a beam structure having three redundants, such as a fixed-end beam, arch, rigid frame, or closed ring. It applies with equal simplicity to either symmetrical or unsymmetrical rings and to any type of loading. The column analogy utilizes the classic fundamental equations of continuity but attributes to them a new, clear-cut significance that eliminates all confusion of signs and manipulation.

BASIC CONCEPT

Let it be assumed that there is under investigation a threefold statically indeterminate beam structure such as a fixed-end beam, arch, rigid frame, or a closed ring, loaded in any manner and that it is required to compute the internal bending moment at successive points on the structure.

Cut the given indeterminate structure in any convenient manner to produce a stable, statically determinate *base structure* and compute, at successive points, the resulting applied moment referred to as M_s, the *static moment*. It then follows that at *any point* in the original uncut structure the actual applied moment, M, can be considered to be made up of two component parts—namely, the statically determinate moment, M_s, as previously defined, and a statically indeterminate moment, called M_i, which is to be determined by use of the column analogy. These two component moments may be additive or subtractive and the relationship can be generalized by the equation

$$M = M_s \pm M_i \tag{1}$$

In Eq. (1) M_s may be positive or negative, according to the sign convention adopted. If the given structure is a horizontal fixed-end beam and the usual sign convention is adopted, then M_s (also M) will be considered as *positive* if it tends to cause *compression* at the *top face* of the beam and negative if opposite. For a closed-ring structure, where there is no clear-cut top and bottom to the ring rib, the usual convention is to designate M_s (also M) as *positive* if it tends to cause *compression* at the *inner face* of the ring and negative if opposite.

The plus-and-minus sign of M_i is merely to indicate that it may add to or subtract from the M_s value at any random station. This is a generalized statement, and in a given solution all ambiguity will be *definitely* removed, as will be shown later, by applying the fundamental principle that M_i must reduce M_s *numerically* at the *point* where M_s is a *maximum*. This condition must be true, otherwise the determinate structure would have smaller moments than the indeterminate structure, which is an obvious fallacy.

An analogous column can now be defined as an *imaginary* column:

(1) Whose height has no significance.

(2) Whose cross section is of such a shape that (a) its centerline is identical to the longitudinal axis of the redundant beam structure under investigation, and (b) its transverse width at any point is numerically equal to the reciprocal of the product, EI, of the redundant beam structure at the corresponding point.

(3) Whose applied compressive (or tensile) unit load (load per unit area such as pounds per square inch) on any differential area, $dA = ds(1/EI)$, of its cross section is *numerically* equal to the static moment, M_s, existing at the corresponding point on the *base structure*.

In part (2b), above, E is the modulus of elasticity of the material constituting the given beam structure and I is the moment of inertia of the beam structure's cross section at the point in question, about its appropriate centroidal axis.

In part 3, a positive M_s will be translated into a compressive (positive) load on the analogous column and a negative M_s into a tensile (negative) load.

Received August 20, 1943.

* Chief of Structures, Nashville Division.

As will be shown later, the reacting stresses at the base of such an analogous column will be *numerically* equal to the indeterminate components, M_i, of the total moments, M, in Eq. (1), and the values are computed in the usual manner of analyzing an eccentrically loaded column, as expressed by:

$$M_i = f = (W/A) \pm (M_z z/I_z) \pm (M_x x/I_x) \quad (2)$$

where

A = $\sum \Delta A = \sum \Delta s(1/EI)$ = total cross-sectional area of the analogous column

x, z = location of any specific area increment, ΔA, of the column section, relative to principal centroidal axes z–z and x–x, respectively

I_x, I_z = moments of inertia of the column section about the x–x and z–z axes, respectively

W = $\sum (M_s)\Delta A$ = total *applied* load on the column

M_x, M_z = total *applied* moments on the column, about the x–x and z–z axes, respectively, due to any eccentricity of load, W

f = reacting stress in the analogous column at any point fixed by the x and z coordinates defined above

The plus-and-minus signs in Eq. (2) are merely generalizations to indicate that the algebraic sum of the stresses is intended—that is, add like stresses and subtract unlike stresses. In an actual application addition only is indicated, and the correct senses of the component parts are automatically taken care of by calling applied compressive loads positive and tensile loads negative and by assigning positive values to the x and z ordinates, which are to the right of and above the z–z and x–x centroidal axes, respectively; negative values, if to the left of and below these axes.

Sign-Convention

As explained above the signs of the M_i values, which are numerically equal to the reacting stresses of the analogous column, follow from the easily remembered rule: *Consider compressive stresses in the column as positive and, in Eq. (2), add like stresses and subtract unlike stresses.*

These individual values of M_i, each obtained from a separate calculation, have *only relative sense.* Their absolute sense, to be used when combined with M_s in Eq. (1) comes automatically from the knowledge, as previously mentioned, that M_i must reduce M_s numerically at the point where M_s is a maximum.

To illustrate, assume that the maximum value of M_s is +15 in.lbs. (compression on inner face of ring) and the corresponding value of M_i, as obtained from Eq. (2), is +12 in.lbs. Since M_i *must* numerically reduce M_s at this critical point, Eq. (1) must read $M = M_s - M_i$ when applied to this problem. This would have been true also if $M_s = -15$ and $M_i = -12$. On the other hand, if $M_s = +15$ and $M_i = -12$ or $M_s = -15$ and $M_i = +12$, then Eq. (1) would have to read $M = M_s + M_i$.

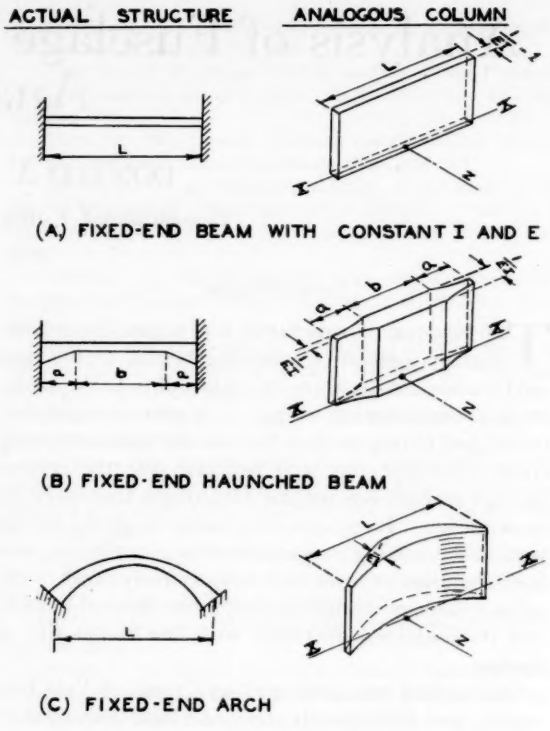

FIG. 1. The analogous columns for typical beam structures.

It may appear, superficially, that this sign convention is little, if any, better than a "hunch" convention and is not foolproof, but this is not the case. A careful analysis of the preceding statements and the succeeding illustrative problems will lead to the positive conclusion that this method is in reality free from any confusion in signs and is thoroughly reliable.

Fig. 1 illustrates the analogous columns for typical beam structures. Applied loads have been omitted for the sake of clarity. It will be noted in Fig. 1(A) that for a beam of constant E and constant I the width of the analogous column section can be assigned a value of unity, since only the relative values of these functions are significant. In Fig. 1(B) the haunched beam has a large I at the ends and a small I in the middle. If E is assumed to be constant (relative value equal to unity), then the width of the analogous column is narrow at the ends and wide at the middle, since the width $b = 1/EI$.

DIRECT DERIVATION OF THE COLUMN ANALOGY

It is possible to arrive at the conception of the column analogy either by application of the conventional Neutral Point method of analysis or by utilizing directly the classic equations of continuity. In order to conserve

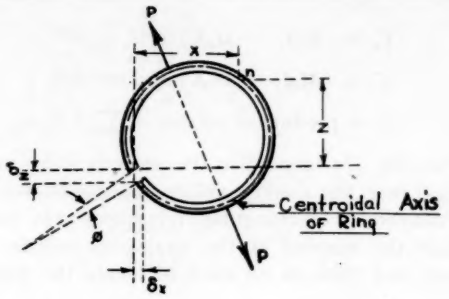

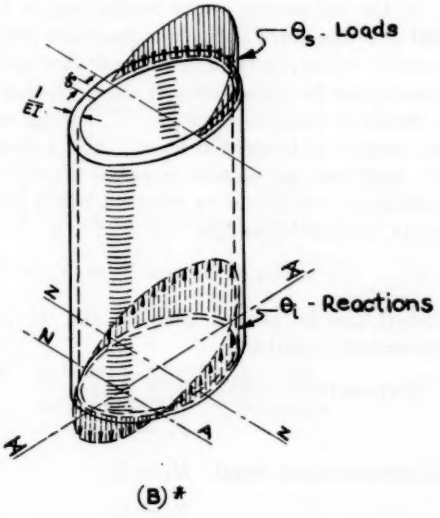

(A)* LOADED RING CUT AT ANY POINT TO FORM BASE STRUCTURE.
(B)* LOADED ANALOGOUS COLUMN.

FIG. 2. The analogous column for a circular ring.

space only the second method will be presented herein.

Consider any closed elastic ring loaded with two equal, opposite, and colinear forces, P, so that the ring is in external equilibrium under the action of these two applied forces, as well as in internal equilibrium. Imagine that the ring is cut entirely through at a single section, as in Fig. 2(A), and that the internal stresses at this section have been replaced by identical external forces to maintain the original state of equilibrium. (These replaced internal stresses are not shown in the figure.) It is evident that the principle of continuity still applies and that there is no relative displacement of the two faces of the cut section. If this relative displacement is resolved into an angular component, ϕ, a horizontal component, δ_x, and a vertical component, δ_z, it follows that:

$$\phi = 0;\ \delta_x = 0;\ \delta_z = 0$$

Each of these displacement components can, in turn, be visualized as made up of two parts: one induced by the external applied loads, P; the other caused by the unknown external reacting forces that have replaced the original internal stresses at the cut section, when both of these force groups act on the determinate cut ring or *base structure*. In accordance with the basic principles of indeterminate stress analysis, it follows that:

$$\phi = \int (M_s ds/EI) + \int (M_i\, ds/EI) = 0 \quad (3)$$

$$\delta_x = \int (M_s\, ds/EI)z + \int (M_i\, ds/EI)z = 0 \quad (4)$$

$$\delta_z = \int (M_s\, ds/EI)x + \int (M_i\, ds/EI)x = 0 \quad (5)$$

where

M_s = the *statically determinate* moment at any point, N, along the centroidal axis of the cut ring, due to the *known applied* loads, P

M_i = the indeterminate moment at the same point, N, due to the *redundant forces* at the *cut section*

I = the moment of inertia of the transverse section of the ring at the point, N, about the appropriate centroidal axis of this section

E = the modulus of elasticity of the ring

x, z = the horizontal and vertical ordinates, respectively, of point, N, with respect to the cut section

ds = a differential length of the ring at point, N

Replace the terms, $M_s\, ds/EI$ and $M_i\, ds/EI$, by the more convenient symbols, θ_s and θ_i, respectively. If the ring axis is divided into relatively small segments, preferably equal, so that the differential, ds, is replaced by the increment, Δs, with the point, N, bisecting this increment, and if the integral sign is replaced by the summation sign; then Eqs. (3), (4), and (5) can be rewritten:

$$\phi = \sum\theta_s + \sum\theta_i = 0 \quad (3a)$$

$$\delta_x = \sum\theta_s z + \sum\theta_i z = 0 \quad (4a)$$

$$\delta_z = \sum\theta_s x + \sum\theta_i x = 0 \quad (5a)$$

If these θ values are visualized as imaginary vertical forces acting on an otherwise unsupported body (the analogous column), the three equations above will express the fact that this body is in equilibrium under the effect of these θ forces—that is:

$$\sum\theta_s + \sum\theta_i = 0 \text{ corresponds to } \sum F_z = 0 \quad (6)$$

$$\sum\theta_s z + \sum\theta_i z = 0 \text{ corresponds to } \sum M_x = 0 \quad (7)$$

$$\sum\theta_s x + \sum\theta_i x = 0 \text{ corresponds to } \sum M_z = 0 \quad (8)$$

Since, for a body in equilibrium, the moments are balanced about any pair of axes, the coordinates x and z will hereafter be considered as referenced to the principal rectangular centroidal axes of the cross section of

the imaginary analogous column—namely, the z–z and x–x axes shown in Fig. 2(B).

If the analogous column is now visualized as indicated in Fig. 2(B) in accordance with the definition previously stated, then—

$\Delta s(1/EI) = \Delta A$, an increment of the cross-sectional area, A

$M_s = p$, the imaginary *applied* load on the column top per unit area

$\theta_s = M_s(\Delta s/EI) = p\Delta A$, the total applied load on ΔA

$M_i = f$, the imaginary *reacting* stress at the column base

$\theta_i = M_i(\Delta s/EI) = f\Delta A$, the total reacting force on ΔA

Referring to Fig. 2 and the preceding discussion, it follows that for the analogous column the *total applied load* is

$$W = \sum\theta_s = \sum p\Delta A = \sum M_s(\Delta s/EI) \qquad (9)$$

The *total tilting moments* caused by any eccentricity of the θ_s loads about the x–x and z–z axes are

$$M_x = \sum(p\Delta A)z = \sum\theta_s z = \sum M_s(\Delta s/EI)z \qquad (10)$$

$$M_z = \sum(p\Delta A)x = \sum\theta_s x = \sum M_s(\Delta s/EI)x \qquad (11)$$

Then, from the conventional theory of combined bending and direct stresses such as used in column design, the resulting *reacting stresses* in the column base are, by Eq. (2),

$$f = (W/A) \pm (M_x z/I_x) \pm (M_z x/I_z)$$

where each term is as previously defined after Eq. (2). Bear in mind that the plus-and-minus signs merely indicate the algebraic sum of the terms, and the result will always be consistent if a compressive load is called *positive* and if *positive* signs are given to z and x ordinates which are *above* and to the *right* of the centroidal axes, with *negative* signs for those opposite. It also follows from the definitions that

$$A = \sum\Delta A = \sum\Delta s(1/EI) \qquad (12)$$

$$I_x = \sum(\Delta A)z^2 \qquad (13)$$

$$I_z = \sum(\Delta A)x^2 \qquad (14)$$

Symmetrical and Unsymmetrical Rings

The analysis of a symmetrical ring (hence, symmetrical analogous column) is easily accomplished through the use of Eq. (2), since an axis of symmetry is also a principal axis; but this equation is tedious when applied to an unsymmetrical ring because it becomes necessary to locate the principal axes. In the latter case of structural dissymmetry it is easier to use the conventional modified form of Eq. (2)—namely,

$$f = (W/A) + C_x x + C_z z \qquad (2a)$$

where

$$C_x = (M_z I_x - M_x K)/(I_x I_z - K^2) \qquad (15)$$

$$C_z = (M_x I_z - M_z K)/(I_x I_z - K^2) \qquad (16)$$

$$K = \text{product of inertia} = \sum(\Delta A)xz \qquad (17)$$

When Eq. (2a) is used in the analysis of an unsymmetrical ring, the x and z values are coordinates along *any* convenient rectangular reference axes passing through the *centroid* of the analogous column cross section, and there is no need to locate the principal axes.

Normal and Shearing Stresses in Ring

At the cut section of the loaded ring in Fig. 2 there will exist the three redundant reactions previously discussed—namely, a bending moment that will have been determined by the solution of the preceding equations; a tensile or compressive force, N_i, normal to the radial cut section (a tangential force); and a shearing force, S_i, along the cut section (a radial force). These two redundant forces can be resolved into x and z components, H_i and V_i, so that

$$H_i = N_{ix} \pm S_{iz} \text{ and } V_i = N_{iz} \pm S_{ix}$$

and it can be proved that H_i and V_i have values *numerically* equal to

(Symmetrical rings) $H_i = M_x/I_x$ (18)

$V_i = M_z/I_z$ (19)

(Unsymmetrical rings) $H_i = C_z$ (20)

$V_i = C_x$ (21)

where C_x and C_z are obtained from Eqs. (15) and (16), respectively. The proper senses of these components can be deduced by inspection of the final moment diagram and the distortion of the given structure.

Once H_i and V_i have been determined, H_n and V_n (the components of the normal and shear forces existing in the ring at any point, N) can be computed by applying $\sum H = 0$ and $\sum V = 0$ in the usual manner, with subsequent determination of N_n and S_n by application of (see Fig. 10)

$$N_n = H_n \cos\alpha_n - V_n \sin\alpha_n \qquad (22)$$

$$S_n = H_n \sin\alpha_n + V_n \cos\alpha_n \qquad (23)$$

Problem 1—Unsymmetrical Ring

Given—The trapezoidal ring shaped and loaded as shown in Fig. 3(A) having a constant cross section and a constant modulus of elasticity.

Required—Compute the internal bending moments at the corners A, B, C, D and the intermediate Stations 1 to 10, inclusive, as well as the normal and shearing forces acting on the cut section.

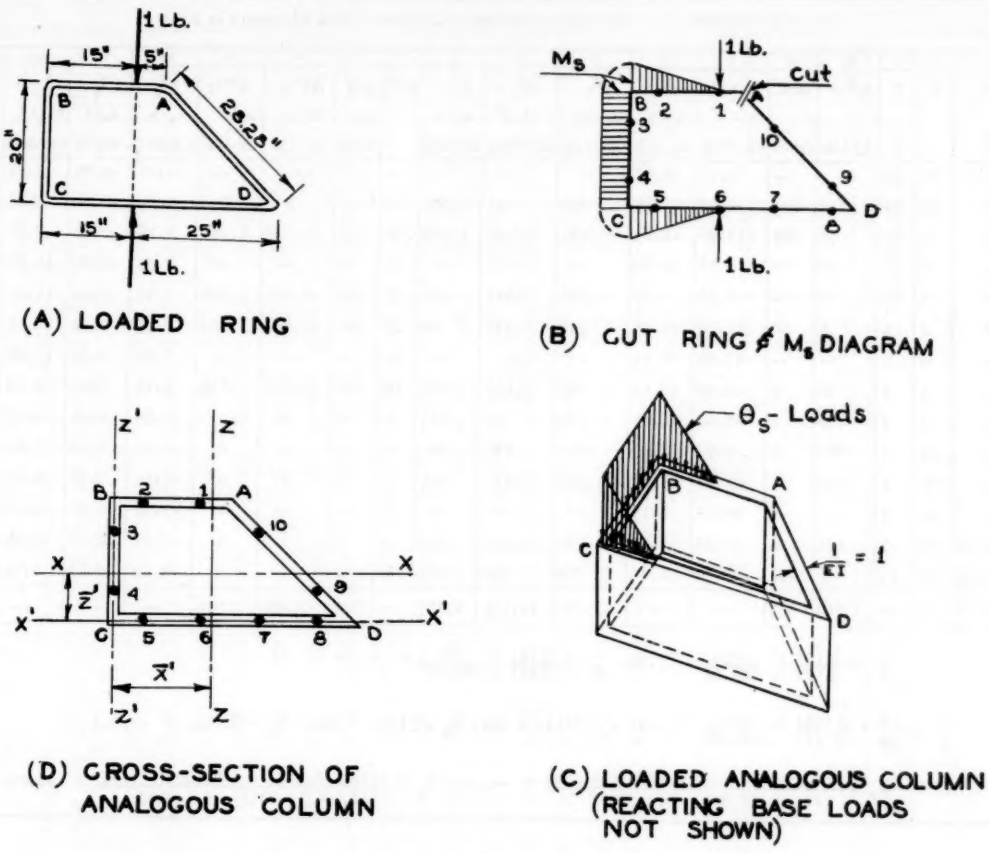

FIG. 3. Unsymmetrical ring analyzed in Problem 1.

Solution (See table 1)

Step 1—Cut the ring at any convenient point, say A, to form the base structure. Divide the ring axis into eight segments 10 in. long ($\Delta s = 10$ in.) and two segments 14.14 in. long ($\Delta s = 14.14$ in.). Locate the centers of these segments and assign to them station numbers 1 to 10, inclusive, see Fig. 3(B). These stations apply also to the section of the analogous column in Fig. 3(D). For each of these divisions compute their respective ΔA values, where $\Delta A = \Delta s/(EI)$, computing the I value at each station point and assuming it to be constant throughout the Δs length. In this problem both E and I are constant and are assigned relative values of unity; hence, in Column (2) of Table 1, $\Delta A = \Delta s$. Note that the accuracy of the solution increases as the "Δs" lengths are decreased, with a consequent increase in the number of stations used.

Step 2—Choose any convenient pair of rectangular references axes, X'–X' and Z'–Z', as in Fig. 3(D). Place in Columns (3) and (4) the x' and z' coordinates of the station centers, calling these values *positive* when to the right of and above the reference axes. Locate the parallel centroidal axes X–X and Z–Z of the analogous column section by extending Columns (5) and (6) and applying equations

$$\bar{x}' = \frac{\sum(\Delta A)x'}{\sum \Delta A} \text{ and } \bar{z}' = \frac{\sum(\Delta A)z'}{\sum \Delta A}$$

Step 3—Compute the section properties of the analogous column with respect to the centroidal axes by extending Columns (7) to (11), inclusive, noting that x and z are *positive* when measured to the right of and above the centroidal axes and *negative* when opposite. This results in

$$A = \sum \Delta A = \sum(2) = 108.28$$
$$K = \sum(\Delta A)xz = \sum(9) = -3290$$
$$I_x = \sum(\Delta A)z^2 = \sum(11) = 6835$$
$$I_z = \sum(\Delta A)x^2 = \sum(10) = 18104$$

Step 4—At each station center compute M_s, the applied moment in the base structure, and place in Column (12), assigning a positive value to any moment tending to cause *compression* on the *inside* of the ring.

Step 5—Extend computations in Columns (13), (14), and (15), resulting in

$$W = \sum M_s(\Delta A) = \sum(13) = 500$$

TABLE 1 (Problem 1). Stresses in Analogous Column, Final Moments in Ring

1	2	3	4	5	6	7	8	9	10	11	12	13	14	15	16	17	18	19
RING STA. NO.	ΔA $\frac{\Delta s}{EI}$	x'	z'	$\Delta A \cdot x'$ (2)·(3)	$\Delta A \cdot z'$ (2)·(4)	x $x'-\bar{x}'$ (3)−17.08	z $z'-\bar{z}'$ (4)−8.15	ΔK $\Delta A \cdot xz$ (2)·(7)·(8)	ΔI_z $\Delta A \cdot x^2$ (2)·(7)·(7)	ΔI_x $\Delta A \cdot z^2$ (2)·(8)·(8)	$p=M_s$	ΔW $p \cdot \Delta A$ (2)·(12)	ΔM_z $\Delta W \cdot x$ (7)·(13)	ΔM_x $\Delta W \cdot z$ (8)·(13)	f_2 $C_x \cdot x$ (−.429)·(7)	f_3 $C_z \cdot z$ (−.071)·(8)	$M_i = f$ $f_1+f_2+f_3$ 4.63+(9)+(17)	M $M_s - M_i$ (12)−(18)
A	--	20	20	--	--	2.92	11.85	--	--	--	0	--	--	--	-1.25	-0.84	2.54	-2.54
1	10	15	20	150	200	-2.08	11.85	-246	43	1,404	0	0	0	0	0.89	-0.84	4.68	-4.68
2	10	5	20	50	200	-12.08	11.85	-1,431	1,459	1,404	10	100	-1,208	1,185	5.19	-0.84	8.98	1.02
B	--	0	20	--	--	-17.08	11.85	--	--	--	15	--	--	--	7.33	-0.84	11.12	3.88
3	10	0	15	0	150	-17.08	6.85	-1,170	2,917	469	15	150	-2,562	1,028	7.33	-0.49	11.47	3.53
4	10	0	5	0	50	-17.08	-3.15	538	2,917	99	15	150	-2,562	-472	7.33	0.22	12.18	2.82
C	--	0	0	--	--	-17.08	-8.15	--	--	--	15	--	--	--	7.33	0.58	12.54	2.46
5	10	5	0	50	0	-12.08	-8.15	985	1,459	664	10	100	-1,208	-815	5.19	0.58	10.40	-0.40
6	10	15	0	150	0	-2.08	-8.15	170	43	664	0	0	0	0	0.89	0.58	6.10	-6.10
7	10	25	0	250	0	7.92	-8.15	-645	627	664	0	0	0	0	-3.40	0.58	1.81	-1.81
8	10	35	0	350	0	17.92	-8.15	-1,460	3,211	664	0	0	0	0	-7.69	0.58	-2.48	2.48
D	--	40	0	--	--	22.92	-8.15	--	--	--	0	--	--	--	-9.84	0.58	-4.63	4.63
9	14.14	35	5	495	71	17.92	-3.15	-798	4,541	140	0	0	0	0	-7.69	0.22	-2.84	2.84
10	14.14	25	15	354	212	7.92	6.85	767	887	663	0	0	0	0	-3.40	-0.49	0.74	-0.74
Σ =	108.28	--	--	1,849	883	--	--	-3,290	18,104	6,835	--	500	-7,540	926	--	--	--	--

$$\bar{x} = \frac{\Sigma(5)}{\Sigma(2)} = \frac{1,849}{108.28} = 17.08; \quad \bar{z} = \frac{\Sigma(6)}{\Sigma(2)} = \frac{883}{108.28} = 8.15''$$

$$f_1 = \frac{W}{A} = \frac{\Sigma(13)}{\Sigma(2)} = \frac{500}{108.28} = 4.63; \; W = \Sigma(13) = 500; \; M_x = \Sigma(15) = 926; \; M_z = \Sigma(14) = -7,540$$

$$C_x = \frac{(-7,540)(6,835) - (926)(-3,290)}{(18,104)(6,835) - (-3,290)^2} = -0.429; \quad C_z = \frac{(926)(18,104) - (-7,540)(-3,290)}{(18,104)(6,835) - (-3,290)^2} = -0.071$$

$$M_x = \sum M_s(\Delta A)z = \sum(15) = 926$$
$$M_z = \sum M_s(\Delta A)x = \sum(14) = -7540$$
$$W/A = 500/108.28 = 4.63$$

$$C_z = \frac{M_xI_z - M_zK}{I_xI_z - K^2} =$$

$$\frac{(-7540)(6835) - (926)(-3290)}{(6835)(18104) - (-3290)^2} = -0.429$$

$$C_x = \frac{M_zI_x - M_xK}{I_xI_z - K^2} = -0.071$$

Step 6—Extend Columns (16), (17), and (18), resulting in $M_i = f = (W/A) + C_x x + C_z z = 4.63 + (-0.429)x + (-0.071)z$. Extend Column (19), completing the first part of the solution by presenting

$$M = M_s - M_i = (12) - (18)$$

It will be noted that, since $M_s = +15$ in.lbs. at the point of maximum value (points B, 3, 4, C) and $M_i = +12.54$ in.lbs. at one of these points (point C) and since M_s here must be reduced numerically by M_i, it is readily seen that Column (19) must in this case read:

$M = M_s - M_i$ or Col. (19) = Col. (12) − Col. (18)

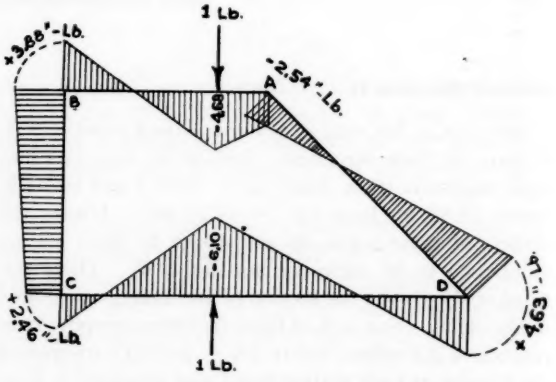

FIG. 4. Final moment diagram of ring.

Fig. 4 represents the final moment values in the ring. A positive moment indicates compression on the inner face of the ring.

Step 7—At A, the cut section in the ring, H_i and V_i, the x and z internal reactions, are numerically equal to

$$H_i = C_z = 0.071 \text{ lb.}$$
$$V_i = C_x = 0.429 \text{ lb.}$$

By inspection of the loaded ring in Fig. 3 and its moment diagram in Fig. 4, it is evident that H_i must

TABLE 1 (Problem 2). Shear Flow

1	2	3	4	5	6	7	8	9	10	11	12	13	14	15	16	17	18	19	20	21
Stringer No.	a Str. Area	x	z	ΔI_x $a\cdot z^2$ (2)·(4)·(4)	ΔI_z $a\cdot x^2$ (2)·(3)·(3)	$\Delta q'_x$ $\frac{S_z}{I_z}\cdot ax$ .538(2)·(3)	$\Delta q'_z$ $\frac{S_x}{I_x}\cdot az$ -.514(2)·(4)	Skin Letter	q' $\frac{\sum(\Delta q'_x+\Delta q'_z)}{\sum[(7)+(8)]}$	$x_{n+1}\cdot z_n$ $(3)_{n+1}\cdot(4)_n$	$x_n\cdot z_{n+1}$ $(3)_n\cdot(4)_{n+1}$	$2A$ (11)−(12)	$q'\cdot 2A$ (10)·(13)	q q_o+q' −9.17+(10)	Δx $x_{n+1}-x_n$ $(3)_{n+1}-(3)_n$	Δz $z_{n+1}-z_n$ $(4)_{n+1}-(4)_n$	Δc $\sqrt{(\Delta x)^2+(\Delta z)^2}$ $\sqrt{(16)^2+(17)^2}$	F_x $q\cdot\Delta x$ (15)·(16)	F_z $q\cdot\Delta z$ (15)·(17)	F $q\cdot\Delta c$ (15)·(18)
1	.302	0	24.22	177	0	0	-3.76													
2	.302	9.75	22.97	159	29	1.58	-3.57	a	-3.76	236	0	236	-887	-12.93	9.75	-1.25	9.83	-126.1	16.2	-127.1
3	.293	18.38	18.42	99	99	2.90	-2.77	b	-5.75	422	179	243	-1397	-14.92	8.63	-4.55	9.76	-128.8	67.9	-145.6
4	.284	23.63	11.12	35	159	3.61	-1.62	c	-5.62	435	204	231	-1298	-14.79	5.25	-7.30	8.99	-77.6	108.0	-133.0
5	.264	26.40	2.52	2	184	3.75	-.34	d	-3.63	294	60	234	-849	-12.80	2.77	-8.60	9.04	-35.5	110.1	-115.7
6	.174	27.70	-6.48	7	133	2.59	.58	e	-.22	70	-171	241	-53	-9.39	1.30	-9.00	9.09	-12.2	84.5	-85.4
7	.097	27.98	-15.78	24	76	1.46	.79	f	2.95	-181	-437	256	755	-6.22	.28	-9.30	9.30	-1.7	57.8	-57.8
8	.127	27.40	-22.98	67	95	1.87	1.50	g	5.20	-432	-644	212	1102	-3.97	-.58	-7.20	7.22	2.3	28.6	-28.7
9	.185	25.12	-29.88	165	117	2.50	2.84	h	8.57	-578	-819	241	2065	-.60	-2.28	-6.90	7.27	1.4	4.1	-4.4
10	.140	16.10	-36.28	184	36	1.21	2.61	i	13.91	-481	-911	430	5981	4.74	-9.02	-6.40	11.06	-42.7	-30.3	52.4
11	.098	4.80	-38.08	142	2	.25	1.92	j	17.73	-174	-613	439	7783	8.56	-11.30	-1.80	11.44	-96.7	-15.4	97.9
11'	.098	-4.80	-38.08	142	2	-.25	1.92	k	19.90	184	-184	368	7323	10.73	-9.60	0	9.60	-103.0	0	103.0
10'	.140	-16.10	-36.28	184	36	-1.21	2.61	j'	21.57	613	174	439	9469	12.40	-11.30	1.80	11.44	-140.1	22.3	141.9
9'	.185	-25.12	-29.88	165	117	-2.50	2.84	i'	22.97	911	481	430	9877	13.80	-9.02	6.40	11.06	-124.5	88.3	152.6
8'	.127	-27.40	-22.98	67	95	-1.87	1.50	h'	23.31	819	578	241	5618	14.14	-2.28	6.90	7.27	-32.2	97.6	102.8
7'	.097	-27.98	-15.78	24	76	-1.46	.79	g'	22.94	644	432	212	4863	13.77	- .58	7.20	7.22	-8.0	99.1	99.4
6'	.174	-27.70	-6.48	7	133	-2.59	.58	f'	22.27	437	181	256	5701	13.10	.28	9.30	9.30	3.7	121.8	121.8
5'	.264	-26.40	2.52	2	184	-3.75	-.34	e'	20.26	171	-70	241	4883	11.09	1.30	9.00	9.09	14.4	99.8	100.8
4'	.284	-23.63	11.12	35	159	-3.61	-1.62	d'	16.17	-60	-294	234	3784	7.00	2.77	8.60	9.04	19.4	60.2	63.3
3'	.293	-18.38	18.42	99	99	-2.90	-2.77	c'	10.94	-204	-435	231	2527	1.77	5.25	7.30	8.99	9.3	12.9	15.9
2'	.302	-9.75	22.97	159	29	-1.58	-3.57	b'	5.27	-179	-422	243	1281	-3.90	8.63	4.55	9.76	-33.7	-17.7	-38.1
								a'	0=(.12)	0	-236	236	0	-9.17	9.75	1.25	9.83	-89.4	-11.5	-90.1
			$\Sigma=$	1945	1860						$\Sigma=$	5894	68528					$\Sigma=$	-1001.7	1004.3	

$\frac{S_x}{I_z} = \frac{1000}{1860} = 0.538$; $\frac{S_z}{I_x} = \frac{-1000}{1945} = -0.514$; $q_o = \frac{-T_{c.g.} - \Sigma q'\cdot(2A)}{\Sigma 2A} = \frac{-(-14{,}480) - 68{,}528}{5894} = -9.17$ Lb./In.

CHECK: Col. 10: Error = $\frac{\Sigma+(10)_4}{\Sigma-(10)} = \frac{29.06}{28.94} = 0.4\%$; F_x: Error = $\frac{1001.7}{1000} = 0.2\%$; F_z: Error = $\frac{1004.3}{1000} = 0.4\%$

act at A toward AB and V_i must act at A *upward* relative to AB.

PROBLEM 2—SYMMETRICAL FUSELAGE RING LOADED UNSYMMETRICALLY

Given—The symmetrical fuselage ring loaded unsymmetrically by means of 1,000-lb. horizontal and vertical forces applied to a bracket as shown in Fig. 5. The shear flow induced in the fuselage skin constitutes the external forces reacting on the ring to maintain equilibrium.

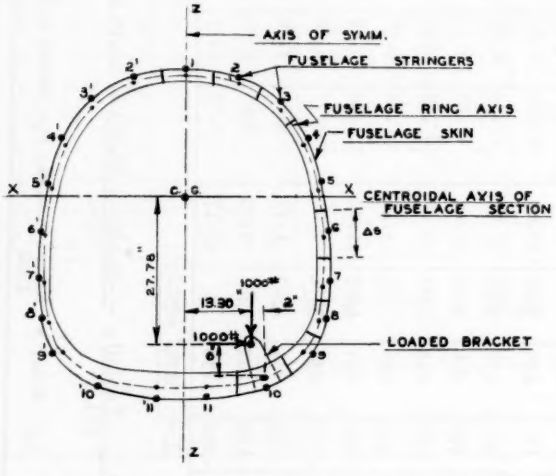

FIG. 5. Symmetrical fuselage ring loaded unsymmetrically.

Required—Compute the bending moments and the normal and shearing forces induced in the ring at successive points along its axis.

Outline

The successive steps in the solution of this problem are:

Step 1—Computation of the reacting shear flow in the fuselage skin, due to the loads applied to the ring through the bracket.

Step 2—Computation of the statically determinate moments, M_s, induced in the cut ring by the ring forces including both the applied 1,000-lb. forces and the reacting shear-flow forces.

Step 3—Computation of the section properties of the analogous column.

Step 4—Computation of the internal reacting stresses in the analogous column due to the applied θ_s forces $[\theta_s = p\Delta A = M_s(\Delta s/EI)]$, by use of Eq. (2): $f = (W/A) \pm (M_z z/I_z) \pm (M_x x/I_z)$. This gives the M_i values in the uncut ring since $f = M_i$.

Step 5—Computation of the internal moments in the uncut ring by application of Eq. (1): $M = M_s \pm M_i$.

Step 6—Computation of the normal and shearing forces in the ring.

Solution

Step 1—Shear-flow computations.

Sign Convention—In order to have results that are correct both numerically and in sense of traverse, the following sign convention is adopted: *positive* values are assigned to

(1) Forces acting *upward* and to the *right*.

(2) Clockwise moments.

(3) Shear-flow forces having a *clockwise* sense of traverse around the fuselage skin.

(4) The x and z coordinates of the stringer units that are to the *right* of and *above* the z–z and x–x centroidal axes of the fuselage section. (Negative values are applied to the opposite characteristics.)

Table 1 presents the necessary computations in proper sequence.

Columns 1, 9—The fuselage stringers are numbered successively in a *clockwise* sense, starting with No. 1 as the top stringer, which is on the z–z axis of symmetry, and ending with No. 11, the last stringer on the right half of the ring. The successive units on the left half are numbered 11′ to 2′ to indicate the existence of symmetry (see Fig. 5). The skin lengths between adjacent stringer units are assigned the letters a, b, c, etc., starting with the length between stringers 1 and 2, and proceeding in a clockwise sense on the right half, and a', b', c', etc., in a counterclockwise sense on the left half because of symmetry.

Columns 2, 3, 4, 5, 6—The area, a, of each stringer unit, and its x and z coordinates referenced to the z–z and x–x centroidal axes are obtained from computations previously used in the fuselage analysis. The total moments of inertia of the stringer areas are obtained by summation of the individual values of az^2 and ax^2.

Columns 7 to 15—Before computing the skin shear-flow reactions the applied 1,000-lb. loads are transferred to act along the centroidal axes of the section along with the torque resulting from this transfer, which will be:

$$T_{c.g.} = 1{,}000 \overset{\curvearrowright}{\times} 13.30 - 1{,}000 \overset{\curvearrowleft}{\times} 27.78 = -14{,}480 \text{ in.lb.} \quad (24)$$

The resulting total shear-flow reaction will be the algebraic sum of the separate effects shown in Fig. 6.

Fig. 6(a) shows the proper sense of the shear-flow reaction in each skin unit, a, b, c, etc., induced by the 1000-lb. horizontal force indicated. The sense of each individual vector is determined by the basic fact that the horizontal component of each vector must oppose the sense of the applied 1,000-lb. horizontal force. The magnitude and sense of each shear-flow increment entering the skin through each stringer connection is determined by application of the basic formula:

$$\Delta q_x' = \left(\frac{S_x}{I_z}\right) Q_s = \left(\frac{S_x}{\sum ax^2}\right) ax = \frac{1{,}000}{\sum ⑥} \cdot ② \cdot ③ \quad (25a)$$

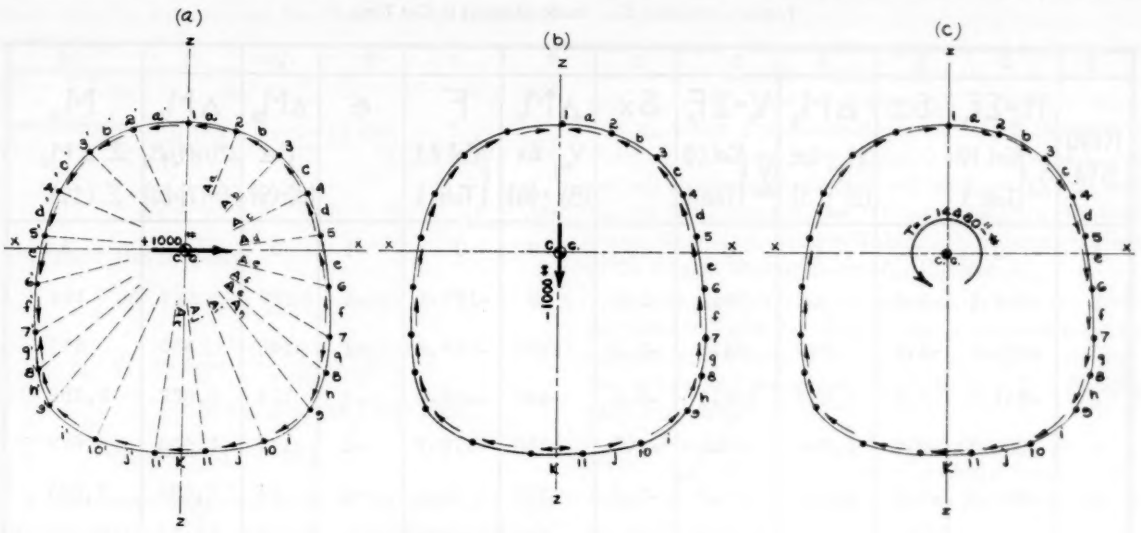

FIG. 6. Component parts of reacting shear-flow.

The sign convention previously described will automatically insure the correct senses of these increments. The numerals in the circles of Eq. (25a) refer to the appropriate columns in Table 1. The actual shear flow, q_n, in any skin unit, N, must be considered broken up, into q_0, the unknown shear flow existing in skin unit a' immediately to the left of initial stringer 1, and $q_n' = \sum_1^n \Delta q_x'$, the accumulating increments entering the skin from stringer 1 to that immediately preceding the skin unit, n. Expressed mathematically, this is:

$$q_n = q_0 + q_{n'} = q_0 + \sum_1^n \Delta q_x' \qquad (26a)$$

The value of the unknown shear flow, q_0, is obtained by use of the equation of equilibrium, $\sum M_{c.g.} = 0$, which is expressed by

$$T_{c.g.} + q_a(2A_a) + q_b(2A_b) + \ldots + q_{b'}(2A_{b'}) + q_0(2A_{a'}) = 0$$

or

$$T_{c.g.} + (q_0 + q_a')2A_a + (q_0 + q_b')2A_b + \ldots + (q_0 + q_{b'})\,2A_{b'} + q_0(2A_{a'}) = 0$$

which simplifies to

$$T_{c.g.} + q_0\sum 2A + \sum q'(2A) = 0 \qquad (27)$$

Since the applied horizontal 1,000-lb. force in Fig. 6(a) acts through the center of gravity of the section, there is no eccentricity and $T_{c.g.} = 0$. Hence, Eq. (27) reduces to

$$q_0 = -\sum q'(2A)/\sum 2A \qquad (28)$$

from which the unknown q_0 is obtained, then substituted in Eq. (26) to determine q_a, q_b, q_c, etc. Fig. 6(a) defines the terms A_a, A_b, A_c, etc. $\sum 2A$ indicates twice the total area enclosed by the fuselage skin. Eqs. (26), (27), and (28) will be recognized as those generally used in the determination of the shear flow in a single-cell wing beam reinforced with stringers. The derivations can be found in several texts, some of which are listed herein.[3]

Fig. 6(b) shows the proper sense of the shear-flow reaction in each skin unit induced by the 1,000-lb. vertical force shown, the sense of which is determined by the basic fact that the vertical components of *each* vector must oppose the sense of the applied 1,000-lb. vertical force. The magnitude and sense of each shear-flow increment is determined by

$$\Delta q_z' = \left(\frac{S_z}{I_z}\right) Q_z = \left(\frac{S_z}{\sum az^2}\right) az = \frac{-1{,}000}{\sum ⑤} \cdot ② \cdot ④ \qquad (25b)$$

and

$$q_n = q_0 + q_n' = q_0 + \sum_1^n \Delta q_z' \qquad (26b)$$

Following the same reasoning applied to Fig. 6(a), and noting that $T_{c.g.} = 0$, since the vertical 1,000-lb. force in Fig. 6(b) acts through the c.g. of the section, q_0 is obtained by application of Eq. (28).

Fig. 6(c) shows the proper sense of the shear-flow reaction in each skin unit, induced by the 14,480-in.lb. torque shown, the sense of which is determined by the basic fact that the reacting moment of each vector must oppose the applied torque. Since there are no applied external shear forces in this case, the shear-flow vector in each skin unit will be:

$$q_n = q_0 \qquad (26c)$$

and q_0 becomes, by application of Eq. (27):

$$q_0 = -T_{c.g.}/\sum 2A \qquad (29)$$

TABLE 2 (Problem 2). Static Moment in Cut Ring

1	2	3	4	5	6	7	8	9	10	11	12
RING STA.	$H_s=\Sigma F_x$ $\sum$ {Col. 19 Tab. 1	δz	ΔM_1 $H_{n-1}\cdot\delta z$ $(2)_{n-1}\cdot(3)$	$V_s=\Sigma F_z$ $\sum$ {Col. 20 Tab. 1	δx	ΔM_2 $V_{n-1}\cdot\delta x$ $(5)_{n-1}\cdot(6)$	F {Col. 21 Tab. 1	e	ΔM_3 Fe $(8)\cdot(9)$	ΔM_s $\Delta M_1+\Delta M_2+\Delta M_3$ $(4)+(7)+(10)$	M_s $\Sigma\,\Delta M_s$ $\Sigma\,(11)$
1	0	0	0	0	0	0	0	-1	0	0	0
2	-126.1	-1.5	0	16.2	-9.2	0	-127.1	-1	127	127	127
3	-254.9	-4.3	540	84.1	-8.5	-138	-145.6	-1	146	550	677
4	-332.6	-7.2	1,835	192.1	-5.3	-446	-133.0	-1	133	1,522	2,199
5	-368.1	-8.4	2,794	302.2	-2.5	-480	-115.7	-1	116	2,430	4,629
6	-380.3	-8.7	3,202	386.7	-1.3	-393	- 85.4	-1	85	2,894	7,523
7	-382.0	-9.2	3,499	444.5	-0.2	- 77	- 57.9	-1	58	3,480	11,003
8	-379.7	-6.7	2,559	473.1	0.8	356	- 28.7	-1.45	42	2,957	13,960
9	-378.3	-6.1	2,316	477.2	2.7	1,277	- 4.4	-2.30	10	3,603	17,563
10A	-421.0	-5.6	2,118	446.9	7.9	3,769	52.4	-2.45	-128	5,759	23,322**
10B	579.0	0	0	-553.1	0	0	--	--	--	-4,000	19,322**
11	482.3	-1.0	- 579	-568.5	10.8	-5,973	97.9	-2.80	-274	-6,826	12,496
11'	379.3	0	0	-568.5	9.6	-5,458	103.0	-2.80	-288	-5,746	6,750
10'	239.2	1.0	379	-546.2	10.8	-6,140	141.9	-2.45	-348	-6,109	641
9'	114.7	5.6	1,340	-457.9	7.9	-4,315	152.6	-2.30	-351	-3,326	- 2,685
8'	82.5	6.1	700	-360.3	2.7	-1,236	102.8	-1.45	-149	- 685	- 3,370
7'	74.5	6.7	553	-261.2	0.8	- 288	99.4	-1	- 99	166	- 3,204
6'	78.2	9.2	685	-139.4	-0.2	52	121.8	-1	-122	615	- 2,589
5'	92.6	8.7	680	- 39.6	-1.3	181	100.8	-1	-101	760	- 1,829
4'	112.0	8.4	778	20.6	-2.5	99	63.3	-1	- 63	814	- 1,015
3'	121.3	7.2	806	33.5	-5.3	- 109	15.9	-1	- 16	681	- 334
2'	87.6	4.3	521	15.7	-8.5	- 285	- 38.1	-1	38	274	- 60
1'=1	- 1.8*	1.5	131	4.2*	-9.2	- 144	- 90.1	-1	90	77	17*

* Note: Col. 2: -1.8 should = 0 (0.2% Error); Col. 5: 4.2 should = 0 (0.4% Error)
Col. 12: 17 should = 0 (0.1% Error)

** Note: At Sta. 10, Use $M_s = \frac{23,322 + 19,322}{2} = 21,322$ in Column Analogy

Since the three cases shown in Fig. 6 actually occur simultaneously, the total shear flow in any skin unit is, by the law of superposition, the algebraic sum of the component values.

In actual application it is not necessary to determine these separate values, since the effects can be combined as follows:

$$q_n' = \sum_1^n \Delta q_x' + \sum_1^n \Delta q_z' = \sum_1^n (⑦ + ⑧) = ⑩_n \quad (30)$$

$$q_0 = \frac{-T_{c.g.} - \sum q'(2A)}{\sum 2A} = \frac{-(-14{,}480) - \sum ⑭}{\sum ⑬} \quad (31)$$

$$q_n = q_0 + q_n' = q_0 + ⑩_n \quad (32)$$

Applied to this problem:

$$\sum ⑭ = 68{,}528; \quad \sum ⑬ = 5{,}894$$

$$q_0 = \frac{-(-14{,}480) - 68{,}528}{5{,}894} = -9.17 \text{ lbs. per linear inch}$$

$$q_n = -9.17 + ⑩_n$$

A convenient numerical check is obtained by noting that the value of q' for skin unit a' in Column 10 should be zero, since, by definition, the total shear flow in a' is q_0. The error in this problem is 0.12 lb. per linear inch, or 0.4 per cent, which is negligible.

Columns 16 to 21—The values in these columns really belong to Step 2 but are placed in Table 1 since they utilize data determined in this table. Columns 16, 17, and 18 give the horizontal, vertical, and resultant distances between adjacent stringer units.

Columns 19 and 20 furnish the total horizontal and vertical components of the shear flow in each skin unit so that $F_x = q(\Delta x)$ and $F_z = q(\Delta z)$. An additional check is obtained on the accuracy of the computations in Table 1 by virtue of the fact that, since $\sum H = 0$ and $\sum V = 0$, $\sum(19) + 1{,}000 = 0$ and $\sum(20) - 1000 = 0$. In this problem: $\sum(19) = -1001.7$, with an error of 0.2 per cent, and $\sum(20) = +1004.3$, with an error of 0.4 per cent, both of which errors are negligible. Column 21 presents the vector sum of F_x and F_z.

Step 2—Computation of static moments, M_s, in cut ring. The fuselage ring is assumed cut at stringer 1 to furnish the determinate base structure and the resulting M_s value are computed in Table 2. Fig. 7 represents the external forces acting on the cut ring between Stations 1 and 2. Since continuity has been destroyed at Station 1 by the cut, it follows that $H_{s_1} = 0$, $V_{s_1} = 0$, and $M_{s_1} = 0$. The resultant of all of the skin shear flow, q_a, which is transferred into the ring in the curved distance, a, will be $F_a = q_a(\Delta c_a)$, the horizontal and vertical components of which will be $F_{a_x} = q_a(\Delta x_a)$ and $F_{a_z} = q_a(\Delta z_a)$, respectively. These values are obtained from Columns 19, 20, 21 of Table 1. The forces applied to the ring at Station 2 are H_{s_2}, V_{s_2}, and M_{s_2}.

Sign Convention—Before proceeding with the computations in Table 2, a definite sign convention must be adopted with reference to Fig. 7 in order to insure correct senses and numerical values in Step 2. *Positive* values are assigned to

(1) Forces acting *upward* and to the *right*.

(2) Shear-flow forces with a *clockwise* sense of traverse. (Note that the above senses permit the use of pertinent values directly from Table 1.)

(3) Moments which cause *compression* on the *inner* face of the ring. (Note that such a moment will be counterclockwise in Fig. 7, which is contrary to the convention used in the shear-flow computations, but this does not matter since Step 2 constitutes a new set of computations.)

(4) δx_n when measured to the right of the moment center.

(5) δz_n when measured below the moment center.

(6) e_n when measured inward from the moment center. (Note that e_n will *always* be negative since the shear-flow force F_n will always be outward from the moment center.)

Note—δx_n and δz_n are the horizontal and vertical distances between Stations N and $(N - 1)$ on ring axis and must not be confused with Δx_n and Δz_n, which are the horizontal and vertical projections of the skin unit between Stations N and $(N - 1)$. Fig. 7 defines the term e_n. From Fig. 7, it is evident that the forces *applied* to the shaded portions of the ring on the section at Station 2 are:

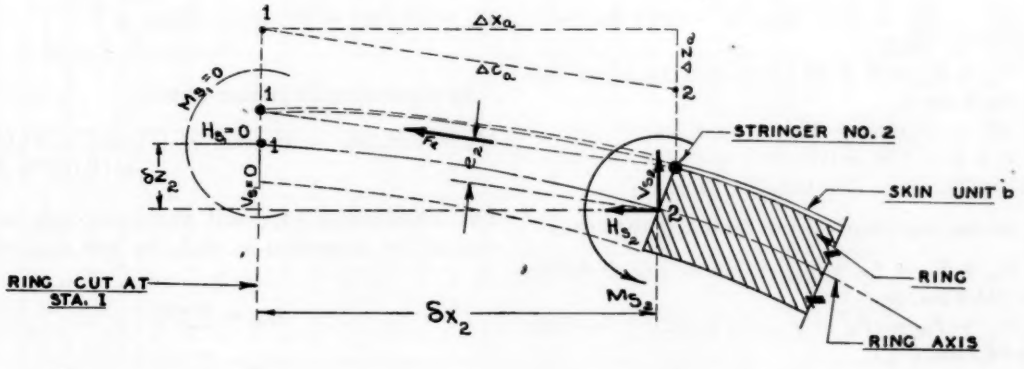

FIG. 7. Moments and forces applied to Station 2 of cut ring.

TABLE 3 (Problem 2). Section Properties of Analogous Column

1	2	3	4	5	6	7	8	9	10
RING STATION	Δs of Ring Rib	I of Ring Rib	ΔA $\frac{\Delta s}{I}$ (2)/(3)	z' From C.G. of Fuselage	$z'\cdot\Delta A$ (4)·(5)	z $z'-\bar{z}'$ (5)−2.5	x From Symm. Axis	ΔI_x $\Delta A\cdot z^2$ (4)·(7)·(7)	ΔI_z $\Delta A\cdot x^2$ (4)·(8)·(8)
1	9.2	1	9.2	23.5	216.2	21.0	0	4,057	0
2	9.4	1	9.4	22.0	206.8	19.5	9.2	3,574	796
3	9.2	1	9.2	17.7	162.8	15.2	17.7	2,126	2,882
4	8.7	1	8.7	10.5	91.4	8.0	23.0	557	4,602
5	8.7	1	8.7	2.1	18.3	−0.4	25.5	1	5,657
6	8.9	1	8.9	−6.6	−58.7	−9.1	26.8	737	6,392
7	7.9	1	7.9	−15.8	−124.8	−18.3	27.0	2,646	5,759
8	6.8	1.66	4.1	−22.5	−92.2	−25.0	26.2	2,563	2,814
9	8.2	5.79	1.4	−28.6	−40.0	−31.1	23.5	1,354	773
10	10.0	7.13	1.4	−34.2	−47.9	−36.7	15.6	1,886	341
11	10.2	6.12	1.7	−35.2	−59.8	−37.7	4.8	2,416	39
$\Sigma(2' \text{ to } 11')$ $=\Sigma(2 \text{ to } 11)$			61.4		55.9			17,860	30,055
		A =	132.0	$\Sigma z'\Delta A$ =	328.0		I_x =	39,777	
								I_z =	60,110

$$\bar{z}' = \frac{\Sigma z'\Delta A}{\Sigma \Delta A} = \frac{\Sigma(6)}{\Sigma(4)} = \frac{328.0}{132.0} = 2.5''$$

$H_{s_2} = H_{s_1} + F_{ax} = 0 - 126.1 = -126.1$ lbs. (←). See Col. 19, Table 1

$V_{s_2} = V_{s_1} + F_{az} = 0 + 16.2 = +16.2$ lbs. (↑). See Col. 20, Table 1

$M_{s_2} = M_{s_1} + H_{s_1}(\delta z_2) + V_{s_1}(\delta x_2) + F_a(e_2)$

$M_{s_2} = 0 + 0\,(-1.5) + 0\,(-9.2) + (-127.1)(-1) = +127$ in.lbs. (↶). See Col. 21, Table 1

In a similar way there exist at Station 3, the forces

$H_{s_3} = H_{s_2} + F_{bx} = F_{ax} + F_{bx} = (-126.1) + (-128.8) = -254.9$ lbs. (←)

$V_{s_3} = V_{s_2} + F_{bz} = F_{az} + F_{bz} = (+16.2) + (+67.9) = +84.1$ lbs. (↑)

$M_{s_3} = M_{s_2} + H_{s_2}(\delta z_3) + V_{s_2}(\delta x_2) + F_b(e_3) = +677$ in.lbs. (↶)

$M_{s_3} = H_{s_1}(\delta z_2) + V_{s_1}(\delta x_2) + F_a(e_2) + H_{s_2}(\delta z_3) + V_{s_2}(\delta x_3) + F_b(e_3)$

By regrouping for similar terms:

$$M_{s_3} = [(H_{s_1}(\delta z_2) + H_{s_2}(\delta z_3)] + [V_{s_1}(\delta x_2) + V_{s_2}(\delta x_3)] + [F_a(e_2) + F_b(e_3)]$$

The relationships expressed above can now be generalized by inspection so that, for *any* ring station, N,

$$H_{s_n} = \sum_1^n F_x \tag{33}$$

$$V_{s_n} = \sum_1^n F_z \tag{34}$$

$$M_{s_n} = \sum_1^n [H_{s_{n-1}}(\delta z_n) + V_{s_{n-1}}(\delta x_n) + F_n(e_n)] \tag{35}$$

TABLE 4 (Problem 2). Stresses in Analogous Column, Final Moments in Ring

1	2	3	4	5	6	7	8	9	10	11	12
RING STA.	ΔA Col. 4 Tab. 3	x Col. 8 Tab. 3	z Col. 7 Tab. 3	$p=M_s$ Col. 12 Tab. 2	$\Delta W=p\cdot\Delta A$ (2)·(5)	ΔM_x $(\Delta W)\cdot z$ (4)·(6)	ΔM_z $(\Delta W)\cdot x$ (3)·(6)	f_2 $C_2\cdot z$ (-138.0)·(4)	f_3 $C_3\cdot x$ (178.4)·(3)	$M_i=f$ $f_1+f_2+f_3$ 2058+(9)+(10)	M M_s-M_i (5)-(11)
1	9.2	0	21.0	0	0	0	0	-2,898	0	-840	840
2	9.4	9.2	19.5	127	1,194	23,283	10,985	-2,691	1,641	1,008	-881
3	9.2	17.7	15.2	677	6,228	94,666	110,236	-2,098	3,158	3,118	-2,441
4	8.7	23.0	8.0	2,199	19,131	153,048	440,013	-1,104	4,103	5,057	-2,858
5	8.7	25.5	-0.4	4,629	40,272	-16,109	1,026,936	55	4,549	6,662	-2,033
6	8.9	26.8	-9.1	7,523	66,955	-609,290	1,794,394	1,256	4,781	8,095	-572
7	7.9	27.0	-18.3	11,003	86,924	-1,590,709	2,346,948	2,525	4,817	9,400	1,603
8	4.1	26.2	-25.0	13,960	57,236	-1,430,900	1,499,583	3,450	4,674	10,182	3,778
9	1.4	23.5	-31.1	17,563	24,588	-764,687	577,818	4,292	4,192	10,542	7,021
10A	--	--	--	23,322	--	--	--	--	--	9,906	13,416
10	1.4	15.6	-36.7	21,322	29,851	-1,095,532	465,676	5,065	2,783	--	--
10B	--	--	--	19,322	--	--	--	--	--	9,906	9,416
11	1.7	4.8	-37.7	12,496	21,243	-800,861	101,966	5,203	856	8,117	4,379
11'	1.7	-4.8	-37.7	6,750	11,475	-432,608	-55,080	5,203	-856	6,405	345
10'	1.4	-15.6	-36.7	641	897	-32,920	-13,993	5,065	-2,783	4,340	-3,699
9'	1.4	-23.5	-31.1	-2,685	-3,759	116,906	88,336	4,292	-4,192	2,158	-4,843
8'	4.1	-26.2	-25.0	-3,370	-13,817	345,425	362,005	3,450	-4,674	834	-4,204
7'	7.9	-27.0	-18.3	-3,204	-25,312	463,210	683,424	2,525	-4,817	-234	-2,970
6'	8.9	-26.8	-9.1	-2,589	-23,042	209,682	617,526	1,256	-4,781	-1,467	-1,122
5'	8.7	-25.5	-0.4	-1,829	-15,912	6,365	405,756	55	-4,549	-2,436	607
4'	8.7	-23.0	8.0	-1,015	-8,830	-70,640	203,090	-1,104	-4,103	-3,149	2,134
3'	9.2	-17.7	15.2	-334	-3,073	-46,710	54,392	-2,098	-3,158	-3,198	2,864
2'	9.4	-9.2	19.5	-60	-564	-10,998	5,189	-2,691	-1,641	-2,274	2,214
A= 132.0				W= 271,685		M_x= -5,489,560	M_z= 10,725,200				

$$C_2=\frac{M_x}{I_x}=\frac{-5,489,560}{39,777}=-138.0;\quad C_3=\frac{M_z}{I_z}=\frac{10,725,200}{60,110}=178.4;\quad f_1=\frac{W}{A}=\frac{271,685}{132}=2,058$$

TABLE 5 (Problem 2). Normal and Shearing Stresses in Ring

1	2	3	4	5	6	7	8	9	10	11	12
RING STA.	$H=H_1+H_2$ $H_1=138$ H_2 (Col. 2 Tab. 2)	$V=V_1+V_2$ $V_1=178$ V_2 (Col. 5 Tab. 2)	α Scaled	SIN α	COS α	$H\sin\alpha$ (2)·(5)	$H\cos\alpha$ (2)·(6)	$V\sin\alpha$ (3)·(5)	$V\cos\alpha$ (3)·(6)	N Comp.+ Ten.- (8)-(9)	S (7)+(10)
1	138	178	0	0	1.0	0	138	0	178	138	178
2	12	194	17.0	.293	.956	4	11	57	185	-46	189
3	-117	262	44.1	.696	.718	-81	-84	182	188	-266	107
4	-195	370	35.3	.909	.418	-177	-82	336	155	-418	-22
5	-230	480	78.7	.981	.196	-226	-45	471	94	-516	-132
6	-242	565	84.2	.995	.101	-241	-24	562	57	-586	-184
7	-244	623	94.3	.997	-.075	-243	18	621	-47	-603	-290
8	-242	651	112.8	.922	-.388	-223	94	600	-253	-506	-476
9	-240	655	133.2	.729	-.685	-175	164	477	-449	-313	-624
10A	-283	625	163.3	.287	-.958	-81	271	179	-599	92	-680
10B	717	-375	163.3	.287	-.958	206	-687	-108	359	-579	565
11	620	-391	177.0	.052	-.999	32	-619	-20	391	-599	423
11'	517	-391	183.0	-.052	-.999	-27	-516	20	391	-536	364
10'	377	-368	196.7	-.287	-.958	-108	-361	106	353	-467	245
9'	253	-280	226.8	-.729	-.685	-184	-173	204	192	-377	8
8'	221	-182	247.2	-.922	-.388	-204	-86	168	71	-254	-133
7'	213	-83	265.7	-.997	-.075	-212	-16	83	6	-99	-206
6'	216	39	275.8	-.995	.101	-215	22	-39	4	61	-211
5'	231	138	281.3	-.981	.196	-227	45	-135	27	180	-200
4'	250	199	294.7	-.909	.418	-227	105	-181	83	286	-144
3'	259	212	315.9	-.696	.718	-180	186	-148	152	334	-28
2'	226	194	343.0	-.293	.956	-66	216	-57	185	273	119

In these equations n indicates the *number* of the particular ring station being considered except when used as a subscript to F. In the latter case it is the *letter* denoting the skin unit between ring stations N and "$N - 1$." It should also be remembered that successive ring stations are taken in a *clockwise* sense of traverse around the ring.

Referring to Table 2, Columns 2 and 5 represent the solution of Eqs. (33) and (34); the numerical values are obtained by summing up the values listed in Columns 19 and 20 of Table 1. The δz and δx values in Columns 3 and 6 are obtained from the original layout of the ring by computation. The e values in Column 9 are scaled off of the same layout with sufficient accuracy since the values of $\Delta M_3 = F(e)$ are relatively small. Columns 4, 7, 10, 11, 12 represent the solution of Eq. (35). The last values in Columns 2, 5, and 12 furnish an arithmetical check since they represent H_{s1}, V_{s1}, and M_{s1} and should equal zero.

The bracket that receives the two 1,000-lb. applied forces is attached to the fuselage ring at Station 10. Hence, these forces must be transferred to act on the ring at this station, together with the resulting moment of transfer, which is:

$$\Delta M_{10} = -1{,}000 \curvearrowright \times 6 + \overset{\curvearrowleft}{1000} \times 2 = -\overset{\curvearrowright}{4{,}000} \text{ in.lbs.}$$
$$\Delta H_{10} = +1{,}000; \text{ lbs. } \Delta V_{10} = -1{,}000 \text{ lbs.}$$

Station 10 is then broken up into Station 10A, a point an infinitely small distance *before* ΔH_{10}, ΔV_{10}, and ΔM_{10} are applied, and Station 10B, a point an infinitely small distance *after* they are applied. When applied as an imaginary load to the analogous column, the value of M_s acting at Station 10 will then be assumed as the *average* of M_{s10A} and M_{s10B}. At Station 10 in this problem M_s will then be:

$$M_{s10} = (1/2)(M_{s10A} + M_{s10B}) = (1/2)(23{,}322 + 19{,}322) = +21{,}322 \text{ in.lbs.}$$

With the sign convention adopted herein, Column 12, Table 2, will automatically furnish the correct numerical values of M_s together with correct senses (positive moments causing compression on inner face of ring, negative moments causing tension).

Step 3—Section properties of analogous column. Table 3 presents the computations of the section properties of the analogous column for the cut ring and is self-explanatory. The values of the moments of inertia in Column 3 are relative only, in terms of unity at Ring Station No. 1. These values were determined separately from the ring details. The Δs distances in Column 2 represent the curved length of each ring increment. They were assumed to be the mean of the *scaled* distances along the ring axis between N, the station considered, and the next adjacent stations, fore and aft—namely, $(N + 1)$ and $(N - 1)$.

Steps 4 and 5—Stresses in analogous column and moments in uncut ring. Table 4 represents the computations for the stresses in the analogous column, when loaded with the M_s values computed in Step 2, and the resulting final moments in the uncut ring. The table is essentially self-explanatory, since it is the solution of the basic Eqs. (1) and (2).

Column 5 lists the M_s values from Table 2, Column 12. These are the imaginary loads applied to the analogous column in pounds per square inch. Positive values represent *compressive* loads and negative values indicate *tensile* loads.

Column 11 represents f, the final combined bending and direct reacting stresses in the column base and is the solution of the basic Eq. (2). Positive values indicate compressive stresses and negative values show tensile stresses. It has already been established that these stresses are numerically equal to the M_t values of Eq. (1); hence, Column 11 also furnishes these M_t values. As has already been emphasized, the signs of these M_t values are only relative.

Column 12 is the solution of the basic Eq. (1). Since the maximum value of M_s is +23,322 in.lbs. at Station 10A and since the corresponding value of M_t is +9,906 in.lbs., Column 12 *must* read $M = M_s - M_t =$ Column 5 − Column 11 so that at this point the actual moment in the uncut ring will be numerically less than the statically determinate moment. The positive and negative signs in Column 12 will, as in Column 5, indicate moments causing compression and tension, respectively, on the inner face of the ring.

Step 6—Normal and shearing stresses in ring. From Eqs. (18) and (19) are determined the numerical values of H_t and V_t, the horizontal and vertical components of normal and shearing forces applied at the section where the ring was cut. ($H_{s1} = 0$, $V_{s1} = 0$ by virtue of the cut.) Therefore

$$H_1 = H_t = M_x/I_x = C_2 = 138 \text{ lbs. (see Table 4)}$$
$$V_1 = V_t = M_z/I_z = C_3 = 178 \text{ lbs. (see Table 4)}$$

To determine the correct senses of these forces refer to Fig. 8(a), which shows the left half of the ring with the internal reactions replaced by equal but opposite applied forces to maintain equilibrium.

Column 12, Table 4, furnishes the moment at Station 1 ($M_1 = +840$ in.lbs.) and at Station 11.5, which is assumed to be the mean of the moments at Stations 11 and 11′ [$M_{11.5} = 1/2(4{,}379 + 345) = +2{,}362$ in.lbs.]. The moment about Station 11.5, because of the applied shear-flow forces in the skin of the half-ring, is assumed to be the mean of the M_s values existing at Stations 11 and 11′, which are listed in Column 5, Table 4 [$M_{s11.1} = 1/2(12{,}496 + 6{,}750) = 9{,}623$]. By applying $\sum M = 0$ about Station 11.5, H_1 becomes the only unknown in the equation and

$$H_1 = (\overset{\curvearrowright}{9{,}623} + \overset{\curvearrowright}{840} - \overset{\curvearrowleft}{2{,}362})/58.7 = 138 \text{ lbs.} \leftarrow$$

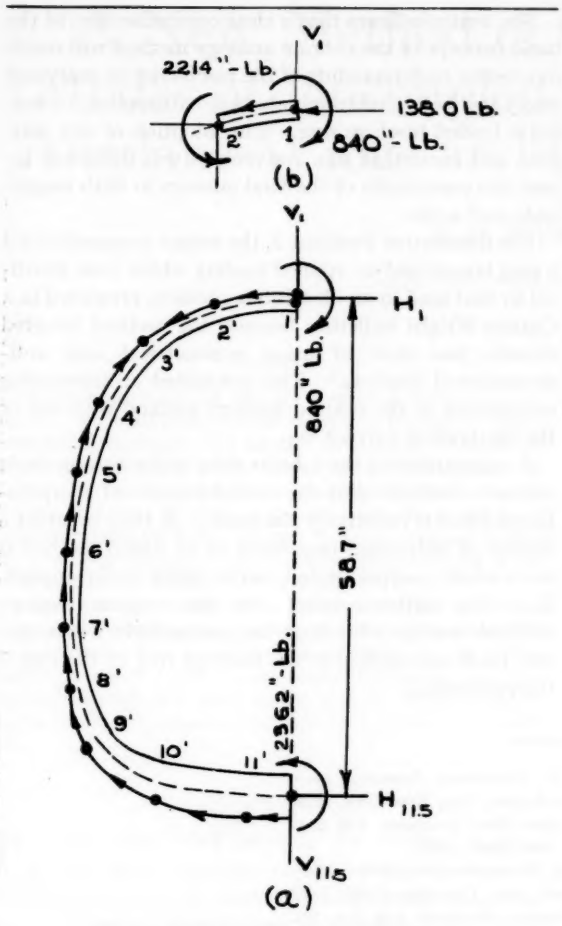

FIG. 8. Half-ring with known moments.

This checks the numerical value of H_1 previously determined and, in addition, establishes the correct sense of H_1. Then, by use of Fig. 8(b), V_1 is obtained by applying $\sum M = 0$ about Station 2', for which $M_2' = +2{,}214$ (Column 12, Table 4) and $M_{z2'} = -60$ (Column 5, Table 4):

$$V_1 = \frac{\overset{\curvearrowleft}{2{,}214} + \overset{\curvearrowleft}{60} + \overset{\curvearrowleft}{138 \times 1.5} - \overset{\curvearrowright}{840}}{9.2} = 178 \text{ lbs.} \downarrow$$

Fig. 9 is similar to Fig. 7 but shows the final moments and forces on the uncut ring at Stations 1 and 2. The values for M_1 and M_2 are taken from Column 12, Table 4; for F_{ax} and F_{az}, from Columns 19 and 20, Table 1; for H_1 and V_1, from the above computations, reversing the senses since they are now applied to the right half of the ring. It then follows that

$$H_2 = H_1 + F_{ax} = +138 - 126 = +12 \text{ lbs.} (\rightarrow)$$
$$V_2 = V_1 + F_{az} = +178 + 16 = +194 \text{ lbs.} (\uparrow)$$

Eqs. (33) and (34) can now be revised to read:

$$H_n = H_1 + \sum_1^n F_x = H_1 + H_{sn} \qquad (33a)$$
$$V_n = V_1 + \sum_1^n F_z = V_1 + V_{sn} \qquad (34a)$$

where H_n and V_n are the final horizontal and vertical components of the forces applied to any ring station, N. The values of H_{sn} and V_{sn} are listed in Columns 2 and 5, Table 2.

Referring to Fig. 10, the normal and shearing forces, N_n and S_n, acting on any ring station, N, are

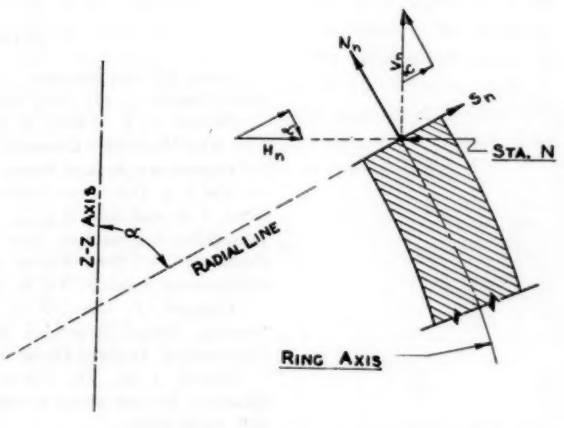

FIG. 10. Normal and shearing forces on typical ring station.

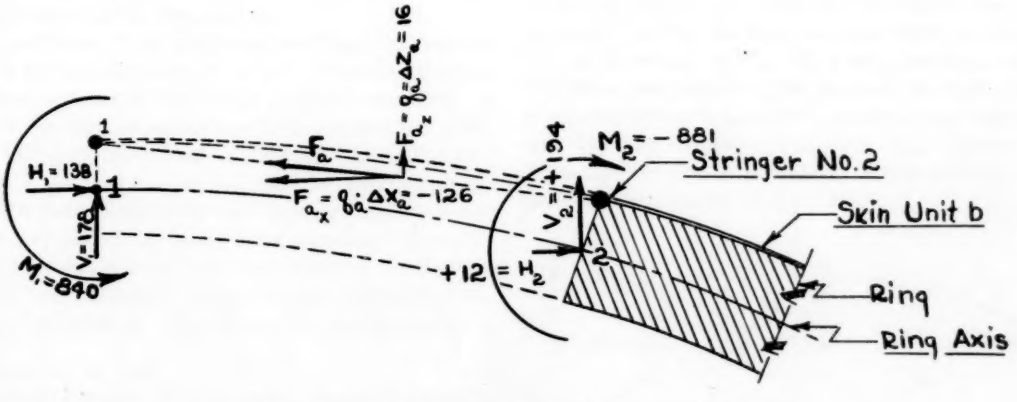

FIG. 9. Moments and forces applied to Station 2 of uncut ring.

$$N_n = H_n \cos \alpha_n - V_n \sin \alpha_n \quad (22)$$

$$S_n = H_n \sin \alpha_n + V_n \cos \alpha_n \quad (23)$$

The signs in Eqs. (22) and (23) are so arranged that, using the sign convention previously adopted for the V and H forces and measuring α as shown, the resulting sign convention for N_n and S_n will be: *Positive* and *negative* values of N_n will indicate *compressive* and *tensile* forces, respectively. *Positive* and *negative* values of S_n will indicate radially *outward* and *inward* shear, respectively.

Table 5 presents the computations for the Normal and Shearing forces acting at the various ring stations.

Conclusion

The arriving at a conclusion upon the completion of an experiment or development of an analytical procedure implies an expression of the personal opinion of the investigator. Since personal opinions vary, the writer presents these closing remarks with a realization that many will disagree with him as to the relative merits of the column analogy method.

The writer believes that a clear comprehension of the basic concept of the column analogy method will result in a better understanding of the mechanics of analyzing many statically indeterminate beam structures, including a loaded fuselage ring. The adoption of any suitable and consistent sign convention will definitely insure the correctness of the final answers in both magnitude and sense.

For illustrative Problem 2, the writer purposely used a ring layout and an applied loading which were identical to that used in an illustrative problem presented in a Curtiss-Wright bulletin,[4] because the method adopted therein was that of using symmetrical and antisymmetrical loadings.[5] This permitted an interesting comparison of the column analogy method with one of the methods in current use.

A comparison of the tabular data in the two methods seems to indicate that the actual amount of computational labor is essentially the same. It then becomes a matter of individual preference as to which method is more easily comprehended, hence, more easily applied. It is the author's belief that the column analogy method is more advantageous, particularly where several loads are applied to the fuselage ring or the ring is unsymmetrical.

References

[1] Cross, H., and Morgan, N. D., *Continuous Frames of Reinforced Concrete*, p. 46; John Wiley & Sons, Inc., New York, 1932.

[2] Grinter, L. E., *Theory of Modern Steel Structures*, Vol. 2, p. 216; The Macmillan Company, New York, 1937.

[3] Deyarmond, A., and Arslan, A., *Fundamentals of Stress Analysis*, Vol. 1, p. 114; Aero Publishers, Inc., Glendale, Calif., 1942. Niles, A. S., and Newell, J. S., *Airplane Structures*, Vol. 2, p. 184; John Wiley & Sons, Inc., New York, 1943. Shanley, F. R., and Cozzone, F. P., *Unit Method of Beam Analysis*, Journal of the Aeronautical Sciences, Vol. 8, No. 6, p. 246, April, 1941.

[4] Chapper, J., Cline, F. B., and Peery, D. J., *Analysis of Fuselage Rings*, Structures Bulletin No. 14, Curtiss-Wright Corporation, Airplane Division, St. Louis Plant, August 1, 1941.

[5] Newell, J. S., *The Use of Symmetric and Anti-Symmetric Loadings*, Journal of the Aeronautical Sciences, Vol. 6, No. 6, p. 235, April, 1939.

A New Method of Calculating Natural Modes of Uncoupled Bending Vibration of Airplane Wings and Other Types of Beams

N. O. MYKLESTAD*

California Institute of Technology

SUMMARY

The main advantage of this new method is perhaps its simplicity. While all other methods known to the author require considerable experience, this tabular method may be performed by inexperienced calculators. Also, the amount of labor involved in using any other method becomes prohibitive as the number of desired frequencies increases, and the accuracy will diminish rapidly for higher modes. With the proposed method any particular frequency may be found independently of the others and to any desired degree of accuracy.

A particular advantage of the proposed method is that by plotting such curves as those in Figs. 6 and 9 no frequencies will be overlooked. This is particularly important for the case of flexibly mounted engines, since many frequencies are then bunched together in a small region, such as shown in Fig. 9, and for this case the proposed method is perhaps the only feasible one.

INTRODUCTION

IN DEVELOPING THIS METHOD for finding natural modes (both frequencies and deflection curves) the assumptions were made that the elastic axis of the unbent beam is a straight line, which bends into a plane curve during vibration, and that the mass is concentrated at several discrete points along this axis. When the mass of the beam is distributed along its length, the accuracy of the results obtained will depend on how many points of concentration are used in the calculations. As a rough rule it may be said that at least twice as many concentrated masses should be used as the number of natural frequencies desired, but, if deflection curves are also needed, the number of concentrated masses should not be less than six.

The principle of the method is analogous to Holzer's method for finding natural modes of torsional vibration, but because of the much greater complexity of the problem the development of this new method is entirely different from that of Holzer. Like Holzer's method it is based on the fact that for a forced vibration with finite amplitude the shaking force becomes zero at any one of the natural frequencies. However, while for torsion it is a simple matter to find the shaking force for any assumed frequency and amplitude this is not so for bending. For this reason the tabular form used to find the bending frequencies by the proposed method are much more complex than those developed by Holzer, and the time consumed in finding a bending frequency is about four to five times as great as that needed to find a torsional frequency of a system with the same number of concentrated masses.

Received July 16, 1943.

* Research Associate in Aeronautics, Daniel Guggenheim Aeronautical Laboratory.

METHOD OF ANALYSIS FOR AN AIRPLANE WING

General Principles

Consider the wing to be weightless and to carry a series of concentrated masses, as shown in Fig. 1. The base of the wing is at the plane of symmetry of the fuselage and the fuselage is considered to be perfectly rigid. One-half the mass of the fuselage is given by m_B in Fig. 1. The distance from the base to each individual station is called x, with appropriate subscript, and the length of wing between stations is indicated by l, with appropriate subscript, as shown in Fig. 1.

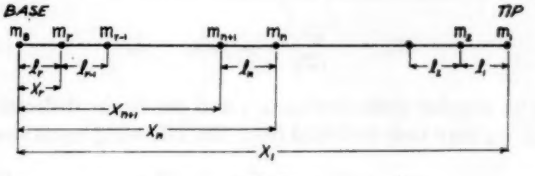

FIG. 1.

Fig. 2 shows the nth section of the wing, between stations n and $n+1$, with the left end of the section clamped. In Fig. 2a there is a unit force on the right end of the wing; in Fig. 2b, a unit bending moment. The linear and angular deflections of the right end due to the unit force are d_{Fn} and v_{Fn}, respectively; due to the unit bending moment, d_{Mn} and v_{Mn}, respectively. These are the elastic constants, which must be calculated for each section of the wing.

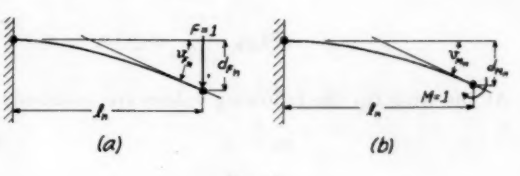

FIG. 2.

Fig. 3 shows the nth section of the wing in its extreme position when the wing is vibrating with a unit amplitude at the tip. The extreme deflection of each of the various stations of the wing is indicated by the letter y, with appropriate subscript, so that y_n is the deflection of the nth mass m_n, etc. If the frequency of the vibration is $\omega/2\pi$ cycles per sec. then the inertia force on each of the masses will be $m\omega^2 y$ and the maximum deflection of the beam during vibration will be the same as if it were statically loaded with these inertia forces. The deflection curve due to this static load is easily found as follows:

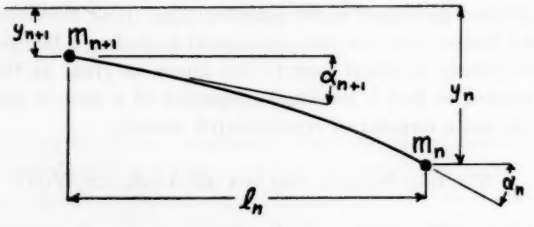

FIG. 3.

Consider the nth section of the wing shown in Fig. 3 and assume that the angular deflection α_n and the linear deflection y_n are both known. The shear force S_n at the left of the nth station is simply the sum of all the inertia forces from this station to the tip, or

$$S_n = \sum_{i=1}^{i=n} m_i\omega^2 y_i \tag{1}$$

The bending moment at the nth station is

$$M_n = \sum_{i=1}^{i=n-1} m_i\omega^2 y_i(x_i - x_n) \tag{2}$$

The angular deflection α_{n+1} and the linear deflection y_{n+1} may now be found from the following equations:

$$\alpha_{n+1} = \alpha_n - S_n v_{Fn} - M_n v_{Mn} \tag{3}$$

$$y_{n+1} = y_n - l_n\alpha_{n+1} - S_n d_{Fn} - M_n d_{Mn} \tag{4}$$

Substituting the values of S_n and M_n from Eqs. (1) and (2) will give

$$\alpha_{n+1} = \alpha_n - \omega^2 v_{Fn} \sum_{i=1}^{i=n} m_i y_i - \omega^2 v_{Mn} \sum_{i=1}^{i=n-1} m_i y_i(x_i - x_n) \tag{5}$$

$$y_{n+1} = y_n - l_n\alpha_{n+1} - \omega^2 d_{Fn} \sum_{i=1}^{i=n} m_i y_i - \omega^2 d_{Mn} \sum_{i=1}^{i=n-1} m_i y_i(x_i - x_n) \tag{6}$$

At the wing tip the following values are assumed:

$$\alpha_1 = \varphi \tag{7}$$

$$y_1 = 1 \tag{8}$$

where φ is an arbitrary tip angle. Eqs. (5) and (6) will give

$$\alpha_2 = \varphi - v_{F1}\omega^2 m_1 = \varphi - f_2 \tag{9}$$

$$y_2 = 1 + l_1 f_2 - d_{F1}\omega^2 m_1 - l_1\varphi = g_2 - l_1\varphi \tag{10}$$

By continuing to use Eqs. (5) and (6), the following general expressions are found:

$$\alpha_n = h_n\varphi - f_n \tag{11}$$

$$y_n = g_n - k_n\varphi \tag{12}$$

where the coefficients h_n, f_n, g_n, and k_n are independent of the arbitrary tip angle φ. How these constants may be obtained by a tabular method will be explained later, but first assume that they have all been obtained for a particular value of ω. At the base of the wing, then, the known values of α and y will be

$$\alpha_B = h_B\varphi - f_B \tag{13}$$

$$y_B = g_B - k_B\varphi \tag{14}$$

Suppose, first, that the airplane is being shaken up and down by a vertical shaking force $2F \cos \omega t$ through the middle of the fuselage, of mass $2m_B$, as shown in Fig. 4. The slope α_B will then be equal to zero and the motion will be a symmetric bending vibration. The corresponding values of φ and y will be denoted by φ' and y'. From Eq. (13), then, $0 = h_B\varphi' - f_B$ or

$$\varphi' = f_B/h_B \tag{15}$$

With this value of φ', all the deflections y' and all the products my' are found. If ω is one of the natural angular frequencies for symmetric bending then $\Sigma my' = 0$, where $\Sigma my' = m_B y_B' + \sum_{i=1}^{i=r} m_i y_i'$. This follows from the fact that at resonance the shaking force is zero, and in order to have equilibrium the sum of all

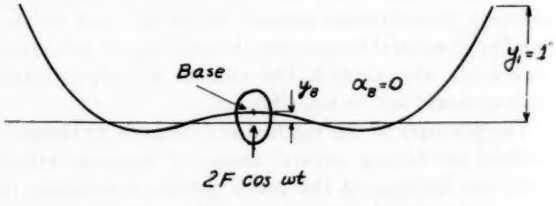

FIG. 4. Symmetric bending vibration.

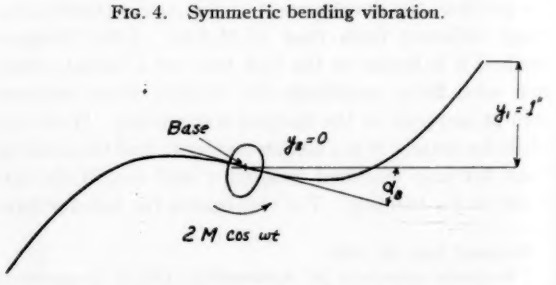

FIG. 5. Antisymmetric bending vibration.

inertia forces, $\Sigma m\omega^2 y'$, must then also be zero. Plotting $\Sigma my'$ against ω will give a curve such as shown in Fig. 6a, and the approximate values of all the symmetric frequencies will be obtained by the points of intersection of this curve and the ω axis.

The region around the desired frequencies may be plotted to a larger scale by calculating several points in each of these regions. If these points are close to the desired frequency, a straight line interpolation will give a good value of this frequency. To obtain the correct values of y', and also as a check, the interpolated value of ω should be used in a final calculation. In this way all the symmetric frequencies and deflection curves may be obtained independently of each other to any desired degree of accuracy.

Now consider the case of the airplane being shaken by a shaking moment $2M \cos \omega t$ about the axis of the fuselage, as shown in Fig. 5. The deflection y_B will then be equal to zero and the motion will be an antisymmetric bending vibration. The corresponding values of φ and y will now be denoted by φ'' and y''. From Eq. (14), then, $0 = g_B - k_B\varphi''$ or

$$\varphi'' = g_B/k_B \tag{16}$$

With this value of φ'' all the deflections y'' and all the products mxy'' are found. If ω is one of the natural angular frequencies for antisymmetric bending, then $\Sigma mxy'' = 0$, where $\Sigma mxy'' = \sum_{i=1}^{i=r} m_i x_i y_i''$. This follows from the fact that at resonance $M = 0$, and in order to have equilibrium of moment about the axis of the fuselage the sum of all inertia moments, $\Sigma m\omega^2 xy''$, must then also be zero. By plotting $\Sigma mxy''$ against ω a curve such as shown in Fig. 6b is obtained. From this curve all the antisymmetric frequencies may be obtained in exactly the same manner as the symmetric ones were obtained from Fig. 6a. It is seen that one set of values of the constants h, f, g, and k will give a point on each of the curves 6a and 6b.

Determination of the Coefficients h, f, g, and k

The initial values of these coefficients are easily obtained from Eqs. (7) and (8) as

$$h_1 = 1 \qquad f_1 = 0 \qquad g_1 = 1 \qquad k_1 = 0 \tag{17}$$

and from Eqs. (9) and (10) the following values are also found:

$$h_2 = 1 \qquad k_2 = l_1 \tag{18}$$

To find the coefficients for any station it is only necessary to substitute Eqs. (11) and (12) into Eqs. (5) and (6), which gives

$$h_{n+1}\varphi - f_{n+1} = h_n\varphi - f_n - \omega^2 v_{Fn} \sum_{i=1}^{i=n} m_i(g_i - k_i\varphi) - \omega^2 v_{Mn} \sum_{i=1}^{i=n-1} m_i(g_i - k_i\varphi)(x_i - x_n) \tag{19}$$

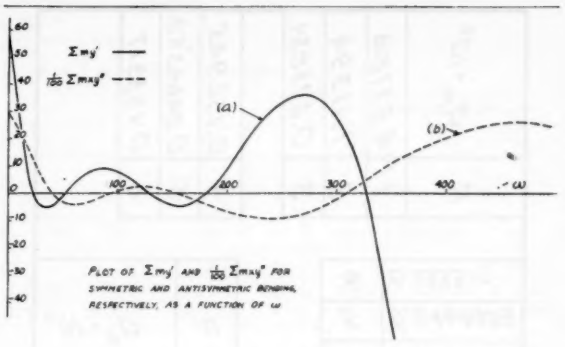

FIG. 6.

$$g_{n+1} - k_{n+1}\varphi = g_n - k_n\varphi - l_n h_{n+1}\varphi + l_n f_{n+1} - \omega^2 d_{Fn} \sum_{i=1}^{i=n} m_i(g_i - k_i\varphi) - \omega^2 d_{Mn} \sum_{i=1}^{i=n-1} m_i(g_i - k_i\varphi) \times (x_i - x_n) \tag{20}$$

By equating the terms containing φ and those not containing φ on the two sides of each of Eqs. (19) and (20), the following equations are obtained

$$h_{n+1} = h_n + \omega^2 v_{Fn} \sum_{i=1}^{i=n} m_i k_i + \omega^2 v_{Mn} \sum_{i=1}^{i=n-1} \left[m_i k_i \sum_{s=i}^{s=n-1} l_s \right] \tag{21}$$

$$k_{n+1} = k_n + l_n h_{n+1} - \omega^2 d_{Fn} \sum_{i=1}^{i=n} m_i k_i - \omega^2 d_{Mn} \sum_{i=1}^{i=n-1} \left[m_i k_i \sum_{s=i}^{s=n-1} l_s \right] \tag{22}$$

$$f_{n+1} = f_n + \omega^2 v_{Fn} \sum_{i=1}^{i=n} m_i g_i + \omega^2 v_{Mn} \sum_{i=1}^{i=n-1} \left[m_i g_i \sum_{s=i}^{s=n-1} l_s \right] \tag{23}$$

$$g_{n+1} = g_n + l_n f_{n+1} - \omega^2 d_{Fn} \sum_{i=1}^{i=n} m_i g_i - \omega^2 d_{Mn} \sum_{i=1}^{i=n-1} \left[m_i g_i \sum_{s=i}^{s=n-1} l_s \right] \tag{24}$$

In the above equations put

$$m\omega^2 k = K \tag{25}$$

$$m\omega^2 g = G \tag{26}$$

Also

$$\sum_{i=1}^{i=n-1} \left[K_i \sum_{s=i}^{s=n-1} l_s \right] = K_1(l_1 + l_2 + \ldots + l_{n-1}) + K_2(l_2 + \ldots + l_{n-1}) + \ldots + K_{n-1}l_{n-1} = l_1K_1 + l_2(K_1 + K_2) + \ldots + l_{n-1}(K_1 + K_2 + \ldots + K_{n-1}) = \sum_{i=1}^{i=n-1} \left[l_i \sum_{s=1}^{s=i} K_s \right]$$

Eqs. (21) to (24) may then be written:

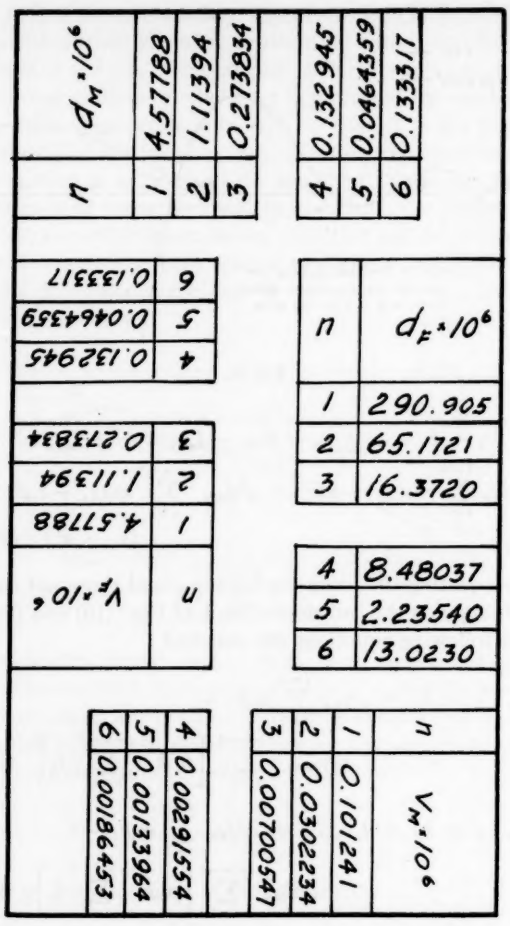

FIG. 7.

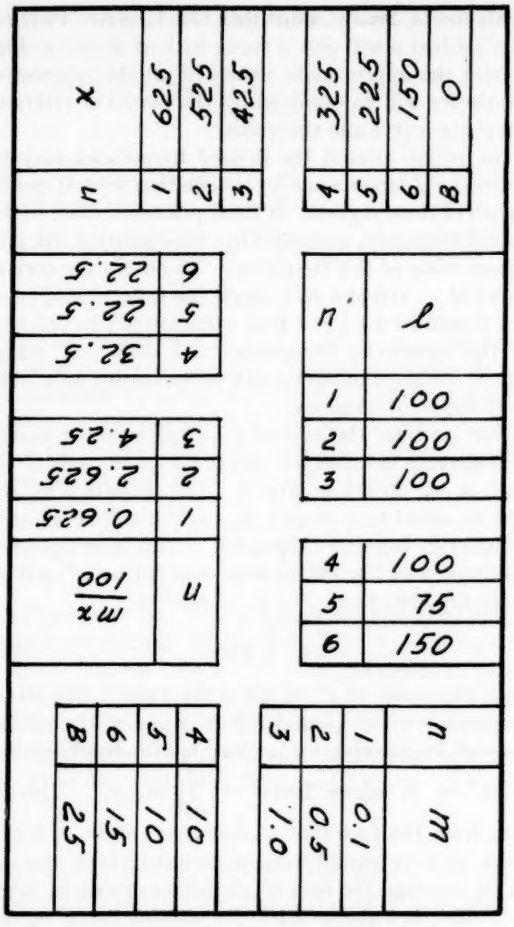

FIG. 8.

$$h_{n+1} = h_n + v_{Fn} \sum_{i=1}^{i=n} K_i + v_{Mn} \sum_{i=1}^{i=n-1} \left[l_i \sum_{s=1}^{s=i} K_s \right] \quad (27)$$

$$k_{n+1} = k_n + l_n h_{n+1} - d_{Fn} \sum_{i=1}^{i=n} K_i - d_{Mn} \sum_{i=1}^{i=n-1} \left[l_i \sum_{s=1}^{s=i} K_s \right] \quad (28)$$

$$f_{n+1} = f_n + v_{Fn} \sum_{i=1}^{i=n} G_i + v_{Mn} \sum_{i=1}^{i=n-1} \left[l_i \sum_{s=1}^{s=i} G_s \right] \quad (29)$$

$$g_{n+1} = g_n + l_n f_{n+1} - d_{Fn} \sum_{i=1}^{i=n} G_i - d_{Mn} \sum_{i=1}^{i=n-1} \left[l_i \sum_{s=1}^{s=i} G_s \right] \quad (30)$$

Illustrative Example

To illustrate the tabular method consider a hypothetic airplane with six stations along the wing at which the weight is concentrated. First calculate the constants v_F, d_F, v_M, and d_M for each section of the wing, as will be shown later, and write these values on a card such as shown in Fig. 7. On the back of this card, or on another card, write the quantities l, m, x, and mx, as shown in Fig. 8. The spacings on these cards should correspond exactly to the horizontal lines in the main table shown in Table 1, as they are used as parts of this table. The left part of this table is used to find all the coefficients h, k, f, and g, starting at the tip and progressing to the base according to Eqs. (27) to (30). After φ' and φ'' have been found, according to Eqs. (15) and (16), the right part of Table 1 is used to find y', my', $\Sigma my'$, y'', mxy'', and $\Sigma mxy''$. This will give one point on each of the two curves of Fig. 6. By going through this table with various values of ω, such curves as (a) and (b) of Fig. 6 are obtained. For this particular example $\omega = 100$.

In Table 1 the following spaces may be filled in at once: for $n = 1$, columns 1, 2, 3, 4, 5, 6, 7, 8, 9, 10, 13, 14, 15, 19, 20, 21, 22, 23, and 24; for $n = 2$, columns 1, 4, 5, and 6; and for the base row, columns 23 and 24. It should also be noted that for increasing values of ω

TABLE 1

$\omega = 100$ $\quad \frac{\omega^2}{10^4} = 0.01$ $\quad f = \frac{60}{2\pi}\omega = 955$ cycles per min.

												Symmetric Bending		
		1	2	3	4	5	6	7	8	9		19	20	21
n	$\frac{m\omega^2}{10^4}$	k	$K \times 10^{-4} = \frac{m\omega^2 k}{10^4}$	$\Sigma K \times 10^{-4}$	$10^{-4}l\Sigma K$ for $n-1$	$\Sigma(4) \times 10^{-4}$	k	$h_{n+1} = v_F(3) + v_M(5) + (6)$	$lh_{n+1} = l(7)$	$k_{n+1} = (1) + (8) - d_F(3) - d_M(5)$	n	$\varphi'(1)$	$y' = (10)-(19)$	my'
1	0.001	0	0	0	0	0	1	1	100	100	1	0	1	0.100000
2	0.005	100	0.5	0.5	0	0	1	1.55697	155.697	223.111	2	1.01967	0.14721	0.07360
3	0.01	223.111	2.23111	2.73111	50	50	1.55697	2.65511	265.511	430.217	3	2.27500	−0.1436	−0.1436
4	0.1	430.217	43.0217	45.7528	273.111	323.111	2.65511	9.67976	967.976	967.236	4	4.38679	−0.08980	−0.8980
5	0.1	967.236	96.7236	142.476	4,575.28	4,898.39	9.67976	22.8578	1,714.34	2,135.62	5	9.86262	0.05019	0.5019
6	0.15	2,135.62	320.343	462.819	10,685.7	15,584.1	22.8578	113.616	17,042.4	11,073.1	6	21.7763	0.0952	1.428
B		11,073.1					113.616				Base	112.909	0.069	1.72

$\varphi' = \frac{(15)_B}{(6)_B} = 0.0101967$ $\qquad \varphi'' = \frac{(10)_B}{(1)_B} = 0.0102029$ $\qquad \Sigma my' = 2.78$

												Antisymmetric Bending		
		10	11	12	13	14	15	16	17	18		22	23	24
n	$\frac{m\omega^2}{10^4}$	g	$G \times 10^{-4} = \frac{m\omega^2}{10^4} g$	$\Sigma G \times 10^{-4}$	$10^{-4}l\Sigma G$ for $n-1$	$\Sigma(13) \times 10^{-4}$	f	$f_{n+1} = v_F(12) + v_M(14) + (15)$	$lf_{n+1} = l(16)$	$g_{n+1} = (10) + (17) - d_F(12) - d_M(14)$	n	$\varphi''(1)$	$y'' = (10)-(22)$	$\frac{mx}{100} y''$
1	0.001	1	0.001	0.001	0	0	0	0.00457788	0.457788	1.16688	1	0	1	0.625000
2	0.005	1.16688	0.0058344	0.0068344	0.1	0.1	0.00457788	0.0152133	1.52133	2.13140	2	1.02029	0.14659	0.3848
3	0.01	2.13140	0.021314	0.0281484	0.68344	0.78344	0.0152133	0.0284097	2.84097	4.29699	3	2.27638	−0.14498	−0.6162
4	0.10	4.29699	0.429699	0.457847	2.81484	3.59828	0.0284097	0.0997691	9.97691	9.91281	4	4.38946	−0.09247	−3.005
5	0.10	9.91281	0.991281	1.44913	45.7847	49.3830	0.0997691	0.233216	17.4912	21.8715	5	9.86861	0.0442	0.994
6	0.15	21.8715	3.28072	4.72985	108.685	158.068	0.233216	1.15851	173.776	112.978	6	21.7895	0.0820	1.845
B		112.978					1.15851				Base	112.978	0	0

$\frac{1}{100} \times \Sigma mxy'' = 0.227$

φ' and φ'' become nearly identical in value and the deflections y are obtained as small differences between large quantities. For this reason it is necessary to use at least eight significant figures to obtain the highest modes, but these will probably never be required.

Flexibly Mounted Engines

The case of flexibly mounted engines may be calculated just like the case of rigid engines except that the masses of the engines must first be multiplied by the factor $1/1 - (\omega^2/\omega_e^2)$, where ω is the angular frequency used in Table 1 and ω_e is the natural angular frequency for vertical motion of the engines. When $\omega > \omega_e$ the above factor becomes negative and may result in negative masses at the engine stations.

When the curves of Fig. 6 are plotted for this case, particular care should be taken to obtain a sufficient number of points in the region $0.9\omega_e < \omega < 1.5\omega_e$, as these curves fluctuate violently in this region and the frequencies are close together.

Fig. 9 shows this particular region for an engine frequency of 200 cycles per minute in the same airplane as was used to plot the curves in Fig. 6. It is seen that no less than nine frequencies, of a possible 17, occur in this region. Outside the region the curves behave in much the same manner as do those of Fig. 6 and the frequencies are spread quite far apart. For higher engine frequencies, however, the fluctuations of the

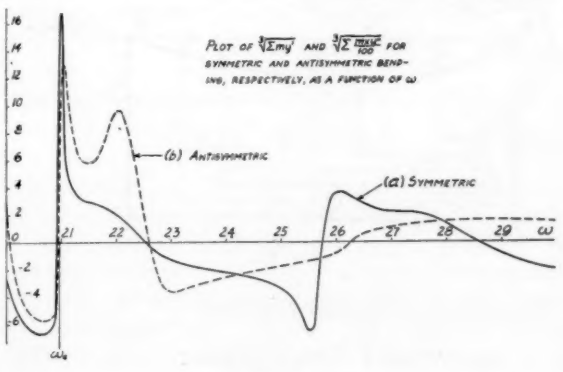

FIG. 9.

curves in Fig. 9 may become less violent because the region will extend over a larger range.

Application to Other Types of Beams

Cantilever Beam

To find the natural frequencies of a cantilever beam with concentrated masses it is merely necessary to shake the support up and down with harmonic motion and find φ just as in the case of symmetric bending previously described. However, the condition of resonance is now that y_B is zero; thus, instead of plotting Σmy, the value of y_B should be plotted against ω. Every time $y_B = 0$ there will be a natural frequency.

Simply Supported Beam

The case of a simply supported beam with concentrated masses may be treated by a method analogous to that for an airplane wing. Considering the vibrating beam of Fig. 10, which is being shaken by a moment $M \cos \omega t$ at its left end, the equations for the shear force and bending moment become

$$S_n = \sum_{i=1}^{i=n} m_i \omega^2 y_i - R_a \tag{31}$$

$$M_n = R_a \sum_{i=1}^{i=n-1} l_i - \sum_{i=1}^{i=n-1} \left[m_i \omega^2 y_i \sum_{s=i}^{s=n-1} l_s \right] + M_a \tag{32}$$

where R_a is the unknown reaction at the right end of the beam in the extreme position and M_a is an arbitrary end moment that is used to take care of a possible overhang, as will be explained later.

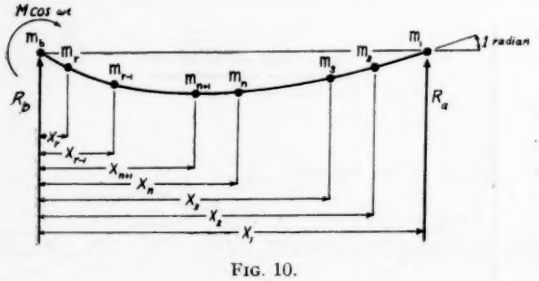

Fig. 10.

From Fig. 11 it is easily seen that

$$\alpha_{n+1} = \alpha_n + S_n v_{Fn} - M_n v_{Mn} \tag{33}$$

$$y_{n+1} = y_n + l_n \alpha_{n+1} - S_n d_{Fn} + M_n d_{Mn} \tag{34}$$

In the same way as was done for a cantilever beam it can be shown that, in general,

$$\alpha_n = h_n - f_n R_a \tag{35}$$

$$y_n = k_n - g_n R_a \tag{36}$$

and

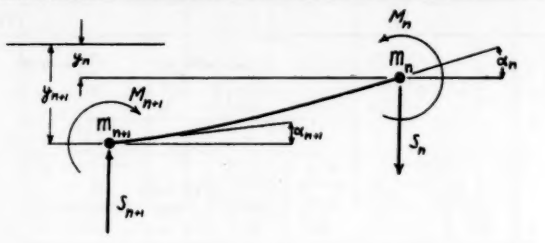

Fig. 11.

$$h_{n+1} = h_n + v_{Fn} \sum_{i=1}^{i=n} K_i + v_{Mn} \sum_{i=1}^{i=n-1} \left[l_i \sum_{s=1}^{s=i} K_s \right] - P_n \tag{37}$$

$$k_{n+1} = k_n + l_n h_{n+1} - d_{Fn} \sum_{i=1}^{i=n} K_i - d_{Mn} \sum_{i=1}^{i=n-1} \left[l_i \sum_{s=1}^{s=i} K_s \right] + Q_n \tag{38}$$

$$f_{n+1} = f_n + v_{Fn} \sum_{i=1}^{i=n} G_i + v_{Mn} \sum_{i=1}^{i=n-1} \left[l_i \sum_{s=1}^{s=i} G_s \right] + T_n \tag{39}$$

$$g_{n+1} = g_n + l_n f_{n+1} - d_{Fn} \sum_{i=1}^{i=n} G_i - d_{Mn} \sum_{i=1}^{i=n-1} \left[l_i \sum_{s=1}^{s=i} G_s \right] - U_n \tag{40}$$

where

$$P_n = v_{Mn} M_a \tag{41}$$

$$Q_n = d_{Mn} M_a \tag{42}$$

$$T_n = v_{Fn} + v_{Mn} \sum_{i=1}^{i=n-1} l_i \tag{43}$$

$$U_n = d_{Fn} + d_{Mn} \sum_{i=1}^{i=n-1} l_i \tag{44}$$

The quantities T_n and U_n may be calculated once and for all and put on a separate card similar to Figs. 7 and 8.

At the right end of the beam the deflection y is zero and an arbitrary angular deflection, say 1 rad., may be assumed. This gives

$$\alpha_1 = 1 \tag{45}$$

$$y_1 = 0 \tag{46}$$

and

$$h_1 = 1 \qquad f_1 = 0 \qquad k_1 = 0 \qquad g_1 = 0 \tag{47}$$

Eqs. (37) to (40) then give

$$f_2 = T_1 \qquad g_2 = l_1 T_1 - U_1 \tag{48}$$

and, for a beam without overhang, $h_2 = 1$ and $k_2 = l_1$.

TABLE 2

		(1)	(2)	(3)	(4)	(5)	(6)		(7)	(8)		(9)	
n	$m\omega^2$	k	$K=m\omega^2k$	ΣK	$l\Sigma K$ for $n-1$	$\Sigma(4)$	h	$P = v_M M_a$	$h_{n+1} = v_F(3) + v_M(5) + (6) - P$	$lh_{n+1} = l(7)$	$Q = d_M M_a$	$k_{n+1} = (1) + (8) + Q - d_F(3) - d_M(5)$	n
1		0	0	0	0	0	1						1
2					0	0							2
.													.
.													.
.													.
r													r
b													b

$$R_a = \frac{(1)_b}{(10)_b} = \text{\_\_\_\_\_}$$

		(10)	(11)	(12)	(13)	(14)	(15)	(16)	(17)	(18)		(19)	(20)	(21)
n	$m\omega^2$	g	G	ΣG	$l\Sigma G$ for $n-1$	Σ (13)	f	$f_{n+1} = v_F(12) + v_M(14) + (15) + T$	$lf_{n+1} = l(16)$	$g_{n+1} = (10) + (17) - U - d_F(12) - d_M(14)$	n	$R_a(10)$	$y = (1) - (19)$	mxy
1		0	0	0	0	0	0	T_1	l_1T_1	$l_1T_1 - U_1$	1	0	0	0
2		$l_1T_1 - U_1$		0	0	T_1					2			
.											.			
.											.			
r											r			
b											b		0	0

Using Eqs. (37) to (40) it is now possible to proceed to the left end of the beam by a tabular method similar to that for a cantilever beam. Table 2 shows this case for a beam with overhang. For a beam without overhang P_n and Q_n are both zero and these columns may then be left out. Also the quantities $h_2 = 1$ and $k_2 = l_1$ may be added.

At the left end of the beam $y_b = 0$, which gives

$$k_b - g_b R_a = 0$$

$$R_a = k_b/g_b \tag{49}$$

With this value of R_a all the deflections y_n may be calculated from Eq. 36, which is done in column 20 of Table 2. In column 21 the quantities mxy are calculated. Finally, the quantity

$$M = R_a l - \omega^2 \Sigma mxy$$

should be plotted as a function of ω, giving a curve similar to Fig. 6a or 6b. When the amplitude M of the shaking moment is zero there will be a natural frequency.

Simply Supported Beam with Overhangs

Fig. 12 shows a vibrating beam with overhangs at both ends and a shaking moment $M \cos \omega t$ at the left support. The right overhang will first be considered. At the right end of the beam assume

$$y_1' = 1 \tag{50}$$

$$\alpha_1' = \varphi' \tag{51}$$

Then proceed by the tabular method of Table 1 until the right support is reached, and find

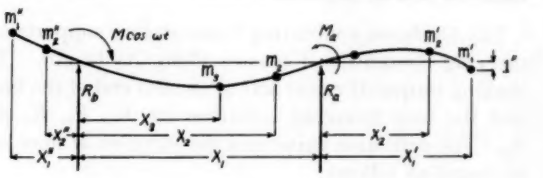

FIG. 12.

$$\varphi' = g_a'/k_a' \tag{52}$$

which makes $y_a = 0$. As the beam is continuous at station a, the value of α_1 for the midspan will be

$$\alpha_1 = \alpha_a' \tag{53}$$

The right end bending moment for the midspan is

$$M_a = -\Sigma\, m'\omega^2 x' y' \tag{54}$$

and the reaction $R_a' = R_a - \Sigma m'\omega^2 y'$, where R_a is the total reaction for the beam with overhang.

Now, consider the main beam and proceed by the tabular method of Table 2, except that $\alpha_1 = \alpha_a'$ instead of unity. At the left support the deflection $y_b = 0$ and R_a' is determined by Eq. (49). This will give all the deflections for the midspan and also the slope $\alpha_b = \alpha_b''$.

For the left overhang start at the left end of the beam with the arbitrary deflections

$$\alpha_1'' = \varphi \tag{55}$$

$$y_1'' = \eta \tag{56}$$

The general case will then be

$$\alpha_n'' = h_n''\varphi'' - f_n''\eta'' \tag{57}$$

$$y_n'' = g_n''\eta'' - k_n''\varphi'' \tag{58}$$

and by proceeding to the left support, according to the tabular method of Table 1, the values

$$\left.\begin{aligned} h_b''\varphi'' - f_b''\eta'' &= \alpha_b \\ -k_b''\varphi'' + g_b''\eta'' &= y_b = 0 \end{aligned}\right\} \tag{59}$$

will be obtained. Solving these two equations simultaneously gives

$$\varphi'' = \alpha_b g_b''/(h_b''g_b'' - k_b''f_b'') \tag{60}$$

$$\eta'' = \alpha_b k_b''/(h_b''g_b'' - k_b''f_b'') \tag{61}$$

With these values of φ'' and η'' the deflections y'' can be found from Eq. (58).

The amplitude of the shaking moment is now

$$M = M_a + R_a'x_1 - \Sigma m\omega^2 xy + \Sigma m''\omega^2 x''y'' \tag{62}$$

where y and y'' are both positive downward and negative upward and all the quantities x and x'' are considered to be positive.

Plotting this quantity against ω will give a curve similar to either of those in Fig. 6, and every time $M = 0$ there will be a natural frequency.

Beam on Several Supports

Fig. 13 shows a vibrating beam on four supports and carrying concentrated masses along its length. The shaking torque $M \cos \omega t$ acts at the left end of the beam and the four unknown reactions are R_a, R_b, R_c, and R_d. The deflection curve and the value of M may now be found as follows:

First consider the right-hand beam shown in Fig. 14a and start with $\alpha_a = 1$ rad. Then go through Table 2 and put $y_b = 0$. Eq. (49) will then give R_a and Eq. (36) will give the deflections y_n. M_b and R_b' will be determined by the equations

$$M_b = L_1R_a - \Sigma m\omega^2 xy \tag{63}$$

$$R_b' = \Sigma m\omega^2 y - R_a \tag{64}$$

Next consider the middle beam shown in Fig. 14b and start with the known end moment M_b and the known angular deflection α_b, obtained from the first beam by means of Eq. (35). Repeat the tabular calculation for this case and obtain R_b'' from the equation

$$R_b'' = k_c/g_c \tag{65}$$

and the deflections y_n from Eq. (36). Also obtain α_c by means of Eq. (35). The moment M_c and reaction R_c' are then

$$M_c = M_b + R_b''L_2 - \Sigma m\omega^2 xy \tag{66}$$

$$R_c' = \Sigma m\omega^2 y - R_b'' \tag{67}$$

Finally, the tabular calculation is performed for the left-hand beam in exactly the same way as for the middle one. This gives

$$R_c'' = k_d/g_d \tag{68}$$

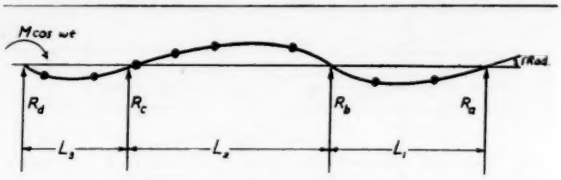

FIG. 13.

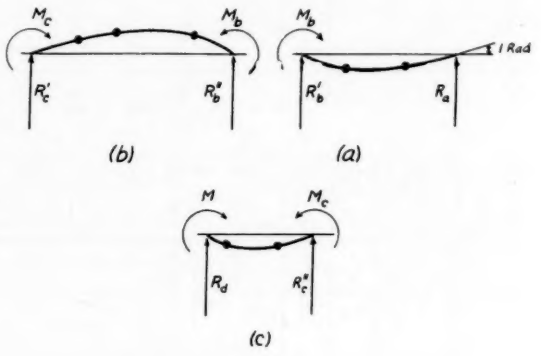

FIG. 14.

$$R_d = \Sigma m\omega^2 y - R_c'' \tag{69}$$

$$M = M_b + R_c''L_3 - \Sigma m\omega^2 xy \tag{70}$$

By plotting the quantity M against ω a curve similar to those on Fig. 6 is obtained. A natural frequency is obtained every time this curve crosses the ω axis.

If the reactions R_b and R_c are desired these are easily obtained as

$$R_b = R_b' + R_b'' \tag{71}$$

$$R_c = R_c' + R_c'' \tag{72}$$

Determination of the Elastic Coefficients v_M, d_M, v_F, and d_F

As these are not basic data but calculated quantities, interrelated in such a way that their accuracy is of paramount importance in the subsequent calculations, they must be computed with extreme care. If more than two modes are desired, it is recommended that seven significant figures be consistently employed throughout the computations of these coefficients and that six significant figures be retained in the vibration calculations. The deflections y' and y'' can then be obtained to a reasonable degree of accuracy for all but the highest modes. If only the two lowest modes are desired it will usually be sufficient to use four significant figures for the calculations in Table 1 and five for the calculations of the elastic coefficients. However, the number of places to which y' and y'' are obtained will serve as a guide in this respect.

Fig. 15 shows a typical bending stiffness curve for an airplane wing, where the moment of inertia of cross-sectional area is plotted against the distance from the

TABLE 3
$EI_0 = 5 \times 10^{10}$

	1	2	3	4	5	6	7	8	9
n	l	a	$a+b$	$\frac{(3)}{(2)}$	ln (4)	b = (3)−(2)	$\frac{l}{b}=\frac{(1)}{(6)}$	$v_M \times 10^9 = \frac{(5)(7)}{50}$	(2)(5)(10^9)
1	100	0.0146	0.026	1.780822	0.5770750	0.0114	8,771.930	101.241	8.425295
2	100	0.026	0.135	5.192308	1.647178	0.109	917.431	30.2234	42.82663
3	100	0.135	0.520	3.851852	1.348554	0.385	259.740	7.00547	182.0548
4	100	0.520	0.884	1.700000	0.5306282	0.364	274.725	2.91554	275.9267
5	75	0.884	1.394	1.576923	0.4554755	0.510	147.059	1.33964	402.6403
6	150	1.394	1.845	1.323529	0.2803015	0.451	332.594	1.86453	390.7403

	10	11	12	13	14	15	16	17	18
n	[(6)−(9)](10^{-5})	(7)(7)(10^{-4})	$v_F \times 10^9 = d_M \times 10^9 = \frac{(10)(11)}{50}$	$\frac{(6)(6)}{2}$(10^9)	(2)(9)(10^9)	(2)(6)(10^9)	[(13) + (14) − (15)] × (10^9)	(7)(11)(10^{-7})	$d_F \times 10^9 = \frac{(16)(17)}{50}$
1	2.974705	7,694.676	4,577.88	0.0649800	0.1230094	0.166440	0.0215494	67497.159	290,905
2	66.17337	84.16796	1,113.94	5.940500	1.113492	2.834000	4.219992	77.2183	65,172.1
3	202.9452	6.74649	273.834	74.11250	24.57740	51.97500	46.71490	1.75233	16,372.0
4	88.0733	7.54738	132.945	66.2480	143.4819	189.2800	20.4499	2.07345	8,480.37
5	107.3597	2.16263	46.4359	130.0500	355.9341	450.8400	35.1441	0.318034	2,235.40
6	60.2597	11.0619	133.317	101.7005	544.6920	628.6940	17.6985	3.67912	13,023.0

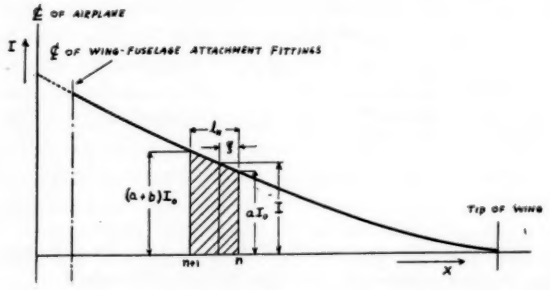

FIG. 15.

fuselage axis as abscissa. The cross-hatched part of the curve, corresponding to the nth section of the wing, may evidently be approximated by a trapezoid. Let I_0 be a reference value of the moment of inertia taken for the wing as a whole; then the two parallel sides of the trapezoid will have the lengths aI_0 and $(a+b)I_0$ as shown in Fig. 15—and for this section of the beam the moment of inertia may be written as

$$I = I_0[a + (b/l)\xi] \tag{73}$$

where ξ is measured along the wing from station n and where a and b are dimensionless quantities.

Using any convenient method for finding angular and linear deflections, it is now easily seen that

$$v_M = \int_0^l \frac{d\xi}{EI_0[a + (b/l)\,\xi]} = \frac{1}{EI_0}\frac{l}{b}\ln\frac{a+b}{a} \tag{74}$$

$$d_M = v_F = \int_0^l \frac{\xi d\xi}{EI_0[a + (b/l)\xi]} = \frac{1}{EI_0}\frac{l^2}{b^2}\left(b - a\ln\frac{a+b}{a}\right) \tag{75}$$

$$d_F = \int_0^l \frac{\xi^2 d\xi}{EI_0[a + (b/l)\xi]} = \frac{1}{EI_0}\frac{l^3}{b^3}\left(\frac{b^2}{2} + a^2\ln\frac{a+b}{a} - ab\right) \tag{76}$$

where

$$\ln\frac{a+b}{a} = 2.302585\log_{10}\frac{a+b}{a} \tag{77}$$

and the subscript n is left out for convenience. In Table 3 these calculations have been performed for a typical example. For this particular case the stiffness curve was continued to the centerline of the airplane, but quite often the stiffness through the fuselage is considered to be infinite. In the latter case, there will be a station added at the wing-fuselage attachment fittings, and the mass of the fuselage may then be concentrated here in order to compensate for its mass moment of inertia about the axis of the airplane in the antisymmetric modes. One more station will then also be needed in Table 1 in order to obtain $y_B = 0$ for the antisymmetric case. However, the last section will have $v_M = d_M = v_F = d_F = 0$ in this case.

APPENDIX

Since this paper was prepared the author has simplified the tabular calculations greatly, as will be described briefly below.

Instead of defining K and G as in the main body of the paper, define them as follows:

$$K_n = \sum_{i=1}^{i=n} m_i\omega^2 k_i \tag{78}$$

$$G_n = \sum_{i=1}^{i=n} m_i\omega^2 g_i \tag{79}$$

TABLE 4

ω =					$\omega^2 \times 10^{-6}$ =		
	1	2	3	4		Symmetric	
$\frac{m\omega^2}{10^6}$	$k = (1) + l(4) - d_F(2) - d_M(3)$ for $n - 1$	$K \times 10^{-6} = \Sigma \frac{m\omega^2}{10^6}(1)$	$K' \times 10^{-6} = \Sigma l(2)$ for $n - 1$	$h_{n+1} = h_n + v_F(2) + v_M(3)$ $h_1 = 1$	n	$y' = g - k\varphi'$	my'
	0	0	0	1	1	1	
			0		2		
					B		
$\varphi' = f_B/h_B$ =				$\varphi'' = g_B/k_B$ =			
	1	2	3	4		Antisymmetric	
$\frac{m\omega^2}{10^6}$	$g = (1) + l(4) - d_F(2) - d_M(3)$ for $n - 1$	$G \times 10^{-6} = \Sigma \frac{m\omega^2}{10^6}(1)$	$G' \times 10^{-6} = \Sigma l(2)$ for $n - 1$	$f_{n+1} = f_n + v_F(2) + v_M(3)$ $f_1 = 0$	n	$y'' = g - k\varphi''$	$\frac{mx}{100} y''$
	1		0		1	1	
					2		
					B	0	0
$(1/\omega^2)(G_B - K_B\varphi')$ =				$(1/100\omega^2)(G_B' - K_B'\varphi'')$ =			

Also, define the following quantities:

$$K_n' = \sum_{i=1}^{i=n-1} l_i K_i \tag{80}$$

$$G_n' = \sum_{i=1}^{i=n-1} l_i G_i \tag{81}$$

Eqs. (27) to (30) may then be written in the form:

$$h_{n+1} = h_n + v_{Fn}K_n + v_{Mn}K_n' \tag{82}$$

$$k_{n+1} = k_n + l_n h_{n+1} - d_{Fn}K_n - d_{Mn}K_n' \tag{83}$$

$$f_{n+1} = f_n + v_{Fn}G_n + v_{Mn}G_n' \tag{84}$$

$$g_{n+1} = g_n + l_n f_{n+1} - d_{Fn}G_n - d_{Mn}G_n' \tag{85}$$

For the airplane wing in symmetric vibration the amplitude F of the shaking force is equal to $G_B - K_B\varphi'$ and the quantity plotted in Fig. 6a is simply $(1/\omega^2)(G_B - K_B\varphi')$.

For the antisymmetric case the moment $M = G_B' - K_B'\varphi''$ and the quantity plotted in Fig. 6b is simply $(1/100\omega^2)(G_B' - K_B'\varphi'')$.

It is therefore not necessary to calculate the values of y', y'', my'', $(mx/100)y''$ except when the amplitudes curve itself is desired.

Table 1 may now be simplified to that of Table 4.

TABLE 5

$d_F \times 10^6$	$\frac{d_M \times 10^6}{v_F \times 10^6}$	$v_M \times 10^6$	n	l	m	$\frac{mx}{100}$
			1			
			B			

For a simply supported beam Eqs. (37) to (40) may be written identically to Eqs. (82) to (85) when

$$K_n = \sum_{i=1}^{i=n} m_i\omega^2 k_i \tag{86}$$

$$G_n = 1 + \sum_{i=1}^{i=n} m_i\omega^2 g_i \tag{87}$$

$$K_n' = \sum_{i=1}^{i=n-1} l_i K_i - M_a \tag{88}$$

$$G_n' = \sum_{i=1}^{i=n-1} l_i G_i \tag{89}$$

and it is not necessary to find the quantities P, Q, T, and U. Table 3 may then be simplified in a similar manner to that of Table 1.

The shaking moment M may now be written as $M = R_a G_b' - K_b'$, and it is not necessary to find the deflections y.

The expressions for F and M are easily obtained from Eqs. (1) and (2) for an airplane wing and Eq. (32) for a simply supported beam.

Finally, it may be said that it has been found simpler to put all the fundamental quantities in a table such as Table 5 rather than on two separate cards as those of Figs. 7 and 8.

A Note on Inelastic Buckling

N. J. HOFF*

Polytechnic Institute of Brooklyn

SINCE THE INVESTIGATIONS of Engesser,[1] von Kármán,[2] and Southwell[3] it has been known that the buckling load of a straight bar can be calculated from the Euler formula even when the critical stress is higher than the proportional limit, provided that Young's modulus is replaced in the formula by the reduced, effective, or double[4] modulus. From the theory developed by these investigators the value of the reduced modulus corresponding to any buckling stress can be calculated if the compressive stress-strain diagram of the material is available. Unfortunately, this diagram varies with chemical composition, heat-treatment, cold-work, and the previous history of the loading of the bar, and in many cases its experimental determination is more difficult than the establishment by experiment of the relationship between the buckling stress and slenderness ratio. For this reason, in aircraft the buckling load of straight bars in the inelastic range is calculated according to empirical formulas developed from buckling tests and prescribed by the licensing authorities.

Comparable established empirical formulas do not exist for the calculation of the inelastic buckling of thin plates and shells or of the inelastic torsional-flexural buckling of bars. Because of this lack of experimental information it appears best to make use, in such calculations, of the connection between the elastic properties of the material and the buckling stress implicitly established by the specification of an empirical short column formula. This was done by several authors, for instance Timoshenko,[5] Osgood,[6] and Lundquist.[7] A simple and convenient procedure—not previously published in this form to the knowledge of the writer—which is based upon the same idea is as follows:

Calculate the buckling load of the bar that fails in torsional-flexural buckling, the thin plate, or the thin shell by the formula valid in the elastic range. Substitute the buckling stress so obtained into the Euler formula and solve for the slenderness ratio. Substitution of this "equivalent" slenderness ratio into the short column formula specified for the material by the licensing authority yields the actual buckling stress of the bar that fails in torsional-flexural buckling, the thin plate, or the thin shell.

Two numerical examples may be given to illustrate the procedure. The buckling load of a plate 3 by 3 by 0.091 in. made of 17 ST aluminum alloy simply supported along its four edges is, if calculated by the formula valid in the elastic range:

$$f_{cr} = 3.62E(t/b)^2 = 35{,}000 \text{ lbs. per sq.in.}$$

Substitution of this value into the Euler formula (as presented in Table 5-1 of ANC-5[8]) gives:

$$f_{cr} = 35{,}000 = \pi^2E/(L/\rho)^2 = 103.8 \times 10^6/(L/\rho)^2$$

From this equation the equivalent slenderness ratio can be calculated:

$$L/\rho = 54.5$$

This value is smaller than the transitional slenderness ratio ("critical slenderness ratio" according to ANC-5), which is 85.7. Substitution of $L/\rho = 54.5$ into the short column formula of the same table gives:

$$f_{cr} = 42{,}500 - 330.5 \times 54.5 = 24{,}500 \text{ lbs. per sq.in.}$$

This is the actual buckling stress of the plate.

As a second example the torsional-flexural buckling load of a channel section is calculated. The formulas and symbols used follow closely those of Goodier.[9] The material of the channel is SAE-1025 steel, the length of the channel is 8 in., the length of the median line of its back is $^3/_4$ in., the length of the median line of its flanges is $^3/_4$ in., and the thickness of its wall is 0.063 in. The cross-sectional area A is 0.1417 sq.in.; the moment of inertia I_x about the axis of symmetry 0.0155 in.^{4}; the other moment of inertia, $I_y = 0.00887$ in.^{4}; the polar radius of gyration ρ about the shear center, 0.706 in.; the distance x_0 of the shear center from the centroid of the section, 0.572 in.; the torsional constant C, according to the Saint-Venant theory, 0.0001875 in.^{4}; and the warping constant, $\Gamma = 0.000888$ in.^{6} If Hooke's law is assumed to be valid beyond the elastic limit, the critical load for symmetric flexural buckling

$$N = \pi^2EI_y/L^2 = 39{,}620 \text{ lbs.}$$

the pure antisymmetric flexural buckling load

$$Q = \pi^2EI_x/L^2 = 69{,}300 \text{ lbs.}$$

the pure torsional buckling load

$$T = (1/\rho^2)[GC + (\pi^2E\Gamma/L^2)] = 12{,}140 \text{ lbs.}$$

From these values P, the smaller of the combined torsional-flexural buckling loads, can be calculated:

$$(1/P) = \frac{1}{2}\left\{\frac{1}{Q} + \frac{1}{T} + \sqrt{\left(\frac{1}{Q} - \frac{1}{T}\right)^2 + \frac{4}{QT}\left(\frac{x_0}{\rho}\right)^2}\right\}$$

Received August 27, 1943.

* Associate Professor of Aeronautical Engineering.

Solution for P gives:

$$P = 10{,}800 \text{ lbs.}$$

P is the smallest of the buckling loads just calculated and thus is the one of practical interest. The compressive stress caused by it is:

$$f_c = 10{,}800/0.1417 = 76{,}400 \text{ lbs. per sq.in.}$$

Substitution of this value into the Euler formula (as presented in Table 4-1 of ANC-5[8]) gives:

$$76{,}400 = \pi^2 E/(L/\rho)^2 = 276 \times 10^6/(L/\rho)^2$$

Consequently, the equivalent slenderness ratio is:

$$(L/\rho) = 60.1$$

This slenderness ratio being smaller than the transitional (critical) one, which is 124, the buckling stress must be reduced. Substitution into the short column formula of Table 4-1 of ANC-5[8] gives:

$$f_{cr} = 36{,}000 - 1.172\ (L/\rho)^2 = 31{,}770 \text{ lbs. per sq.in.}$$

and thus the buckling load

$$P = 31{,}770 \times 0.1417 = 4{,}500 \text{ lbs.}$$

The procedure just described is based on the fact that the specification of a short column formula for columns of a given cross section establishes a uniquely determined connection between $\alpha = E_{red}/E$ and the actual critical stress, and another between α and the critical stress as calculated from the Euler formula. (In the following α denotes the value of E_{red}/E as calculated from the short column formula specified by the licensing authority.) That the functions expressing these connections are little influenced by the cross-sectional shape of the straight bar was shown by von Kármán[2] and Southwell.[3] Thus it is permissible to use the formulas specified for round tubing in the calculation of the flexural buckling of straight bars of other sections.

The considerations leading to the suggestion of a procedure for the calculation of the torsional-flexural buckling load in the inelastic range are more complex since this load depends both on E_{red} and G_{red}. In the "flexural" terms of the relevant formulas the use of $E_{red} = \alpha E$ is obviously indicated; in the "torsional" terms $G_{red} = (1/2)(\alpha + \sqrt{\alpha})G$ was suggested by Lundquist and Fligg.[10] The suggestion was based on theoretic and experimental work carried out by Kollbrunner[11] with angle sections, but the accuracy of Kollbrunner's conclusions is impaired by the assumption in his theory that the common edge of the two legs of the angle remains straight at buckling. This assumption is untenable in the light of the recent theory of flexural-torsional buckling. Although the axis about which the angle "twists away" is close to the edge of the angle, the deviation is sufficiently large to cause changes in the calculated buckling stress which are of the same order of magnitude as those caused by the assumption of a different formula for the reduced modulus of elasticity in shear, for instance $G_{red} = \alpha G$. Thus Kollbrunner's reduced shear modulus is likely to lead to good agreement between theory and experiment only if it is used in the formula he developed which contains an empirical coefficient.

The procedure suggested in the present paper is based upon the assumption that $G_{red} = \alpha G$. This assumption was made for the following reasons: (1) It permits the use of the simple procedure just described, while any other assumption requires more elaborate calculations; (2) the true connection between G_{red} and the critical stress is not known; (3) the difference in the calculated buckling stress is small even though the difference between αG and the true value of G_{red} is large; (4) the assumption causes an error to the safe side.

The buckling load of plates was investigated in detail by Timoshenko.[12] He showed that in the case of the inelastic buckling of a rectangular plate simply supported along its four edges the value of the reduced modulus must lie between αE and $\sqrt{\alpha}E$. Thus the assumption of $E_{red} = \alpha E$ is again safe, and permits the use of the simple procedure suggested here. It follows from Timoshenko's statements in his *Theory of Elastic Stability*[13] that the same conclusions hold true also for the inelastic buckling of thin cylindric shells.

References

[1] Engesser, Fr., *Ueber Knickfragen*, Schweizerische Bauzeitung, Vol. 26, No. 4, p. 24, July 27, 1895.

[2] von Kármán, Th., *Untersuchungen ueber Knickfestigkeit*. No. 81; Forschungsheft des Vereins Deutscher Ingenieure, Berlin, 1910.

[3] Southwell, R. V., *The Strength of Struts*, Engineering, Vol. XCIV, p. 249, August 23, 1912.

[4] Osgood, William R., *Column Curves and Stress Strain Diagrams*, Research Report No. 492, Journal of Research of the National Bureau of Standards, Vol. 9, pp. 571–582, October, 1932.

[5] Timoshenko, S., *Theory of Elastic Stability*, p. 388; McGraw-Hill Book Company, Inc., New York and London, 1936.

[6] Osgood, William R., and Holt, Marshall, *The Column Strength of Two Extruded Aluminum-Alloy H-Sections*, N.A.C.A. T.R. No. 656, 1939.

[7] Lundquist, Eugene E., *Local Instability of Symmetrical Rectangular Tubes under Axial Compression*, N.A.C.A. T.N. No. 686, February, 1939.

[8] ANC-5, *Strength of Aircraft Elements*, Army-Navy-Civil Committee, Aeronautical Board, U.S. Government Printing Office, December, 1942.

[9] Goodier, J. N., *Torsional and Flexural Buckling of Bars of Thin-Walled Open Section under Compression and Bending Loads*, Journal of Applied Mechanics, Vol. 9, No. 3, p. A-103, September, 1942.

[10] Lundquist, E. E., and Fligg, Claude M., *A Theory of Primary Failure of Straight Centrally Loaded Columns*, N.A.C.A. T.R., No. 582, 1937.

[11] Kollbrunner, Curt F., *Das Ausbeulen des auf Druck Beanspruchten Freistehenden Winkels*, Dissertation; Federal Polytechnic Institute, Zurich, Switzerland, 1935.

[12] *See* p. 384 of reference 5.

[13] *See* p. 442 of reference 5.

Analysis of the General Beam-Column by the Collocation Method

YVES NUBAR*

York Research Corporation

SUMMARY

The method of collocation is applied to the determination of critical axial loads and deflection curves for the general type of beam-columns under any conditions of end fixity, lateral loading, and flexural rigidity distribution. Slope deflection equations are also derived and the expressions for fixed-end moments, stiffness and carry-over factors established for use in the rigid frame analysis of structures involving such members. For the purpose of illustration and comparison, the method is applied to several problems, some of which have already been solved by standard methods.

INTRODUCTION

THE SECOND-ORDER LINEAR DIFFERENTIAL EQUATIONS of beam-column problems cannot be integrated exactly except in a few cases where the flexural rigidity EI varies along the member according to some simple law (reference 1, p. 358); even in many such cases the solution involves the somewhat unfamiliar Bessel's functions.

For the analysis of the general beam-column of irregular EI distribution, with arbitrary lateral loading and end conditions, recourse must be had to approximate methods. The method of collocation[2, 3] belongs to this category; it is applicable to the approximate solution of equations of many types encountered in engineering. In common with other methods of approximation enjoying wider dissemination and popularity,[1–6] it can yield results as nearly correct as desired, the accuracy obtainable being limited only by the amount of numerical work involved. The method consists in setting up a function $y = f(x)$ which fulfills exactly the boundary conditions of the given equation and also satisfies it at a number of prescribed values of x; at these stations, y and the exact solution will have the same "locations."† The particular form of this function is generally suggested, within rather wide limits, by the physical nature of the problem at hand; an expression involving a sine series will be found advantageous in many engineering problems.

In addition to the possibility the method offers of quickly determining certain elements of the problem which may be of special interest (such as critical loads, end slopes, center deflection, etc.), it affords a fair visualization of the deviation of the results from the exact solution; this will help in maintaining the errors within acceptable limits by readjusting the collocation stations or increasing their number. This number need not exceed three or four in the average type of problems; in many cases, a smaller number will be sufficient. In order to keep it a minimum, the given $1/EI$ distribution must be faired to such an extent as seems strictly necessary; experience and judgment will naturally help in this process. A helpful feature is that the overall properties of a member, such as deflections, periods of vibration, critical loads, etc., are rather insensitive to local changes in stiffness. This is verified by the illustrative examples given in this paper in which results correct within 3 per cent are obtained in spite of a somewhat crude fairing. A further reason why the fairing of the $1/EI$ distribution curve mentioned above should not greatly affect the results lies in the fact that such a fairing is used in only one part of the operations involved.

SYMBOLS

l	= span
P	= axial load
E	= modulus of elasticity
I	= moment of inertia
t	= Pl^2/π^2EI
y	= transverse displacement
Ω_1, Ω_2	= rotations at ends 1 and 2
d_2	= transverse displacement of end 2 relative to end 1
M	= bending moment
m	= bending moment for the member assumed on simple supports
M_1, M_2	= moments exerted by joints 1 and 2 upon the member
A, B, C	= areas of diagrams in Figs. 2, 3, and 4
a', b, c	= ratios locating centers of gravity of these areas
A_x^m, B_x^m, C_x^m	= bending moments at point x due to loading represented by Figs. 2, 3, and 4, respectively
A_x^s, B_x^s, C_x^s	= shears at point x due to loading represented by Figs. 2, 3, and 4, respectively
a_1, a_2, etc.	= coefficients
u	= variable abscissa
S_1, C_1, D_1, F_1, etc.	= coefficients in slope deflection equations

Received September 2, 1943.

* Senior Aerodynamics Engineer, Aircraft Division.

† NOTE: Strictly speaking, when differential equations are solved by this method, the curves for the approximate and exact solutions will not pass exactly through the same points for these stations, although the error will be small; these two solutions will actually coincide only in the case of algebraic or transcendental equations.

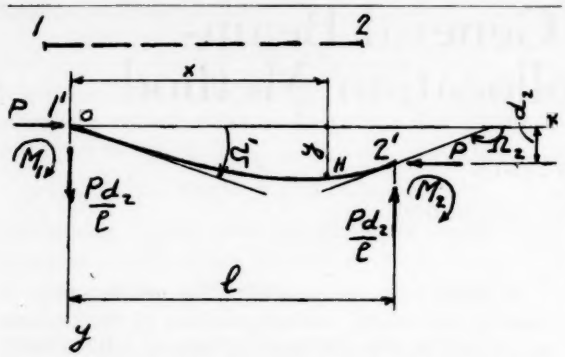

FIG. 1. Original and deformed position of member.

ANALYSIS OF BEAM-COLUMNS

Fig. 1 shows the original and deflected positions of a beam-column 1-2, acted upon by an axial load P (assumed to move with the ends of the member) and an arbitrary lateral loading—(this loading and the corresponding reactions are not shown in the figure). The structure of which this member is a part exerts upon it the moments M_1 and M_2 at ends 1 and 2, respectively; arrows in Fig. 1 indicate the positive directions of the end moments and rotations.

The bending moment at a point H of the member is given by

$$M = Py - Pd_2\frac{x}{l} + M_1\left(1 - \frac{x}{l}\right) - M_2\frac{x}{l} + m \quad (1)$$

where m stands for the simple moment at H due to the lateral loading alone. With the coordinate axes as adopted, the deflection curve y of the member is given by

$$(d^2y/dx^2) + (M/EI) = 0$$

or

$$\frac{d^2y}{dx^2} + \frac{1}{EI}\left[-Pd_2\frac{x}{l} + M_1\left(1 - \frac{x}{l}\right) - M_2\frac{x}{l} + m + Py\right] = 0 \quad (2)$$

in which E is the Young's modulus and I is the moment of inertia at point H.

Let y_1 be a solution of the equation

$$\frac{d^2y_1}{dx^2} + \frac{1}{EI}\left[-Pd_2\frac{x}{l} + M_1\left(1 - \frac{x}{l}\right) - M_2\frac{x}{l} + m\right] = 0 \quad (3)$$

satisfying the conditions $y_1 = 0$ for $x = 0$ and $x = l$. (It may be noted that, except for the term in P, y_1 is the deflection curve due only to the lateral loads and the end moments.)

The following expression, which satisfies the boundary conditions (namely: for $x = 0$: $y = 0$, $d^2y/dx^2 = -M_1/EI_1$; for $x = l$: $y = d_2$, $d^2y/dx^2 = +M_2/EI_2$), will be made to represent the general solution of Eq. (2):

$$y = y_1 + \frac{Pd^2}{6EI_2l}(l^2 - x^2)x + \frac{d_2x}{l} + a_1\sin\frac{\pi x}{l} + a_2\sin\frac{2\pi x}{l} + a_3\sin\frac{3\pi x}{l} + \ldots . \quad (4)$$

where a_1, a_2, a_3, etc., are coefficients as yet indeterminate. Its substitution into Eq. (2) gives

$$\left[t_2 - t - tt_2\left(1 - \frac{x^2}{l^2}\right)\frac{\pi^2}{6}\right]d_2\frac{x}{l} - ty_1 + (1 - t)a_1\sin\frac{\pi x}{l} + (4 - t)a_2\sin\frac{2\pi x}{l} + (9 - t)a_3\sin\frac{3\pi x}{l} + \ldots . = 0 \quad (5)$$

in which $t = Pl^2/\pi^2EI$ and $t_2 = Pl^2/\pi^2EI_2$.

It may be seen that this last equation reduces to an identity for $x = 0$ and $x = l$. By writing that it is also satisfied at a certain number of points along the member, an equal number of coefficients a may be determined. Therefore, since y, given by Eq. (4), satisfies the boundary conditions of the problem, it can be made to express the solution of Eq. (2) as closely as desired.

Determination of Function y_1

First, the solution y_1 of Eq. (3) will be determined. Integrating this equation twice,

$$y_1 + \frac{M_1}{l}\int_0^x dx\int_0^x\frac{(l - x)}{EI}dx - \frac{(M_2 + Pd_2)}{l}\times\int_0^x dx\int_0^x\frac{x}{EI}dx + \int_0^x dx\int_0^x\frac{m}{EI}dx + C'x + C'' = 0 \quad (6)$$

C' and C'' being constants of integration.

Making use of the known identity

$$\int_0^x dx\int_0^x f(x)\,dx = \int_0^x (x - u)f(u)\,du \quad (7)$$

(u being the variable in the integration process), Eq. (6) may be written

$$y_1 + \frac{M_1}{l}\int_0^x (l - u)(x - u)\frac{du}{EI} - \frac{(M_2 + Pd_2)}{l}\times\int_0^x u(x - u)\frac{du}{EI} + \int_0^x m(x - u)\frac{du}{EI} + C'x + C'' = 0 \quad (8)$$

The condition $y_1 = 0$ for $x = 0$ gives $C'' = 0$; the condition $y_1 = 0$ for $x = l$ determines the value of C' which, when replaced in Eq. (8), yields the following equation:

$$y_1 = \left[\frac{x}{l}\int_0^l (l - u)m\frac{du}{EI} - \int_0^x (x - u)m\frac{du}{EI}\right] - \frac{(M_2 + Pd_2)}{l}\left[\frac{x}{l}\int_0^l (l - u)u\frac{du}{EI} - \int_0^x (x - u)u\frac{du}{EI}\right] + \frac{M_1}{l}\left[\frac{x}{l}\int_0^l (l - u)^2\frac{du}{EI} - \int_0^x (l - u)(x - u)\frac{du}{EI}\right] \quad (9)$$

The three brackets appearing in this expression have simple interpretations: lay out diagram m/EI (Fig. 2),

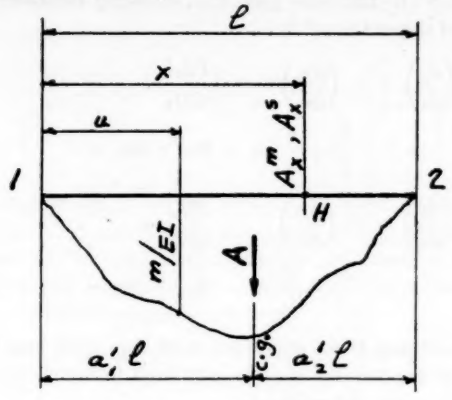

FIG. 2. m/EI diagram.

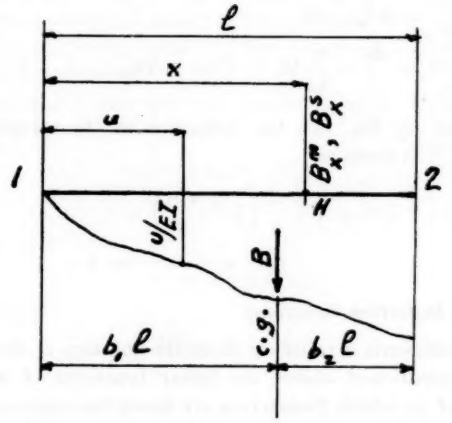

FIG. 3. u/EI diagram.

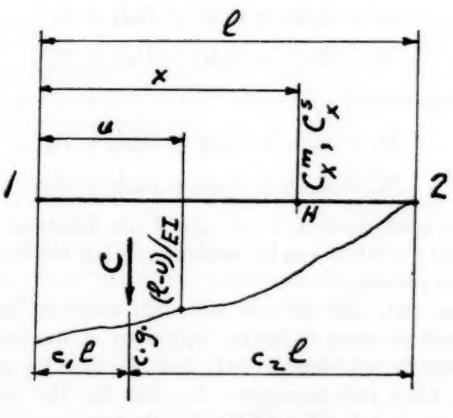

FIG. 4. $(l-u)/EI$ diagram.

diagram u/EI (Fig. 3), and diagram $(l-u)/EI$ (Fig. 4) and denote their areas by A, B, and C, respectively, located at their centroids as shown. It may be easily seen that the expressions in the first, second, and third brackets in Eq. (9) are the bending moments at point H of the member (considered on simple supports), assumed to be loaded, respectively, by the loading diagrams represented by Figs. 2, 3, and 4. Designating these bending moments by A_x^m, B_x^m, and C_x^m, Eq. (9) may be written

$$y_1 = A_x^m - \frac{(M_2 + Pd_2)}{l} B_x^m + \frac{M_1}{l} C_x^m \quad (10)$$

Similarly, the derivatives dA_x^m/dx, dB_x^m/dx, dC_x^m/dx are, respectively, the shears at point H of the member due to the loading diagrams of Figs. 2, 3, and 4; denoting these shears by A_x^s, B_x^s, and C_x^s, dy_1/dx may be written as follows:

$$\frac{dy_1}{dx} = A_x^s - \frac{(M_2 + Pd_2)}{l} B_x^s + \frac{M_1}{l} C_x^s \quad (11)$$

Considering that $A_0^s = Aa_2'$, $B_0^s = Bb_2$, $C_0^s = Cc_2$, $A_l^s = -Aa_1'$, $B_l^s = -Bb_1$, $C_l^s = -Cc_1$, Eq. (11) reduces at the boundaries to

$$\left.\begin{aligned}\left(\frac{dy_1}{dx}\right)_{x=0} &= Aa_2' - \frac{(M_2 + Pd_2)}{l} Bb_2 + \frac{M_1}{l} Cc_2 \\ \left(\frac{dy_1}{dx}\right)_{x=l} &= -Aa_1' + \frac{(M_2 + Pd_2)}{l} Bb_1 - \frac{M_1}{l} Cc_1\end{aligned}\right\} \quad (12)$$

The useful relation $Bb_2 = Cc_1$ is self evident by comparison of Figs. 3 and 4.

Coefficients A, B, C, A_x^m, B_x^m, C_x^m, A_x^s, B_x^s, C_x^s may be determined conveniently by decomposition of areas into trapezoidal elements or by the use of a planimeter.

It may be noted that up to this point no fairing of the $1/EI$ distribution curve is necessary (beyond the negligible amount involved in such a decomposition).

Determination of Coefficients

The determination of the coefficients a_1, a_2, etc., in Eq. (4) will now be considered.

For each point $x = x_n$ along the member at which Eq. (5) is satisfied, a coefficient a_n can be determined; when these coefficients, determined as a group as will be shown presently, are substituted in Eq. (4), the approximate deflection curve y represented by this equation is collocated with the true deflected position of the member at all stations such as x_n. The greater the number of these stations, the closer will the two curves lie together; on the other hand, the smaller this number, the easier will be the numerical work involved.

The choice as to the number of these selected stations and their location depends a great deal upon the given distribution of EI and the degree of precision which any particular problem may require. In the majority of practical cases, it is believed that six or seven stations at the most will furnish amply accurate results; this number will provide for some extremely irregular cases of rigidity distribution. Frequently, this number may be much less, say two or three. In the case of members symmetric about their midpoint, as to lateral

loading, stiffness, and end restraints, with $d_2 = 0$ and antisymmetric modes disregarded, the collocation stations may be reduced by half; for such cases, the even coefficients a_2, a_4, etc., will drop out of Eqs. (4) and (5).

Among other points at which collocation may be desirable, two important ones are those infinitesimally near each end; collocation at these points will collocate the end tangents, since the boundary conditions for the displacements at the ends are already satisfied. This may be achieved by taking the derivatives of Eq. (5) and equating to zero their values for $x = 0$ and $x = l$; in this process, $1/EI$ (or t) may be treated as a constant over the infinitesimal lengths at the ends. The resulting two relations are:

$$\frac{l\,t_1}{\pi}\left[\left(\frac{dy_1}{dx}\right)_{x=0} - t_2\left(\frac{1}{t_1} - \frac{1}{t_2} - \frac{\pi^2}{6}\right)\frac{d_2}{l}\right] = (1 - t_1)a_1 + 2(4 - t_1)a_2 + 3(9 - t_1)a_3 + \ldots \quad (13)$$

$$\frac{l\,t_2}{\pi}\left[\left(\frac{dy_1}{dx}\right)_{x=l} - t_2 d_2 \frac{\pi^2}{3l}\right] = -(1 - t_2)a_1 + 2(4 - t_2)a_2 - 3(9 - t_2)a_3 + \ldots . \quad (14)$$

in which the expressions for $(dy_1/dx)_{x=0}$ and $(dy_1/dx)_{x=l}$ are given by Eq. (12).

In addition to these two end points, collocation at any other point, say $x = x_3$, may be established by making this substitution in Eq. (5); this gives:

$$\left[-t_2 + t_3 + t_2 t_3\left(1 - \frac{x_3^2}{l^2}\right)\frac{\pi^2}{6}\right]d_2\frac{x_3}{l} + t_3(y_1)_{x=x_3} = (1 - t_3)a_1 \sin\frac{\pi x_3}{l} + (4 - t_3)a_2 \sin\frac{2\pi x_3}{l} + (9 - t_3)a_3 \sin\frac{3\pi x_3}{l} + \ldots . \quad (15)$$

where $(y_1)_{x=x_3}$ is obtained by applying Eq. (10) at $x = x_3$.

If equations such as Eq. (15) are written for $n - 2$ points along the member, they will form, together with Eq. (13) and (14) relative to the end tangents, a system of n linear equations in a_1 to a_n, inclusive; the determinant Δ of this system, involving the n ratios t_1 to t_n, inclusive $\left(\text{that is, } \frac{Pl^2}{\pi^2 EI_1}, \ldots, \frac{Pl^2}{\pi^2 EI_n}, \text{ etc.}\right)$, will be a polynomial of degree n in P. Setting $\Delta = 0$ will furnish n critical loads, each corresponding to one of the modes of the deflection curve y; only the smallest of the roots of $\Delta = 0$ is of interest in the generality of engineering problems; it can be found by any of several methods in common use for such cases, for instance that of successive substitutions. Assuming that Δ is different from 0—that is, the axial load does not coincide with any of the critical values—the system can be solved for the n coefficients a; replacing them in Eq. (4), the deflection curve y of the member will be determined. The end slopes can then be found by differentiating the expression y and making $x = 0$ and $x = l$; this will give the following relations for the end slopes Ω_1 and Ω_2:

$$\Omega_1 = \left(\frac{dy}{dx}\right)_{x=0} = \left(\frac{dy_1}{dx}\right)_{x=0} + \frac{Pd_2 l}{6EI_2} + \frac{d_2}{l} + \frac{\pi}{l}(a_1 + 2a_2 + 3a_3 + \ldots .) \quad (16)$$

$$\Omega_2 = \left(\frac{dy}{dx}\right)_{x=l} = \left(\frac{dy_1}{dx}\right)_{x=l} - \frac{Pd_2 l}{3EI_2} + \frac{d_2}{l} - \frac{\pi}{l}(a_1 - 2a_2 + 3a_3 - \ldots .) \quad (17)$$

Combining these equations with Eqs. (13) and (14), simpler expressions may be obtained in terms of coefficients a just determined:

$$\Omega_1 = \frac{t_2}{t_1}\frac{d_2}{l} + \frac{\pi}{t_1 l}[a_1 + 2^3 a_2 + 3^3 a_3 + \ldots .] \quad (18)$$

$$\Omega_2 = \frac{d_2}{l} - \frac{\pi}{t_2 l}[a_1 - 2^3 a_2 + 3^3 a_3 - \ldots .] \quad (19)$$

Also, by Eq. (4), the deflection of the member at $x = l/2$ is given as:

$$(y)_{x=l/2} = (y_1)_{x=l/2} + \frac{d_2}{2}\left(1 + \frac{\pi^2 t_2}{8}\right) + a_1 - a_3 + a_5 - a_7 + \ldots . \quad (19a)$$

Slope Deflection Equations

Coefficients a resulting from the solution of the system mentioned above are linear functions of dy_1/dx and of y_1, which themselves are linear functions of M_1, M_2, and d_2 because of Eqs. (10) and (12). Therefore, Eqs. (18) and (19) may be written symbolically as:

$$\Omega_1 = S_1 M_1 + C_1 M_2 + D_1 d_2 + F_1 \quad (20)$$

$$\Omega_2 = C_2 M_1 + S_2 M_2 + D_2 d_2 + F_2 \quad (21)$$

and conversely:

$$M_1 = S_{12}\Omega_1 + C_{12}\Omega_2 + D_{12} d_2 + F_{12} \quad (22)$$

$$M_2 = C_{21}\Omega_1 + S_{21}\Omega_2 + D_{21} d_2 + F_{21} \quad (23)$$

where coefficients S, C, D, and F are functions of P, t's, and x's, which can be written explicitly for each particular problem.

Eqs. (20) and (21) or Eqs. (22) and (23) are the generalized slope deflection equations of the member. It may be established easily that F_{12} and F_{21} are the fully fixed end moments; S_{12} and S_{21}, the stiffness factors; and C_{21}/S_{12} and C_{12}/S_{21}, the carry-over factors at ends 1 and 2, respectively. In Eqs. (20) and (21), F_1 and F_2 are the end rotations for the member assumed on simple supports.

Test of Accuracy Attained

The degree of approximation obtained in building up the curve y (Eq. 4), through collocational representa-

tion as described above, may be ascertained by plotting the curve

$$\frac{1}{EI'} = -\frac{d^2y}{dx^2}\Big/\left[Py - Pd_2\frac{x}{l} + M_1\left(1 - \frac{x}{l}\right) - M_2\frac{x}{l} + m\right] \quad (24)$$

and comparing it to the given $1/EI$ distribution for possible wide variations; these two curves will coincide exactly for each collocation station; their proximity over the length of the member will be a measure of the degree of accuracy attained.

Illustration

Example 1

Beam-column of length l and simple ends (level), under axial load P and uniform lateral load of w lbs. per in. (I constant).

The exact solution for this case is known (reference 4, pp. 8, 9, etc.).

$$P_{cr} = \frac{EI\pi^2}{l^2}, \frac{9EI\pi^2}{l^2}, \frac{25EI\pi^2}{l^2}, \text{ etc.}$$

Center deflection

$$\delta = (5wl^4/384EI)C_1$$

End slope

$$\Omega = (wl^3/24EI)C_2$$

where

$$C_1 = \frac{4.8}{v^4}\left(\sec v - 1 - \frac{v^2}{2}\right), \quad C_2 = \frac{3}{v^3}(\tan v - v)$$

in which $v = (l/2)\sqrt{P/EI}$. Because of symmetry, the even coefficients a_2, a_4, etc., will disappear from the collocation equations. Only two terms a_1 and a_3 will be taken and collocation established at $x = 0 + dx$ and $x = l/2$. Eq (4) for this case is

$$y = y_1 + a_1 \sin\frac{\pi x}{l} + a_3 \sin\frac{3\pi x}{l} \quad (4)'$$

[$y_1 = (wx/24EI)(l^3 - 2lx^2 + x^3)$ is the known deflection curve for uniformly loaded simple beam of constant EI.] Eq. (13) and (15) become

$$(1 - t)a_1 + 3(9 - t)a_3 = \frac{lt}{\pi}\left(\frac{dy_1}{dx}\right)_{x=0} = \frac{t}{\pi}\frac{wl^4}{24EI} \quad (13)'$$

$$(1 - t)a_1 - (9 - t)a_3 = t(y_1)_{x=l/3} = t\frac{5wl^4}{384EI} \quad (15)'$$

Critical loads are given by

$$\Delta = \begin{vmatrix} 1-t & 3(9-t) \\ 1-t & -(9-t) \end{vmatrix} = -4(1-t)(9-t) = 0$$

the roots of which are $t_{cr} = 1$ and 9 or $P_{cr} = EI\pi^2/l^2$ and $9EI\pi^2/l^2$; they are identical with the true solutions.

Assuming Δ different from 0, Eqs. (13)′ and (15)′ give

$$a_1 = \frac{1}{4(1-t)}\left(\frac{16}{\pi} + 15\right)\frac{wl^2t^2\pi^2}{384P}$$

$$a_3 = \frac{1}{4(9-t)}\left(\frac{16}{\pi} - 5\right)\frac{wl^2t^2\pi^2}{384P}$$

From Eq. (4)′,

$$(y)_{x=l/3} = (y_1)_{x=l/3} + a_1 - a_3 = \frac{5wl^4}{384EI}C_1'$$

where

$$C_1' = \left[1 + \frac{t}{4(1-t)}\left(\frac{16}{5\pi} + 3\right) - \frac{t}{4(9-t)}\left(\frac{16}{5\pi} - 1\right)\right]$$

From Eq. (18)

$$\Omega_1 = \frac{\pi}{tl}(a_1 + 3^3a_3) = \frac{wl^3}{24EI}C_2'$$

in which

$$C_2' = \frac{\pi}{64}\left[\frac{1}{1-t}\left(\frac{16}{\pi} + 15\right) + \frac{27}{9-t}\left(\frac{16}{\pi} - 5\right)\right]$$

A comparison between the exact coefficients C_1, C_2 and the corresponding approximate coefficients C_1' and C_2' for several values of t is included in Table 1. The results indicate close agreement.

As a further test, it may be interesting to determine the flexural rigidity distribution corresponding to the assumed deflection curve (4)′. Designating this rigidity by $1/EI'$

$$P/EI' = -(d^2y/dx^2)/[y + (m/P)]$$

where m is the simple moment $wx(l - x)/2$.

After development and simplification, this equation is given the form

$$\frac{t' - t}{t} = \frac{-16\left(\frac{x}{l} - \frac{2x^3}{l^3} + \frac{x^4}{l^4}\right) + \frac{1}{4}\left(\frac{16}{\pi} + 15\right)\sin\frac{\pi x}{l} + \frac{1}{4}\left(\frac{16}{\pi} - 5\right)\sin\frac{3\pi x}{l}}{+16\left(\frac{x}{l} - \frac{2x^3}{l^3} + \frac{x^4}{l^4}\right) + \frac{192}{\pi^2 t}\left(\frac{x}{l} - \frac{x^2}{l^2}\right) + \frac{1}{4(1-t)}\left(\frac{16}{\pi} + 15\right)\sin\frac{\pi x}{l} + \frac{1}{4(9-t)}\left(\frac{16}{\pi} - 5\right)\sin\frac{3\pi x}{l}} \quad (25)$$

in which t' stands for Pl^2/π^2EI'. For $x/l = {}^1/_2$, it is seen that $(t' - t)/t = 0$. For $x = 0$, Eq. (25) has the form 0/0; lifting the indetermination by taking the ratio of the derivatives of both numerator and denominator and making $x = 0$, the result is again found to be zero; these results were naturally to be expected, since coefficients a_1 and a_3 were obtained by collocation at $x = dx$ and $x = l/2$.

TABLE 1

		Deflection at Center			End Slope		
v	t	C_1	C_1'	C_1''	C_2	C_2'	C_2''
0.50	0.1013	1.11360	1.11319	1.11272	1.1112	1.1113	1.0924
0.70	0.1986	1.24748	1.24886	1.24781	1.2445	1.2447	1.2250
0.85	0.2928	1.41609	1.41579	1.41402	1.4085	1.4088	1.3882
1.00	0.4053	1.68384	1.68447	1.68152	1.6722	1.6728	1.6508
1.15	0.5360	2.15986	2.16025	2.15517	2.1392	2.1402	2.1158
1.25	0.6333	2.73325	2.73470	2.72707	2.7027	2.7044	2.6772
1.30	0.6850	3.18190	3.18433	3.17460	3.1435	3.1459	3.1166
1.40	0.7944	4.87734	4.88132	4.86381	4.8082	4.8122	4.7750
1.50	0.9120	11.38915	11.41128	11.36364	11.2013	11.2333	11.1562

That the ratio $(t' - t)/t$ given by Eq. (25) is small at all other points may be seen by substituting several values of x/l and testing the result for different values of t; for instance, for $x/l = 1/4$, Eq. (25) gives

$$\frac{t' - t}{t} = \frac{-3.5625 + 3.5683}{+3.5625 + \dfrac{3.65}{t} + 3.56t\left[\dfrac{1}{1 - t} + \dfrac{1}{200(9 - t)}\right]}$$

which is small for all finite values of t. This can also be ascertained by developing the numerator of the second member of Eq. (25) into a power series.

As a matter of curiosity, the results of a collocation at one point only, $x = l/2$ will be investigated; a_3 and Eq. (13)′ will drop out, Eq. (15)′ will give $a_1 = 5wl^4t/384EI(1 - t)$; then $y = y_1 + (5wl^4t/384EI(1 - t) \times \sin \pi x/l$ and

$$(y)_{x=l/2} = \frac{5wl^4}{384EI} C_1'', \quad \Omega_1 = \frac{wl^2}{24EI} C_2''$$

with

$$C_1'' = 1/(1 - t), \qquad C_2'' = 5\pi/16(1 - t)$$

For comparison, the coefficients C_1'' and C_2'' are also listed in Table 1; it is seen that their agreement with the other values is quite sufficient for all practical purposes.

Example 2

To find critical load for the column shown in Fig. 5. (In reference 4, p. 130, its exact value is given as $P_{cr} = 4.22EI_3/l^2$ or $t_{3(cr)} = 4.22/\pi^2 = 0.427$.)

Again, only symmetric modes will be considered, and the deflection curve will be taken as

$$y = a_1 \sin \frac{\pi x}{l} + a_3 \sin \frac{3\pi x}{l} + a_5 \sin \frac{5\pi x}{l}$$

which does not contain the function y_1 because of the absence of lateral loads.

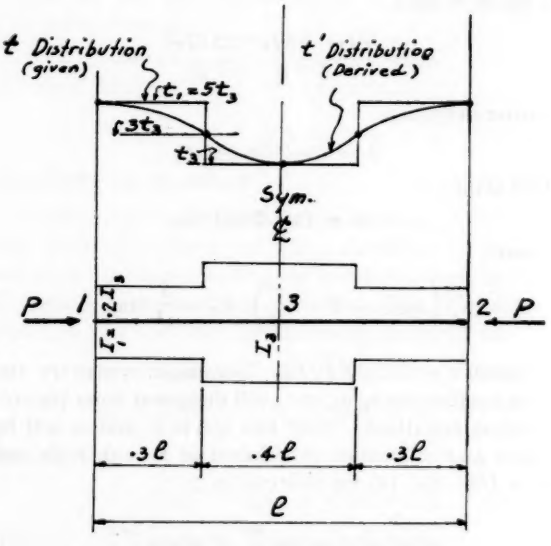

FIG. 5. Sketch of column in example 2.

Collocation will be established at $0 + dx$ with $t = t_1 = 5t_3$; at $l/2$, with $t = t_3$; and at $3l/10$ with $t = (t_1 + t_3)/2 = 3t_3$. The following equations correspond to Eqs. (13) and (15):

$$\left.\begin{aligned} \text{at } 0 + dx: &\quad (1 - 5t_3)a_1 + 3(9 - 5t_3)a_3 + 5(25 - 5t_3)a_5 = 0 \\ \text{at } l/2: &\quad (1 - t_3)a_1 - (9 - t_3)a_3 + (25 - t_3)a_5 = 0 \\ \text{at } 3l/10: &\quad (1 - 3t_3)0.809a_1 + (9 - 3t_3)0.309a_3 - (25 - 3t_3)a_5 = 0 \end{aligned}\right\} \tag{26}$$

The roots of the equation

$$\Delta = \begin{vmatrix} 1 - 5t_3 & 3(9 - 5t_3) & 5(25 - 5t_3) \\ 1 - t_3 & -(9 - t_3) & 25 - t_3 \\ 0.809(1 - 3t_3) & 0.309(9 - 3t_3) & -(25 - 3t_3) \end{vmatrix} = 0$$

will furnish the critical values for t_3; by a few substitutions, the smallest root is found to be $t_{3(cr)} = 0.415$, which differs by about 3 per cent from the exact solution $t_{3(cr)} = 0.427$. With $t_3 = 0.415$, coefficients a_1 and a_3 are determined by using only two of Eq. (26): $a_1 = -510a_5$; $a_3 = -31.9a_5$.

The resulting $1/EI'$ distribution is given by $P/EI' = -(d^2y/dx^2)/y$ or

$$t' = \frac{Pl^2}{\pi^2 EI'} = \frac{510 \sin \frac{\pi x}{l} + 287 \sin \frac{3\pi x}{l} - 25 \sin \frac{5\pi x}{l}}{510 \sin \frac{\pi x}{l} + 31.9 \sin \frac{3\pi x}{l} - \sin \frac{5\pi x}{l}}$$

The substitution of several values for x/l yields the following results: $t'_{(x=0)} = 2.074$; $t'_{(x=l/10)} = 2.0$; $t'_{(x=3l/10)} = 1.735$; $t'_{(x=2l/10)} = 1.242$; $t'_{(x=4l/10)} = 0.678$; $t'_{(x=l/2)} = 0.415$.

It is seen that, as it should be, $t'_{(x=0)} = 5t'_{(x=l/2)}$ and $t'_{(x=3l/10)} = {}^1/_2[t'_{(x=0)} + t'_{(x=l/2)}]$.

The t' distribution is shown in Fig. 5, together with the given one for comparison. The small error of 3 per cent in P_{cr} resulting from the use of the collocation method indicates that these two distributions are nearly equivalent as far as the critical load is concerned.

That this is not a "freak" case may be seen by applying an identical analysis to another column, represented again by Fig. 5, in which the only change is $I_1 = 0.4I_3$ instead of $0.2I_3$; taking now $t_1 = 2.5t_3$ and $t_{(3l/10)} = {}^1/_2(t_3 + 2.5t_3) = 1.75t_3$, the collocation equations, applied at the same points as before, are:

$$(1 - 2.5t_3)a_1 + 3(9 - 2.5t_3)a_3 + 5(25 - 2.5t_3)a_5 = 0$$
$$(1 - t_3)a_1 - (9 - t_3)a_3 + (25 - t_3)a_5 = 0$$
$$(1 - 1.75t_3)a_1 0.809 + (9 - 1.75t_3)a_3 0.309 - (25 - 1.75t_3)a_5 = 0$$

The smallest root of the determinant of this system equated to zero is found to be $t_{3(cr)} = 0.66$; by reference 4, the critical load for this case is $6.68EI_3/l^2$—that is, $t_{3(cr)} = 0.677$, which differs from the approximate value 0.66 by about 3 per cent.

Example 3

As an illustration of slope deflection equations in a beam-column, the following case will be treated (Fig. 6): a symmetric member on level supports of unequal restraints, loaded as shown, EI_x varying according to the law $EI_x = EI_3/2[1 - (x/l)]$—that is, $t_x = 2[1 - (x/l)]t_3$.

The deflection curve will be taken with five coefficients a, to be determined at the five collocation points: $0 + dx$, $(t_1 = 2t_3)$; $l/4$, $(t_4 = 3/2t_3)$; $l/2$, (t_3); $3l/4$, $(t_5 = 3/2t_3)$; $l - dx$, $(t_2 = 2t_3)$. Eq. (4) is therefore written as

$$y = y_1 + a_1 \sin \frac{\pi x}{l} + a_2 \sin \frac{2\pi x}{l} + a_3 \sin \frac{3\pi x}{l} + a_4 \sin \frac{4\pi x}{l} + a_5 \sin \frac{5\pi x}{l}$$

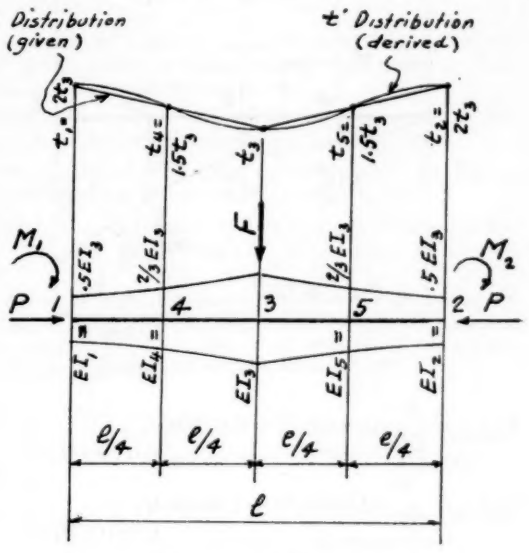

FIG. 6. Sketch of member in example 3.

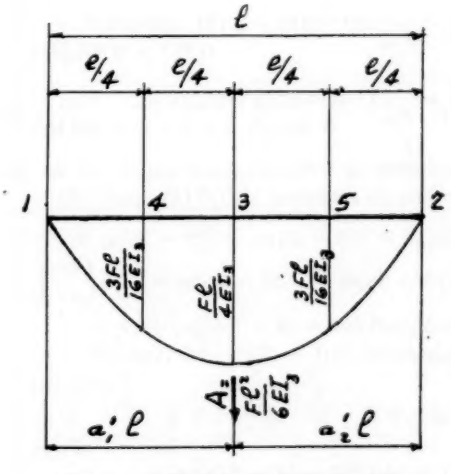

FIG. 7. m/EI diagram for example 3.

To determine y_1 at the several stations and dy_1/dx at the ends, the diagrams m/EI (Fig. 7) and u/EI (Fig. 8) are plotted; because of symmetry in $1/EI$ distribution, diagram $(l - u)/EI$ is omitted. By decomposition of areas into elementary trapezoids, the following quantities are determined:

$$A = 0.1666 \frac{Fl^2}{EI_3}, a_1' = a_2' = \frac{1}{2}, B = C = 0.751 \frac{l^2}{EI_3},$$
$$b_1 = c_2 = 0.695, b_2 = c_1 = 0.305$$

By application of Eqs. (10) and (12)

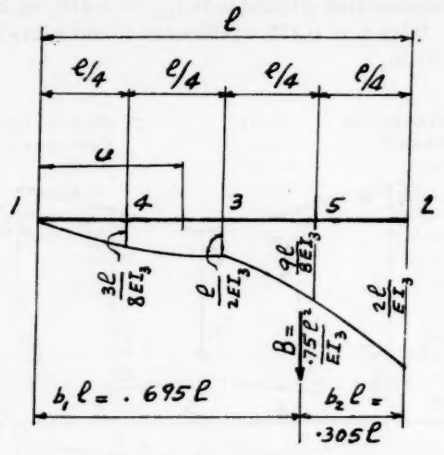

FIG. 8. u/EI diagram for example 3.

$$
\left.\begin{aligned}
(y_1)_{l/4} &= \frac{l^2}{EI_3}(0.01872Fl + 0.07760M_1 - 0.05282M_2)\\
(y_1)_{l/2} &= \frac{l^2}{EI_3}(0.02590Fl + 0.08160M_1 - 0.08160M_2)\\
(y_1)_{3l/4} &= \frac{l^2}{EI_3}(0.01872Fl + 0.05282M_1 - 0.07760M_2)\\
\left(\frac{dy_1}{dx}\right)_0 &= \frac{l}{EI_3}(0.0833Fl + 0.751 \times 0.695M_1 - 0.751 \times 0.305M_2)\\
\left(\frac{dy_1}{dx}\right)_l &= \frac{l}{EI_3}(-0.0833Fl - 0.751 \times 0.305M_1 + 0.751 \times 0.695M_2)
\end{aligned}\right\} \quad (27)
$$

The following collocation equations are set up, corresponding to relations (13), (14), and (15):

$$
\left.\begin{aligned}
&(1 - 2t_3)a_1 + 2(4 - 2t_3)a_2 + 3(9 - 2t_3)a_3 + 4(16 - 2t_3)a_4 + 5(25 - 2t_3)a_5 = \frac{l}{\pi}2t_3\left(\frac{dy_1}{dx}\right)_0\\
&(1 - 1.5t_3)a_1 0.707 + (4 - 1.5t_3)a_2 + (9 - 1.5t_3)a_3 0.707 + 0 - (25 - 1.5t_3)a_5 0.707 = 1.5t_3(y_1)_{l/4}\\
&(1 - t_3)a_1 + 0 - (9 - t_3)a_3 + 0 + (25 - t_3)a_5 = t_3(y_1)_{l/2}\\
&(1 - 1.5t_3)a_1 0.707 - (4 - 1.5t_3)a_2 + (9 - 1.5t_3)a_3 0.707 + 0 - (25 - 1.5t_3)a_5 0.707 = 1.5t_3(y_1)_{3l/4}\\
&-(1 - 2t_3)a_1 + 2(4 - 2t_3)a_2 - 3(9 - 2t_3)a_3 + 4(16 - 2t_3)a_4 - 5(25 - 2t_3)a_5 = \frac{l}{\pi}2t_3\left(\frac{dy_1}{dx}\right)_l
\end{aligned}\right\} \quad (28)
$$

The critical axial load is found by determining the smallest root of the determinant of this system equated to zero; as some of the coefficients are missing in these equations, the evaluation of this fifth order determinant is not too involved; it yields $t_{3(cr)} = 0.80$, corresponding to $P_{cr} = 7.9EI_3/l^2$. The member is stable for any value of t_3 less than this amount. The remainder of the computations will be performed on the assumption that t_3 is given as $1/3$. Making use of Eq. (27), the solution for the coefficients a with this value of t_3 is facilitated by first combining the first with the fifth, and the second with the fourth, of the equations of Eq. (28); this determines a_2 and a_4 directly, leaving a system involving only the three remaining unknowns. As a result:

$$
\left.\begin{aligned}
a_1 &= \frac{[654.9Fl + 2197.2(M_1 - M_2)]l^2}{34816EI_3}\\
a_2 &= 61.6(M_1 + M_2)l^2/34816EI_3\\
a_3 &= \frac{[15.8Fl + 67.8(M_1 - M_2)]l^2}{34816EI_3}\\
a_4 &= 10.9(M_1 + M_2)l^2/34816EI_3\\
a_5 &= \frac{[0.02Fl + 2.8(M_1 - M_2)]l^2}{34816EI_3}
\end{aligned}\right\} \quad (29)
$$

Applying now Eqs. (18) and (19)

$$
\left.\begin{aligned}
\Omega_1 &= \frac{(5101.5Fl + 26261.4M_1 - 15022.3M_2)l}{34816EI_3}\\
\Omega_2 &= \frac{(-5101.5Fl - 15022.3M_1 + 26261.4M_2)l}{34816EI_3}
\end{aligned}\right\} \quad (30)
$$

Solving for the end moments

$$
\left.\begin{aligned}
M_1 &= \frac{EI_3}{l}(1.971\Omega_1 + 1.131\Omega_2) - 0.123Fl\\
M_2 &= \frac{EI_3}{l}(1.131\Omega_1 + 1.971\Omega_2) + 0.123Fl
\end{aligned}\right\} \quad (31)
$$

These are the slope deflection equations for the member. Fixed-end moments are $\pm 0.123Fl$, while the stiffness and carry-over factors are $1.971EI_3/l$ and $1.131/1.971 = 0.575$, respectively. As a comparison, the corresponding elements for the same member with the axial load removed are: fixed-end moments—$0.111Fl$, stiffness factor—$2.38EI_3/l$, carry-over factor—0.44; these values are easily obtained by consideration of the expressions for $(dy_1/dx)_0$ and $(dy_1/dx)_l$ written previously in the development of this problem (Eq. (27)).

The $1/EI'$ distribution corresponding to the resulting deflection curve y may now be ascertained for comparison with the given distribution; this can be done by writing

$$
\frac{1}{EI'} = -\frac{d^2y}{dx^2}\Big/\left[Py + M_1\left(1 - \frac{x}{l}\right) - M_2\frac{x}{l} + m\right] \quad (32)
$$

or, after transformation,

$$\frac{t'-t}{t}=\frac{-y_1+\left(\frac{1-t}{t}\right)a_1\sin\frac{\pi x}{l}+\left(\frac{4-t}{t}\right)a_2\sin\frac{2\pi x}{l}+\ldots.+\left(\frac{25-t}{t}\right)a_5\sin\frac{5\pi x}{l}}{+y_1+a_1\sin\frac{\pi x}{l}+\ldots.a_5\sin\frac{5\pi x}{l}+\frac{l^2}{\pi^2EIt}\left[M_1\left(1-\frac{x}{l}\right)-M_2\frac{x}{l}+m\right]} \tag{33}$$

If y_1 and coefficients a are replaced by their Eqs. (27) and (29), it is seen that this ratio is equal to zero at the five stations $0+dx$, $l/4$, $l/2$, $3l/4$, $l-dx$; its maximum value along the member is found to be about 4 per cent for varying values of the ratio of end moments to lateral load. The general shape of the derived t' distribution is shown in Fig. 6, for comparison with the given distribution of t.

References

[1] von Kármán, Th., and Biot, M. A., *Mathematical Methods in Engineering*, 1st Edition; McGraw-Hill Book Company, Inc., New York, 1940.

[2] Frazer, R. A., Jones, W. B., and Skan, S. W., *R. and M.*, No. 1799 (2913), A.R.C. Technical Report (1937), Air Ministry, London; His Majesty's Stationery Office.

[3] Keller, E. G., *Mathematics of Modern Engineering*, 1st Edition, Vol. II; John Wiley & Sons, Inc., New York, 1942.

[4] Timoshenko, S., *Theory of Elastic Stability*, 1st Edition; McGraw-Hill Book Company, Inc., New York, 1936.

[5] Niles, A. S., and Newell, J. S., *Airplane Structures*, 2nd Edition, Vol. II; John Wiley & Sons, Inc., New York, 1938.

[6] Newmark, N. M., *Numerical Procedure for Computing Deflections, Moments and Buckling Loads*, Proceedings American Society of Civil Engineers, May, 1942. (See list of several references given in this paper.)

Errata

In the article "Contraction Cone for a Wind Tunnel" by Boleslaw Szczeniowski (Journal of the Aeronautical Sciences, Vol. 10, No. 8, pp. 311, 312, October, 1943) there were errors in the formulas. The corrections are shown in the following table.

Original Formulas	Corrected Formulas
$u=\frac{(\mu+1)u_0}{2}+\ldots\ldots$ (6)	$u=\frac{(\mu+1)u_0}{2}-\ldots\ldots$ (6)
$\psi=-\frac{\mu u_0r^2}{4}+\frac{(\mu-1)u_0ar}{2}\sum_{m=1}^{\infty}\frac{(-1)^{m-1}}{m^2}\ldots\ldots$ (9)	$\psi=-\frac{\mu u_0r^2}{2}+\frac{(\mu-1)u_0ar}{2}\sum_{m=1}^{\infty}\frac{(-1)^{m-1}}{m}\ldots\ldots$ (9)
$u=\frac{\mu u_0}{2}-(\mu-1)u_0\sum_{m=1}^{\infty}\frac{(-1)^{m-1}}{m}\ldots\ldots$ (10)	$u=\mu u_0-(\mu-1)u_0\sum_{m=1}^{\infty}(-1)^{m-1}\ldots\ldots$ (10)
$v=(\mu-1)u_0\sum_{m=1}^{\infty}\frac{(-1)^m}{m}\ldots\ldots$ (11)	$v=(\mu-1)u_0\sum_{m=1}^{\infty}(-1)^m\ldots\ldots$ (11)
$\psi=-\frac{u_0r^2}{4}-\frac{(\mu-1)u_0ar}{2}\sum_{m=1}^{\infty}\frac{(-1)^{m-1}}{m^2}\ldots\ldots$ (12)	$\psi=-\frac{u_0r_2}{2}-\frac{(\mu-1)u_0ar}{2}\sum_{m=1}^{\infty}\frac{(-1)^{m-1}}{m}\ldots\ldots$ (12)
$u=\frac{u_0}{2}+(\mu-1)u_0\sum_{m=1}^{\infty}\frac{(-1)^{m-1}}{m}\ldots\ldots$ (13)	$u=u_0+(\mu-1)u_0\sum_{m=1}^{\infty}(-1)^m\ldots\ldots$ (13)
$v=(\mu-1)u_0\sum_{m=1}^{\infty}\frac{(-1)^m}{m}\ldots\ldots$ (14)	$v=(\mu-1)u_0\sum_{m=1}^{\infty}(-1)^m\ldots\ldots$ (14)
$\frac{\psi}{a^2u_0}\leqq\ldots\ldots+\left(\frac{r}{a}\right)^2\Big]$ (16a)	$\frac{\psi}{a^2u_0}\leqq\ldots\ldots+2\left(\frac{r}{a}\right)^2\Big]$ (16a)
$\left(\frac{\psi}{a^2u_0}\right)_{x\geq 0}\leqq-\frac{\mu}{4}\left(\frac{r}{a}\right)^2+\ldots\ldots-\frac{1}{4}e^{-4(x/a)}J_1\left(\frac{4x}{a}\right)\Big]$ (17)	$\left(\frac{\psi}{a^2u_0}\right)_{x\geq 0}\leqq-\frac{\mu}{2}\left(\frac{r}{a}\right)^2+\ldots\ldots-\frac{1}{2}e^{-4(x/a)}J_1\left(\frac{4r}{a}\right)\Big]$ (17)
$\left(\frac{\psi}{a^2u_0}\right)_{x<0}\leqq-\frac{1}{4}\left(\frac{r}{a}\right)^2-\ldots\ldots-\frac{1}{4}e^{4(x/a)}J_1\left(\frac{4x}{a}\right)\Big]$ (18)	$\left(\frac{\psi}{a^2u_0}\right)_{x<0}\leqq-\frac{1}{2}\left(\frac{r}{a}\right)^2-\ldots\ldots-\frac{1}{2}e^{4(x/a)}J_1\left(\frac{4r}{a}\right)\Big]$ (18)

The Effects of a Fuselage upon the Stability of an Airplane

C. E. PAPPAS*

Republic Aviation Corporation

Introduction

This paper deals with the determination of fuselage moments and shows the change in moment as fineness ratio, depth, and width of fuselage are varied. In addition, the change in moments for a circular fuselage resulting from the interference effects of a wing can be found from the figures presented in the main body of the paper.

The determination of the unstable moment of a body immersed in an inviscous, incompressible fluid can be made in terms of additional apparent mass coefficients. Coefficients of additional apparent mass have been calculated for a body of revolution by Lamb,[1] and the unstable moment has been determined by Munk[2] in terms of these coefficients.

O'Donnell in his doctor's dissertation[3] has taken into account the variation of the additional apparent mass coefficients when the shape departs from a true prolate ellipsoid.

Boundary layer effects were considered by Smith[4] in the determination of the longitudinal additional apparent mass coefficient, and it was shown that the coefficient increased when the energy of the boundary layer was taken into account.

Theoretic coefficients of additional apparent mass for an ellipsoid of three unequal axes are presented. In order to indicate the change in the theoretic coefficients when boundary layer, interference, and turbulence effects are considered, wind-tunnel tests on circular fuselages alone and in combination with a wing were used to determine the extent of the variation in the theoretic coefficients.

An attempt has been made to give the necessary theory associated with the concept of additional apparent mass so that the reader may better understand the actual variation of moment of a body moving in a viscous fluid in terms of the mass coefficients.

Concept of Additional Apparent Mass

The concept of the additional apparent mass of a body is based upon an inviscous fluid. A body in steady motion in such a fluid possesses no resultant body forces, i.e., lift or drag. When a body moves through an inviscous fluid, however, a certain amount of energy is stored up in the stream lines of the fluid, the energy being a function of the body shape. When the body is at rest no energy field exists. In order to start the body in motion it is necessary to overcome the inertia of the body and the inertia of the fluid, since the shape of the body will cause the fluid to diverge at the nose and to converge at the rear of the body. Considering the body and the fluid medium as one system, the total kinetic energy may be written as $(MU^2/2) + (M_aU^2/2)$ where M is the mass of the body, M_a is the ratio of the kinetic energy of the fluid to $U^2/2$, and U is the speed of the body. The quantity M_a is called the additional apparent mass of the body.

There is an important difference, however, between the mass of the body and the apparent mass of the body. The former is the same for all directions of motion but the latter is not necessarily so. This is associated with the fact that the resultant momentum of the flow is generally not parallel to the direction of motion. There are, however, at least three axes of the body, mutually at right angles to each other and designated principal axes, for which the momentum is parallel to the direction of motion if the direction of motion coincides with one of these axes.[5] Moreover, if M_a, M_b, and M_c denote the additional apparent masses when the direction of motion coincides successively with each of these axes, the total kinetic energy for any direction of motion can be written as

$$(M/2)(U^2 + V^2 + W^2) + (M_aU^2/2) + (M_bV^2/2) + (M_cW^2/2)$$

where U, V, and W are the components of the velocity along the principal axes.

Considering now motion parallel to one of the principal axes, the term $M_aU^2/2$ is the energy that goes into deflecting the stream lines around the body during the process of accelerating the body from rest. The energy remains in the stream lines around the body when it is moving with steady motion and is given up to the body only as the body comes to rest.

When a body is in steady motion, the forward part of the body supplies energy to the fluid, and at the rear portion of the body energy is being transmitted to it by the fluid, the difference in energy in front of and at the rear of the body being zero. The energy in the stream lines remains within the stream lines as long as the body is in steady motion.

The energy stored up in the stream lines should not be confused with the pressure drag of a body moving in

Received June 2, 1943.

* Chief, Aerodynamics and Flight Test Department.

a viscous fluid. In such a case a drag results because of the boundary layer which exists over the body and which increases in thickness along the length of the body. It is because of this boundary layer resulting from viscosity that a pressure drag exists in a viscous fluid. This drag results since full atmospheric pressure recovery at the trailing edge of the body is not possible. In contradistinction to a viscous fluid, full pressure recovery is realized at the trailing edge of the body.

The kinetic energy imparted to the inviscous fluid due to the motion of a body through it will be determined by consideration of the concept of impulsive pressure. An inviscous, incompressible, and irrotational fluid having no circulation is set in motion only by the surface-body normal velocity components. The motion of the fluid can be considered as having been produced from rest by a series of impulses applied by the surface of the body. If an element of the fluid is considered:

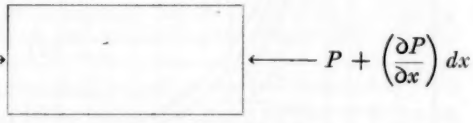

we have $\{P - [P + (\partial P/\partial x)dx]\}\, dy\, dz$ = impulsive force = Fdt, where P is an impulsive pressure.

But $Fdt = mdU$, where m is an elemental mass of fluid and dU is the increment in velocity of the body in the X-direction.

$mdU = mU$, assuming the body to have started from rest.

$mU = \rho\, dx\, dy\, dz\, U$, where ρ is the mass density of the fluid.

Then,

$$\{P - [P + (\partial P/\partial x)dx]\}dy\, dz = \rho\, dx\, dy\, dz\, U$$
$$-\partial P/\partial x = \rho U$$

For a potential flow we have $\partial\Phi/\partial x = U$

$$\rho(\partial\Phi/\partial x) = -\partial P/\partial x$$

or $P = -\rho\Phi$, where ρ is the density of the fluid and Φ is a velocity potential function. The impulsive force, normal to the surface dS, acting on the fluid is $-\rho\Phi\, dS$. $\partial\Phi/\partial n$ is the velocity normal to the element of surface dS, where dn is drawn from the body into the fluid. Then, the work done by the impulse = impulse times the average of the initial and final normal velocities in the direction of the impulse

$$= -\int \rho\Phi\left[\frac{0 + (\partial\Phi/\partial n)}{2}\right]dS$$

Since the work done by the impulse is equal to the kinetic energy imparted to the inviscous fluid,

$$T = -\rho/2 \int \Phi(\partial\Phi/\partial n)dS \qquad (1)$$

and therefore

$$M_a = \frac{T}{U^2/2} = \frac{-\rho/2\int\Phi(\partial\Phi/\partial n)\, dS}{U^2/2}$$

The additional apparent mass coefficient, k, is defined as the ratio of the kinetic energy of the fluid to the kinetic energy of the body—that is, $T/[M(\text{velocity of body})^2/2]$. The longitudinal additional apparent mass coefficient for translational motion is $T_{x\text{ axis}}/(MU^2/2)$ or $k_1 = M_a/M$. The transverse coefficients are $T_{y\text{ axis}}/(MV^2/2)$, or $k_2 = M_b/M$ and $T_{z\text{ axis}}/(MW^2/2)$, or $k_3 = M_c/M$, respectively.

In order to illustrate the concept of additional apparent mass, consider a sphere. Applying Eq. (1) to the case of a sphere moving through an inviscous fluid, it can be shown that $T = [(4/3)\pi r^3\rho]\, U^2/4 = M'U^2/4$, where M' is the mass of the fluid displaced by the sphere and r is its radius. The additional apparent mass of the sphere is, therefore, $T/(U^2/2) = (M'U^2/4)/(U^2/2)$ or $M'/2$. For the derivation of T for a sphere moving in an infinite mass of liquid which is at rest at infinity see pages 123–124 of reference 1. If M is the mass of the sphere, the total kinetic energy of the liquid and sphere considered as one dynamic system is

$$[M + (M'/2)]\, U^2/2 = (M + M_a)U^2/2 \qquad (2)$$

since $M'/2 = M_a$.

This means, therefore, that the effect of the presence of the fluid is equivalent to an addition to the inertia of the sphere of one-half of the mass of the liquid displaced.

When referring to a body having a certain mass one should not think of a lead body or a body having a concrete mass. The body under discussion is formed by the closed stream line which results from the sink-source distribution selected to represent the particular body. The mass of the body, M, can then be represented as $Q\rho$, where Q is the actual volume of the body and ρ is the density of the fluid medium for an incompressible fluid. Since M' is equal to the mass of fluid displaced by the body, M is numerically equal to M' for an incompressible fluid. In order to take into account the presence of the fluid as an item separate from the body alone, the term M' will be maintained in the following discussion.

The additional apparent mass coefficient of the sphere is

$$k = (M'U^2/4)/(MU^2/2) = (M'/2)/M = 0.50$$

In like manner, the kinetic energy of the fluid due to the motion of a circular cylinder moving through it with its axis perpendicular to the direction of motion is $T = M'U^2/2$, where $M' = \pi r^2\rho$ is the mass of fluid displaced by a unit length of cylinder and r is the radius of the cylinder. In this case $k = (M'U^2/2)/(MU^2/2) = 1.0$.

Let K = volume of apparent mass. Then, for the case of the sphere, we have $[M + (M'/2)]/\rho = K$. But $\rho = M/Q$, where M = mass of the body having

the same density as the fluid. Therefore, $\{[M + (M'/2)]/M\}Q = K$ or

$$(1 + k)Q = K$$

since $k = (M'/2)/M$ for the sphere.

The physical interpretation of this general expression is of interest. If each side of the last expression is multiplied by ρ,

$$Q\rho + kQ\rho = K\rho$$

where $Q\rho$ represents the mass of the body; $kQ\rho$ represents the additional mass that must be added to the mass of the body having the same density as the fluid to allow for the effect of the presence of the fluid (k is the additional apparent mass coefficient); and $K\rho$ represents the total apparent mass of the system which is composed of the body and the presence of the surrounding fluid.

Fuselage Moments for a Body of Revolution

The theoretic pitching moment acting on a body immersed in an inviscous fluid can be determined from the principle of the rate of change of moment of momentum, i.e.,

$$(d/dt) \sum (K\rho Ul) = M$$

where $K\rho$ is the total apparent mass of the system, U is the velocity of the body, l is the moment arm for the components of momentum, and M is the pitching moment of the body.

A body moving with a constant velocity U in the X-direction and an angle of attack, α, possesses momentum with the components $K_1\rho(U \cos \alpha)$ along the principal longitudinal axis and $K_2\rho$ $(U \sin \alpha)$ along the principal transverse axis which is perpendicular to the principal longitudinal axis and lies in a vertical plane. To determine the rate of change of moment of momentum a point is chosen in the plane of the longitudinal and transverse axes and moments are taken about the point. We obtain, as the moment M, assuming stalling moments positive,

$$-K_1\rho(U \cos \alpha)(U \sin \alpha) + K_2\rho(U \sin \alpha)(U \cos \alpha) = M$$

$$U^2\rho K_2 \sin \alpha \cos \alpha - U^2\rho K_1 \sin \alpha \cos \alpha = M$$

$$(\rho U^2/2)\ (K_2 - K_1) \sin 2\alpha = M$$

(For a more detailed discussion of the last expression see reference 2) where K_1 is the longitudinal apparent mass coefficient along the principal longitudinal axis and where K_2 is the transverse apparent mass coefficient along the principal transverse axis which is perpendicular to the longitudinal axis and lies in a vertical plane.

Since $(1 + k_1)Q = K_1$ and $(1 + k_2)Q = K_2$, upon substituting in the above equation,

$$M = (\rho U^2/2)\ (K_2 - k_1)Q \sin 2\alpha \qquad (3)$$

where k_1 equals the additional apparent mass coefficient along the principal longitudinal axis of the body and where k_2 equals the additional apparent mass coefficient along the principal transverse axis which is perpendicular to the principal longitudinal axis and lies in a vertical plane.

Since $k_2 > k_1$ for a body moving in an inviscous fluid (see Fig. 1), the moment will be an unstable one since positive moments are stalling moments.

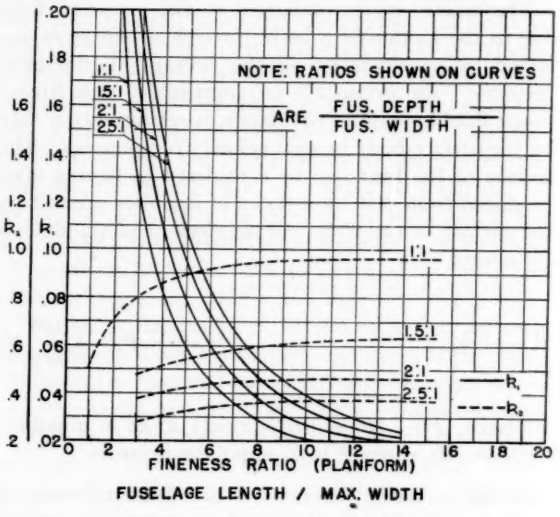

FIG. 1. Additional apparent mass coefficients k_1 and k_2 vs. fineness ratio for longitudinal stability.

In like manner, the theoretic yawing moment is

$$N = (\rho U^2/2)(k_3 - k_1)Q \sin 2\Psi \qquad (4)$$

where k_3 equals the additional apparent mass coefficient along the principal transverse axis which is perpendicular to the principal longitudinal axis and lies in a horizontal plane.

Since $k_3 > k_1$ (see Fig. 2), the moment will be unstable.

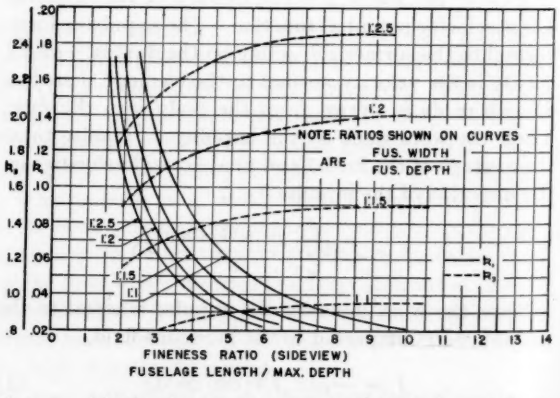

FIG. 2. Additional apparent mass coefficients k_1 and k_3 vs. fineness ratio for directional stability.

An axis of symmetry of the body is also a principal axis. Lamb[1] has derived the general energy expression of the fluid in terms of 21 coefficients when no stipulation is made in regard to the principal planes of the body. When the three principal axes of equilibrium are considered, the energy of the fluid can be expressed as

$$T = (\rho/2)(K_1U^2 + K_2V^2 + K_3W^2)$$

(for pure translational flow in a three-dimensional flow) where K_1, K_2, and K_3 are the apparent mass coefficients referred to the three mutually orthogonal principal axes of equilibrium, U being the longitudinal velocity, V being the transverse velocity in a vertical plane containing K_1 and K_2, and W being the transverse velocity in a horizontal plane containing K_1 and K_3.

For a body of revolution, $k_2 = k_3$, since an angle of attack is equivalent to an angle of yaw. Coefficients k_1 and k_2 have been computed by Lamb[1] and are shown in Figs. 1 and 2. The coefficients have been computed for a prolate ellipsoid in which the centroid of the body is located at the midpoint of the length of the body.

For shapes that depart from the prolate ellipsoid and in particular when the nose section and/or the tail section are so modified that the centroid moves toward the nose of the body, curves of k_2 and k_1 are replotted from reference 3 and are shown in Fig. 3. In order to define the shift in the centroid of the body from the midlength of the body, the term "conicity"[3] is introduced and is defined as: C = distance along the axis of symmetry from the midpoint of the length to the centroid of volume divided by the length of the body.

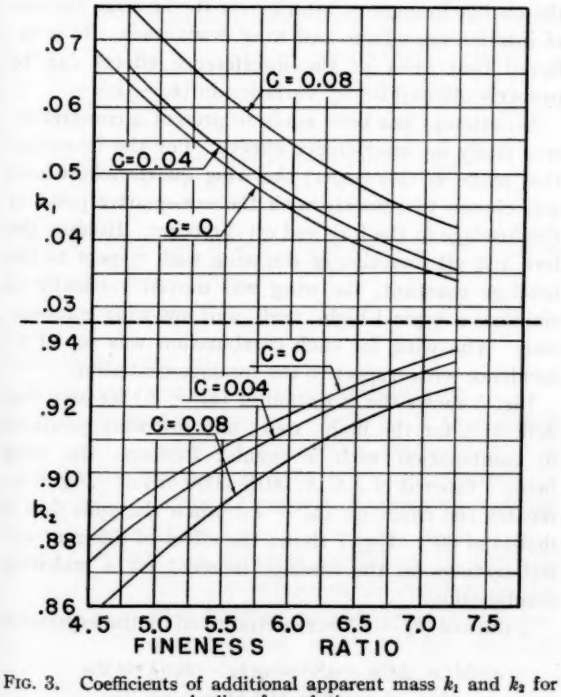

FIG. 3. Coefficients of additional apparent mass k_1 and k_2 for bodies of revolution.

Fig. 3 shows the effect of conicity on the additional apparent mass coefficients for $C = 0$ (prolate ellipsoid) and $C = 0.04$ and 0.08 for various fineness ratios. It is interesting to note that $(k_2 - k_1)$ for a given conicity and fineness ratio does not differ appreciably for the same fineness ratio and conicity = 0.

Smith[4] has shown the effect of a viscous fluid on the longitudinal additional apparent mass coefficient k_1 by taking into account the additional energy contained in the boundary layer on the airship "Akron." The coefficient k_1 increased 35 per cent over that for an inviscous fluid, the value of k_1 for the "Akron" being 0.0534 based on an inviscous fluid and 0.0721 when viscosity was taken into account.

Circular Fuselage—Pitching Moments

To show further the effects of a viscous fluid on $(k_2 - k_1)$, the pitching moments of the "Akron" were computed according to Eq. (3) and were compared with the moments obtained from reference 6 taken about the quarter-point of the body length. The following table shows the modified values of $(k_2 - k_1)$ determined in accordance with

$$M = q(k_2 - k_1)Q \sin 2\alpha = (C_{M_F})qQ$$

where q equals $\rho V^2/2$, C_{M_F} equals the pitching moment coefficient of "Akron" referred to the quarter-length of the body, and $k_2 - k_1 = C_{M_F}/\sin 2\alpha$.

In determining $(k_2 - k_1)$ it should be noted that the angle of attack α also changes because of boundary layer effects. Experiments indicate, however, that the change in α as well as in angle of yaw, Ψ, is small. On this basis the entire effect of viscosity will be taken into account in the factor $(k_2 - k_1)$.

TABLE 1

α	C_{M_F}	2α	$\sin 2\alpha$	$(k_2 - k_1)$
0	0.003	0	0	...
3	0.0685	6	0.1045	0.656
6	0.125	12	0.2079	0.603
9	0.165	18	0.3090	0.534
12	0.191	24	0.4067	0.470

The fineness ratio of the "Akron" is 5.9 and $C = 0.036$. From reference 3, $k_2 - k_1 = 0.912 - 0.048 = 0.864$ (see Fig. 3).

It is apparent that viscosity and the large boundary layer effects, especially at the higher angles of attack, have a pronounced effect on the coefficients. The effect, however, is to reduce the unstable moment of the body, the moment being a function of $(k_2 - k_1)$. Values of $(k_2 - k_1)$ are listed in Table 1 for various angles of attack.

Values of $(k_2 - k_1)$ were also obtained from data given in reference 7. The fuselage tested was circular in cross section and had a fineness ratio of 5.9. Values

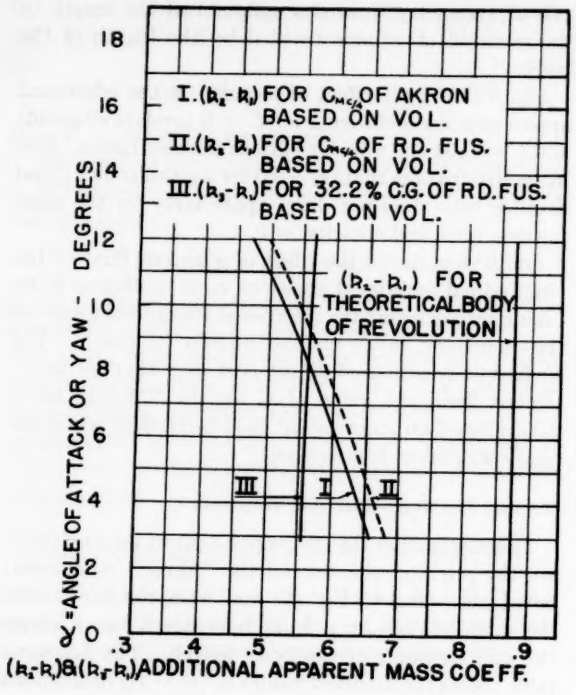
I.(k2-k1) FOR Cmc/4 OF AKRON BASED ON VOL.
II.(k2-k1) FOR Cmc/4 OF RD. FUS. BASED ON VOL.
III.(k3-k1) FOR 32.2% C.G. OF RD. FUS. BASED ON VOL.
(k2-k1) FOR THEORETICAL BODY OF REVOLUTION
α = ANGLE OF ATTACK OR YAW - DEGREES
(k2-k1)&(k3-k1) ADDITIONAL APPARENT MASS COEFF.

FIG. 4. Additional apparent mass coefficient vs. angle of attack or yaw.

of $(k_2 - k_1)$ vs. angle of attack are plotted for both the "Akron" and the circular fuselage in Fig. 4. The moments were taken about an axis 25 per cent of the fuselage length.

Circular Fuselage—Yawing Moments

The theoretic yawing moment of a body of revolution is given by

$$N = q(k_3 - k_1)Q \sin 2\Psi = q(k_2 - k_1)Q \sin 2\Psi$$

since $k_3 = k_2$.

Theoretically, then, the pitching moment of a body of revolution should be the same as the yawing moment. To show that this is practically the case, the data from reference 15 were used to determine values of $(k_3 - k_1)$. The results are shown in Fig. 4. Curve III of Fig. 4 is obtained by evaluation of

$$k_3 - k_1 = \frac{C_N}{\sin 2\Psi}\left(\frac{S\bar{b}}{Q}\right) = \frac{\Psi(dC_N/d\Psi)\ (Sb/Q)}{\sin 2\Psi}$$

where Ψ = the angle of yaw
C_N = yawing moment coefficient (N/qSb)
q = dynamic pressure $(\rho V^2/2)$
S = wing area
b = wing span
Q = fuselage volume

It is assumed that $dC_N/d\Psi = 0.0006$ for an angle of attack range from 0° to 15° (see Fig. 8, reference 15). This assumption is not strictly correct, since C_N is not a linear function of the angle of yaw throughout the yawing range. As a result, the slope of Curve III differs from the slopes of Curves I and II, and, as indicated by Curves I and II in Fig. 4, the slope of Curve III should change in sign and magnitude as the angle of yaw is increased. The yawing moments were obtained about an axis 32.2 per cent of the fuselage length. The fuselage was similar to the one tested in reference 7.

Effect of Wing-Fuselage Interference—Pitching Moments

The N.A.C.A. has conducted a thorough series of tests to determine the effects of aerodynamic interference between wings and fuselages at a large value of the Reynolds Number.[7–12] The program included tests on circular and rectangular fuselages in combination with various wings having different airfoil sections. The quarter-chord axis of the wing was placed at several positions with respect to the quarter-point of the fuselage in the fore and aft direction, and the vertical position of the wing was varied to simulate high-, mid-, and low-wing combinations. The vertical displacement of the wing quarter-chord axis was measured with respect to the quarter-point of the fuselage. Tests were also made with various wing-fuselage fillets and split flaps deflected 60°. All tests were conducted in the Variable Density Tunnel of the N.A.C.A.

The results show that wing-fuselage interference has a pronounced effect on the magnitude of the fuselage unstable pitching moments. Reference to Figs. 5 to 7 show clearly the effect of interference on fuselage moments.

In determining $(k_2 - k_1)$ no allowance was made for the change in angle of attack over the fuselage because of interference effects and wing down-wash. It is believed that most of the interference effects can be properly allowed for by variation in $(k_2 - k_1)$.

No attempt has been made to present a comprehensive study on interference effects. For the investigation made in this paper, the wing quarter-chord axis was chosen to coincide with the one-quarter point of the fuselage in the fore and aft direction. Holding the fore and aft direction of the wing with respect to the fuselage constant, the wing was moved vertically to simulate a typical high-, mid-, and low-wing combination. The wing for each combination was set at 0° incidence with respect to the fuselage centerline.

Fig. 5 shows the variation of $(k_2 - k_1)$ for zero flap deflection for the high-, mid-, and low-wing positions in combination with a circular fuselage, the wing being a tapered N.A.C.A. 0018–0009 airfoil. Fig. 6 indicates the effect on $(k_2 - k_1)$ when the split flap is deflected 60°. Fig. 7 shows the effect of different airfoil sections on the fuselage moment for a mid-wing combination.

Values of $(k_2 - k_1)$ were determined by the expression

$$M = \Delta C_{M_{c/4}} qS\bar{c} = q(k_2 - k_1)Q \sin 2\alpha$$
$$(k_2 - k_1) = (S\bar{c}/Q)(\Delta C_{M_{c/4}}/\sin 2\alpha)$$

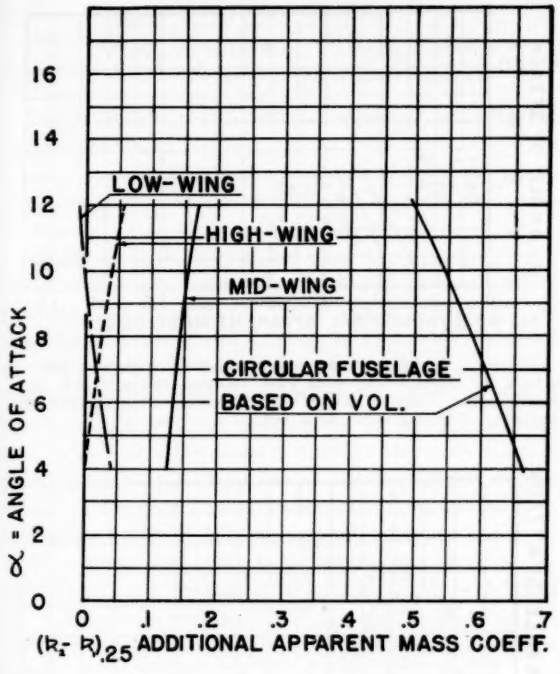

FIG. 5. Additional apparent mass coefficient vs. angle of attack for round fuselage plus wing interference. $\delta_f = 0°$. Tapered N.A.C.A. 0.0018–0.0009 airfoil, tapered fillets.

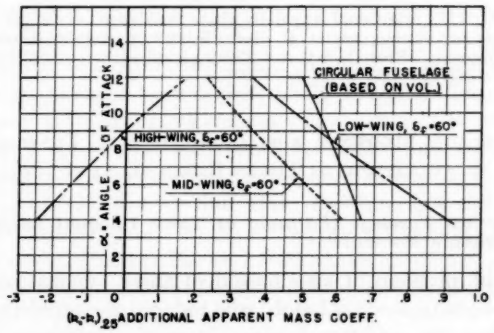

FIG. 6. Additional apparent mass coefficient vs. angle of attack. Round fuselage plus interference. Rect. N.A.C.A. 0.0012 airfoil, tapered fillets.

where S = wing area

$\bar{c}$ = mean aerodynamic chord of wing

Q = fuselage volume, which can be determined easily by integrating mechanically the area under the curve determined by plotting cross-sectional area vs. fuselage length

$\Delta C_{M_{c/4}}$ = pitching moment coefficient of fuselage plus interference of the fuselage in the wing-fuselage combinations about the quarter-chord point of the fuselage given in references 6–11, inclusive—that is, the difference between the characteristics of the combination and the characteristics of the wing alone

α = angle of attack

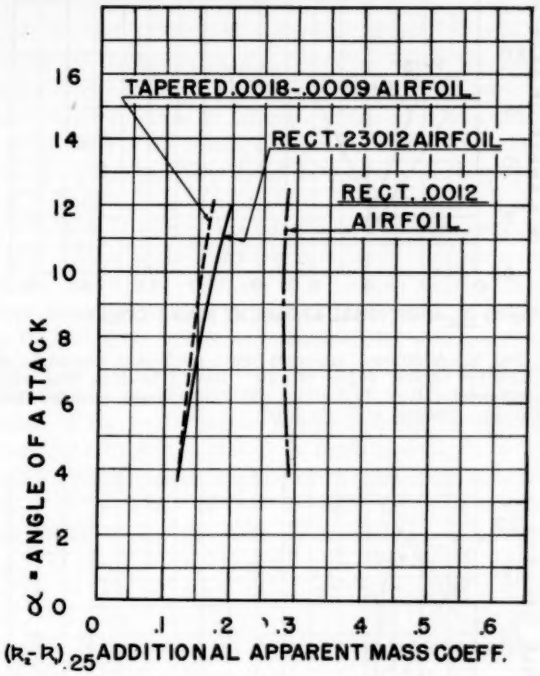

FIG. 7. Effect of airfoil section on $(k_2 - k_1)$. Round fuselage, tapered fillets. Midwing.

Yawing Moments

An extensive wind-tunnel investigation has been made at the N.A.C.A. to determine the effect of yaw on lateral-stability characteristics including the effects of aerodynamic interference between wings and fuselages. Various wings and wings in combination with a circular fuselage have been tested (refs. 13–15, inclusive). The yawing moments were taken about an axis located 32.2 per cent of the fuselage length from the leading edge of the fuselage. Coefficients $(k_3 - k_1)$ were computed for a circular fuselage of fineness ratio 5.9 and include wing-fuselage interference effects resulting from the 23012 rectangular wing with rounded tips installed on the circular fuselage.[15]

Values of $(k_3 - k_1)$ vs. angle of attack for various angles of yaw are plotted on Figs. 8 to 12, inclusive. For the zero flap deflection, a midwing and low wing were chosen, the wing having a 5° dihedral. The high-wing results are not shown, since the $(k_3 - k_1)$ values were quite erratic at an angle of attack of 15°, due possibly to wing stalling.

Figs. 10, 11, and 12 show $(k_3 - k_1)$ for the 60° split flap and for a high, mid, and low wing, the wing in this case having 0° dihedral.

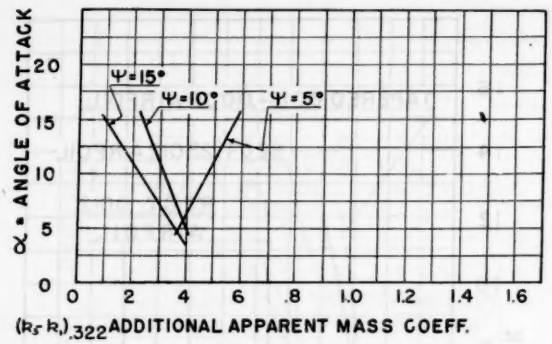

FIG. 8. Additional apparent mass coefficient vs. angle of attack for various angles of yaw. Round fuselage plus wing interference. Rect. N.A.C.A. 23012 airfoil with rounded tips. Midwing, dihedral = 5°, $\delta_f = 0°$.

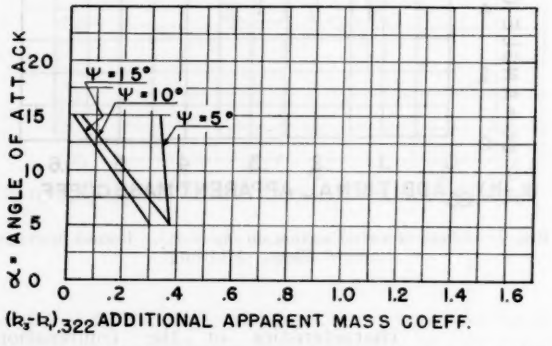

FIG. 9. Additional apparent mass coefficient vs. angle of attack for various angles of yaw. Round fuselage plus wing interference. Rect. N.A.C.A. 23012 airfoil with rounded tips. Low wing, dihedral = 5°, $\delta_f = 0°$.

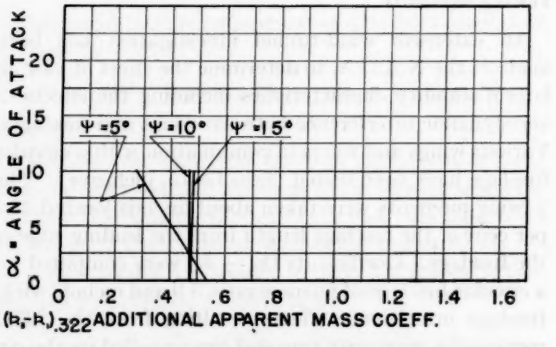

FIG. 10. Additional apparent mass coefficient vs. angle of attack for various angles of yaw. Round fuselage plus wing interference. Rect. N.A.C.A. 23012 airfoil with rounded tips. High wing, dihedral = 0°, $\delta_f = 60°$.

Values of $(k_3 - k_1)$ were determined from

$$(k_3 - k_1) = (Sb/Q)(\Delta C_{N_{32\cdot2}\%}/\sin 2\Psi)$$

where $\Delta C_{N_{32\cdot2}\%}$ is the yawing moment coefficient of fuselage plus interference of the fuselage in the wing-fuselage combinations given in reference 15 and where Ψ equals angle of yaw.

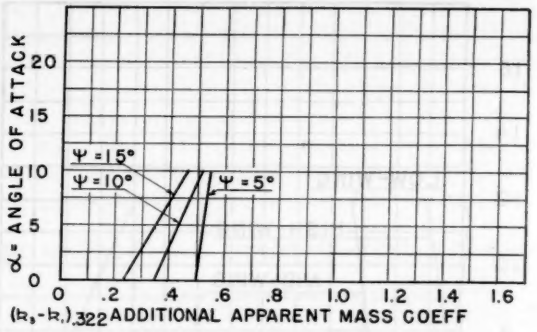

FIG. 11. Additional apparent mass coefficient vs. angle of attack for various angles of yaw. Round fuselage plus wing interference. Rect. N.A.C.A. 23012 airfoil with rounded tips. Midwing, dihedral = 0°, $\delta_f = 60°$.

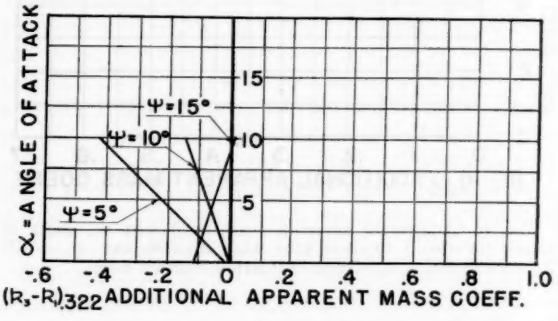

FIG. 12. Additional apparent mass coefficient vs. angle of attack for various angles of yaw. Round fuselage plus wing interference. Rect. N.A.C.A. 23012 airfoil with rounded tips. Low wing, dihedral = 0°, $\delta_f = 60°$.

FUSELAGE MOMENTS FOR AN ELLIPTICAL FUSELAGE (ELLIPSOID OF THREE UNEQUAL AXES)

Elliptical Fuselage (Ellipsoid of Three Unequal Axes)—Pitching Moments

The problem of an ellipsoid of three unequal axes has been treated by Lamb[1] who reduced the problem of finding the additional apparent mass coefficients in terms of elliptic integrals. Munk[16] reduces these integrals to a form which is readily usable; viz.

$$\alpha_0 = \frac{2abc}{\sqrt{(a^2 - c^2)^3}}\left(\frac{1}{k^2}\right)\left[F(u) - E(u)\right]$$

$$\beta_0 = \frac{2abc}{\sqrt{(a^2 - c^2)^3}}\left[\frac{1}{k^2(1 - k^2)}\right]\times$$

$$\left[E(u) - (1 - k^2)F(u) - k^2\sqrt{\frac{(a^2 - c^2)c^2}{a^2b^2}}\right]$$

$$\gamma_0 = \frac{2abc}{\sqrt{(a^2 - c^2)^3}}\left(\frac{1}{1 - k^2}\right)\left[\sqrt{\frac{(a^2 - c^2)b^2}{a^2c^2}} - E(u)\right]$$

where $a > b > c$ = the semiaxes of the ellipsoid

$k = \sin\alpha = \sqrt{(a^2 - b^2)/(a^2 - c^2)}$

$$\sin \Phi = \sqrt{(a^2 - c^2)/a^2}$$
$$F(u) = F(k, \Phi) \text{ is given in reference 17}$$
$$E(u) = E(k, \Phi) \text{ is given in reference 17}$$

The coefficients of additional apparent mass for the three axes are

$$k_1 = \frac{\alpha_0}{2 - \alpha_0} \qquad k_2 = \frac{\beta_0}{2 - \beta_0} \qquad k_3 = \frac{\gamma_0}{2 - \gamma_0}$$

Values of k_1, k_2, and k_3 have been plotted in Figs. 1 and 2. The coefficients k_1 and k_2 are plotted against fineness ratio based on the fuselage length to the maximum width of the fuselage in plan view. Curves for various ratios of maximum depth to maximum width of fuselage are shown in Fig. 1. For the yawed flight condition values of k_1 and k_3 are plotted vs. fineness ratio where the fineness ratio in this case is based on fuselage length to maximum fuselage depth in side view. Curves for various ratios of maximum width to maximum depth of fuselage appear in Fig. 2.

An analysis was made to determine the effect of viscosity and wing-fuselage interference on $(k_2 - k_1)$ and $(k_3 - k_1)$ for an elliptical fuselage, but, because of the restricted status of the data, the results cannot be published.

General Discussion

The fuselages that have been discussed so far are rounded-nose bodies that are commonly used in liquid-cooled engine installations. The question naturally arises as to whether the fuselage moments obtained for a rounded-nose body apply equally as well to a radial-engine installation. Examination of Table II of reference 7 shows that the rounded-nose fuselage and the radial-engine cowl installation fuselage moments do not vary appreciably for flow along the longitudinal axis. The radial-engine installation apparently behaves like a flat plate in that the air ahead of the engine piles up to such an extent that an equivalent rounded-nose body results, the air particles moving along a stream line that hypothetically extends the blunt radial-engine fuselage body to a rounded-nose shape.

The data presented do not allow for any appendages on the fuselage such as canopy, underslung ducts, or gun turrets. In most normal installations, however, the canopy is so arranged that its side area is nearly symmetrically placed with respect to the c. g. and, as a result, no substantial change in fuselage yawing moment should result. If the duct is not symmetrically placed with respect to the c. g. a rough approximation can be made as to the increment or decrement in fuselage yawing moment by assuming the flow around the duct to be equal to the flow around an elliptical or circular cylinder, depending upon the shape of the duct. The change in yawing moment due to a gun turret can be approximated in a manner similar to the duct. For changes in the pitching moment due to the canopy or duct the pressure distribution for an airfoil section approaching the appendage can be used. In the case of a gun turret near the tail, the effect on pitching moment should be negligible inasmuch as the boundary layer thickness there is appreciable. For the gun turret in the forward part of the fuselage an estimate of the change in pitching moment of the fuselage can be made if one performs a strip analysis making use of data on circular or elliptical cylinders.

If Curve II in Fig. 4 is taken as the average curve of $(k_2 - k_1)$ vs. angle of attack, it is found that the slope of the curve $d(k_2 - k_1)/d\alpha$ is -0.02 per degree. The experimental value of $(k_2 - k_1)$ at zero angle of attack is 0.75. This value was obtained by extrapolating Curve II to zero angle of attack where it is believed the boundary layer effects are a minimum. The theoretic value of $(k_2 - k_1)$ for a circular fuselage of fineness ratio 5.9 is $(0.915 - 0.046) = 0.869$ (see Fig. 1 or 3). The correction to be applied to the theoretic value of $(k_2 - k_1)$ is 0.85. If the correction factor of 0.85 is multiplied by the theoretic value of $(k_2 - k_1)$ at zero angle of attack, it is then possible to construct the curve of $(k_2 - k_1)$ vs. angle of attack by making use of $d(k_2 - k_1)/d\alpha = -0.02$ per degree. On this basis it is possible to determine the pitching moment of a circular fuselage having a fineness ratio other than 5.9. The first step would be to find from Fig. 1 the value of $(k_2 - k_1)$ for the fineness ratio under consideration. By assuming a correction factor of 0.85 at zero angle of attack, the curve of $(k_2 - k_1)$ vs. α can be found from $d(k_2 - k_1)/d\alpha = -0.02$ per degree.

Examination of Figs. 1 and 2 shows the marked change in the values of $(k_2 - k_1)$ and $(k_3 - k_1)$ for an ellipsoid of three unequal axes relative to a body of revolution. For a fineness ratio of 8 in plan form the values of $k_2 - k_1$ are (see Fig. 1) shown in Table 2.

Table 2

Maximum Depth of Fuselage: Maximum Width	k_2	k_1	$k_2 - k_1$	$\frac{k_2 - k_1}{0.921}$
1:1	0.95	0.029	0.921	1.00
1.5:1	0.59	0.038	0.552	0.60
2:1	0.45	0.048	0.402	0.44
2.5:1	0.36	0.055	0.305	0.33

Table 2 shows the theoretic variation in $(k_2 - k_1)$ as the maximum depth of fuselage to maximum width is increased. The last column indicates the reduction in pitching moment for an elliptical fuselage as compared to a circular fuselage of fineness ratio 8. The ratio of

$$\frac{(k_2 - k_1)_{\text{Elliptical Fuselage}}}{(k_2 - k_1)_{\text{Circular Fuselage}}} \text{ vs. } \frac{\text{Maximum Depth of Fuselage}}{\text{Maximum Width of Fuselage}}$$

is plotted in Fig. 13 for fineness ratios of 4, 6, 8, and 10 in plan form. For fineness ratios of 4, 6, and 10, the

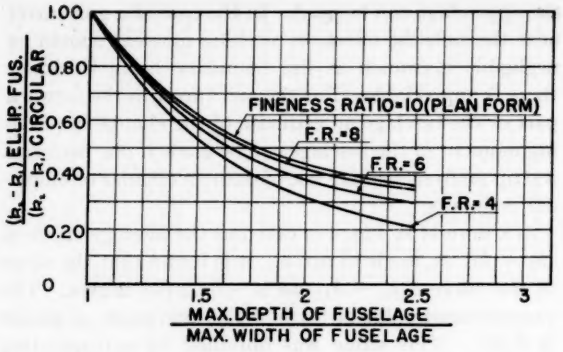

FIG. 13. Variation of $(k_2 - k_1)$ vs. maximum depth of fuselage to maximum width.

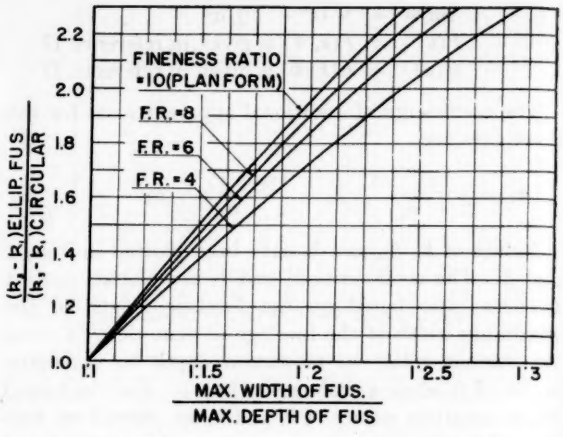

FIG. 14. Variation of $(k_3 - k_1)$ vs. maximum width of fuselage to maximum depth.

values of $(k_2 - k_1)$ for the circular fuselage are 0.778, 0.875, and 0.939, respectively.

TABLE 3

Maximum Width of Fuselage: Maximum Depth	Fineness Ratio in Side View	k_2	k_1	$k_3 - k_1$	$\frac{k_3 - k_1}{0.921}$
1:1	8.0	0.95	0.029	0.921	1.00
1:1.5	5.3	1.43	0.038	1.392	1.50
1:2	4.0	1.79	0.048	1.742	1.89
1:2.5	3.2	2.16	0.055	2.105	2.28

Table 3 shows the theoretic variation in $(k_3 - k_1)$ and indicates the rapid increase in yawing moment of an elliptical fuselage as the depth increases. The ratio of

$$\frac{(k_3 - k_1)_{\text{Elliptical Fuselage}}}{(k_3 - k_1)_{\text{Circular Fuselage}}} \quad \text{vs.} \quad \frac{\text{Maximum Width of Fuselage}}{\text{Maximum Depth of Fuselage}}$$

is plotted in Fig. 14 for fineness ratios of 4, 6, 8, and 10 in plan form. The fineness ratio in side view is included in this table in order that k_3 may be found from Fig. 2.

The method presented herein can be applied to determine the pitching and yawing moments of engine nacelles of multiengined airplanes.

REFERENCES

[1] Lamb, H., *Hydrodynamics*, 6th Edition; Cambridge University Press, London, 1932.

[2] Ames, Joseph S., *A Résumé of the Advances in Theoretical Aeronautics made by Max M. Munk*, N.A.C.A. T. R. No. 213, 1928.

[3] O'Donnell, William J., *On the Motion of Elongated Bodies of Revolution Through a Perfect Fluid;* A Dissertation Submitted to the Faculty of the Graduate School of Arts and Sciences of the Catholic University of America in Partial Fulfillment of the Requirements for the Degree of Doctor of Philosophy, the Catholic University of America, Washington, D.C. 1938.

[4] Smith, Richard H., *Longitudinal Potential Flow about an Arbitrary Body of Revolution with Application to the Airship "Akron,"* Journal of the Aeronautical Sciences, Vol. 3, No. 1, pp. 26–31, September, 1935.

[5] Munk, Max M., *Fundamentals of Fluid Dynamics for Aircraft Designers;* The Ronald Press Co., New York, 1929.

[6] Freeman, H. B., *Force Measurements on a 1/40-Scale Model of the U.S. Airship "Akron,"* N.A.C.A. T.R. No. 432, 1932.

[7] Jacobs, E. N., and Ward, K. E., *Interference of Wing and Fuselage from Tests of 209 Combinations in the N.A.C.A. Variable-Density Tunnel*, N.A.C.A. T.R. No. 540, 1935.

[8] Sherman, A., *Interference of Wing and Fuselage from Tests of 28 Combinations in the N.A.C.A. Variable-Density Tunnel*, N.A.C.A. T.R. No. 575, 1936.

[9] Sherman, A., *Interference of Wing and Fuselage from Tests of 18 Combinations in the N.A.C.A. Variable-Density Tunnel. Combinations with Split Flaps*, N.A.C.A. T.N. No. 640, 1938.

[10] Sherman, A., *Interference of Wing and Fuselage from Tests of 17 Combinations in the N.A.C.A. Variable-Density Tunnel. Combinations with Special Junctures*, N.A.C.A. T.N. No. 641, 1938.

[11] Sherman, A., *Interference of Wing and Fuselage from Tests of Eight Combinations in the N.A.C.A. Variable-Density Tunnel. Combinations with Tapered Fillets and Straight-Side Junctures*, N.A.C.A. T.N. No. 642, 1938.

[12] Sherman, A., *Interference of Tail Surfaces and Wing and Fuselage from Tests of 17 Combinations in the N.A.C.A. Variable-Density Tunnel*, N.A.C.A. T.R. No. 678, 1939.

[13] Imlay, F. M., *The Estimation of the Rate of Change of Yawing Moment with Sideslip*, N.A.C.A. T.N. No. 636, 1938.

[14] Bamber, M. J., and House, R. O., *Wind-Tunnel Investigation of Effect of Yaw on Lateral-Stability Characteristics. I—Four N.A.C.A. 23012 Wings of Various Plan Forms with and Without Dihedral*, N.A.C.A. T.N. No. 703, 1939.

[15] Bamber, M. J., and House, R. O., *Wind-Tunnel Investigation of Effect of Yaw on Lateral-Stability Characteristics. II—Rectangular N.A.C.A. 23012 Wing with a Circular Fuselage and Fin*, N.A.C.A. T.N. No. 730, 1939.

[16] Durand, W. F., *Aerodynamic Theory*, Vol. I, Div. C., Fluid Mechanics, Part II, Max M. Munk, pp. 301–302; Julius Springer, Berlin, 1934.

[17] Peirce, B. O., *A Short Table of Integrals;* Ginn and Co., Boston, 1929.

Notes on Rudder Pedal-Force Characteristics

H. R. PASS*

Hughes Aircraft Company

SUMMARY

From an analysis of the geometric and airflow parameters that affect the free-floating characteristics of an unstalled rudder during steady sideslips, the effects of these parameters on the rudder pedal-force characteristics have been studied. The results of this study indicate that rudder pedal-force lightenings or reversals are more likely to occur for rudders having large chords or balancing tabs than for rudders having small chords or horn balances. In addition, the results indicate that these undesirable pedal-force characteristics are extremely likely to occur in power-on flight at the sideslip angles at which the vertical tail emerges from the slipstream.

INTRODUCTION

IN ORDER TO HAVE satisfactory directional control during normal flight operations, the pilot of an airplane requires that the rudder, in addition to being capable of producing any desired yawing moment, should possess the following pedal-force characteristics:

(1) When right rudder deflections are required for some flight condition, the right pedal should be moved forward and should be held with a right pedal push force. Left rudder deflections should be obtained in a similar manner.

(2) As the rudder deflection increases, the corresponding pedal push should increase. There should not be any lightening of the pedal push as the rudder is further deflected from neutral.

Most rudders have these desirable pedal-force characteristics. There have been some airplanes, however, for which—usually in high-power low-speed flight during steady sideslips—the right rudder deflection, for example, would have to be held by a pull on the right pedal or, since this is usually impossible with conventional pedal arrangements, would have to be held by a push on the left pedal. This reversal of pedal force is extremely disconcerting to the pilot and may be dangerous because it could lead to catastrophic instability if the pilot could not exert enough push on the left pedal to prevent the rudder from further deflecting to the right.

Rudder pedal-force reversals are obviously caused by a reversal of the rudder hinge moment and, as indicated by Schairer,[1] may occur with the vertical tail in either a stalled or unstalled state. Rudder pedal-force reversals with the vertical tail in a stalled state are particularly dangerous because the pilot usually has little warning; the relative importance of the various factors that affect rudder pedal-force reversals with the vertical tail in a stalled state have been amply discussed by Schairer[1] and Johnson.[2] It is the object of this paper to indicate qualitatively the parameters that affect rudder-pedal force reversals with the vertical tail in an unstalled state; rudder pedal-force lightenings, while not so dangerous as rudder pedal-force reversals, are more frequent occurrences, and the parameters affecting them will also be indicated.

Received November 9, 1943.

* Senior Aerodynamicist.

SYMBOLS

b = span

$\bar{c}$ = mean geometric chord

C_{H_R} = rudder hinge-moment coefficient, (hinge moment $\div q S_R \bar{c}_R$)

C_n = yawing-moment coefficient, (yawing moment $\div q_o S_w b_w$)

C_N = normal-force coefficient, (normal force/qS_T)

q = effective dynamic pressure at tail

(q/q_o) = ratio of effective dynamic pressure at tail to free-stream dynamic pressure

S = area

u = hinge-moment parameter, $(\partial C_{H_R}/\partial C_{N_T})_{\delta_R}$

v = hinge-moment parameter, $(\partial C_{H_R}/\partial \delta_R)_{C_{N_T}}$

α = angle of attack, degrees

β = angle of sideslip, degrees (positive when left wing tip is forward)

δ = control surface deflection, degrees (positive when trailing edge of rudder moves toward right wing tip)

σ = local sidewish angle measured from the wind axes, degrees (negative when it increases the angle of attack of the yawed vertical tail)

τ = relative rudder effectiveness, $\left(\frac{dC_{N_T}}{d\delta_R}\Big/\frac{dC_{N_T}}{d\alpha_T}\right)$

Subscripts:

A = airplane

B = balance

FF = free-floating

o = free-stream

R = rudder

T = vertical tail

TR = trim

w = wing

ANALYSIS

Although rudder pedal-force reversals or lightenings may occur either with the airplane in curvilinear or rectilinear flight, only those reversals or lightenings that occur with the airplane in rectilinear flight will be studied; the results of this study may probably be applied, with some modifications, to curvilinear flight.

Rudder Pedal-Force Reversals

The hinge moment of the rudder of an unstalled vertical tail in a steady sideslip may be expressed as

$$\text{hinge moment} = C_{H_R} q S_R \bar{c}_R \tag{1}$$

in which

$$C_{H_R} = (\delta_{R_{TR}} - \delta_{R_{FF}})(\partial C_{H_R}/\partial \delta_R)_{\alpha_T} \tag{2}$$

where $(\partial C_{H_R}/\partial \delta_R)_{\alpha_T}$, the rate of change of hinge-moment coefficient with rudder angle, is sensibly constant throughout a considerable sideslip range, so that, as indicated in Fig. 1:

(1) If $\delta_{R_{FF}}$ is less than $\delta_{R_{TR}}$ (Case 1), the rudder pedal force will be in the correct direction—that is, right pedal pushes are required for right rudder deflections.

(2) If $\delta_{R_{FF}}$ is equal to $\delta_{R_{TR}}$, the rudder pedal force will be zero.

(3) If $\delta_{R_{FF}}$ is greater than $\delta_{R_{TR}}$ (Case 2), the rudder pedal force will be reversed—that is, left pedal pushes are required to hold right rudder deflections.

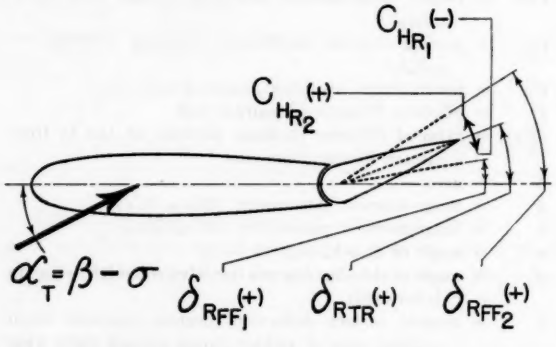

FIG. 1. Effect of the rudder free-floating angle on the direction of the rudder hinge-moment coefficient for a given rudder trim angle in a steady sideslip.

Thus, and most significantly, as the free-floating tendency of the rudder is decreased, $\delta_{R_{FF}} \to 0$, the likelihood of rudder pedal-force reversals diminishes.

The free-floating angle of the rudder, the angle at which the hinge moment is zero, may be calculated by setting

$$C_{H_R} = uC_{N_T} + v\delta_{R_{FF}} = 0 \tag{3}$$

where the coefficients are based on local dynamic pressure and u and v, the hinge-moment parameters of Glauert,[3] are functions of S_R/S_T and S_B/S_R and also of the type of aerodynamic balance and are related to the more familiar hinge-moment parameters by

$$(\partial C_{H_R}/\partial \alpha_T)_{\delta_R} = u(dC_{N_T}/d\alpha_T) \tag{3a}$$

and by

$$(\partial C_{H_R}/\partial \delta_R)_{\alpha_T} = v + u(dC_{N_T}/d\alpha_T)_\tau \tag{3b}$$

Expressing

$$C_{N_T} = (dC_{N_T}/d\alpha_T)_o(\alpha_T + \tau\delta_{R_{FF}}) \tag{4}$$

where $\alpha_T = \beta - \sigma$, substituting this expression in Eq. (3), and then transposing, the free-floating angle of the rudder at any sideslip angle may finally be obtained as

$$\delta_{R_{FF}} = -R_K(\beta - \sigma) \tag{5}$$

where

$$R_K = [(dC_{N_T}/d\alpha_T)_o u]/[(dC_{N_T}/d\alpha_T)_o u\tau + v] \tag{5a}$$

Eqs. (5) and (5a) indicate that the free-floating characteristics of the rudder are functions solely of the geometric parameters and of the angle of attack of the vertical tail and are independent of the dynamic pressure at the tail. For design purposes, Eq. (5a), which will be used to evaluate the effects of the geometric parameters on the rudder free-floating characteristics, might perhaps be more usefully written, using Eqs. (3a) and (3b), as

$$R_K = (\partial C_{H_R}/\partial \alpha_T)_{\delta_R}/(\partial C_{H_R}/\partial \delta_R)_{\alpha_T} \tag{5b}$$

Rudder Pedal-Force Lightenings

From Eq. (2), the rate of change of rudder hinge-moment coefficient with angle of sideslip is

$$\frac{dC_{H_R}}{d\beta} = \left(\frac{d\delta_{R_{TR}}}{d\beta} - \frac{d\delta_{R_{FF}}}{d\beta}\right)\left(\frac{\partial C_{H_R}}{\partial \delta_R}\right)_{\alpha_T} \tag{6}$$

so that, as indicated in Fig. 2, which may be representative of wind-tunnel results,

(1) If $d\delta_{R_{FF}}/d\beta$ is less than $d\delta_{R_{TR}}/d\beta$, the rudder pedal force increases with sideslip.

(2) If $d\delta_{R_{FF}}/d\beta$ is equal to $d\delta_{R_{TR}}/d\beta$, the rudder pedal-force does not vary with sideslip.

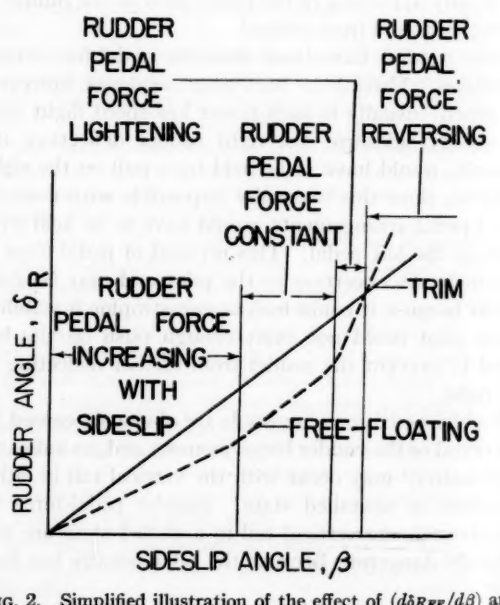

FIG. 2. Simplified illustration of the effect of $(d\delta_{R_{FF}}/d\beta)$ and $(d\delta_{R_{TR}}/d\beta)$ on the variation of the rudder pedal force with sideslip angle.

(3) If $d\delta_{R_{FF}}/d\beta$ is greater than $d\delta_{R_{TR}}/d\beta$, the rudder pedal-force will decrease or lighten with sideslip.

Thus, as $d\delta_{R_{FF}}/d\beta$ decreases, the likelihood of rudder pedal-force lightenings diminishes. Eq. (5) indicates that

$$d\delta_{R_{FF}}/d\beta = -R_K[1 - (d\sigma/d\beta)] \qquad (7)$$

Application

Eqs. (5) and (7) indicate the parameters that by affecting the rudder free-floating tendencies affect the rudder pedal-force characteristics. These parameters may conveniently be considered in the following groups: the geometric parameters—$dC_{N_T}/d\alpha_T$, τ, and u and v—which depend on the geometry of the isolated vertical tail, and the airflow parameters—σ and $d\sigma/d\beta$—which depend on the location of the vertical tail with respect to the wing, propeller(s), and fuselage.

Geometric Parameters

The geometric parameters, $dC_{N_T}/d\alpha_T$ and u and v, are functions of the tail aspect ratio and functions of S_R/S_T, S_B/S_R, and the type of aerodynamic balance, respectively. The effect of these parameters on the rudder pedal-force characteristics is determined by the factor R_K, which, as shown in Eqs. (5) and (7), is directly proportional to the rudder free-floating tendencies so that, as the numerical value of this factor for a given rudder is reduced, the likelihood of a rudder pedal-force lightening or reversal diminishes (Eqs. 2 and 6).

As indicated by the results of calculations (Fig. 3), assuming an end-plate factor of 1.55,[4, 5] $S_R/S_T = 0.55$ and $S_B/S_R = 0.20$ (all of which correspond to a typical vertical tail with axial balance on a single-engine airplane), tail aspect ratio has practically a negligible effect on R_K, although there is a slightly greater tendency toward rudder pedal-force lightenings or reversals with high than with low aspect ratios. S_R/S_T, S_B/S_R, and particularly the type of aerodynamic balance—axial or overhang, horn, or balancing tab—have, on the other hand, marked effects on R_K and, hence, on the rudder pedal-force characteristics.

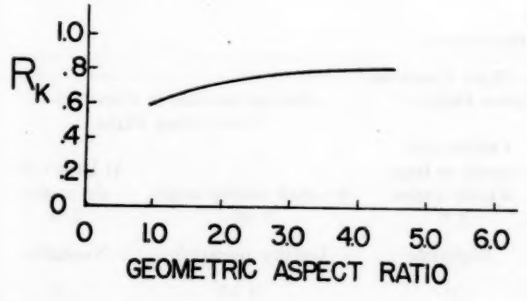

FIG. 3. Effect of geometric aspect ratio on R_K; $S_R/S_T = 0.55$; $S_B/S_R = 0.20$.

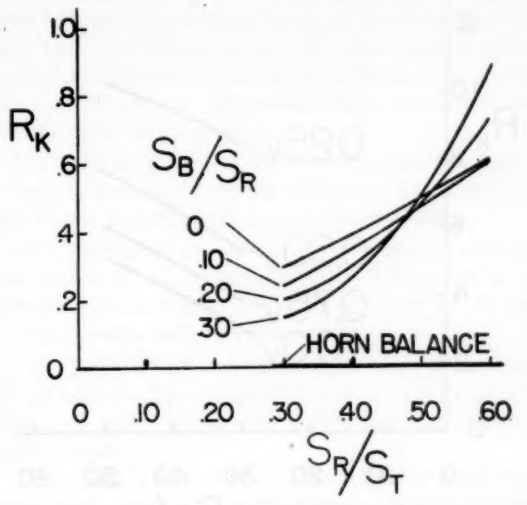

FIG. 4. Variation of R_K with S_R/S_T and S_B/S_R for rudders with axial and horn balance; $(dC_{N_T}/d\alpha_T)_o = 0.040$.

Axial or Overhang Balance: For an axial or overhang balance, the variation of u, v, and τ with S_R/S_T and S_B/S_R has been taken from design charts[5] and, assuming $(dC_{N_T}/d\alpha_T)_o = 0.040$, the variation of R_K with S_R/S_T and S_B/S_R has been calculated. The results, presented in Fig. 4, indicate that:

(1) There is a much greater tendency toward rudder force reversals or lightenings with large-chord rudders than with small chord rudders.

(2) For large-chord rudders, the tendency toward rudder force reversals or lightenings markedly increases as the amount of axial balance increases.

(3) For small-chord rudders, on the other hand, the tendency toward rudder force reversals or lightenings slightly decreases as the amount of axial balance increases.

Horn Balance: With a properly proportioned horn balance, u may be reduced to zero or may even be made positive, while v would remain negative. As indicated in Eqs. (5) and (7), the rudder, in these instances, either will be nonfloating ($\delta_{R_{FF}} = d\delta_{R_{FF}}/d\beta = 0$) or will float against the wind, so that rudder pedal-force reversals or lightenings are highly unlikely with horn-balanced rudders (Fig. 4).

Balancing Tab: Unlike a horn balance, a balancing tab scarcely affects u but, depending upon its proportions and gearing, may produce any desired value of v. Assuming various rudders with balancing tabs that reduce v to $^1/_4$, $^1/_2$, and $^3/_4$ of the value that the rudders would have without any balancing tab, the variation of R_K with S_R/S_T (taking values of u, v, and τ for rudders without balancing tabs from design charts[5]) has been calculated using $(dC_{N_T}/d\alpha_T)_o = 0.040$. The results, presented in Fig. 5, strikingly indicate that, since the free-floating tendency of the rudder is markedly in-

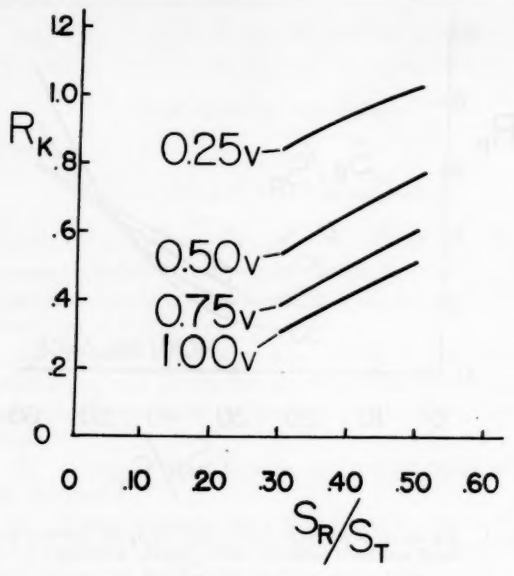

FIG. 5. Variation of R_K with S_R/S_T and with values of v corresponding to various balancing tab effectiveness; $S_B/S_R = 0$; $(dC_{N_T}/d\alpha_T)_o = 0.040$.

creased by reducing the numerical value of v, the use of balancing tabs markedly increases the likelihood of rudder pedal-force reversals or lightenings and this likelihood sharply increases as the balancing tab effectiveness increases.

Airflow Parameters

As indicated in Eqs. (5) and (7), the side-wash at the vertical tail during various flap and power flight conditions obviously affects the free-floating tendencies of the rudder. The only available experimental data[6] on this parameter does not, unfortunately, include the marked and important effects of slipstreams on the airflow at the vertical tail.

Values of this airflow parameter and the flow pattern at the vertical tail, however, can at least be estimated from previous slipstream studies on the horizontal tail.[7, 8] By analogy, the increased dynamic pressure in the slipstream behind a yawed propeller is probably confined to a sharply defined region, and the increased side-wash, caused primarily by the unsymmetrical span loading on the wing and by the side force on a yawed propeller, is probably evident at considerable distances from this region. For a typical single-engined monoplane with dihedral and with contrarotating propellers that eliminate slipstream twist, the order of magnitude of the airflow parameters has been estimated as shown in Table 1. The variation of $d\sigma/d\beta$ with wing position has previously been discussed in other notes,[5, 6] which were also used in estimating the values for propellers-windmilling flight.

Using these estimates, values of $d\delta_{R_{FF}}/d\beta$ have been calculated from Eq. (7) for the various flight conditions for a typical vertical tail with axial balance—$S_R/S_T = 0.55$, $S_B/S_R = 0.20$, and $(dC_{N_T}/d\alpha_T)_o = 0.040$. The results, which are presented in Table 2, imply that there is a slightly greater tendency toward rudder pedal-force reversals or lightenings with low-wing airplanes than with high-wing airplanes. The results would also seem to indicate that in general there is no marked change in the rudder free-floating characteristics as the sideslip angle increases in either propeller-windmilling or power-on flight. In power-on flight, however, since it seems evident that the rudder trim characteristic—$d\delta_{R_{TR}}/d\beta = (dC_n/d\beta)_A/(dC_n/d\delta_R)$—would similiarly be unaffected as the sideslip angle increases, Eqs. (1) and

TABLE 2

$(d\delta_{R_{FF}}/d\beta)$ at the Various Flight Conditions

Flight Condition	$d\delta_{R_{FF}}/d\beta$ High wing	Midwing	Low wing
Steady sideslip in low-speed high-power flight with the vertical tail at small sideslip angles	−0.41	−0.51	−0.53
Same with vertical tail just outside slipstream	−0.44	−0.53	−0.56
Same with vertical tail outside slipstream at large sideslip angles	−0.59	−0.59	−0.59
Steady sideslip in propellers-windmilling flight at small sideslip angles	−0.50	−0.59	−0.62
Same at large sideslip angles	−0.59	−0.59	−0.59

TABLE 1

Estimated Airflow Parameters

	Flight Condition				
	—Steady Sideslips in High-Power Low-Speed Flight— with the Vertical Tail			—Steady Sideslips in Propellers— Windmilling Flight	
Airflow Parameters	Within the slipstream at small sideslip angles	Just outside slipstream	Outside slipstream at large sideslip angles	At small sideslip angles	At large sideslip angles
q/q_o	2.5	1.0	1.0	0.95	1.0
$\frac{d(q/q_o)}{d\beta}$	Usually negligible	Negligible	Negligible	Usually negligible	Negligible
$\frac{d\sigma}{d\beta}$ High Wing	0.30	0.25	0	0.15	0
$\frac{d\sigma}{d\beta}$ Midwing	0.15	0.10	0	0	0
$\frac{d\sigma}{d\beta}$ Low Wing	0.10	0.05	0	−0.05	0

(6) indicate that the sudden drop in the local dynamic pressure when the vertical tail emerges from the slipstream would undoubtedly cause a rudder pedal-force lightening.

Conclusions

Eqs. (2) and (6) indicate that airplanes that require large rudder trim angles and, hence, large $d\delta_{R_{TR}}/d\beta$, are probably less likely to have rudder pedal-force lightenings or reversals in steady sideslips than airplanes that require small rudder trim angles. These rudder trim characteristics obviously depend not only on the geometry of the vertical tail but also, and to the same degree, on the geometry of the complete airplane, although in general large- and small-chord rudders produce, respectively, small and large rudder trim angles; small-chord rudders are therefore less likely to have rudder pedal-force lightenings or reversals than large-chord rudders.

Considering only the free-floating characteristics of an *unstalled* vertical tail, the qualitative results may be summarized as follows:

(1) For a rudder with axial balance, rudder pedal-force lightenings or reversals are less likely to occur with small-chord rudders than with large-chord rudders. Increasing the axial balance of small-chord rudders tends to reduce further the likelihood of rudder pedal-force lightenings or reversals, whereas increasing the axial balance of large-chord rudders tends to further increase this likelihood.

(2) The likelihood of rudder pedal-force lightenings or reversals may be virtually eliminated by using a rudder with a properly proportioned horn balance.

(3) The use of balancing tabs on a rudder increases the likelihood of rudder pedal-force lightenings or reversals; this likelihood markedly increases as the balancing tab effectiveness increases.

(4) There is a slightly greater tendency toward rudder pedal-force lightenings or reversals for vertical tails with high aspect ratios than for vertical tails with low aspect ratios.

(5) There is no tendency toward rudder pedal-force lightenings or reversals as the sideslip angle increases in propeller-windmilling flight.

(6) Rudder pedal-force lightenings or reversals are most likely to occur in power-on flight at the sideslip angles at which the vertical tail emerges from the slipstream.

References

[1] Schairer, George S., *Directional Stability and Vertical Tail Stalling*. Journal of the Aeronautical Sciences, Vol. 8, No. 7, pp. 270–275, May, 1941.

[2] Johnson, Clarence L., *Rudder Control Problems on Four-Engined Airplanes*. S.A.E. Journal, Vol. 46, No. 6, pp. 262–270, June, 1940.

[3] Glauert, H., *Theoretical Relationships for an Airfoil with Hinged Flap*. R. & M. No. 1095, British A.R.C., 1927.

[4] Katzoff, S., and Mutterperl, Wm., *The End Plate Effect of a Horizontal Tail Surface*, N.A.C.A. T.N. No. 797, 1941.

[5] Pass, H. R., *Analysis of Wind-Tunnel Data on Directional Stability and Control*, N.A.C.A. T.N. No. 775, 1940.

[6] Recant, Isidore G., and Wallace, Arthur R., *Wind-Tunnel Investigation of the Effect of Vertical Position of the Wing on the Side Flow in the Region of the Vertical Tail*, N.A.C.A. T.N. No. 804, 1941.

[7] Katzoff, S., *Longitudinal Stability and Control with Special Reference to Slipstream Effects*, N.A.C.A. T.R. No. 690, 1940.

[8] Goett, Harry J., and Pass, H. R., *Effect of Propeller Operation on the Pitching Moments of Single-Engine Monoplanes*, N.A.C.A. A.C.R., May, 1941.

SUGGESTIONS FOR CONTRIBUTORS TO THE PUBLICATIONS *of the* INSTITUTE *of the* AERONAUTICAL SCIENCES

The Institute of the Aeronautical Sciences invites both members and nonmembers from any country to submit papers for publication in the JOURNAL OF THE AERONAUTICAL SCIENCES and the AERONAUTICAL ENGINEERING REVIEW. The Institute, following the practice of other societies, does not pay for contributions.

The following directions for the preparation of papers, if followed by authors, will save correspondence, avoid the return of papers for changes, minimize the work of preparation for the printer, and save the expense due to the charges made for "author's corrections."

MANUSCRIPTS: Papers must be written in English, in original typewriting on one side only of white paper sheets, consecutively numbered and be double or triple spaced with wide margins. Manuscripts should be prepared with great care so that they will be typographically accurate. Paragraphing should be given special attention. Papers should be written in the third person, reference to the writer being made as "the author." Avoid the use of the words "I," "we," and "you." Blueprint copies of papers are unacceptable as it is impossible to mark directions to the printer on them. Correcting, changing, or adding to papers after they are in type is costly. It is, therefore, imperative that papers submitted be in final form. Typographical errors may be corrected on proofs, but if authors wish to add material, they may do so at their own expense. In mailing, drawings may be rolled, but manuscripts should be sent flat. Send by first class mail (register if you wish for your own protection) to the Editorial Office, Institute of the Aeronautical Sciences, 1505 RCA Bldg. West, 30 Rockefeller Plaza, New York 20, N. Y. All manuscripts will be examined by the Editorial Committee and by the Editor. Authors will be advised as promptly as possible whether the paper is acceptable for publication.

TITLES: The title of the paper should be brief. The name and initials of the author should be written as he prefers. The use of the full name of an author is advocated because of the frequent duplication of initials and surnames which sometimes makes it difficult to establish the identity of the author. This is particularly important for large annual indexing and abstracting services. All titles and degrees or honors are omitted. The name of the organization with which the author is associated should be placed after his name on a separate line. The date on which the paper is received will be inserted by the Editor.

SUMMARIES OR ABSTRACTS: An abstract to be printed at the beginning should accompany each article. It should be adequate as an *index* and as a *summary*. It should contain a statement of major conclusions reached, since summaries in many cases constitute the only source of information used in compiling scientific reference indexes. Abstracts printed in other journals, especially foreign, in most cases, consist of summaries from printed papers. The summary should explain as adequately as possible the major conclusions to a nonspecialist in the subject. The summary should contain from 100 to 300 words, depending on the length of the paper.

SUBHEADINGS: Subheadings should be inserted by the author at frequent intervals. The work of editorial preparation will be simplified by the author providing many subheadings. Owing to the breaking of columns and the insertion of illustrations, some of the subheadings may have to be omitted.

SHORTENING OF PAPERS: Some papers, at the end, fill in only a portion of a page. This leaves much wasted blank space as succeeding articles are started at the top of a page. Authors should indicate by notation on the left-hand side of the page what matter may be omitted when "runovers" occur. This request is important as the Journal cannot afford in the future, as it has in its earlier issues, to have blank half pages or more at the end of papers.

MATTER USUALLY DELETED: Acknowledgments of assistance in preparation of paper, except by collaborators. Photographs or illustrations of little technical interest and not showing advances in general practice. Too detailed tabular matter (general results of such tables may be included in the text). Lengthy descriptions of materials or processes or of preliminary experiments or theories that preceded final results; salient features only are of interest.

REFERENCES AND FOOTNOTES: References should appear as footnotes only, numbered consecutively, grouped together at the end of the manuscript. The arrangement should be as follows: (for books)—[1] Durand, W. F., *Aerodynamic Theory*, 1st Edition, Vol. 1, p 23; Julius Springer, Berlin, 1934. (For magazines)—[1]Englund, C. R., Crawford, A. B., and Mumford, W. W., *Some Results of a Study of Ultra-Short-Wave Transmission Phenomenon*, Proc. I. R. E., Vol. 20, No. 12, pp. 481 and 482, March, 1933. Please give author, title, edition, volume, page, publisher and date of publication as indicated. Omission of one required fact causes much extra editorial work and possible inaccuracies. All references are grouped at the end of the article.

ILLUSTRATIONS: Illustrations should accompany manuscripts and each should always be referred to in the text, preferably by number. Drawings or graphs should not be larger than 12 × 16 inches, and must be made with jet black India Ink on white paper or tracing cloth, the latter being preferred. *Do not use typewriter for lettering.* The smallest lettering on 8 × 10 inch figures should be no less than 1/4 inch high. Cross-section paper (white with black lines) may be used, but should not have more than 4 lines per inch. If finer ruled paper is used, the major division lines should be drawn in with black ink, omitting the finer divisions. In the case of finely ruled paper, only blue-lined paper can be accepted. *Tracing paper and blueprints* are not acceptable. Lettering and all markings must be large enough to be readable after reduction. Mail rolled or flat, never fold. Drawings that cannot be reproduced (including pencil drawings) will be returned to the author for redrawing, thus delaying publication of the paper. Photographs should be very distinct and show clear black and white contrasts. They must be on glossy white paper. Avoid round and oval photographs.

CAPTIONS AND LEGENDS: Legends or captions must accompany each drawing or photograph submitted. If written on the drawing or photograph, they should be placed below and well outside the part to be reproduced. It is better to place them on separate sheets of paper pasted to the back of the drawings or photographs. Each table should have a caption such as Table 1, Table 2, Table 3, etc. Captions should be complete in themselves so as to make the data intelligible to the reader without reference to the text. A duplicate list of captions for figures should be included as the last page of the manuscript. Use "Fig. 1" (not Figure 1), Figs. 3 and 4, etc., in both the text and the numbering of illustrations. In the text, "Eq. (1)," or "Eqs. (1) and (2)" are preferable to "Equation (1)." In captions and legends, except for "Fig." and "Eq." and table headings, write all words in full; do not abbreviate. Avoid placing explanatory written matter in the drawings; it should be in the text.

MATHEMATICAL WORK: Only the simplest formulas should be typewritten; all others should be carefully written in pen and ink, the writing to be large enough so that ample room is provided to mark mathematical matter for the printer. A considerable space for marking should be allowed above and below all equations. All complicated equations should be repeated on separate sheets with plenty of space left for marking. The solidus should be used for simple fractions appearing within the text. Make all expressions clear to the typesetter. Greek letters used in formulas should be clearly designated by name on the margin of the manuscript. All symbols should be clearly written and carefully checked. The difference between capital and lower-case letters should be clearly distinguished and care taken to avoid confusion between zero (0) and the letter (o), between the numeral (one) and the letter (ell) and the prime ('), between alpha and a, kappa and k, u and mu, v and nu, n and eta. All subscripts and exponents should be clearly marked and dots and bars over letters or mathematical expressions should be avoided. Avoid complicated exponents and subscripts. When it is necessary to repeat a complicated expression, it should be represented by some convenient symbol.

NOMENCLATURE AND ABBREVIATIONS: The National Advisory Committee for Aeronautics Nomenclature should be used in preference to any others. Standard abbreviations should be used, and it should be noted that most abbreviations are lower case, such as m.p.h., b.m.e.p., i.hp., b.hp., hp., . . etc.